Akademia Techniczno-Humanistyczna

Wydział Inżynierii Materiałów, Budownictwa i Środowiska

Katedra Inżynierii Materiałowej

Rozprawa doktorska

pod tytułem

Badania nad otrzymywaniem i właściwościami materiałów celulozowych modyfikowanych nanododatkami węglowymi

mgr inż. Tobiasz Gabryś

Praca wykonana pod kierunkiem

dr hab. inż. Beaty Fryczkowskiej, prof. ATH

w Katedrze Inżynierii Materiałów ATH w Bielsku-Białej

Bielsko-Biała 2023

Pragnę podziękować również moim współpracownikom

z Katedry Inżynierii Materiałów za okazaną pomoc

w codziennej pracy zawodowej.

Streszczenie

Biopolimerem powszechnie występującym w przyrodzie jest tania i ogólnie dostępna celuloza. Celuloza jest polimerem, który można modyfikować, zarówno fizycznie, jak i chemicznie. Wiele możliwości, jakie daje ten biopolimer skłaniają do tworzenia nowych materiałów, które sprostają naszym oczekiwaniom.

Rozwój nowych materiałów był możliwy dzięki m.in. nanotechnologii, która w dużej mierze bazuje na nanomateriałach węglowych. Do nanostruktur węglowych zaliczane są między innymi nanorurki, fulereny, grafen, czy tlenek grafenu (GO). Ten ostatni jest utlenioną pochodną grafitu i charakteryzuje się zawartością różnego rodzaju grup tlenowych. Budowa chemiczna tlenku grafenu sprzyja tworzeniu kompozytów na bazie celulozy, w wyniku czego otrzymywane są nowe, biodegradowalne materiały o nieopisanych dotąd i ciekawych właściwościach.

W niniejszej dysertacji podjęto zadanie opracowania, wytworzenia i szczegółowego scharakteryzowania materiałów celulozowych modyfikowanych tlenkiem grafenu. Materiały te otrzymywano w dwojaki sposób. Pierwszy polegał na rozpuszczeniu celulozy drzewnej w octanie 1-etylo-3-metyloimidazolu, po czym wprowadzeniu dodatku GO (zdyspergowanego w dimetyloformamidzie), a następnie formowaniu włókien metodą mokrą. W ten sposób otrzymywano włókna kompozytowe na bazie celulozy regenerowanej. Druga metoda polegała na biochemicznej syntezie celulozy bakteryjnej, w trakcie której *in situ* wprowadzano wodną dyspersję GO. W wyniku tego doświadczenia otrzymano nanowłókniny kompozytowe o budowie warstwowej.

W pracy badano wpływ dodatku tlenku grafenu na właściwości otrzymanych kompozytów na osnowie celulozy. Wykazano, że nanododatek wprowadzony do matrycy celulozowej wpływa na strukturę, właściwości fizykochemiczne, mechaniczne i mikrobiologiczne. Pod wpływem GO wzrasta stopień krystaliczności dla celulozy regenerowanej, natomiast zmniejsza się dla bakteryjnej. Włókna modyfikowane GO, jak i modyfikowane włókniny kompozytowe, charakteryzują się wyższą temperaturą rozkładu termicznego. Zatem dodatek GO zwiększa stabilność termiczną włókien kompozytowych. Mikroskopia skaningowa potwierdziła, że GO jest wbudowany wewnątrz struktury włókien kompozytowych oraz włókniny, co zapewnia bezpieczeństwo stosowania wytworzonych materiałów kompozytowych. Jednocześnie

otrzymane materiały kompozytowe posiadają właściwości biobójcze. W wyniku prowadzonych badań otrzymano nowe, nieopisane dotąd materiały kompozytowe o unikalnych właściwościach.

Abstract

Cellulose is a biopolymer commonly found in nature, which is cheap and easily accessible. Cellulose is a polymer that can be modified, both physically and chemically. The many possibilities offered by this biopolymer encourage the creation of new materials that meet our expectations.

The development of new materials was possible by nanotechnology, which is largely based on carbon nanomaterials. Carbon nanostructures include, among others, nanotubes, fullerenes, graphene or graphene oxide. The last one is an oxidized derivative of graphite and is characterized by the content of various types of oxygen groups. The chemical structure of graphene oxide is promotes to the creation of cellulose-based composites, resulting in new, biodegradable materials with previously undescribed and interesting properties.

In this dissertation, the task of developing, manufacturing and detailing cellulose materials modified with graphene oxide was undertaken. These materials were obtained in two ways. The first consisted in dissolving wood cellulose in 1-ethyl-3-methylimidazole acetate, followed by the introduction of the additive GO (dispersed in dimethylformamide), followed by the formation of fibers by the wet method. In this way, composite fibers based on regenerated cellulose were obtained. The second method consisted in the biochemical synthesis of bacterial cellulose, during which aqueous dispersion of GO was introduced in situ. As a result of this experiment, composite nanotextiles with a layered structure were obtained. The effect of graphene oxide addition on the properties of the obtained cellulose matrix composites was investigated. It has been shown that the nanoadditive introduced into the cellulose matrix affects physicochemical, structural, mechanical and microbiological properties. Under the influence of GO, the degree of crystallinity increases for regenerated cellulose, while it decreases for bacterial cellulose. GO modified fibers as well as modified composite nonwovens are characterized by a higher temperature of thermal decomposition. Thus, the addition of GO increases the thermal stability of composite fibers. Scanning microscopy confirmed that GO is embedded inside the structure of composite fibers and non-woven fabrics, which ensures the safety of using the manufactured composite materials. At the same time, the obtained composite materials have biocidal properties. As a result of the conducted research, new, previously undescribed composite materials with unique properties were obtained.

Spis treści

1. Wprowadzenie

Niekorzystne zmiany w środowisku naturalnym, które mają miejsce podczas produkcji, użytkowania i utylizacji tworzyw sztucznych skłaniają do zastępowania ich polimerami biodegradowalnymi. Biopolimerem powszechnie występującym w przyrodzie jest tania i ogólnie dostępna celuloza. Znajduje ona zastosowanie w wielu dziedzinach naszego życia, zarówno w formie nieprzetworzonej, jak i przetworzonej. Celuloza jest polimerem, który można również modyfikować fizycznie, jak i chemicznie. Wiele możliwości, jakie daje ten biopolimer skłaniają do tworzenia nowych materiałów, które sprostają naszym oczekiwaniom.

Rozwój nowych materiałów był możliwy dzięki mi.in. nanotechnologii, która powstała pod koniec XX wieku. Nauka ta bazuje w dużej mierze na nanomateriałach węglowych. Do nanostruktur węglowych zaliczane są nanorurki, fulereny, grafen, czy tlenek grafenu. Ten ostatni jest utlenioną pochodną grafitu i charakteryzuje się zawartością różnego rodzaju grup tlenowych. Budowa chemiczna tlenku grafenu sprzyja tworzeniu kompozytów na bazie biopolimerów, w tym celulozy. W wyniku intensywnie prowadzonych badań otrzymywane są nowe, biodegradowalne materiały o ciekawych właściwościach.

1.1. Budowa chemiczna i właściwości celulozy

Jednym z najobficiej występujących w przyrodzie związków organicznych jest celuloza. Syntezowana jest przez rośliny zielone w złożonym procesie fotosyntezy, w którym światło słoneczne dostarcza energii do przekształcenia dwutlenku węgla w glukozę. Celuloza roślinna powstaje w wyniku reakcji polikondensacji ogromnej ilości cząsteczek β-glukopiranozy, tworząc bardzo długie, proste, nierozgałęzione łańcuchy. Do otrzymywania tego biopolimeru są przystosowane również wyspecjalizowane mikroorganizmy, które ją syntezują tworząc nanofibrylarną, trójwymiarową sieć [1].

Makrocząsteczka celulozy cechuje się bardzo dużą długością łańcucha, wynoszącą 3000 – 14000 jednostek D-glukozy. Stopień polimeryzacji w istotnej mierze zależy od źródła pochodzenia. Dla celulozy natywnej oraz celulozy bakteryjnej może on dochodzić do 9000 jednostek. Natomiast po obróbce chemicznej, w wyniku której otrzymuje się celulozę regenerowaną, stopień polimeryzacji wynosi zaledwie 300–500 jednostek D-glukozy [2].

Pod względem chemicznym celuloza jest liniowym homopolisacharydem zbudowanym z cząsteczek β-D-glukopiranozy połączonej wiązaniami β-1,4-glikozydowymi [3,4]. Konfiguracja β pozwala na tworzenie długich łańcuchów, w których każda kolejna reszta glukozy obrócona jest o 180° względem sąsiedniej. W wyniku tego między atomem tlenu pochodzącym z pierścienia jednej β-D-glukopiranozy i grupą –OH następnej powstaje wewnątrzcząsteczkowe wiązanie wodorowe (zaznaczone kolorem niebieskim na Rysunku 1).
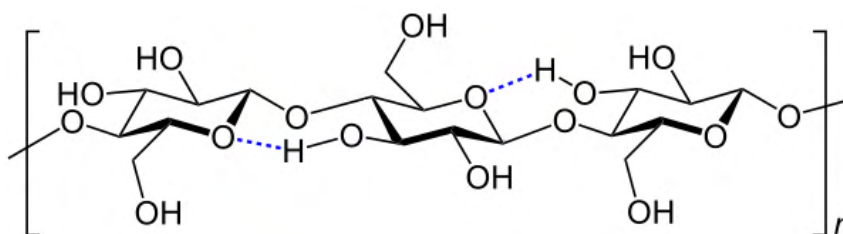
Rysunek 1. Chemiczna struktura celulozy [5]

Poszczególne cząsteczki celulozy oddziałują ze sobą, tworząc wielkie agregaty utrzymywane przez międzycząsteczkowe wiązania wodorowe. Skutkiem obecności licznych wiązań wodorowych jest wysoka wartość energii kohezji molekularnej, która sprawia, że celuloza jest trudnorozpuszczalna w klasycznych rozpuszczalnikach, co stwarza spore problemy przetwórcze [6].

W każdym merze β-D-glukopiranozy przy 2, 3 i 6 atomie węgla występują grupy -OH. Natomiast na końcach łańcucha celulozy występują charakterystyczne grupy końcowe: hydroksylowe i aldehydowe. Dzięki obecności tych grup funkcyjnych celuloza może również ulegać reakcjom estryfikacji i eteryfikacji.

Obecny stan wiedzy pozwala na przypisanie celulozie budowy krystaliczno-amorficznej, zwanej inaczej budową semikrystaliczną. Wyróżniamy w niej obszary zorientowane – krystaliczne oraz obszary bezpostaciowe. Te pierwsze charakteryzują się doskonałym uporządkowaniem we wszystkich kierunkach przestrzeni. Z kolei drugie, tzw. obszary amorficzne, odznaczają się mniej doskonałym porządkiem w ułożeniu cząsteczek oraz mniejszym natężeniem sił van der Waalsa i wiązań wodorowych.

Celuloza występuje w kilku odmianach polimorficznych, różniących się kształtem komórki elementarnej i jej parametrami. Odmiany te są numerowane cyframi rzymskimi i różnią się od siebie rodzajem sieci krystalicznej, układem wiązań wodorowych i

orientacją łańcuchów w sieci. Wyróżnia się cztery główne odmiany krystalograficzne celulozy, o charakterystycznych parametrach sieci krystalicznej (Tabela 1) [7].

Tabela 1. Parametry komórki elementarnej różnych odmian celulozy [7]

Typ odmiany	a (Å)	b (Å)	c (Å)	α (°)	β (°)	γ (°)
Iα	6,717	5,962	10,400	118,08	114,8	80,37
Iβ	7,784	8,201	10,380	90	90	96,55
II	8,10	9,03	10,31	90	90	117,1
III	4,45	7,85	10,31	90	90	105,1
IV	8,03	8,13	10,34	90	90	90

Celuloza I jest najczęściej spotykaną odmianą celulozy, gdyż jest odmianą naturalną (natywną). W strukturze tej odmiany łańcuchy polisacharydu ułożone są w równoległych warstwach. Występowanie odmian polimorficznych α i β oraz ich wzajemne proporcje zależą od pochodzenia surowca. Celuloza II jest nazywana celulozą regenerowaną, powstającą w trakcie obróbki chemicznej celulozy I. Jest ona najstabilniejszą termodynamicznie odmianą celulozy. Różni się od celulozy I tym, że w jej strukturze sąsiednie łańcuchy polisacharydu są zorientowane przeciwnie. Natomiast celuloza III oraz IV są odmianami, które nie występują w warunkach naturalnych [1].
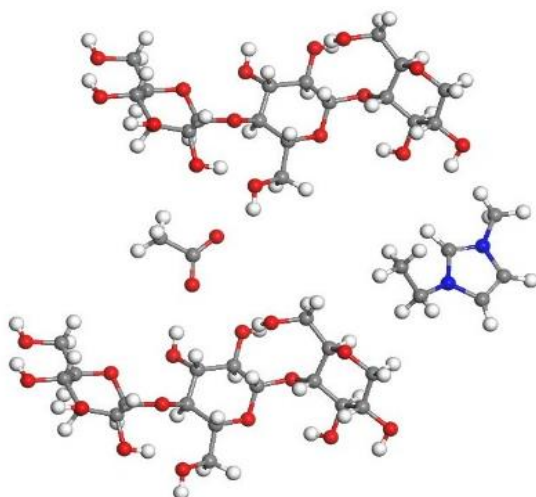
1.2. Proces rozpuszczania celulozy

Celuloza jest polimerem liniowym, połączonym stabilnymi wiązaniami glikozydowymi, którym towarzyszą wewnątrz- i międzycząsteczkowe wiązania wodorowe. Obecność tych wiązań, oraz występowanie obszarów krystalicznych w celulozie powoduje, iż polimer ten jest nierozpuszczalny w wodzie oraz w większości rozpuszczalników organicznych. Wysoka wartość energii kohezji molekularnej sprawia spore problemy przetwórcze [8,9].

Opracowano wiele układów zdolnych do rozpuszczenia polimeru, pośród których można wymienić: $NaOH/CS_2$, DMSO/TBAF, $NMMO/H_2O$, LiCl/DMAc, N_2O_4/DMF, które mają takie wady, jak: lotność, toksyczność, czy łatwopalność [9–11].

Oprócz klasycznych, znanych od lat metod rozpuszczania celulozy, pojawiły się nowe rozpuszczalniki nazywane cieczami jonowymi. Ciecze jonowe znajdują zastosowanie jako rozpuszczalniki bezpośrednie biopolimerów opartych o polisacharydy [12]. Możliwość rozpuszczania celulozy w cieczach jonowych pozwala na stosunkowo proste przetwórstwo tego polimeru, pozwalające otrzymać włókna, nanowłókna, granulki, żele, kłaczki i membrany [6,13,14].

Pod względem chemicznym ciecze jonowe zbudowane są z dużego organicznego kationu oraz mniejszego organicznego lub nieorganicznego anionu [9]. Proces rozpuszczania celulozy przez ciecze jonowe jako pierwszy opisał Swatolski i współautorzy [15]. Koncepcja rozpuszczania celulozy przez te związki polega na wnikaniu cieczy jonowej pomiędzy makrocząsteczki celulozy i pękaniu wiązań wodorowych (Rysunek 2).

Rysunek 2. Rysunek przedstawiający proces rozpuszczania celulozy przez ciecz jonową EMIMAc [16]

Badania cieczy jonowych prowadzone przez szereg lat wskazują na to, że jedną z najlepszych cieczy jonowych jest octan 1-etylo-3-metyloimidazolu (EMIMAc). Stosując tą ciecz można otrzymać roztwory celulozy o stężeniu do 25% wagowych. Ważną cechą EMIMAc jest to, że należy do grupy niskotemperaturowych cieczy jonowych (RTIL-*room temperaturę ionic liquid)*. Inną jej zaletą jest niska toksyczność, wynosząca ED50 = 2860 mg/dm^3 [17].

1.3. Celuloza bakteryjna

Celuloza bakteryjna (BC) jest biopolimerem produkowanym przez niepatogenne bakterie, które występują w środowisku naturalnym. Najwydajniejszymi producentami tego rodzaju celulozy są Gram ujemne bakterie z rodziny *Acetobacter*. Biopolimer ten może być również produkowany przez inne bakterie Gram ujemne (np. *Gluconacetobacter xylinus* [18] *Agrobacterium* [19] i *Rhizobium* [20] oraz Gram dodatnie np. *Sarcina* [21].

Budowa chemiczna celulozy bakteryjnej jest taka sama, jak celulozy roślinnej. Makrocząsteczka cechuje się długością łańcucha wynoszącą do 15000 jednostek D-glukozy [22]. Liniowe łańcuchy β-1,4-glukopiranozy tworzą nanofibryle widoczne na mikrofotografiach wykonanych za pomocą skaningowego mikroskopu elektronowego (SEM) (Rysunek 3).
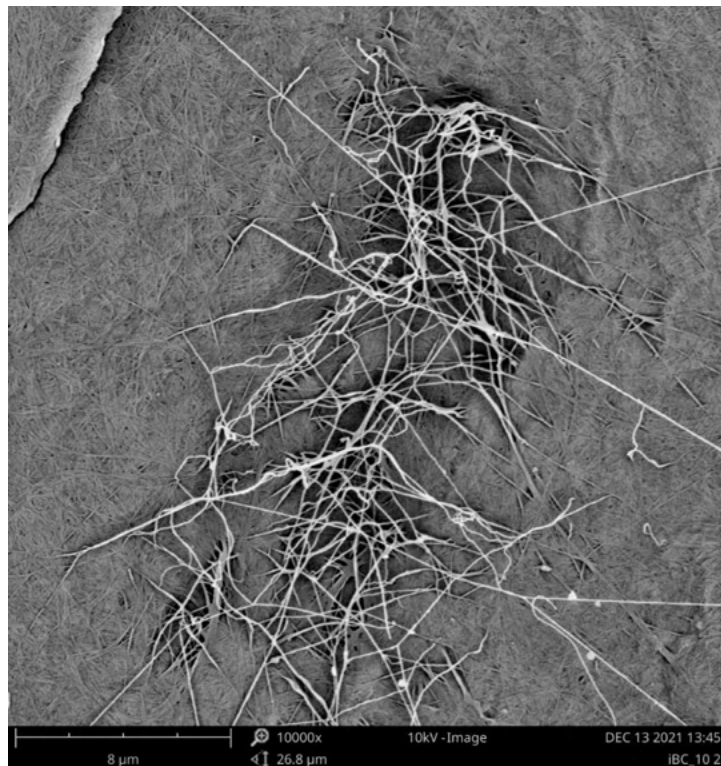
Rysunek 3. Zdjęcie SEM celulozy bakteryjnej [opracowanie własne].

Celuloza bakteryjna zbudowana jest z czystego biopolimeru i w odróżnieniu od tej pochodzenia roślinnego, nie zawiera lignin, ani hemicelulozy. Włókna celulozy bakteryjnej są tysiąc razy cieńsze niż włókna celulozy roślinnej. Ponadto stopień

krystaliczności tego biopolimeru wynosi do 80% [24–26]. Wszystko to sprawia, że celuloza bakteryjna cechuje się takimi właściwościami, jak nietoksyczność, hipoalergiczność, biofunkcjonalność, biokompatybilność i biodegradowalność. Do obszarów jej zastosowań można zaliczyć medycynę, przemysł spożywczy, kosmetyczny oraz papierniczy [27].

1.4. Nanododatki węglowe

Pod koniec XX wieku rozwinęła się nanotechnologia, która opierała się na nanomateriałach węglowych, czyli alotropowych odmianach węgla, takich, jak fulereny i nanorurki, nanodruty i kropki kwantowe. W późniejszym czasie odkryto i badano grafen oraz tlenek grafenu.

Okrycie fulerenów i rozszyfrowanie ich budowy przestrzennej datuje się na rok 1985. Cząsteczki fulerenu zbudowane są z parzystej liczby atomów węgla (od 28 do 15000) z pustą przestrzenią w środku, przypominającą wyglądem sferę (Rysunek 4–d). Powierzchnia fulerenów składa się z układu sprzężonych pierścieni składających się z pięciu i sześciu atomów węgla [28]. Posiadają własności nadprzewodzące i półprzewodnikowe. Można je mieszać z polimerami, tworząc środki smarujące. Ponadto poddaje się je funkcjonalizacji, otrzymując katalizatory orozwiniętej powierzchni właściwej [28].

W trakcie badań nad syntezą fulerenów odkryto nanorurki węglowe. Struktura przestrzenna nanorurek oparta jest o dwuwymiarową płaszczyznę grafenową zwiniętą w rurkę (Rysunek 4–f). Wyróżnia się nanorurki jedno- oraz wielościenne. Cechują się one bardzo wysoką wytrzymałością na rozciąganie oraz sztywnością, dobrymi właściwościami elektrycznymi (zachowują się jak metale i półprzewodniki), cieplnymi i dużą powierzchnią właściwą. Znajdują bardzo szerokie zastosowanie, zarówno w nano-, jak i makroskali [28,29].

Ostatnim, odkrytym w 2004 roku nanomateriałem jest grafen (Rysunek 4–b). To płaska, dwuwymiarowa struktura, w której atomy węgla są połączone w sześciokąty i przypominają wyglądem plaster miodu. Grafen posiada unikatowe właściwości, pośród których warto wymienić bardzo dobrą przewodność cieplną, wytrzymałość na rozciąganie, elastyczność, dobre właściwości optyczne. Ponadto jest dobrym

przewodnikiem prądu, a po domieszkowaniu – półprzewodnikiem [30]. W związku z tym, grafen znajduje potencjalne zastosowanie w bardzo wielu dziedzinach życia.
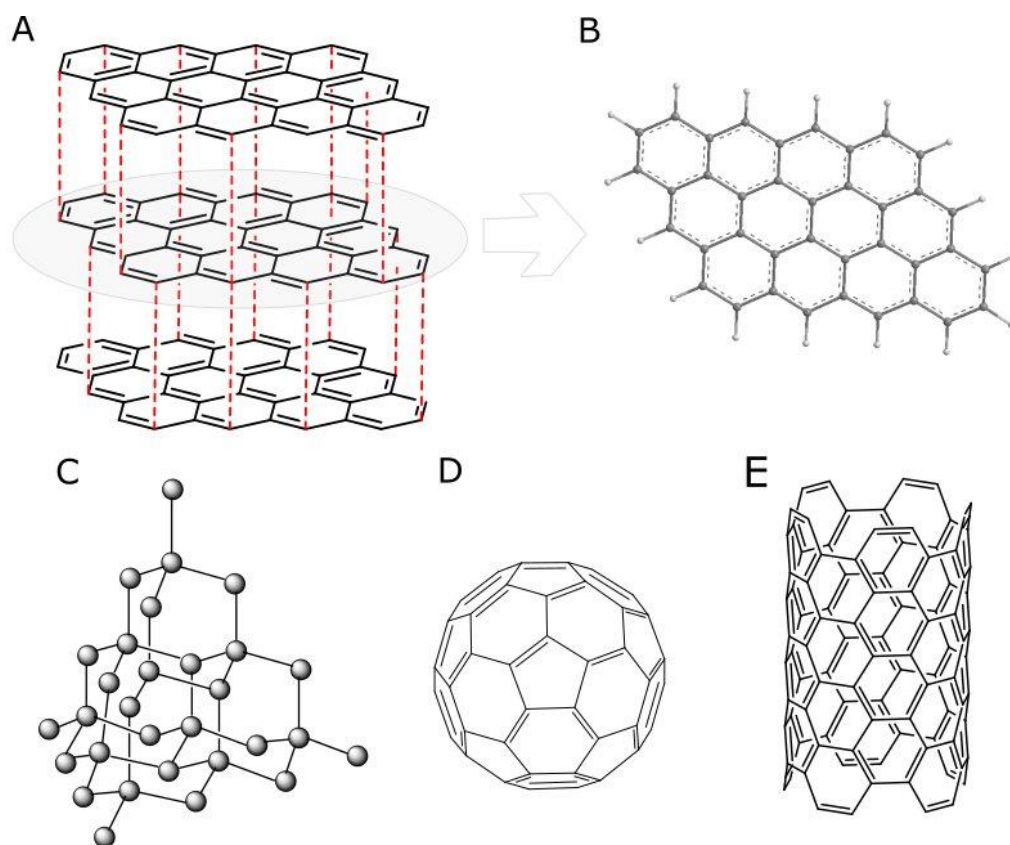
Rysunek 4. Odmiany alotropowe węgla: (A) grafit, (B) grafen, (C) diament, (D) fulereny, (E) nanorurki [31].

1.5. Oddziaływania na granicy celuloza – tlenek grafenu

Tlenek grafenu jest utlenioną formą grafenu, w którym do płaszczyzny węglowej dołączone są liczne tlenowe grupy funkcyjne. Strukturalnie ma postać monowarstwy węglowej o grubości około $1,1 \pm 0,2$ nm, w której grupy funkcyjne występują po obu stronach płaszczyzny oraz na jej brzegach (Rysunek 5). Grupy te nie tylko powiększają odległość międzypłaszczyznową, ale również nadają właściwości hydrofilowe. Te utlenione płaszczyzny mogą ulec dalszemu rozwarstwieniu pod wpływem np. sonifikacji. Proces rozwarstwiania grafitu, prowadzący do powstania tlenku grafenu nazywamy eksfoliacją.

Podstawowym źródłem tlenku grafenu jest grafit (Rysunek 4–a). Dzięki wprowadzeniu grup tlenowych do struktury grafitu możliwe jest jego rozwarstwienie, w wyniku czego otrzymuje się GO, zawierający od kilku do kilkudziesięciu warstw. Samo otrzymywanie tlenku grafenu jest możliwe na różne sposoby, które można sklasyfikować, jako metody fizyczne oraz chemiczne [30]. Wśród metod fizycznych swoje zastosowanie znajduje mechaniczne odspajanie warstw węglowych poprzez działanie np. ultradźwiękami. Chemiczne metody opierają się na eksfoliacji warstw węglowych, poprzez działanie na grafit silnymi utleniaczami. Jako pierwszy metodę tą opisał Hummers w swojej pracy, w 1958 roku [32]. W efekcie otrzymywane są płaszczyzny węglowe jedno- lub kilkuwarstwowe zwane tlenkiem grafenu.
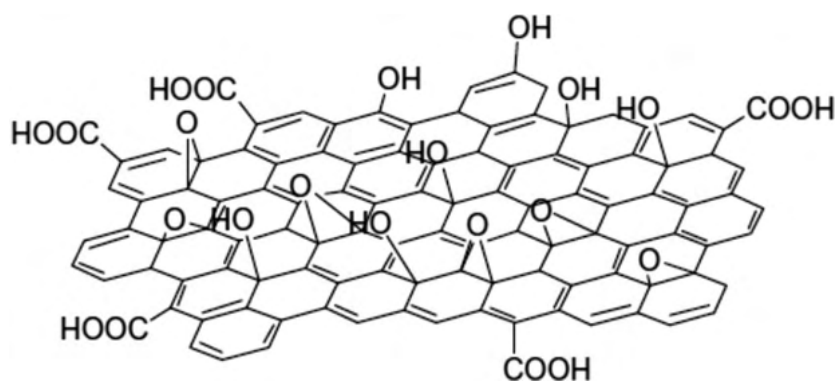
Rysunek 5. Budowa strukturalna GO z licznymi grupami tlenowymi [23]

Budowa chemiczna tlenku grafenu sprzyja tworzeniu kompozytów z polimerami posiadającymi grupy funkcyjne. Do takich polimerów można zaliczyć celulozę, która przy 2, 3 i 6 atomie węgla w ogniwie merowym zawiera grupy –OH.
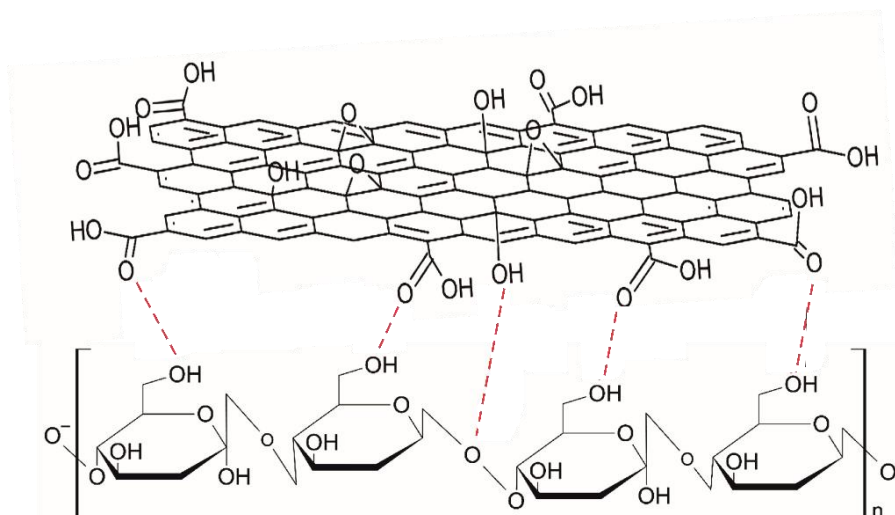
Rysunek 6. Powstawanie wiązań wodorowych między celulozą, a tlenkiem grafenu

[opracowanie własne]

Obecność ugrupowań tlenowych w ogniwie merowym biopolimeru sprawia, że pomiędzy celulozą, a tlenowymi grupami funkcyjnymi GO, powstają między innymi mostki wodorowe (Rysunek 6). Powstałe oddziaływania wpływają na zmianę właściwości fizykochemicznych powstałego kompozytu [33–35] oraz jego struktury. Powstanie dodatkowych wiązań wodorowych pomiędzy celulozą, a tlenkiem grafenu, skutkuje reorganizacją, inaczej rekrystalizacją tego polisacharydu i powstaniem nowych obszarów o wysokim stopniu uporządkowania zwanych micelami [36–38].

1.6. Podsumowanie przeglądu literatury

Materiały kompozytowe są w obecnych czasach bardzo powszechnie stosowane w wielu dziedzinach ludzkiego życia. Są to najczęściej wyroby wieloskładnikowe, które w dużej mierze zawierają tworzywa sztuczne. Niestety, pomimo ogromu swoich zalet, są wyrobami, których recykling jest bardzo utrudniony, albo wręcz niemożliwy.

W związku z powyższym, trwają intensywne prace nad możliwością zastąpienia klasycznych polimerów syntetycznych – biopolimerami. Jednym z nich jest szeroko rozpowszechniona w przyrodzie celuloza. Polisacharyd ten można z powodzeniem przetwarzać i modyfikować, projektując na osnowie celulozy materiały o nowych, nieopisanych wcześniej właściwościach. Istnieje wiele doniesień literaturowych, w których tworzy się kompozyty tego polisacharydu z dodatkami nieorganicznymi (np. nanocząsteczkami metali) oraz organicznymi. Dużym zainteresowaniem cieszą się szeroko rozumiane dodatki węglowe, w tym GO, który został krótko omówiony w poprzednim podrozdziale. To właśnie w obecności tlenku grafenu celuloza tworzy nowe wiązania, w wyniku czego można otrzymywać całkowicie biodegradowalne, przez co ekologiczne, wyroby o dowolnym kształcie. Materiały kompozytowe na osnowie celulozy z dodatkiem GO można również z powodzeniem poddawać recyklingowi energetycznemu. Dzięki niemu minimalizuje się zagrożenia środowiskowe związane z przedostawaniem się nanocząstek do ekosystemów.

2. Teza, założenia i cel pracy

Możliwe jest otrzymanie kompozytowych materiałów na osnowie celulozy modyfikowanych tlenkiem grafenu, który zapewnia poprawę właściwości użytkowych oraz nadanie nowych, nie wynikających z właściwości samej celulozy, co poszerza możliwości aplikacyjne otrzymanych kompozytów włóknistych.

Rozwój nanotechnologii, a także wzrost zainteresowania biopolimerami, w tym pochodzenia naturalnego, były podstawą do badań nad tworzeniem nowych materiałów kompozytowych, o nieznanych dotąd właściwościach. Celuloza jest naturalnym polisacharydem, który można modyfikować zarówno fizycznie, jak i chemicznie. Chemiczna modyfikacja jest możliwa do przeprowadzenia w procesie pęcznienia lub podczas rozpuszczania tego biopolimeru. Podczas, gdy poszczególne łańcuchy celulozy są rozluźnione można prowadzić reakcje chemiczne z udziałem grup hydroksylowych, a także wprowadzać różne nanododatki. Natomiast modyfikację celulozy bakteryjnej można prowadzić na gotowym wyrobie lub *in situ*, czyli równolegle do trwającej syntezy.

Badania nad otrzymywaniem membran kompozytowych [39–41] oraz granulek [42] na osnowie celulozy, domieszkowanych tlenkiem grafenu (GO) były prowadzone przez B. Fryczkowską w Katedrze Inżynierii Materiałowej na Wydziale Inżynierii Materiałów, Budownictwa i Środowiska ATH w Bielsku-Białej. Ważnym aspektem prowadzonych badań było otrzymanie nowego materiału, który w trakcie użytkowania zapewniłby brak możliwości przenikania nanocząstek do środowiska naturalnego. Cel ten został osiągnięty poprzez takie poprowadzenie procesu formowania membran i granulek, by dodatek GO zostawał „uwięziony" wewnątrz kompozytu na osnowie celulozy. Równocześnie wytworzono materiał kompozytowy, który wykazywał właściwości biobójcze.

Prace eksperymentalne rozpoczęto od prób polegających na wprowadzaniu – do 5% roztworu celulozy w EMIMAc – nanododatków węglowych, w postaci zredukowanego tlenku grafenu (rGO) i tlenku grafenu (obydwa nanododatki zostały zsyntezowane w ATH) oraz wielościennych nanorurek węglowych (WMCNT – NC7000TM zostały zakupione w firmie Nanocyl Sambreville, Belgia). Przeprowadzone badania wykazały, że w trakcie ich mieszania zarówno w postaci stałej, jak i dyspersji w

rozpuszczalnikach (DMF, DMAc – N,N-dimetyloacetamid, DMSO – dimetylosulfotlenek) z roztworem celulozy w cieczy jonowej (CEL/EMIMAc), powstawały mieszaniny niejednorodne, a nanocząstki rGO oraz WMCNT ulegały aglomeracji. Zatem wykluczono możliwość użycia zredukowanego tlenku grafenu i wielościennych nanorurek węglowych w procesie otrzymywania materiałów celulozowych modyfikowanych dodatkami węglowymi. Odmiennie natomiast zachowywał się GO, który zdyspergowany w DMF tworzył jednorodne mieszaniny z roztworem CEL/EMIMAc. Zatem do formowania włókien kompozytowych na osnowie celulozy wytypowano dodatek w postaci tlenku grafenu.

Pozytywne wyniki otrzymane w trakcie prowadzonych wcześniej badań nad otrzymywaniem membran skłoniły do ich rozszerzenia w kierunku formowania antyseptycznych, włókien kompozytowych na osnowie celulozy. Wyroby te potencjalnie mają dużo szersze zastosowanie, aniżeli membrany, czy granulki. Ciekawym wyzwaniem wydawało się również przeprowadzenie syntezy celulozy bakteryjnej (BC) w obecności biobójczego GO, w kierunku otrzymywania nowego materiału kompozytowego.

Właściwości biobójcze GO zostały szeroko opisane w literaturze. Tlenek grafenu niszczy komórki bakterii (zarówno Gram dodatnich, jak i Gram ujemnych) oraz grzybów. Proces niszczenia patogenów ma różne mechanizmy. Jeden polega na uszkodzeniu błony komórkowej, poprzez jej przecięcie (*z ang. nano-catting*), po czym wycieku składników komórkowych i śmierci komórki [43]. Inny polega na owinięciu płatków GO wokół komórki bakterii (*z ang. nano-wraping* lub *nano-trapping*), które następnie prowadzi do stresu oksydacyjnego, w efekcie którego komórka umiera [44].

W związku z powyższym, jako cel pracy obrano dwa główne problemy badawcze:

1. Otrzymanie włókien kompozytowych na osnowie celulozy z dodatkiem GO poprzez rozpuszczanie celulozy drzewnej w cieczy jonowej (octanie 1-etylo-3-metyloimidazolu), wprowadzanie dyspersji tlenku grafenu w N,N-dimetyloformamidzie, po czym formowanie włókien metodą mokrą.

2. Otrzymanie kompozytowych nanowłóknin z celulozy bakteryjnej w formie membrany poprzez prowadzenie biosyntezy w obecności tlenku grafenu zdyspergowanego w wodzie.

Pierwszy z tych celów stanowi modyfikację właściwości włókien z celulozy regenerowanej poprzez wprowadzenie nanododatku w postaci tlenku grafenu. Z kolei drugi obejmuje opracowanie warunków biosyntezy celulozy bakteryjnej w obecności GO, w celu otrzymywania warstwowego nanokompozytu metodą *in situ*.

W związku z postawieniem sobie powyższych celów, w pracy zrealizowano następujące cele szczegółowe:

- Zbadanie wpływu dodatku tlenku grafenu na właściwości reologiczne roztworów celulozy w cieczy jonowej - octanie 1-etylo-3-metyloimidazolu.

- Określenie warunków otrzymywania włókien celulozowych domieszkowanych tlenkiem grafenu, w tym dobór odpowiedniego koagulanta.

- Zaprojektowanie i wykonanie linii do laboratoryjnego otrzymywania kompozytowych włókien.

- Zbadanie struktury oraz właściwości fizykochemicznych, mechanicznych i mikrobiologicznych włókien kompozytowych na osnowie celulozy domieszkowanej tlenkiem grafenu.

- Określenie możliwości i warunków syntezy celulozy bakteryjnej w bezpośredniej obecności tlenku grafenu oraz jego wpływu na produkcję celulozy z wykorzystaniem różnych szczepów bakteryjnych.

- Dobór odpowiedniej metody nanoszenia tlenku grafenu podczas syntezy celulozy bakteryjnej, parametrów czasowych i ilościowych.

- Zbadanie wpływu tlenku grafenu na strukturę, właściwości fizykochemiczne i mechaniczne otrzymanych kompozytów warstwowych na bazie celulozy bakteryjnej.

- Zbadanie możliwości zastosowania materiałów kompozytowych na bazie celulozy bakteryjnej i tlenku grafenu jako opatrunków aktywnych.

3. Zakres prac eksperymentalnych

W ramach pracy doktorskiej wykonano szereg eksperymentów, począwszy od zaprojektowania stanowiska badawczego, po dobór parametrów otrzymywania kompozytów, aż po wykonanie materiału badawczego, a następnie poddanie go badaniom w celu określenia struktury, właściwości fizykochemicznych, wytrzymałościowych i mikrobiologicznych.

3.1. Materiały i metody formowania materiałów kompozytowych

Materiałem badawczym, który stanowił osnowę kompozytu była celuloza. Do badań wytypowano dwa rodzaje celulozy: celulozę drzewną oraz celulozę bakteryjną. Dodatkiem do materiału kompozytowego na osnowie celulozy był tlenek grafenu.

Celuloza drzewna o symbolu C 6663, została zakupiona w firmie Sigma Aldrich. Wzór sumaryczny $(C_6H_{10}O_5)_n$ oraz strukturalny (Rysunek 1). Gęstość nasypowa $0,3$ g/cm^3. Celuloza drzewna była rozpuszczana w cieczy jonowej - octanie 1-etylo-3-metyloimidazolu, który zakupiono w firmie Sigma Aldrich. Wzór sumaryczny $C_8H_{14}N_2O_2$ oraz strukturalny (Rysunek 7). Czystość $> 97\%$. Masa cząsteczkowa $170,21$ g/mol. Gęstość $1,101$ g/cm^3.
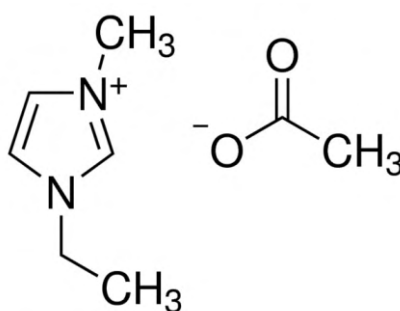
Rysunek 7. Wzór strukturalny octanu 1-etylo-3-metyloimidazolu [17]

Tlenek grafenu został otrzymany według zmodyfikowanej metody Hummersa [32]. Do syntezy zastosowano grafit o wielkości cząstek < 20 μm, który zakupiono w firmie Sigma-Aldrich. Sposób otrzymywania GO został opisany w artykule [45]. Na początku do kolby umieszczonej w łaźni lodowej wprowadzono 1 g NaNO$_3$ i 46 cm^3 H$_2$SO$_4$ oraz 2 g proszku grafitowego. Całość mieszano przez 30 minut, a następnie powoli,

porcjami wprowadzano 6 g KMnO$_4$, tak aby temperatura układu nie przekroczyła 20°C. Po wprowadzeniu całego KMnO$_4$ odczekano 5 minut, po czym mieszaninę reakcyjną ogrzano do 35°C. W tej temperaturze mieszaninę reakcyjną mieszano przez 4 h. Następnie ostrożnie, porcjami dodawano 92 cm^3 wody destylowanej. Na koniec usunięto nieprzereagowany KMnO$_4$. W tym celu do mieszaniny reakcyjnej wprowadzono 80 cm^3 wody destylowanej o temperaturze 60°C oraz 50 cm^3 3% H$_2$O$_2$. Na koniec otrzymany tlenek grafenu odwirowano i przemywano kilkakrotnie wodą destylowaną, aż do uzyskania pH = 7, otrzymując mokry tlenek grafenu.

W celu zastosowania GO jako dodatku do włókien kompozytowych na bazie celulozy regenerowanej, otrzymany w syntezie mokry tlenek grafenu poddano procesowi suszenia w suszarce laboratoryjnej, w temperaturze 60°C, uzyskując brązowy osad. Następnie proszek GO dyspergowano w N,N-dimetyloformamidzie (DMF), wykorzystując do tego celu łaźnię ultradźwiękową. W wyniku doświadczenia otrzymano mieszaninę o stężeniu 2,1% GO/DMF.

Natomiast do reakcji biosyntezy, prowadzącej do otrzymania kompozytu na osnowie celulozy bakteryjnej przygotowano wodną dyspersję GO o stężeniach: 10, 25 i 50 ppm. W tym celu mokry GO zdyspergowano w wodzie, stosując do tego sondę ultradźwiękową.

Włókna kompozytowe otrzymywano klasyczną metodą wytłaczania na mokro (*z ang. wet spinning*). Na wstępie przygotowano 5% roztwór z celulozy drzewnej w cieczy jonowej - octanie 1-etylo-3-metyloimidazolu (EMIMAc), z dodatkiem dyspersji GO w N,N-dimetyloformamidzie (DMF). Kąpiel koagulacyjną stanowiła woda destylowana (w publikacjach I–III – oznaczenie 1) oraz metanol (w publikacjach I–III – oznaczenie 2). Płyny przędzalnicze cechowały się wzrostową zawartością procentową tlenku grafenu. Procent wagowy GO w finalnych włóknach wynosił kolejno: 0,21; 0,5; 0,98; 1,97% (oznaczenie próbek w pracach odpowiednio: A, B, C, D). Przygotowano również próbę kontrolną, w której zawartość GO była zerowa (próbka 0). Do otrzymania monofilamentu wykorzystano skonstruowaną na potrzeby badawcze laboratoryjną linię produkcyjną składającą się z sekcji wytłaczania, koagulacji, odbierania wraz z suszeniem i nawijarki (Rysunek 8).
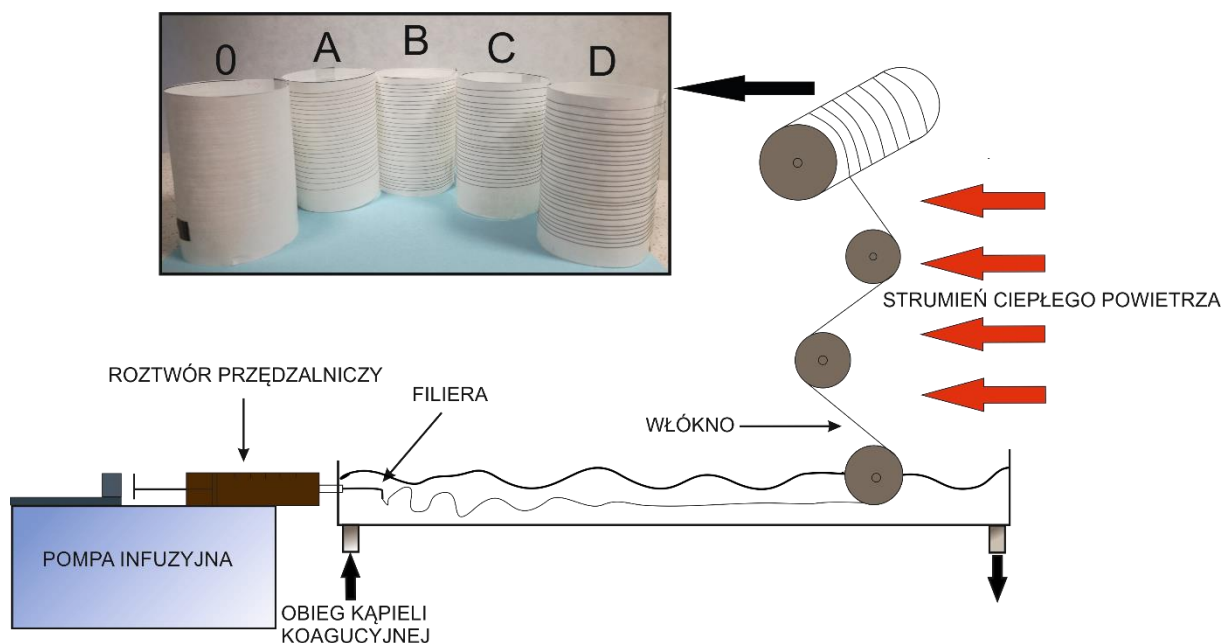
Rysunek 8. Schemat laboratoryjnej linii do otrzymywania włókien wraz z systemem

odbioru włókien. Włókna celulozowe (0) oraz kompozytowe GO/CEL (A-D)

[opracowanie własne]

Celulozę bakteryjną otrzymywano w dwojaki sposób. W pierwszej metodzie (publikacja IV) do biosyntezy wykorzystano szczepy bakterii kwasu octowego występujące naturalnie w owocach (jabłkach odmiany Golden Delicious). Do produkcji celulozy bakteryjnej przygotowano płynną pożywkę sacharozową o stężeniu 110 g/dm^3, do której wprowadzono odpowiednie ilości otrzymanego wcześniej octu jabłkowego oraz fragment "matki octowej", po czym dokładnie wymieszano. Następnie w temperaturze 25°C prowadzono hodowlę celulozy bakteryjnej, dodając do kolejnych próbek odpowiednie ilości dyspersji GO (publikacja IV – Tabela 1). W wyniku tego doświadczenia w prosty – nieopisany dotąd w literaturze – sposób otrzymano kompozyt celulozy bakteryjnej z dodatkiem tlenku grafenu (w ilości 3,7; 5,4; 7,1% w/w) metodą *in situ*.

W drugiej metodzie (publikacja V) wytypowano i zastosowano wyselekcjonowane szczepy bakterii: *Komagataei intermedius* LMG 18909 i *Komagataei sucrofermentas* LMG 18788 otrzymując kompozyty celulozy bakteryjnej oznaczone w pracy odpowiednio iBC oraz sBC. Bakterie te wyizolowano w Laboratorium Mikrobiologii, Zakładu Biologii, Wydziału Nauk Przyrodniczych i Matematyki Uniwersytetu w Mariborze. Do produkcji celulozy bakteryjnej

przygotowano pożywkę RAE (*z ang. reinforced acetic acid-ethanol)* [46], którą zaszczepiono pojedynczą kolonią bakteryjną i inkubowano w łaźni wodnej w temperaturze 30°C. Przez pierwsze 24 godziny kolby mieszano przez wytrząsanie liniowe, po czym bioreakcja była kontynuowana w warunkach statycznych. Równocześnie w odpowiednich odstępach czasowych dodawano wodą dyspersję GO (publikacja V – Tabela 1), otrzymując kompozyt celulozy bakteryjnej z dodatkiem tlenku grafenu metodą *in situ.*

W efekcie prowadzonych badań opracowano warunki prowadzenia biosyntezy, które obejmowały: dostosowanie pH do warunków sprzyjających namnażaniu celulozy przez bakterie, dobór odpowiedniego stężenia dyspersji GO/H_2O i określenie odstępów czasowych pomiędzy kolejnymi cyklami nanoszenia nanododatku. Rysunek 9 przedstawia proces otrzymywania nanokompozytu na osnowie celulozy bakteryjnej.
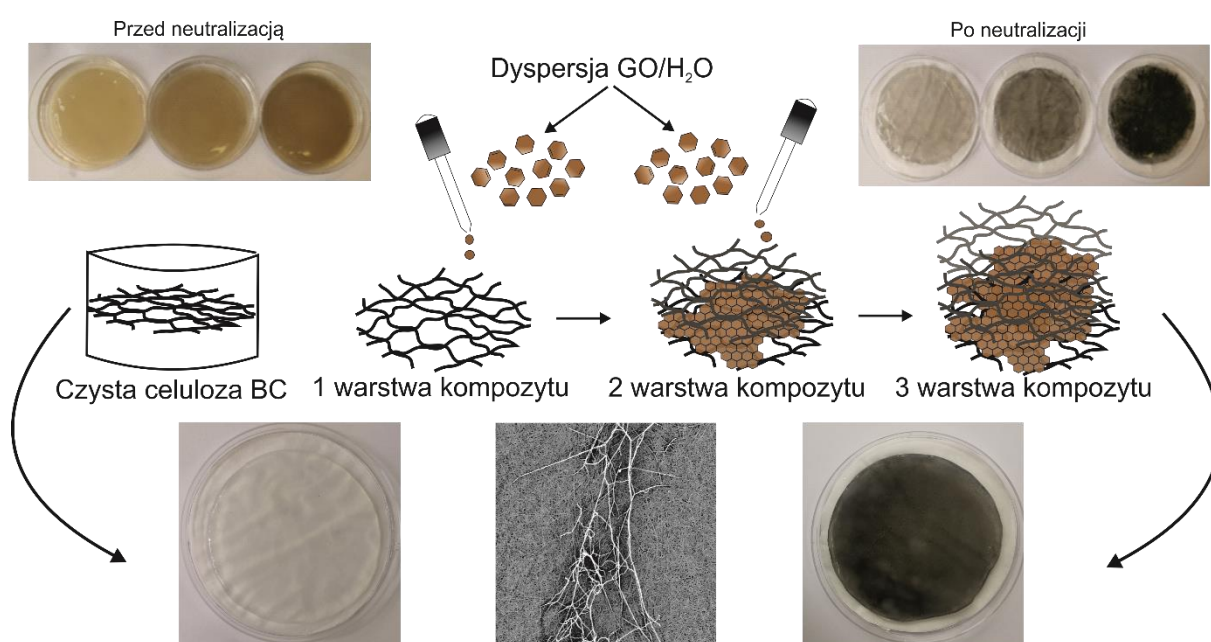
Rysunek 9. Schemat procesu otrzymywania celulozy bakteryjnej modyfikowanej GO in situ.

W górnej części rysunku ukazano przykładowe próbki przed oraz po procesie oczyszczania. [opracowanie własne]

3.2. Metody badawcze

W niniejszej pracy, prezentującej wyniki badań, służące do realizacji założonych celów badawczych wykorzystano następujące metody badawcze:

- Mikroskopia optyczna

Badania mikroskopowe prowadzono celem określenia stopnia zdyspergowania tlenku grafenu w osnowie celulozowej. Badania wykonano w świetle transmisyjnym, przy użyciu płynu immersyjnego, celem zminimalizowania negatywnych efektów optycznych. Obserwacji dokonano przy użyciu mikroskopu optycznego OptaTech z zastosowaniem powiększenia 10×.

- Skaningowa mikroskopia elektronowa

Badania techniką skaningowej mikroskopii elektronowej prowadzono z wykorzystaniem stołowego mikroskopu skaningowego Phenom ProX, wyposażonego w wolframową katodę oraz detektor EDS. Obserwacje prowadzono przy napięciu przyspieszającym równym 10 kV. Preparaty do badań pokrywano warstwą złota o grubości od 10 nm do 20 nm metodą dyfuzyjną przy użyciu niskopróżniowej napylarki marki Leica EM Ace 200, wyposażoną w kwarcową wagę monitorującą grubość naniesionej powłoki.

Próbki mocowano w uchwycie przy użyciu przewodzącej taśmy węglowej. Obserwacje przekrojów włókien prowadzono w analogiczny sposób, z wykorzystaniem holderów pionowych o orientacji 90°. Przełomy uzyskiwano poprzez łamanie próbek w ciekłym azocie.

- Szerokokątowa dyfraktometria rentgenowska (WAXS - *wide-angle X-ray scattering*)

W szerokokątowych badaniach rozpraszania promieniowania rentgenowskiego wykorzystano dwa dyfraktometry.

Pierwsze urządzenie to dyfraktometr URD-65 Seifert wykorzystujący metodę odbiciową w geometrii Bragga-Brentano. Promieniowanie CuK_α ($\lambda = 1,54$ Å) było emitowane przy napięciu przyspieszającym równym 40 kV i natężeniu prądu anodowego równym 30 mA. Monochromatyzacja wiązki promieniowania została uzyskana za pomocą monochromatyzatora grafitowego umieszczonego w torze wiązki odbitej. Jako detektor użyto licznika scyntylacyjnego. Badania przeprowadzono w zakresie kąta 2θ od 5° do 60° w krokach co 0,1°.

Drugie urządzenie to dyfraktometr D2 Phaser (Bruker AXS GmbH, Germany) wykorzystujący metodę odbiciową w geometrii Bragga-Brentano. Promieniowanie CuK_α

($\lambda = 1,54$ Å) było emitowane przy napięciu przyspieszającym równym 30 kV i natężeniu prądu anodowego równym 10 mA. Jako detektor użyto licznika scyntylacyjnego. Badania przeprowadzono w zakresie kąta 2θ od 5° do 60° w krokach co 0,03° przy czasie ekspozycji równym 0,25 s przypadającym na jeden krok.

- Małokątowa dyfraktometria rentgenowska (SAXS-*small-angle X-ray scattering*)

Małokątowe badania rozpraszania promieniowania rentgenowskiego przeprowadzono z użyciem kompaktowej kamery Kratky'ego, wyposażonej w system optyczny SWAXS (HECUS-MBRAUN). Źródłem promieniowania ($\lambda = 1,54$ Å) była lampa rentgenowska z anodą miedzianą pracująca przy parametrach: U = 30 kV, I = 20 mA. Dane SAXS zebrano jako funkcję wektora rozpraszania q = ($4\pi/\lambda$) $\sin\theta$, gdzie 2θ jest kątem rozpraszania. Do określenia współczynnika absorpcji próbki zastosowano metodę ruchomej szczeliny. Tło uchwytu próbki zostało odjęte od krzywych SAXS, a kolejne krzywe skorygowano biorąc pod uwagę zarówno grubość, jak i transmitancję próbki.

- Spektroskopia FTIR (*Fourier Transform Infrared Spectroscopy*)

Analizę spektroskopową w podczerwieni z transformacją Fouriera wykonano za pomocą spektrometru Nicolet 6700 FT-IR (Thermo Electron Corp., Madison, WI, USA) wyposażonego w przystawkę fotoakustyczną MTEC model 300. Zastosowano następujące parametry pomiarowe: rozdzielczość: 4 cm^{-1}, detektor fotoakustyczny; liczba skanów: 256. Dla każdej próbki zebrano widmo w zakresie od 4000 do 500 cm^{-1}. Obróbkę danych przeprowadzono przy użyciu oproGramowania OMNIC (v. 9.0, Thermo Electron Corp.).

Analizę ATR-FTIR (*Attenuated Total Reflection Fourier Transform Infrared*) wykonano za pomocą spektrometru Spectrum GX FTIR (PerkinElmer, Waltham, USA) z przystawką Golden Gate ATR z kryształem diamentu. Widma transmisyjne uzyskano w zakresie 4000-650 cm^{-1}, z wykonaniem 16 skanów i rozdzielczością 4 cm^{-1}. Wszystkie pomiary wykonano w temperaturze pokojowej.

- Analiza termograwimetryczna (TGA – *Thermogravimetric Analysis*)

Badania termograwimetryczne przeprowadzono za pomocą analizatora termograwimetrycznego TA Instruments Q500. Pomiary przeprowadzono w atmosferze

azotu (przepływ gazu na poziomie 60 ml/min), w zakresie temperatur od 30 do 500°C, przy szybkości ogrzewania 20°/min. Krzywe TG i DTG analizowano za pomocą oprogramowania Universal V2.6D TA Instruments.

- Pomiar kąta zwilżania

Pomiary kąta zwilżania wody przeprowadzono za pomocą urządzenia optycznego OCA 35 (DataPhysic Instruments GmbH, Filderstadt, Niemcy) wyposażonego w system pomiaru wideo z kamerą optyczną i wysokowydajnym adapterem stołowym. Objętość kropli wody wynosiła 3 µL. Wszystkie pomiary przeprowadzono w temperaturze pokojowej, w trzech powtórzeniach, z wyznaczeniem wartości średniej i odchylenia standardowego.

- Badania reologiczne

Badanie lepkości płynów przędzalniczych przeprowadzono na wiskozymetrze rotacyjnym Myr V2-L wyposażonym we wrzeciono L3 oraz termoparę (Especialidades Medicas Myr, SL, Tarragona, Spain). Parametry reologiczne, takie jak: energia aktywacji lepkości (E) oraz stała A, wyznaczono na podstawie równania Arrheniusa-Guzmana (wzór 1):

$$\eta = A \cdot exp(E/RT) \tag{1}$$

gdzie: η – lepkość dynamiczna [Pa·s]; A – stała charakterystyczna dla danej cieczy [-], E - energia aktywacji przepływu lepkiego [kJ/mol], R – stała gazowa [8,314 J/mol·K], T - temperatura [K].

- Pomiar rezystywność skrośnej

Pomiary rezystywności skrośnej (objętościowej) nanokompozytu na bazie celulozy bakteryjnej przeprowadzono zgodnie z normą ASTM D275 przy użyciu miernika Keithley'a model 6517A (Cleveland, OH, USA) oraz komory testowej Keithely, model 8009 (Cleveland, OH, USA). Próbki badanego materiału umieszczono w celi pomiarowej między układem elektrod. Pomiar przeprowadzono przy napięciu 50 V DC w czasie elektryfikacji 10 s. Dla każdej próbki wykonano 5 pomiarów, z których wyznaczono wartość średnią. Przeprowadzono również pomiar dla próbki odniesienia bez dodatku GO.

- Pomiar potencjału Zeta

Pomiary potencjału Zeta próbek płynnych wykonano przy użyciu analizatora Litesizer 500 (Anton Paar GmBH, Graz, Austria) wraz z kuwetą pomiarową typu Omega. Pomiary wykonano w termostatowanej komorze w temperaturze 25°C. Potencjał Zeta mierzono w zakresie pH od 2 do 12, wartość pH ustalano poprzez wprowadzanie odpowiedniej ilości NaOH (0,01 M) lub HCl (0,01 M).

Potencjał Zeta ciała stałego mierzono metodą potencjału strumieniowego z wykorzystaniem analizatora elektrokinetycznego SurPASS 3 (Anton Paar GmBH, Graz, Austria) zgodnie z prawem Helmholtza-Smoluchowskiego. Pomiary potencjału Zeta przeprowadzono w cylindrycznej celi dla pH z zakresu od 3 do 10. Do badanego roztworu dozowano odpowiednie ilości 0,1 M HCl, a następnie 0,1 M KOH. Dla każdej wartości pH przeprowadzono trzy cykle płukania i cztery pomiary potencjału Zeta. Podczas badań wyznaczono również punkt izoelektryczny (IEP) dla każdej z badanych próbek.

- Badania wytrzymałościowe

Dla badanych próbek włókien parametry wytrzymałościowe wyznaczono biorąc pod uwagę zalecenia normy ISO 5079. Pomiary przeprowadzono przy użyciu maszyny wytrzymałościowej INSTRON 5544 z głowicą ściskająco-rozciągającą o zakresie pomiarowym 0–10 N. Badania prowadzono przy jednakowej dla wszystkich próbek prędkości zrywania 10 mm/min. Dla określenia parametrów wytrzymałościowych: średniej siły zrywającej i względnego średniego wydłużenia zrywającego wykonano po 20 zrywów dla każdego wariantu, zakładając błąd przypadkowy równy 2% wartości średniej siły zrywającej. Odległość pomiarowa między szczękami wynosiła 20 mm. Badania wykonano w warunkach klimatu normalnego.

Moduł rozciągania, wytrzymałość na rozciąganie i elastyczność nanokompozytu na bazie BC określono za pomocą uniwersalnej elektromechanicznej maszyny testowej Shimadzu, AG-X plus 10 kN. Suche próbki o wymiarach 10 mm × 20 mm były montowane pionowo. Odległość pomiędzy szczękami mocującymi wynosiła 25 mm. Siła rozciągająca (10 kN) działała na próbki z prędkością rozciągania 1 mm/min. Wykonano 5 zrywów dla każdej próbki, po czym obliczono wartości średnie i odchylenia standardowe.

4. Znaczenie naukowe badań objętych pracą

Badania składające się na rozprawę doktorską są badaniami nowatorskimi, czego dowodem są publikacje w renomowanych czasopismach o zasięgu międzynarodowym. Ważnym dokonaniem opisanym w niniejszej rozprawie jest opracowanie metod aplikacji tlenku grafenu w materiałach kompozytowych na bazie celulozy tak, aby zwiększyć ich potencjalne zastosowania. Interdyscyplinarność jest domeną prowadzonych badań naukowych. Ważnym elementem tworzenia nowych materiałów jest poznawanie ich struktury cząsteczkowej oraz nadcząsteczkowej, właściwości fizykochemicznych oraz użytkowych, co stało się przedmiotem przedstawionej rozprawy doktorskiej.

Pierwszym celem pracy były badania nad otrzymywaniem, właściwościami i strukturą kompozytowych włókien na osnowie celulozy modyfikowanych tlenkiem grafenu. Badania te wpisują się w coraz to popularniejszy trend, polegający na powrocie do biopolimerów oraz ich modyfikacji poprzez wprowadzanie nanododatków. W przedstawionych publikacjach (I-III) szczegółowo omówiono metodykę otrzymywania włókien kompozytowych, w których istotną rolę odgrywał rodzaj koagulanta. W czasie procesu formowania włókien kompozytowych prowadzonego w wodzie, obserwowano zjawisko porządkowania łańcuchów polisacharydu, co bezpośrednio wpływało na ich budowę wewnętrzną. W toku badań fizykochemicznych, strukturalnych, wytrzymałościowych i mikrobiologicznych wykazano istotny wpływ dodatku GO na matrycę celulozową. Potwierdzono także możliwość powstawania wiązań wodorowych pomiędzy łańcuchami celulozy, a cząsteczkami GO, co przekłada się na wzrost wytrzymałości włókien oraz wzrost stopnia krystaliczności. Badania mikrobiologiczne wykazały również bakterio- i grzybobójcze właściwości opracowanych włókien. Wyniki badań dotyczące wpływu potencjału Zeta powierzchni włókien na właściwości mikrobiologiczne, w szczególności wartości punktu izoelektrycznego IEP, dostarczyły cennych i nowatorskich informacji. Wynika z nich ścisła korelacja pomiędzy właściwościami biobójczymi a wartością punktu izoelektrycznego zdeterminowanego przez chemiczny charakter powierzchniowych grup funkcyjnych włókien GO/CEL. W wyniku przeprowadzonych badań otrzymano włókna kompozytowe o nieopisanych dotąd właściwościach, które mogą stanowić świetny materiał do wyrobu specjalistycznej odzieży lub innych wyrobów włókienniczych, gdzie priorytetem jest aseptyka

(np. w szpitalnictwie). Ważną właściwością otrzymanych kompozytów jest „zakotwiczenie" GO wewnątrz włókna, zapewnia ich bezpieczeństwo toksykologiczne.

Opracowanie nowych włókien na osnowie celulozy z dodatkiem GO doprowadziły do prac nad syntezą celulozy bakteryjnej modyfikowanej GO *in situ*. Celuloza bakteryjna jest nanobiomateriałem, stosowanym w leczeniu dużych ran skóry (jak oparzenia, czy owrzodzenia). Poprzez nadanie temu materiałowi szczególnych właściwości, głównie bakteriobójczych dzięki dodatku GO, istnieje szansa na zastosowanie go jako opatrunek aktywny, zawierający substancje czynne. W pracy (IV) opracowano nieopisaną dotąd, prostą metodę otrzymywania celulozy bakteryjnej, w której do biosyntezy wykorzystano szczepy bakterii kwasu octowego pozyskane z jabłek odmiany Golden Delicious. Jednym z najważniejszych osiągnięć nad otrzymywaniem celulozy bakteryjnej, modyfikowanej GO było szczegółowe opracowanie warunków tej biosyntezy, które rozwiązało problem śmierci bakterii w obecności biobójczego GO. W pracach IV oraz V opisano wpływ pH roztworu na aglomerację nanocząstek GO, a także wpływ GO na wzrost wydajności syntezy celulozy bakteryjnej. Modyfikowana *in situ* celuloza bakteryjna zawierająca w swojej strukturze dodatek GO może być nośnikiem niesteroidowego leku przeciwzapalnego o wysokim współczynniku uwalniania. Ponadto w pracach badawczych wykazano pozytywny wpływ tego dodatku na parametry użytkowe takie jak wytrzymałość i chłonność wody.

5. Ramowe streszczenia artykułów składających się na rozprawę

Na niniejszą rozprawę doktorską składa się pięć monotematycznych artykułów naukowych (oznaczonych w pracy numerami **I-V**). Są nimi:

I. T. Gabryś, Cz. Ślusarczyk, Effect of graphene oxide additive on the structure of composite cellulose fibers, *Polimery*, tom 65, nr 9, s. 646-649 (2020)
IF = 1,471, punkty MEiN: 70

II. T. Gabryś, B. Fryczkowska, Cz. Ślusarczyk, D. Biniaś, J. Fabia, Preparation and properties of composite cellulose fibres with the addition of graphene oxide, *Carbohydrate polymers*, vol. 254, article number 117436, s. 1-11 (2021)
IF = 10,723, punkty MEiN: 140

III. T. M. Gabryś, B. Fryczkowska, A. Machnicka, T. Graczyk, Nanocomposite cellulose fibres doped with graphene oxide and their biocidal properties, *Polymers*, vol. 13, iss. 2, s. 1-18 (2021)
IF = 3,42, punktacja MEiN: 100

IV. T. Gabryś, B. Fryczkowska, J. Fabia, D. Biniaś, Preparation of an active dressing by in situ biosynthesis of a bacterial cellulose - graphene oxide composite*, Polymers*, vol. 14, iss. 14, s. 1-21 (2022)
IF = 4,967, punktacja MEiN:100

V. T. Gabryś, B. Fryczkowska, U. Jančič, J. Trček, S. Gorgieva, GO-enabled bacterial cellulose membranes by multistep, in situ loading : effect of bacterial strain and loading pattern on nanocomposite properties*, Materials*, vol. 16, iss. 3, s. 1-19 (2023)
IF = 3,748, punktacja MEiN: 140

W pracy I, Cz. Ślusarczyk wykonał pomiary SAXS, natomiast opracowanie wyników badań i wynikające z nich wnioski przygotował doktorant. W pozostałych pracach (II-V) koncepcję, wykonanie materiału badawczego i ostateczną redakcję wyżej wymienionych wieloautorskich prac przygotował doktorant. Szczegółowy udział doktoranta oraz pozostałych współautorów w każdej z publikacji został zamieszczony na końcu poszczególnych publikacji.

W tym miejscu zostały zamieszczone ramowe streszczenia prac, składających się na rozprawę doktorską.

Effect of graphene oxide additive on the structure of composite cellulose fibers [I]
(Wpływ dodatku tlenku grafenu na strukturę kompozytowych włókien celulozowych)

Przedmiotem badań tej pracy było wykazanie wpływu dodatku tlenku grafenu oraz warunków formowania na budowę strukturalną kompozytowych włókien celulozowych przy wykorzystaniu dyfraktometrii rentgenowskiej.

Analiza dyfraktogramów WAXS wskazała we wszystkich badanych próbkach obecność w strukturze nadcząsteczkowej celulozy typu II, co jest typowym zjawiskiem dla celulozy otrzymanej na drodze regeneracji z roztworu. Krzywe dyfrakcyjne (I – Fig. 1) wykazały obecność pików charakterystycznych wynoszących dla kąta 2θ kolejno: 12º, 20º i 21º. Wartości pików charakterystycznych są zbliżone do wyników uzyskanych przez zespół Mazlana, który jednak zamiast cieczy jonowej wykorzystał schłodzony układ NaOH/mocznik/woda do rozpuszczenia celulozy [47]. Istotnym faktem jest to, że struktura nadcząsteczkowa jest lepiej wykształcona we włóknach koagulowanych w wodzie, niż metanolu i może to być spowodowane różnicą w polarności koagulanta. Podobne wyniki uzyskali inni badacze, którzy poddali koagulacji w wodzie destylowanej i etanolu celulozę rozpuszczoną w cieczy jonowej [33,48,49]. Ich badania WAXS wskazują, że dobór koagulanta znacząco wpływa na strukturę nadcząsteczkową regenerowanej celulozy. Wyznaczony stopień krystaliczności (I – Fig. 2) charakteryzuje się trendem wzrostowym wraz z zawartością GO, który mieści się w zakresie 31% - 41% (dla próbek 0-1, A-1, B-1, C-1, D-1) oraz 23%–26% (dla próbek 0-2, A-2, B-2, C-2, D-2). Wzrost stopnia

krystaliczności wraz ze wzrostem zawartości GO we włóknach może być uwarunkowany powstawaniem dodatkowych wiązań wodorowych na drodze rekombinacji GO-CEL, które poprzez łączenie łańcuchów polimerowych mostkami wodorowymi tworzą wysoce uporządkowane obszary tzw. micele krystaliczne.

Analiza SAXS na podstawie różnic gęstości elektronowej w próbce pozwoliła na wyznaczenie takich parametrów jak porowatość Φ (%) oraz wielkość porów R (nm) (I – Table 2). Wynika z niej, że zarówno porowatość oraz wielkość porów dla wszystkich włókien koagulowanych w metanolu jest istotnie wyższa w porównaniu do włókien koagulowanych w wodzie. Próbki referencyjne (0-1 i 0-2) wykazują nieznacznie mniejszą porowatość w odniesieniu do włókien domieszkowanych tlenkiem grafenu. Zależność ta wynika z polarności koagulanta. Wraz ze spadkiem polarności koagulanta, proces zestalania i koagulacji trwa dłużej, co sprzyja tworzeniu się nanoporów [49]. Podobny efekt został osiągnięty i opisany w innej pracy, w której roztwór celulozy w cieczy jonowej EMIMAc był koagulowany w wybranych alkoholach pierwszorzędowych. Wraz ze wzrostem liczby atomów węgla w cząsteczce, a tym samym spadkiem polarności, wzrastała porowatość otrzymanych granul [50]. W tym przypadku moment dipolowy dla wody wynosi 1,85 (D) natomiast dla metanolu 1,7 (D). Obszerne badania w kierunku doboru polarności koagulanta przeprowadził From wraz z zespołem, w których dowiódł, że oprócz polarności istotna jest także jego mieszalność z wodą [51]. Badacze sugerują, że mieszalność koagulanta z wodą, tak samo jak polarność, kontroluje końcową krystaliczność folii celulozowych, co z kolei determinuje inne właściwości materiału. Dzieje się tak ze względu na różną kinetykę dyfuzji rozpuszczalnika i „nierozpuszczalnika" (koagulanta), która również kontroluje szybkość koagulacji i zestalania celulozy, a w tym przypadku włókien celulozowych zawierających dodatek tlenku grafenu.

***Preparation and properties of composite cellulose fibres with the addition of graphene oxide* [II]**

(Otrzymywanie i właściwości kompozytowych włókien celulozowych z dodatkiem tlenku grafenu)

Praca ta jest kontynuacją badań nad otrzymywaniem i właściwościami kompozytowych włókien GO/CEL. W pracy zawarto badania strukturalne, fizykochemiczne, mikroskopowe a także przeprowadzono analizę reologiczną płynów przędzalniczych.

W wyniku przeprowadzonych badań reologicznych wyznaczono takie parametry jak: energię aktywacji przepływu lepkiego (E), stałą charakterystyczną dla danej cieczy (A) oraz lepkość dynamiczną (η). Z przeprowadzonych badań wynika, że niewielki dodatek GO skutkuje zmniejszeniem tarcia wewnętrznego i gwałtownym spadkiem lepkości (II – Table 2). Efekt ten jest spowodowany silnymi właściwościami poślizgowymi GO. Literatura dość szeroko opisuje wykorzystanie właściwości smarnych GO do produkcji środków zmniejszających tarcie, co stanowi istotny aspekt w tribologii [52,53]. Warstwowa budowa GO zmniejsza tarcie międzypłaszczyznowe, powodując swobodne przemieszczanie się łańcuchów polimerowych CEL w ośrodku rozpuszczalnika. Wartość energii aktywacji przepływu lepkiego E jest potencjalną wartością graniczną, zależną od wielkości oddziaływań między molekularnych, którą musi pokonywać cząsteczka przemieszczając się względem sąsiednich cząsteczek. Cząsteczka może przejść do innego położenia równowagi jeśli uzyska odpowiednią energię. Tylko cząsteczki posiadające energię większą od tej wartości mogą się poruszać pomiędzy innymi cząsteczkami cieczy. W związku ze zmniejszonym tarciem międzycząsteczkowym, wywołanym obecnością GO w płynie przędzalniczym zaobserwowano, że wartość energii aktywacji przepływu lepkiego E obniża się wraz ze wzrostem stężenia tego dodatku.

Analiza mikroskopowa przekrojów włókien wskazuje na wysoki stopień zdyspergowania GO wewnątrz wszystkich włókien oraz jego równomierne rozmieszczenie, nie zaobserwowano zjawiska migracji nanododatku (II – Fig. 2). Mikrofotografie SEM pozwoliły na obserwację powierzchni włókien, która różni się w zależności od rodzaju koagulanta (II – Fig. 3). Podczas koagulacji w wodzie powstają podłużne i liczne wgłębienia wzdłuż włókien, które są zdecydowanie płytsze mniej

zauważalne w przypadku koagulacji w metanolu. Ponadto ilość, jak i wielkość powierzchniowych wgłębień we włóknach GO/CEL jest skorelowana z zawartością GO. Zwiększa się ona w kierunku: 0, A, B, C, D; a więc wraz z zawartością GO we włóknie. Mikroskopia SEM pozwoliła również na wyjaśnienie różnic w wartościach kąta zwilżania. Hydrofilowy charakter funkcyjnych grup tlenowych występujących na powierzchni GO wpłynął na obniżenie wartości kąta zwilżania wraz ze wzrostem jego stężenia we włóknach. Ponadto, bardziej rozbudowana powierzchnia włókien zawierających tlenek grafenu w porównaniu do gładkich włókien prób referencyjnych (0-1, 0-2), sprzyja fizycznemu wiązaniu wody wnikającej w pory włókien.

Spektroskopia w podczerwieni (FTIR) wykazała występowanie charakterystycznych pasm drgań rozciągających O-H, między 3700–2400 cm^{-1} oraz około 1640 cm^{-1} odpowiedzialnych za powstawanie wiązań wodorowych. Ponadto obserwuje się poszerzenie tego pasma, wraz z ilością wprowadzanego GO do włókien. Prawdopodobnie dodatek GO powoduje rozluźnienie struktury pomiędzy łańcuchami makrocząsteczek celulozy poprzez wprowadzenie dodatkowych grup hydroksylowych. Dla włókien kompozytowych GO/CEL obserwuje się wzrost intensywności pasm przy liczbie falowej około 1740 cm^{-1} oraz około 1640 cm^{-1}, odpowiadającym za drgania grup C=O w GO. Równocześnie nie obserwuje się pasma 1404 cm^{-1} charakterystycznego dla zastosowanej cieczy jonowej, co potwierdza całkowite usunięcie EMIMAc z włókien w procesie przędzenia (II – Fig. 4).

Analizując przebieg krzywych TG dla próbek włókien można zauważyć, że proces uwalniania wody przebiega do ok. 200°C i przechodzi bezpośrednio w proces rozkładu termicznego (II – Fig. 6). Ponadto, temperatura początku rozkładu termicznego jest najniższa w przypadku włókien bez dodatku modyfikatora, natomiast dodatek GO powoduje wyraźne podwyższenie tej temperatury (temperatury ekstrapolowanego początku przemiany) w przypadku wszystkich włókien modyfikowanych. Największe przesunięcie (o 16,8°C) obserwowane jest w przypadku włókien B-1. W przypadku włókien, które były koagulowane w metanolu zarejestrowano najniższą temperaturę początku rozkładu dla niemodyfikowanego włókna celulozowego 0-2. Dodanie GO we wszystkich włóknach zwiększa temperaturę rozkładu. Można wywnioskować, że dodanie GO zwiększyło stabilność termiczną kompozytowych włókien. Zjawisko to może być spowodowane grupami epoksydowymi, hydroksylowymi i karbonylowymi, obecnymi na powierzchni GO, które oddziałując z celulozą bogatą w grupy hydroksylowe, tworzą

nowe wiązania wodorowe [47,54]. Innym możliwym powodem poprawy stabilności termicznej celulozy może być warstwowa struktura GO, która ma tendencję do oferowania jedynie pośrednich dróg dla lotnych produktów degradacji, opóźniając degradację całego kompozytu [55]. Proces rozkładu termicznego badanych włókien, we wszystkich przypadkach (niezależnie od zastosowanego koagulanta) kończy się w temperaturze nieco ponad 390°C. Końcowy etap rozkładu dla wszystkich próbek przebiega niemal identycznie z maksimum szybkości w temperaturze około 436°C. Oznaczenie pozostałości po wygrzaniu próbek do 650°C w atmosferze azotu, potwierdza zwiększoną zawartość skondensowanych struktur węglowych w przypadku włókien GO/CEL. Zawartość ta zmienia się monotonicznie od 16,5% do 19,1% dla włókien koagulowanych w wodzie oraz odpowiednio od 13,4% do 16,6% dla włókien zestalanych w metanolu.

Nanocomposite cellulose fibres doped with graphene oxide and their biocidal properties [III]
(Nanokompozytowe włókna celulozowe domieszkowane tlenkiem grafenu i ich właściwości biobójcze)

Praca ta opisuje wpływ tlenku grafenu na właściwości użytkowe i biobójcze włókien celulozowych domieszkowanych tym nanododatkiem. W pracy, oprócz oceny parametrów wytrzymałościowych przed i po procesie prania, zawarto wyniki badań mikrobiologicznych oceniających właściwości bakterio- i grzybobójcze modyfikowanych włókien. Najistotniejszym aspektem niniejszej pracy jest skorelowanie właściwości biobójczych włókien z wartością punktu izoelektrycznego (IEP) wyznaczonego na podstawie pomiaru strumieniowego potencjału Zeta.

Szczegółowej analizie metrologicznej zostały poddane włókna GO/CEL, zarówno przed, jak i po procesie prania. W skład analizy weszły pomiary grubości włókien oraz wyznaczenie parametrów wytrzymałościowych (III – Table 3,4). Zaobserwowano szereg zmian fizykochemicznych, które zaszły podczas procesu prania. Wykazano, że po procesie prania grubość wszystkich włókien zmniejszyła się średnio od 7% do 15% w porównaniu do grubości włókien niepranych. Może to być efekt wymycia resztek cieczy jonowej z wnętrza włókien. Badania wytrzymałościowe dostarczyły cennych informacji

na temat wpływu GO na właściwości mechaniczne. Wynika z nich jasno, że dla wszystkich włókien, niezależnie od rodzaju koagulanta, dodatek GO w ilości 0,5% wpłynął istotnie na wzrost wytrzymałości na zerwanie. Wartością graniczną, po której następował stopniowy spadek wytrzymałości jest 0,5% stężenia GO we włóknie. Zastosowanie wyższych stężeń tj. 0,98% i 1,97% skutkuje zmniejszeniem wytrzymałości, co może być spowodowane stopniową agregacją nanododatku, przez co powstają we włóknie obszary niehomogeniczne, które osłabiają ciągłość włókna. Do podobnego wniosku doszedł Wang, który pisze w swojej pracy, że wzrost zawartości GO w cienkich filmach celulozowych powyżej 1% skutkuje osłabieniem parametrów wytrzymałościowych [56]. Analogiczne wyniki uzyskali Mazlan oraz Gan, którzy otrzymywali włókna celulozowe w podobny sposób. Stwierdzili, że zwiększenie zawartości GO do określonego poziomu powoduje spadek siły zrywającej włókna [47,54]. To pokazuje, że efekt wzrostu wytrzymałości jest ściśle powiązany z homogenicznością w osnowie polimeru i zaburzeniem interkalacji między celulozą a GO podczas procesu regeneracji. Sam proces prania włókien najmocniej wpłynął na ich wytrzymałość, która we wszystkich przypadkach wzrosła o około 80%. Bez wątpienia nastąpiła tutaj przebudowa struktury wewnętrznej zwana rekrystalizacją. Kolejnym parametrem mechanicznym, który uległ istotnej zmianie podczas procesu prania jest moduł sprężystości, którego wartości zmniejszyły się kilkukrotnie. Jest to najprawdopodobniej związane z wypłukaniem pozostałości cieczy jonowej z włókien, co potwierdzają także pomiary grubości.

Badania mikrobiologiczne prowadzono z wykorzystaniem bakterii Gram-dodatnich, Gram-ujemnych oraz grzybów. Próbki włókien w formie włókien ciągłych oraz ciętych umieszczono na podłożach selektywnych z mikroorganizmami, a właściwości biobójcze określano poprzez pomiar wielkości stref zatrzymania wokół próbek. Wraz ze wzrostem stężenia GO we wszystkich włóknach obserwowano powiększanie się stref zatrzymania, przy czym nie wykazano istotnych różnic między próbkami koagulowanymi w wodzie i metanolu. Natomiast próbki włókien ciętych posiadały 2–3 krotnie większe strefy zatrzymania niż ich odpowiedniki w formie włókien ciągłych (III – Fig. 7). Tlenek grafenu posiadający właściwości bakterio- i grzybobójcze jest równomiernie rozmieszczony wewnątrz włókna. Nie zaobserwowano zjawiska migracji nanododatku do warstwy naskórkowej włókna. Dlatego cięte włókna, z odsłoniętym przekrojem silniej oddziałują na otaczające

je drobnoustroje, czego skutkiem są większe strefy zatrzymania (III – Fig. 8). Właściwości biobójcze GO są dobrze znane badaczom. Przyjmuje się, że GO działa jak nano-ostrze (inhibitor komórek bakteryjnych), gdy jest w bezpośrednim kontakcie z bakteriami, uszkadzając błonę komórkową i prowadząc do wycieku składników wewnątrzkomórkowych i śmierci komórki [57]. Mechanizm niszczenia drobnoustrojów poprzez mechaniczne uszkadzanie ścian komórkowych nie jest jedynym z możliwych sposobów, w jaki kompozytowe włókna GO/CEL ukazują swoje właściwości antybakteryjne. Może wystąpić bowiem kilka innych mechanizmów, w tym wystąpienie stresu oksydacyjnego, uszkodzenie błony komórkowej oraz zahamowanie metabolizmu [44,58]. Większa strefa zahamowania wokół *Escherichia coli* w porównaniu z *Staphylococcus aureus* może być związana z grubszą warstwą peptydoglikanu w bakteriach Gram-dodatnich (*S. aureus*), która chroni komórkę bakteryjną przed pełnym kontaktem z GO.

Zależność stopnia właściwości biobójczych od potencjału Zeta wyznaczono w oparciu o punkt izoelektryczny (IEP) włókien. Czyste włókna CEL w porównaniu do włókien kompozytowych wykazują bardziej ujemną wartość potencjału Zeta, co wynika z występowania w celulozie grup hydroksylowych. Dodatek GO (który również posiada liczne ugrupowania tlenowe) do osnowy celulozowej, powoduje powstawanie wiązań wodorowych pomiędzy celulozą, a tlenkiem grafenu. W efekcie czego, wraz ze wzrostem stężenia GO we włóknach, spada kwasowy charakter włókien GO/CEL, wyrażający się zmianą kształtu krzywej $\zeta = f(pH)$ (III – Fig. 9). Wiąże się to z przesunięciem IEP ku wyższym wartościom pH. Właściwości bakteriobójcze włókien GO/CEL w głównej mierze wynikają ze wzrostu wartości IEP [59,60]. Dla wszystkich włókien wartości IEP wzrastają wraz ze wzrostem stężenia GO we włóknach. Wyniki przeprowadzonych badań wskazują na ścisłą korelację pomiędzy wartością IEP, a właściwościami bakteriobójczymi, zarówno w przypadku bakterii Gram-ujemnych (*E. coli*), jak i Gram-dodatnich (*S. aureus*) (III – Fig. 10). Efekt ten jest również spowodowany powstaniem oddziaływań elektrostatycznych pomiędzy powierzchnią włókien GO/CEL, a ścianą komórkową bakterii, co uniemożliwia pobieranie substancji odżywczych i powoduje śmierć komórki. Zależność tą ciekawie opisał w swojej pracy nad nanowłóknami z polianiliny Mirmohseni [61]. Oddziaływania te są wynikiem różnic potencjału między powierzchnią włókien, a ujemną powierzchnią komórek bakterii [62]. Dlatego dzięki powstaniu wiązań wodorowych na drodze celuloza-tlenek grafenu oraz

przyciąganiu elektrostatycznemu pomiędzy powierzchnią kompozytowych włókien, a komórkami bakterii, włókna wykazują właściwości biobójcze [61].

***Preparation of an active dressing by in situ biosynthesis of a bacterial cellulose - graphene oxide composite* [IV]**

(Otrzymywanie opatrunku aktywnego metodą biosyntezy in situ celulozy bakteryjnej z tlenekiem grafenu)

W pracy zaprezentowano prostą metodę otrzymywania celulozy bakteryjnej modyfikowanej tlenkiem grafenu metodą *in situ* oraz wykazano wpływ nanocząstek na strukturę i właściwości otrzymanych kompozytowych membran. Cechą wyróżniającą niniejszą pracę jest to, że do otrzymania BC wykorzystano mikroorganizmy pozyskane na drodze naturalnej fermentacji octowej towarzyszącej produkcji octu, a modyfikacja tlenkiem grafenu przebiegała *in situ* tj. w trakcie procesu biosyntezy. Otrzymane membrany przebadano pod kątem zastosowania jako opatrunki aktywne zawierające niesteroidowy lek przeciwzapalny. Membrany zawierały tlenek grafenu w ilości kolejno: 0%, 3,7%, 5,4% oraz 7,1% (oznaczenie w pracy jako BC/0; BC/GO/I; BC/GO/II; BC/GO/III).

Badanie właściwości fizykochemicznych membran uzupełniono o badania mikroskopowe z zastosowaniem elektronowej mikroskopii skaningowej. Na fotografiach zamieszczonych w pracy wyraźnie widać, że membrany są zbudowane z nanowłókien celulozowych o przypadkowym ułożeniu, jak w klasycznej włókninie. Analiza SEM wykazała, że tlenek grafenu nie występuje bezpośrednio na powierzchni membran kompozytowych, lecz znajduje się pomiędzy poszczególnymi warstwami nanowłókien BC, co utrudnia jego obserwację (IV – Fig. 6). Jest to odmienne zjawisko w porównaniu do badań Luo i wsp. którzy na mikrofotografiach SEM stwierdzają obecność GO również na powierzchni membran [63].

Badanie kinetyki uwalniania substancji czynnej z membran wykonywano w roztworze soli fizjologicznej buforowanej fosforanem (PBS) o temperaturze 37°C. Roztwór taki naśladuje stężenie jonów, osmolarność i pH płynów ustrojowych ludzkiego ciała [64]. Do badań sorpcji substancji czynnej wytypowano Paracetamol, który jest powszechnie stosowany jako skuteczny lek przeciwbólowy i przeciwzapalny. Membrany przebadano w stanie wilgotnym, gdyż w takiej postaci mają zastosowanie jako opatrunki

aktywne. Analizując właściwości sorpcyjne otrzymanych membran względem Paracetamolu można stwierdzić, że lek jest dobrze sorbowany na otrzymanych membranach. Całkowita ilość zaadsorbowanego leku po 24 godzinach wynosi 63,3 mg/1g BC (dla membrany BC/0) i nieznacznie maleje wraz ze wzrostem zawartości GO w membranach kompozytowych do wartości 62,4 mg/1g BC (dla membrany BC/GO/III). Natomiast badania desorpcji po 24 godzinach wykazały, że membrany kompozytowe desorbują więcej Paracetamolu, aniżeli próbka referencyjna BC/0 (34,9 mg/1g BC) w kolejności odpowiednio BC/GO/I (35,3 mg/1g BC), BC/GO/II (41,7 mg/1g BC) oraz BC/GO/III (42,0 mg/1g BC) (IV – Fig. 5a). Wynika to z faktu, że w próbce z czystej celulozy bakteryjnej reaktywne ugrupowania hydroksylowe są w stanie wejść w reakcję z jednym z podstawników aktywujących w cząsteczce Paracetamolu, tym samym go wiążąc, podczas, gdy w membranie kompozytowej większość grup -OH w łańcuchu celulozy wytworzyła na wcześniejszym etapie mostki wodorowe z ugrupowaniami tlenowymi GO, stając się niezdolnymi do reakcji z grupą hydroksylową, czy aminową w Paracetamolu [65,66].

Interesujące wyniki przedstawiają badania kinetyki uwalniania leku z badanych membran (IV - Fig. 5b). Wynika z nich, że dla dróbki BC/0 współczynnik uwalniania po 80 minutach wynosi niecałe 50%. Natomiast membrana o najniższej zawartości GO (3,7% w/w) już po 25 minutach cechuje się bardziej intensywną desorpcją leku (współczynnik uwalniania ~55%). Krzywe uwalniania substancji czynnej z membran kompozytowych BC/GO/III oraz BC/GO/II mają zbliżone charakterystyki, a ich współczynniki uwalniania po 80 minutach są wysokie i wynoszą około 67%. Podobne badania przeprowadzone przez Urbina wykazały ponad dwukrotnie niższe wartości współczynnika uwalniania. Bowiem po 80 minutach wynosił on zaledwie 30% [67]. Rozbieżności mogą wynikać z kilku powodów. Po pierwsze, badacze ci otrzymali sferyczne granulki poprzez intensywne mieszanie inoculum podczas inkubacji oraz dodali tlenek grafenu bezpośrednio do płynnej pożywki. Po drugie, jako lek wytypowali Ibuprofen, który mógł w inny sposób wejść w reakcję z badanym nośnikiem leku.

Na podstawie krzywych dyfrakcyjnych WAXS wyznaczono parametry strukturalne otrzymanych membran. Krzywe wykazują charakterystyczne piki dla celulozy typu I, których położenia kątowe 2θ przypadają na 14,5º, 16,7º oraz 22,7º. Oznacza to, że dodatek GO nie wpłynął na zmianę struktury BC, gdyż nie obserwuje się

istotnych przesunięć (IV – Fig. 9). Z przeprowadzonych badań wynika, że stopień krystaliczności czystej celulozy bakteryjnej (BC/0) jest wysoki i wynosi 66%. Ponadto obserwuje się spadek stopnia krystaliczności wraz ze wzrostem zawartości GO w matrycy celulozowej. Zjawisko to wynika z faktu, że dodatki, a zwłaszcza nanododatki, zaburzają proces tworzenia nanofibryli, tak że obszary krystaliczne o wysokim uporządkowaniu stanowią mniejszość w ogólnej strukturze materiału, co bezpośrednio przejawia się niższym stopniem krystaliczności [24].

Analiza porównawcza widm FTIR wskazuje, że próbki BC z dodatkiem GO zachowały wszystkie charakterystyczne cechy pasm celulozy bakteryjnej, co potwierdza zachowanie tej samej struktury chemicznej.

Na podstawie wyników badań termograwimetrycznych można stwierdzić, że proces rozkładu termicznego przebiega jednoetapowo i w dość szerokim zakresie temperatur: od około 250 do 400°C. Temperatura ekstrapolowanego początku procesu degradacji osnowy, wyznaczona na podstawie krzywych DTG, jest najniższa dla membrany BC/0 (298,6°C), a najwyższa dla membrany BC/GO/III (317,4°C). Ponadto stwierdza się, że maksymalna temperatura rozkładu termicznego wzrasta monotonicznie wraz ze wzrostem zawartości modyfikatora (IV – Fig. 11). Zależność ta jest często obserwowana w badaniach innych naukowców i podobnie jak w przypadku włókien celulozowych modyfikowanych tlenkiem grafenu, poprawa stabilności termicznej może być skutkiem warstwowej struktury GO, która sprzyja powstaniu jedynie pośrednich dróg dla lotnych produktów degradacji, opóźniając degradację całego kompozytu [55].

GO-enabled bacterial cellulose membranes by multistep, in situ loading: effect of bacterial strain and loading pattern on nanocomposite properties [V]
(Membrany z celulozy bakteryjnej modyfikowane GO wieloetapową metodą in situ: wpływ szczepu bakteryjnego i ilości dodatku na właściwości nanokompozytu)

W pracy tej przedstawiono wyniki kolejnych badań nad otrzymywaniem i właściwościami kompozytu z celulozy bakteryjnej modyfikowanej tlenkiem grafenu metodą *in situ*. Do biosyntezy wykorzystano dwa wyselekcjonowane szczepy bakteryjne: *Komagataeibacter intermedius* i *Komagataeibacter sucrofermentans*. Opracowano prostą metodę biosyntezy, w której do pożywki RAE dodawano dyspersję wodną GO w

stężeniach: 10 ppm, 25 ppm i 50 ppm, w odstępach 24 h i 48 h. W rezultacie otrzymano kompozytową membranę GO/BC o warstwowej budowie. Ponadto dodatek GO wpłynął na zwiększenie wydajności syntezy. Poprawa kluczowych właściwości (wytrzymałość, przewodnictwo elektryczne) wskazuje na możliwość zastosowania membrany GO/BC w ogniwach paliwowych (MEA).

W pierwszym etapie prac badawczych skupiono się na opracowaniu optymalnej metody wprowadzenia dyspersji GO do tworzącej się na powierzchni pożywki celulozy bakteryjnej. W tym celu wytypowano trzy stężenia dyspersji GO oraz dwa odstępy czasowe, po których ponawiano immersję powstającego filmu celulozowego. Pomimo stabilności dyspersji GO w wodzie przy pH równym 4,1; które odpowiada zastosowanej pożywce, (potencjał Zeta dla wodnej dyspersji GO przy pH = 4,1 wynosi -27 mV) w chwili kontaktu tlenku z pożywką ulega on natychmiastowej agregacji. Powodem agregacji jest znaczna zawartość jonów w złożonym (wieloskładnikowym) ośrodku RAE, powodująca rozległe ekranowanie ładunku. Z tego względu, rozproszona warstwa dielektryczna wokół powierzchni cząstek GO jest cieńsza, co sprawia, że siły van der Waalsa dominują w oddziaływaniu międzycząsteczkowym prowadząc do agregacji i sedymentacji [68]. W związku z tym zastosowano wodną dyspersję GO jako środek immersyjny.

Przeprowadzona analiza statystyczna wybranych właściwości fizykochemicznych otrzymanych membran (wydajność produkcyjna, grubość, kąt zwilżania) wykazała występowanie istotnych statystycznie różnic pomiędzy celulozą produkowana przez dwa wspomniane szczepy bakteryjne (V – Fig. 7, Table 2). *K. sucrofermentas* produkuje więcej, lecz cieńsze i bardziej zwarte strukturalne membrany, co utrudnia wnikanie wody pomiędzy gęstą sieć nanowłókien, stąd tak znaczna różnica w wartościach kąta zwilżania. Ponadto wykazano, że niezależnie od zastosowanych interwałów czasowych, dodatek GO do szczepu *K. intermedius* wpływa na zwiększenie średniej produkcji celulozy.

Analiza wyników rezystywności objętościowej pokazuje różnice w zależności od ilości wprowadzonego nanododatku (V – Table 5). Wyniki wskazują na spadek rezystywności wraz ze wzrostem zawartości GO w materiale, jednak zmiana ta jest niewielka i obejmuje maksymalnie do dwóch rzędów wielkości. Wynika to z hybrydyzacji sp^3 atomów węgla obecnych w tlenku grafenu.

Właściwości mechaniczne wykazują znaczne różnice między próbkami z czystej celulozy bakteryjnej, a próbkami zawierającymi GO. Wyniki analizy statystycznej porównującej próbki iBC i sBC pod względem parametrów mechanicznych (wytrzymałość na rozciąganie, moduł sprężystości i wydłużenie) wykazały na poziomie istotności 5%, że dla pierwszego kryterium różnica między wartościami średnimi nie jest istotna, podczas gdy pod względem dwóch pozostałych parametrów próbki te różnią się znacząco, co oznacza, że rodzaj szczepu bakteryjnego wpływa na te parametry. Dla próbek zawierających najmniejszy dodatek GO (iBC_10/3 i sBC_10/2) wytrzymałość na rozciąganie wzrosła ponad trzykrotnie, co świadczy o pozytywnym wpływie GO (V – Table 4). Luo oraz Iguchi tłumaczą poprawę parametrów wytrzymałościowych w następujący sposób. Po pierwsze, zjawisko to związane jest z pojawieniem się oddziaływań krótkiego zasięgu pomiędzy GO, a osnową celulozową, takich jak wiązania wodorowe. Po drugie, naprzemienny sposób przenikania kolejnych warstw podczas syntezy poprawia dyspersję nanocząstek GO w osnowie celulozy bakteryjnej. Wreszcie, zjawisko interkalacji ułatwia mechaniczne łączenie nanocząstek płatkowego tlenku o strukturze 2D przez nanowłókna celulozowe, którym można przypisać budowę 1D, co skutkuje powstaniem struktury przypominającej unerwiony liść (*z ang. leaf vein*). Silne wiązania wodorowe, zwarta struktura, oraz homogeniczność są odpowiedzialne za poprawę właściwości mechanicznych [63,69].

6. Podsumowanie wyników badań i wnioski końcowe

W trakcie realizacji niniejszej rozprawy doktorskiej przeprowadzono szereg nowatorskich badań, wyniki których zostały opublikowane w renomowanych czasopismach naukowych, tworząc cykl pięciu monotematycznych artykułów (I – V), stanowiący trzon prezentowanej rozprawy. Wpisują się one w nurt najnowszych badań, których celem jest otrzymanie materiałów kompozytowych na osnowie szeroko pojętych biopolimerów z nanododatkami węglowymi.

Należy stwierdzić, że pierwszy z celów rozprawy, sformułowany w pkt. 2 (str. 14) został osiągnięty, przy czym należy podkreślić, że jego realizacja wymagała od Autora rozprawy zaprojektowania i wykonania linii do laboratoryjnego formowania włókien na mokro. Ponadto zebrane w trakcie realizacji tego celu spostrzeżenia prowadzą do następujących wniosków:

- Nawet niewielki dodatek dyspersji tlenku grafenu w DMF, wprowadzony do roztworu celulozy w EMIMAc, powoduje gwałtowny spadek lepkości roztworu przędzalniczego.
- Dobrym koagulantem dla powstającego kompozytu GO/CEL jest woda, ponieważ cechuje się dobrą mieszalnością z EMIMAc, co ma bezpośredni wpływ na krystaliczność celulozy i na pozostałe właściwości fizykochemiczne i mechaniczne.
- Otrzymane włókna kompozytowe na osnowie celulozy z dodatkiem tlenku grafenu wykazują właściwości biobójcze.
- Wartość punktu izoelektrycznego jest ściśle powiązana z właściwościami mikrobiologicznymi badanych włókien.

Drugi z celów pracy, sformułowany w pkt 2 (str. 14) został także w pełni osiągnięty, co wymagało:

- Wykazania możliwości prowadzenia syntezy celulozy bakteryjnej w obecności biobójczego GO.
- Opracowania nieopisanej dotąd biosyntezy nanokompozytu z celulozy bakteryjnej modyfikowanej in situ z pomocą GO, którą można prowadzić w obecności naturalnych szczepów bakterii, pochodzących np. z jabłek.

- Szczegółowego opracowania warunków prowadzenia syntezy bionanokompozytu, w obecności wyselekcjonowanych szczepów bakteryjnych.

Ponadto w trakcie realizacji tego celu:

- Dowiedziono wpływ obecności nanocząstek GO na wzrost wydajność syntezy celulozy bakteryjnej.

- Wykazano wpływ dodatku GO w nanowłókninie z celulozy bakteryjnej na wzrost właściwości wytrzymałościowych.

Realizacja drugiego celu prezentowanej rozprawy zaowocowała opracowaniem nanowłókniny kompozytowej o potencjalnie dużych możliwościach aplikacyjnych, jako opatrunek aktywny zaopatrzony w substancję leczniczą.

7. Bibliografia

1. Wertz Jean-Luc; Bedue Olivier; Mercier Jean P. Structure and Properties od Cellulose. In *Cellulose Science and Technology*; Girault Hubert, Ed.; Lausanne; pp. 87–140 ISBN 978-2-940222-41-4.

2. Dumitriu, S. *Polysaccharides : structural diversity and functional versatility*; Marcel Dekker, 2005; ISBN 0824754808.

3. Wertz Jean-Luc; Bedue Olivier; Mercier Jean P. Biosynthesis of cellulose. In *Cellulose Science and Technology*; Girault Hubert, Ed.; Lausanne, 2010; pp. 46–80 ISBN 978-2-940222-41-4.

4. Wenhua, Z.X.; Liheng, G.; Wu, C.; Runge, L.J.Y.Z.T. A comparison of cellulose nanofibrils produced from Cladophora glomerata algae and bleached eucalyptus pulp. *Cellulose* **2016**, *23*, 493–503.

5. Budowa cząsteczki celulozy Available online: https://www.wikiwand.com/pl/Celuloza (accessed on Jul 10, 2022).

6. Mohd, N.; Draman, S.F.S.; Salleh, M.S.N.; Yusof, N.B. Dissolution of cellulose in ionic liquid: A review. In Proceedings of the AIP Conference Proceedings; American Institute of Physics Inc., 2017; Vol. 1809, p. 020035.

7. Zugenmaier, P. *Crystalline Cellulose and Cellulose Derivatives: Characterization and Structures. Springer Series in Wood Science*; 2008; ISBN 9783540261230.

8. Jin, H.; Zha, C.; Gu, L. Direct dissolution of cellulose in NaOH/thiourea/urea aqueous solution. *Carbohydr. Res.* **2007**, *342*, 851–858.

9. Cao, Y.; Zhang, R.; Cheng, T.; Guo, J.; Xian, M.; Liu, H. Imidazolium-based ionic liquids for cellulose pretreatment: recent progresses and future perspectives. *Appl. Microbiol. Biotechnol.* **2017**, *101*, 521–532.

10. Mohan, T.; Hribernik, S.; Kargl, R.; Karin, K. *Cellulose - Fundamental Aspects and Current Trends*; Poletto, M., Heitor, O., Eds.; InTech, 2015; ISBN 978-953-51-2229-6.

11. Pinkert, A.; Marsh, K.N.; Pang, S.; Staiger, M.P. Ionic liquids and their interaction with cellulose. *Chem. Rev.* **2009**, *109*, 6712–6728.

12. Fukaya, Y.; Hayashi, K.; Kim, S.S.; Ohno, H. Design of polar ionic liquids to solubilize cellulose without heating. In Proceedings of the ACS Symposium

Series; 2010; Vol. 1033, pp. 55–66.

13. Wendler, F.; Todi, L.N.; Meister, F. Thermostability of imidazolium ionic liquids as direct solvents for cellulose. *Thermochim. Acta* **2012**, *528*, 76–84.

14. Wang, S.; Lu, A.; Zhang, L. Recent advances in regenerated cellulose materials. *Prog. Polym. Sci.* 2016, *53*, 169–206.

15. Swatloski, R.P.; Spear, S.K.; Holbrey, J.D.; Rogers, R.D. Dissolution of cellulose with ionic liquids. *J. Am. Chem. Soc.* **2002**, *124*, 4974–4975.

16. Fryczkowska, B.; Kowalska, M.; Biniaś, D.; Ślusarczyk, C.; Janicki, J.; Sarna, E.; Wyszomirski, M. Properties and Structure of Cellulosic Membranes Obtained from Solutions in Ionic Liquids Coagulated in Primary Alcohols. *Autex Res. J.* **2018**, *18*, 232–242.

17. Merck 1-Ethyl-3-methylimidazolium acetate Available online: https://www.sigmaaldrich.com/PL/pl/product/aldrich/689483.

18. Torres, F.G.; Troncoso, O.P.; Lopez, D.; Grande, C.; Gomez, C.M. Reversible stress softening and stress recovery of cellulose networks. *Soft Matter* **2009**, *5*, 4185–4190.

19. Thompson, M.A.; Onyeziri, M.C.; Fuqua, C. Function and Regulation of Agrobacterium Tumefaciens Cell Surface Structures That Promote Attachment. In *Agrobacterium Biology. Current Topics in Microbiology and Immunology*; Gelvin, S., Ed.; Springer:Cham, Switzerland, 2018; Vol. 418, pp. 143–184 ISBN 9783030032562.

20. Stumpf, T.R.; Yang, X.; Zhang, J.; Cao, X. In situ and ex situ modifications of bacterial cellulose for applications in tissue engineering. *Mater. Sci. Eng. C* **2018**, *82*, 372–383.

21. Tanskul, S.; Amornthatree, K.; Jaturonlak, N. A new cellulose-producing bacterium, Rhodococcus sp. MI 2: Screening and optimization of culture conditions. *Carbohydr. Polym.* **2013**, *92*, 421–428.

22. Kubiak, K.; Kalinowska, H.; Peplinska, M.; Bielecki, S. Celuloza bakteryjna jako nanobiomaterial. *Postępy Biol. Komórki. Supl.* **2009**, *25*, 85–98.

23. Budowa GO Available online: http://www.nanomaterials.pl/graphene?lang=PL (accessed on Jul 10, 2022).

24. Troncoso, O.P.; Torres, F.G. Bacterial cellulose—graphene based nanocomposites. *Int. J. Mol. Sci.* **2020**, *21*, 1–17.

25. Czaja, W.; Krystynowicz, A.; Bielecki, S.; Brown, R.M. Microbial cellulose - The natural power to heal wounds. *Biomaterials* **2006**, *27*, 145–151.

26. Singhsa, P.; Narain, R.; Manuspiya, H. Physical structure variations of bacterial cellulose produced by different Komagataeibacter xylinus strains and carbon sources in static and agitated conditions. *Cellulose* **2018**, *25*, 1571–1581.

27. Rosa, H.; Strzelczyk, A.; Jabłońska, E.; Kozielec, T.; Karbowska-Berent, J. Badania nad zastosowaniem celulozy bakteryjnej w konserwacji i restauracji dzieł sztuki. *Acta Univ. Nicolai Copernici Zabytkozn. i Konserw.* **2012**, *410*, 287.

28. Przygocki, W.; Włochowicz, A. *Fulereny i nanorurki*; Wydawnictwa naukowo-techniczne, 2001; ISBN 83-204-2645-6.

29. Kurzydłowski, K.; Lewandowska Magdalena *Nanomateriały inżynierskie, konstrukcyjne i funkcjonalne*; Wydwnictow Naukowe PWN: Warszawa, 2011; ISBN 978-83-01-16418-8.

30. Andrzej, H.; Agnieszka, D.; Kurcz, M. *Grafen. Otrzymywanie, charakterystyka, zastosowania.*; 1st ed.; Wudawnictwa Uniwersytetu Warszawskiego: Warszawa, 2016; ISBN 978-83-235-2314-7.

31. Jelińska, Z. Grafen - świat w dwóch wymiarach Available online: http://laborant.pl/index.php/grafen-swiat-w-dwoch-wymiarach.

32. Hummers, W.S.; Offeman, R.E. Preparation of Graphitic Oxide. *J. Am. Chem. Soc.* **1958**, *80*, 1339.

33. Ślusarczyk, C.; Fryczkowska, B. Structure-property relationships of pure cellulose and GO/CEL membranes regenerated from ionic liquid solutions. *Polymers (Basel).* **2019**, *11*.

34. Rashidian, E.; Babaeipour, V.; Khodamoradi, N.; Omidi, M. Synthesis and characterization of bacterial cellulose / graphene oxide nano-biocomposites. **2021**, 1–9.

35. Tian, M.; Qu, L.; Zhang, X.; Zhang, K.; Zhu, S.; Guo, X.; Han, G.; Tang, X.; Sun, Y. Enhanced mechanical and thermal properties of regenerated cellulose/graphene composite fibers. *Carbohydr. Polym.* **2014**, *111*, 456–462.

36. Nam, S.; French, A.D.; Condon, B.D.; Concha, M. Segal crystallinity index revisited by the simulation of X-ray diffraction patterns of cotton cellulose Iβ and cellulose II. *Carbohydr. Polym.* **2016**, *135*, 1–9.

37. French, A.D. Idealized powder diffraction patterns for cellulose polymorphs.

Cellulose **2014**, *21*, 885–896.

38. Palomba, M.; Longo, A.; Carotenuto, G. Gel-Phase Reduction of Graphene Oxide Coatings by L-Ascorbic Acid. **2021**, 33.

39. Fryczkowska, B.; Wiechniak, K. Preparation and properties of cellulose membranes with graphene oxide addition. *Polish J. Chem. Technol.* **2017**.

40. Fryczkowska, B.; Biniaś, D.; Ślusarczyk, C.; Fabia, J.; Janicki, J. Properties and application of cellulose membranes with graphene oxide addition for removal of heavy metals from aqueous solutions. *Desalin. Water Treat.* **2018**, *117*, 66–77.

41. Machnicka, A.; Fryczkowska, B. Bioactive membranes from cellulose with a graphene oxide admixture. *J. Ecol. Eng.* **2018**, *19*, 231–240.

42. Fryczkowska, B.; Wyszomirski, M.; Puzoń, M. Obtaining and Application of New Cellulose- and Graphene Oxide-Based Adsorbents for Treatment of Industrial Waste Containing Heavy Metals. *J. Ecol. Eng.* **2017**, *18*, 43–52.

43. Yaghoubidoust, F.; Salimi, E. A Simple Method for the Preparation of Antibacterial Cotton Fabrics by Coating Graphene Oxide Nanosheets. *Fibers Polym.* **2019**, *20*, 1155–1160.

44. Chen, H.; Gao, D.; Wang, B.; Palmieri, V.; Lauriola, M.C.; Ciasca, G. The graphene oxide contradictory effects against human pathogens. *Nanotechnology* **2017**, *28*, 1–18.

45. Fryczkowska, B.; Sieradzka, M.; Sarna, E.; Fryczkowski, R.; Janicki, J. Influence of a graphene oxide additive and the conditions of membrane formation on the morphology and separative properties of poly(vinylidene fluoride) membranes. *J. Appl. Polym. Sci.* **2015**, *132*, 42789.

46. Sokollek, S.J.; Hammes, W.P. Description of a starter culture preparation for vinegar fermentation. *Syst. Appl. Microbiol.* **1997**, *20*, 481–491.

47. Mazlan, N.S.N.; Salleh, K.M.; Khairunnisa-Atiqah, M.K.; Ainul Hafiza, A.H.; Mostapha, M.; Ellis, A. V.; Zakaria, S. Macro-Size Regenerated Cellulose Fibre Embedded with Graphene Oxide with Antibacterial Properties. *Polymers (Basel).* **2023**, *15*.

48. Surma-Ślusarska, B.; Danielewicz, D.; Kaleta, M. Porównanie właściwości różnych rodzajów celulozy przed i po regeneracji z cieczy jonowych. *Prz. Pap.* **2012**, *68*, 99–103.

49. Östlund, Å.; Idström, A.; Olsson, C.; Larsson, P.T.; Nordstierna, L. Modification

of crystallinity and pore size distribution in coagulated cellulose films. *Cellulose* **2013**, *20*, 1657–1667.

50. Gabrys, T.; Fryczkowska, B. Preparing and using cellulose granules as biodegradable and long-lasting carriers for artificial fertilizers. *J. Ecol. Eng.* **2018**, *19*.

51. From, M.; Larsson, P.T.; Andreasson, B.; Medronho, B.; Svanedal, I.; Edlund, H.; Norgren, M. Tuning the properties of regenerated cellulose: Effects of polarity and water solubility of the coagulation medium. *Carbohydr. Polym.* **2020**, *236*.

52. Gan, C.; Liang, T.; Li, W.; Fan, X.; Zhu, M. Amine-terminated ionic liquid modified graphene oxide/copper nanocomposite toward efficient lubrication. *Appl. Surf. Sci.* **2019**, *491*, 105–115.

53. Xue, S.; Li, H.; Guo, Y.; Zhang, B.; Li, J.; Zeng, X. Water lubrication of graphene oxide-based materials. *Friction* **2022**, *10*, 977–1004.

54. Gan, S.; Zakaria, S.; Syed Jaafar, S.N. Enhanced mechanical properties of hydrothermal carbamated cellulose nanocomposite film reinforced with graphene oxide. *Carbohydr. Polym.* **2017**, *172*, 284–293.

55. Gan, S.; Zakaria, S.; Chia, C.H.; Kaco, H. Effect of graphene oxide on thermal stability of aerogel bio-nanocomposite from cellulose-based waste biomass. *Cellulose* **2018**, *25*, 5099–5112.

56. Chem, J.M.; Wang, B.; Lou, W.; Hao, J. Relationship between dispersion state and reinforcement effect of graphene oxide in microcrystalline cellulose – graphene oxide composite films. **2012**, 12859–12866.

57. Kumar, P.; Huo, P.; Zhang, R.; Liu, B. Antibacterial properties of graphene-based nanomaterials. *Nanomaterials* 2019, *9*.

58. Xiao, S.; Lu, X.; Gou, L.; Li, J.; Ma, Y.; Liu, J.; Yang, K.; Yuan, B. Graphene oxide as antibacterial sensitizer: Mechanically disturbed cell membrane for enhanced poration efficiency of melittin. *Carbon N. Y.* **2019**, *149*, 248–256.

59. Thomas Luxbacher *The Zeta Potential for Solid Surface Analysis*; first.; Anton Paar GmbH: Graz, 2014;

60. Kelly, A.M.; Kaltenhauser, V.; Mühlbacher, I.; Rametsteiner, K.; Kren, H.; Slugovc, C.; Stelzer, F.; Wiesbrock, F. Poly(2-oxazoline)-derived Contact Biocides: Contributions to the Understanding of Antimicrobial Activity.

Macromol. Biosci. **2013**, *13*, 116–125.

61. Mirmohseni, A.; Azizi, M.; Dorraji, M.S.S. Cationic graphene oxide nanosheets intercalated with polyaniline nanofibers: A promising candidate for simultaneous anticorrosion, antistatic, and antibacterial applications. *Prog. Org. Coatings* **2020**, *139*.

62. Kumar, R.; Oves, M.; Ameelbi, T.; Al-Makishah, N.H.; Barakat, M.A. Hybrid chitosan/polyaniline-polypyrrole biomaterial for enhanced adsorption and antimicrobial activity. *J. Colloid Interface Sci.* **2017**, *490*, 488–496.

63. Luo, H.; Dong, J.; Yao, F.; Yang, Z.; Li, W.; Wang, J.; Xu, X. Layer-by-Layer Assembled Bacterial Cellulose / Graphene Oxide Hydrogels with Extremely Enhanced Mechanical Properties. *Nano-Micro Lett.* **2018**, *10*, 1–10.

64. Bhusal, P.; Rahiri, J.L.; Sua, B.; McDonald, J.E.; Bansal, M.; Hanning, S.; Sharma, M.; Chandramouli, K.; Harrison, J.; Procter, G.; et al. Comparing human peritoneal fluid and phosphate-buffered saline for drug delivery: Do we need bio-relevant media? *Drug Deliv. Transl. Res.* **2018**, *8*, 708–718.

65. Wen, H.; Morris, K.R.; Park, K. Hydrogen bonding interactions between adsorbed polymer molecules and crystal surface of acetaminophen. **2005**, *290*, 325–335.

66. Leyk, E.; Wesolowski, M. Interactions Between Paracetamol and Hypromellose in the Solid State. **2019**, *10*, 1–11.

67. Urbina, L.; Eceiza, A.; Gabilondo, N.; Corcuera, M.Á.; Retegi, A. Tailoring the in situ conformation of bacterial cellulose-graphene oxide spherical nanocarriers. *Int. J. Biol. Macromol.* **2020**, *163*, 1249–1260.

68. Szabo, T.; Maroni, P.; Szilagyi, I. Size-dependent aggregation of graphene oxide. *Carbon N. Y.* **2020**, *160*, 145–155.

69. Iguchi, M.; Yamanaka, S.; Budhiono, A. Bacterial cellulose — a masterpiece of nature ' s arts. *J. Mater. Sci.* **2000**, *35*, 261–270.

8. Wykaz artykułów naukowych wchodzących w skład rozprawy

Effect of graphene oxide additive on the structure of composite cellulose fibers*)

Tobiasz Gabryś[1), **)], Czesław Ślusarczyk[1)]

Abstract: The paper presents results of investigations on the effect of the addition of graphene oxide (GO) on the structural properties of composite cellulose fibers (CEL). GO/CEL fibers were obtained from a solution of CEL in ionic liquid – 1-ethyl-3-methylimidazole acetate – with the addition of GO dispersion in DMF. A classic wet spinning method was used using water and methanol as coagulants. Results have shown that the addition of GO increases the crystallinity of fibers to 31–40.8%. Moreover, these results indicate a significant impact of the coagulant used in the fiber forming process. Methanol coagulated fibers have greater porosity and larger pore sizes than water coagulated fibers.

Keywords: cellulose, graphene oxide, ionic liquids, composite fibers, WAXS, SAXS.

Wpływ dodatku tlenku grafenu na strukturę kompozytowych włókien celulozowych

Streszczenie: Przedstawiono badania wpływu dodatku tlenku grafenu (GO) na właściwości strukturalne kompozytowych włókien celulozowych (CEL). Włókna GO/CEL otrzymywano z roztworu CEL w cieczy jonowej – octanie 1-etylo-3-metyloimidazolu – z dodatkiem dyspersji GO w DMF. Zastosowano klasyczną metodę formowania włókien na mokro z zastosowaniem wody oraz metanolu jako koagulantów. Badania wykazały, że dodatek GO wpływa na wzrost stopnia krystaliczności włókien do wartości 31–40,8%. Ponadto wyniki te wskazują na znaczny wpływ koagulantu stosowanego w procesie formowania włókien na ich strukturę. Włókna koagulowane metanolem mają większą porowatość i większe rozmiary porów niż włókna koagulowane wodą.

Słowa kluczowe: celuloza, tlenek grafenu, ciecz jonowa, włókna kompozytowe, WAXS, SAXS.

Cellulose (CEL) is an available, low-cost and biodegradable polymer that can be processed from the following systems: *N*-methylmorpholine-*N*-oxide (NMMO), ionic liquids (ILs), LiCl/*N*,*N*-dimethylacetamide (LiCl/DMAc), NaOH aqueous solution, alkali/urea and NaOH/thiourea aqueous solution, tetrabutyl ammonium fluoride/dimethyl sulfoxide system (TBAF/DMSO), metal complex solutions and molten inorganic salt hydrates [1].

IL dissolves cellulose relatively easily and the regeneration of this biopolymer occurs under the influence of polar solvents [2, 3]. One of the best ionic liquids for dissolving cellulose is 1-ethyl-3-methylimidazolium acetate (EMIMAc) which belongs to the room temperature ionic liquids (RTILs) group [2]. Literature describes the conditions for dissolving cellulose in EMIMAc and then forming it in different forms [4, 5].

Cellulose in the form of a solution can be modified by the introduction of organic additives, inorganic additives (*e.g.* silver [6, 7], silicon [8]) or polymers, resulting in composites. An interesting and modern addition is graphene oxide (GO). In its structure it has many different oxygen function groups [9–11] which make it easier to disperse with different solvents [12, 13]. These groups also facilitate the dispersion of GO in polymers with functional groups [10, 14], including cellulose.

This paper presents research on the effect of the GO additive on the structure of GO/CEL composite fibers. The fibers were formed by wet spinning method using spinning solutions of cellulose and the additive in ionic liquid 1-ethyl-3-methylimidazolium acetate (EMIMAc). The process of fiber formation, consisting of extrusion spinning liquid into different baths: water (1) and methanol (2), was described in previous work [15] and was similar to that described in the literature [6]. The CEL and composite GO/CEL fibers obtained in this way differed in structural properties depending on the amount of GO in the cellulose matrix and the type of coagulant used. Crystallinity

---

[1)] University of Bielsko-Biala, Faculty of Materials, Civil and Environmental Engineering, Institute of Textile Engineering and Polymer Materials, Willowa 2, 43-309 Bielsko-Biala, Poland.

**) Author for correspondence: tgabrys@ath.bielsko.pl

of the cellulose matrix was investigated by means of the Wide Angle X-ray Scattering (WAXS) method, whereas an analysis of the porous structure of that matrix by means of the Small Angle X-ray scattering (SAXS) method. Using this method, the pore dimensions and the pore volume fraction were determined. The studies characterize pore sizes on length scales from 1 nm to 60 nm, according to the resolution of the SAXS equipment used.

EXPERIMENTAL PART

Materials

Cellulose long fibers C 6663 and 1-ethyl-3-methylimidazolium acetate (EMIMAc) 97% (w/w) purity were purchased from Sigma-Aldrich Sp. z o.o. (Poznań, Poland). Methanol 99.8% and *N,N*-dimethylformamide (DMF) were purchased from Avantor Performance Materials Poland S.A. (Gliwice, Poland). All the chemicals were used without further purification.

Preparation of spinning solutions and fibers spinning

GO/CEL fibers were produced using the wet spinning method. For this purpose single syringe infusion pump KDS-100 (KD Scientific Inc. Holliston, USA), equipped with a 10 cm³ syringe and a needle with an internal diameter of 0.7 mm, was used. The monofilament extrusion rate was 23 cm/min and the stretch ratio was $S = 1$. The fibers were extruded at room temperature directly into a bath containing distilled water or methanol. The coagulation process lasted 30 minutes, and after that the fibers were taken up onto a spool and dried with air at 60°C. The process of preparation of spinning solutions and the method of obtaining fibers are describe in our unpublished work [16]. The mass composition of ingredients needed to prepare individual spinning solutions and sample description system are listed in Table 1.

T a b l e 1. The composition of the solutions for the fibers spinning and description system

Determination of the spinning solution	0	A	B	C	D
W/w conc. of GO in fiber, %	0	0.21	0.50	0.98	1.97
W/w conc. of CEL in fiber, %	100	99.79	99.50	99.02	98.03
Type of coagulant	Designation				
Distilled water	1				
Methanol	2				

Methods of testing

WAXS measurements

Wide Angle X-ray Scattering (WAXS) investigations were carried out with a URD-65 Seifert (Germany) diffrac-

tometer using the reflection method in Bragg-Brentano geometry. CuKα radiation was used at 40 kV and 30 mA. Monochromatization of the beam was obtained by means of a graphite crystal monochromator placed in the diffracted beam path. A scintillation counter was used as a detector. Investigations were performed in the 2θ angle range of 3 to 60° in steps of 0.1°. Before measurements fibers were powdered using Hardy's microtome.

SAXS measurements

The Small Angle X-ray scattering (SAXS) measurements were carried out with the compact Kratky camera, equipped with the SWAXS optical system of HECUS-MBRAUN (Austria). The Cu target X-ray tube, operated at: $U = 30$ kV, $I = 20$ mA was used as a radiation source ($\lambda = 0.154$ nm). The primary beam was monochromatized by Ni filter and a pulse-height discrimination. Measurements were made on powdered fibers, *i.e.* the same samples as in WAXS tests. The SAXS data were collected as a function of the scattering vector $q = (4\pi/\lambda) \sin\theta$, where 2θ is the scattering angle. The moving slit method [17] was applied for determination of the transmittance factor of the sample. The sample holder background was subtracted from the SAXS curves and next curves were corrected taking into consideration both sample thickness and transmittance. The data were converted to absolute intensities with a calibrated Lupolen® (polyethylene) standard [18].

RESULTS AND DISCUSSION

The available literature shows the presence of several varieties of crystalline cellulose, differing in the shape of an elementary cell and parameters [19]. Native cellulose is known as cellulose type I. On the other hand, cellulose regenerated after dissolving in EMIMAc and then precipitating in the form of fiber in water and methanol has the characteristics of cellulose II. This is a phenomenon known as the dissolving effect of cellulose in most known solvents and the occurrence of so-called hydratecellulose. The crystalline level test was performed for GO/CEL fibers with different GO content.

A variety of crystalline cellulose II was found in the supramolecular structure of all GO/CEL fibers tested. It is significantly higher and better shaped for fibers coagulated in water. The characteristic peak at 2θ angle 12° does not occur at all in fibers coagulated in methanol (Fig. 1).

Similar results were obtained by other researchers who precipitated cellulose in distilled water and ethanol [20]. Their WAXS studies indicate that the selection of coagulant significantly affects the supramolecular structure of the regenerated cellulose.

The degree of crystallinity of GO/CEL composite fibers was determined by WAXS curve analysis. To this end, each WAXS diffractogram was deconvoluted into indi-
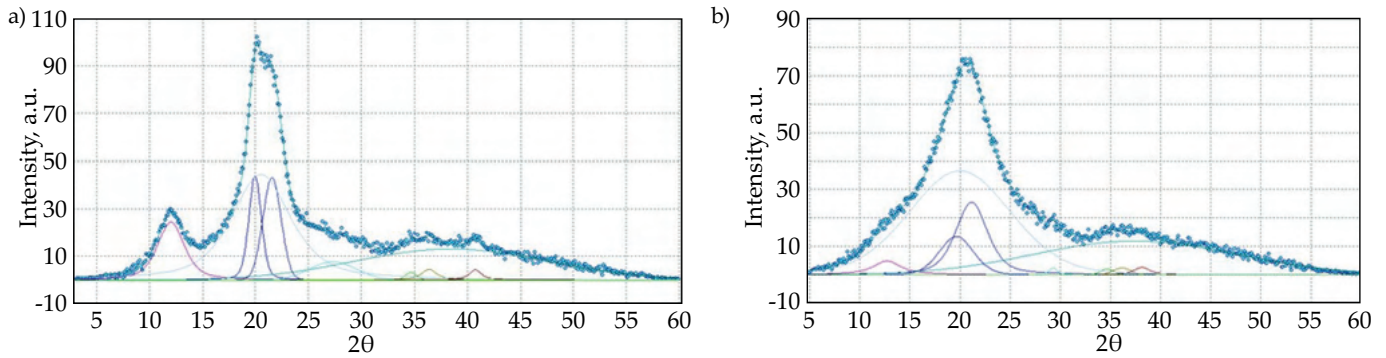
Fig. 1. Crystalline and amorphous components distribution for fiber sample: a) coagulated in water, b) coagulated in methanol

vidual crystalline and amorphous components using WaxsFit software [21]. The shape of each peak was approximated using Gauss and Cauchy function. Examples of deconvoluted diffraction pattern for coagulated fibers in water and methanol are shown in Fig. 1. The degree of crystallinity was determined as the ratio of the summary of the surface fields below the crystalline peaks to the total surface area below the scattering curve.

Studies show that the crystallinity of the fibers obtained in water was between 31 and 40.8% and fibers from methanol between 21.6–26.2% (Fig. 2). The analysis of the results obtained also indicates an increase in the degree of crystallinity as the GO content in the cellulose matrix increases, as shown in Fig. 2. It is also important that all coagulated fibers in methanol have a lower degree of crystallinity compared to the fibers obtained in water. This is due to the coagulation rate. Longer coagulation time – in the case of water – promotes the formation of a crystalline structure. The increase in the crystallinity is the most intense for fibers with the GO content of up to 0.5 wt %. In the case of fibers with the GO content more than 0.5 wt %, the degree of crystallinity increases slowly. This may indicate that there is no need for higher concentrations of graphene oxide, because the most available function groups in the cel-

lulose chain are taken by GO. The increase in the degree of crystallinity with the increase of GO content in the fibers may be conditioned by the presence of numerous hydrogen bonds formed by the combination of cellulose and graphene oxide. These bonds, by linking cellulose, chains together, can form some ordered areas, called lamellas.

The SAXS patterns of investigated fibers are shown in Fig. 3. The dominant feature of these patterns is the appearance of the scattering maximum which can be interpreted based on the standard theory of X-ray scattering at small angles. According to this theory small-
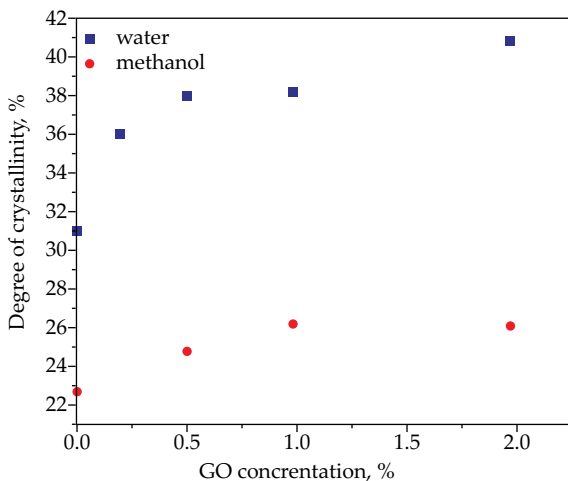

Fig. 2. Dependence of the degree of crystalline on the type of coagulant and the content of graphene oxide in GO/CEL fibers; parameters determined by WAXS curve analysis
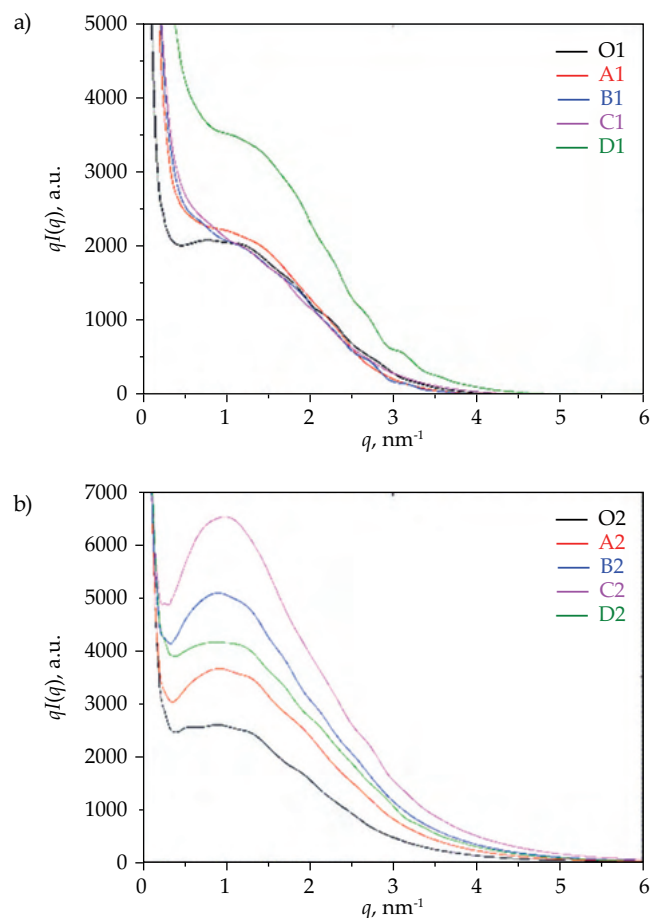

Fig. 3. SAXS patterns for pure cellulose fibers (black) and fibers spun with addition of GO (other colors, respectively): a) coagulated in water, b) coagulated in methanol

angle X-ray scattering is conditioned by the existence of the electron density in homogeneities in the sample, which in the case of fibers studied is due to the existence of pores in them, the higher intensity is caused by higher content of the pores in these fibers.

Content of pores can be determined by calculating the so-called the scattering power, or invariant Q, using the equation:

$$Q = \int_0^\infty q^2 I(q) \mathrm{d}q = \varphi(1 - \varphi)(\Delta \varrho)^2 \qquad (1)$$

where $I(q)$ – the corrected SAXS intensity, φ – the volume fraction of pores, $\Delta \varrho$ – the electron density difference between the pores and cellulose. The pores may be assumed to be entirely air filled in dry fibers. The electron density difference between cellulose and pores was calculated to be $\Delta \varrho = 511$ electrons/nm^3 [22]. The φ values calculated by the Eq. (1), shown in Table 2, indicate a slight but clear influence of the coagulant used in the fiber forming process.

T a b l e 2. The volume fraction of pores (φ) and the radii of pores (R) obtained by SAXS

Sample	φ, %	q_{max}, nm^{-1}	R, nm
01	0.40	0.91 ± 0.05	6.36 ± 0.35
A1	0.52	1.05 ± 0.05	5.52 ± 0.26
B1	0.52	0.99 ± 0.07	5.80 ± 0.42
C1	0.53	1.01 ± 0.06	5.70 ± 0.34
D1	0.90	1.09 ± 0.05	5.31 ± 0.24
02	0.51	0.82 ± 0.05	7.06 ± 0.43
A2	0.70	0.95 ± 0.04	6.06 ± 0.26
B2	0.94	0.90 ± 0.05	6.37 ± 0.36
C2	1.20	0.96 ± 0.04	5.99 ± 0.25
D2	0.84	0.94 ± 0.04	6.15 ± 0.27

For all types of fibers, the values of this parameter are higher for fibers coagulated in methanol. Furthermore φ value oscillating around 1%, allow the assumption that in terms of SAXS theory, the investigated fibers can be treated as dilute system of pores dispersed in a cellulose matrix. For such system, we may assume that the scattering intensity is the sum of scattering intensities coming from the individual pores [23]. Experimentally recorded distribution of the scattering intensity for this system is the basis for the calculation of the sizes of individual pores, because the intensity for spherical particle of radius R scattering X-rays is given by Equation (2):

$$I(q) = 9(\Delta \varrho)^2 V^2 \left[\frac{\sin(qR) - qR\cos(qR)}{(qR)^3} \right]^2 \qquad (2)$$

where V – the volume of the particle.

The first two maxima are located at an angle satisfying the relations

$$q_i R = \begin{cases} 5.765 \text{ for } i = 1 \\ 9.100 \text{ for } i = 2 \end{cases}$$

The calculated values of the radii of pores and the position of the maxima (q_{max}) are presented in Table 2. Again, the pore sizes in all methanol coagulated fibers are larger than sizes in water coagulated fibers. For the first type of fibers, the value of R is greater than 6nm, while for the second type of fibers are less than this value. The difference in pore sizes can be seen both for CEL as GO/CEL fibers.

CONCLUSIONS

This work examines the effect of the coagulant type and the GO additive on the structural properties of composite cellulose fibers. The fibers were formed by wet spinning method from GO/DMF/CEL/EMIMAC solution in distilled water and methanol.

Studies have shown that the coagulant type has a significant impact on the structural properties of CEL and GO/CEL fibers. Namely, the formation of fibers in distilled water (0-1; A-1; B-1; C-1; D-1) results in fibers with higher degree of crystallinity, which is 31–40.8%, because distilled water slows down coagulation process, making it possible to self-assembly crystalline structure. In contrast, fibers coagulated in methanol (0-2; A-2; B-2; C-2; D-2) have a less perfect crystalline structure and the degree of crystallinity of 21.6–26.1%.

Results has shown also that the crystallinity of composite fibers increases with the GO content in the CEL matrix. The observed phenomenon may be the result of the formation of many hydrogen bonds between GO and CEL, which can create certain clusters of ordered areas. Moreover, methanol coagulated fibers are characterized by greater porosity and larger pore sizes than water coagulated fibers.

REFERENCES

[1] Wang S., Lu A., Zhang L.: *Progress in Polymer Science* **2016**, *53*, 169.
http://dx.doi.org/10.1016/j.progpolymsci.2015.07.003
[2] Isik M., Sardon H., Mecerreyes D.: *International Journal of Molecular Sciences* **2014**, *15*, 11922.
http://dx.doi.org/10.3390/ijms150711922
[3] Pinkert A., Marsh K.N., Pang S., Staiger M.P.: *Chemical Review* **2009**, *109*, 6712.
http://dx.doi.org/10.1021/cr9001947
[4] Fukaya Y., Hayashi K., Kim S.S., Ohno H.: *Proceedings of the ACS Symposium Series* **2010**, *1033*, 55.
http://dx.doi.org/10.1021/bk-2010-1033.ch002
[5] Ries M.E., Radhi A., Keating A.S. *et al.*: *Biomacromolecules* **2014**, *15*, 609.
http://dx.doi.org/10.1021/bm401652c
[6] Rac-Rumijowska O., Fiedot M., Karbownik I. *et al.*: *Cellulose* **2017**, *24*, 1355.

http://dx.doi.org/10.1007/s10570-016-1168-7

[7] Rac-Rumijowska O., Maliszewska I., Fiedot-Toboła M. *et al.*: *Polymers* **2019**, *11*, 562.
http://dx.doi.org/10.3390/polym11030562

[8] Andersson Trojer M., Olsson C., Bengtsson J. *et al.*: *Journal of Colloid and Interface Science* **2019**, *553*, 167.
http://dx.doi.org/10.1016/j.jcis.2019.05.084

[9] Guerrero-Contreras J., Caballero-Briones F.: *Materials Chemistry and Physics* **2015**, *153*, 209.
http://dx.doi.org/10.1016/j.matchemphys.2015.01.005

[10] Ghosh T., Biswas C., Oh J. *et al.*: *Chemistry of Materials* **2012**, *24*, 594.
http://dx.doi.org/10.1021/cm2033838

[11] Teodoro K.B.R., Migliorini F.L., Facure M.H.M., Correa D.S.: *Carbohydrate Polymers* **2019**, *207*, 747.
http://dx.doi.org/10.1016/j.carbpol.2018.12.022

[12] Konkena B., Vasudevan S.: *The Journal of Physical Chemistry Letters* **2012**, *3*, 867.
http://dx.doi.org/10.1021/jz300236w

[13] Paredes J.I., Villar-Rodil S., Martínez-Alonso A., Tascón J.M.D.: *Langmuir* **2008**, *24*, 10560.
http://dx.doi.org/10.1021/la801744a

[14] Hwang T., Oh J.-S., Yim W. *et al.*: *Separation and Purification Technology* **2016**, *166*, 41.
http://dx.doi.org/10.1016/j.seppur.2016.04.018

[15] Fryczkowska B., Wiechniak K.: *Polish Journal of Chemical Technology* **2017**, *19*, 41.
http://dx.doi.org/10.1515/pjct-2017-0066

[16] Gabryś T., Fryczkowska B., Biniaś D. *et al.*: *Carbohydrate Polymer,* in print.

[17] Stabinger H., Kratky O.: *Die Makromolekulare Chemie* **1978**, *179*, 1655.
https://doi.org/10.1002/macp.1978.021790630

[18] Kratky O., Pilz I., Schmitz P.J.: *Journal of Colloid Interface Science* **1966**, *21*, 24.
https://doi.org/10.1016/0095-8522(66)90078-X

[19] Zugenmaier P.: "Crystalline cellulose and cellulose derivatives, characterization and structure", (Eds. Timell T.E., Wimmer R.), Springer Series in Wood Science, Heidelberg 2008.

[20] Surma-Ślusarska B., Danielewicz D., Kaleta M.: *Przegląd Papierniczy* **2012**, *68*, 99.

[21] Rabiej M.: *Journal of Applied Crystallography* **2017**, *50*, 221.
http://dx.doi.org/10.1107/S160057671601983X

[22] Crawshaw J., Cameron R.E.: *Polymer* **2000**, *41*, 4691.
https://doi.org/10.1016/S0032-3861(99)00502-9

[23] Porod G.: "Small-Angle X-ray Scattering" (Eds. Glatter O., Kratky O.), Academic Press, New York 1982, pp. 17–51.

Preparation and properties of composite cellulose fibres with the addition of graphene oxide

Tobiasz Gabryś [a], Beata Fryczkowska [b],*, Dorota Biniaś [a], Czesław Ślusarczyk [a], Janusz Fabia [a]

[a] *Faculty of Materials, Civil and Environmental Engineering, Institute of Textile Engineering and Polymer Materials, University of Bielsko-Biala, Willowa 2, 43-309 Bielsko-Biala, Poland*
[b] *Faculty of Materials, Civil and Environmental Engineering, Institute of Environmental Protection and Engineering, University of Bielsko-Biala, Willowa 2, 43-309 Bielsko-Biala, Poland*

ABSTRACT

The paper presents the results of a study on the preparation of cellulose-based composite fibres (CEL) with graphene oxide addition (GO). Composite fibres (GO/CEL) were prepared via the wet spinning method from CEL solutions in 1-ethyl-3-methylimidazolium acetate (EMIMAc) that contained a nano-addition of GO dispersion in *N,N*-dimethylformamide (DMF). The GO contents of the composite fibres were 0, 0.21, 0.50, 0.98, and 1.97 % w w. The fibres were coagulated in two solvents: distilled water and methanol. The results demonstrated that the amount of GO additive and the type of coagulant significantly impact the physicochemical, mechanical and structural properties of the CEL and GO/CEL fibres. The use of distilled water in a coagulation bath causes a degree of crystallinity of 31.0–40.8 % (WAXS) and a shift in the thermal decomposition temperature (by approximately 19 °C) towards higher temperatures (TGA). The results demonstrate improvements in the mechanical properties of the GO/CEL fibres, which were at the level of 9.43–14.18 cN/tex. In addition, the GO/CEL fibres exhibit satisfactory GO dispersion throughout their volume.

1. Introduction

The degradation of the environment that occurs during the production, use, storage and disposal of plastics is resulting in a return to polymers of natural origin. Cellulose is the polysaccharide that is present in nature in the highest amount; hence, it is available, cheap, biodegradable and biocompatible. Regenerated cellulose can be obtained via physical dissolution followed by regeneration. Among the systems that are used to dissolve cellulose, we distinguish the following: *N*-methylmorpholine-*N*-oxide (NMMO), ionic liquids (ILs), LiCl/*N,N*-dimethylacetamide (LiCl/DMAc), NaOH aqueous solution, alkali/urea and NaOH/thiourea aqueous solution, and the tetrabutyl amonium fluoride/dimethyl sulfoxide system (TBAF/DMSO). Regenerated cellulose can be formed as fibres, films and membranes, microspheres and granules, hydrogels and airgels, and bioplastics (Wang, Lu, & Zhang, 2016).

Ionic liquids are among the compounds that may replace the traditional systems that are used to dissolve cellulose in the future. Their advantage is easy dissolution and precipitation of cellulose with polar solvents (Pinkert, Marsh, Pang, & Staiger, 2009). The solubility of ILs in water depends on the nature of the anion, the temperature and the length of the alkyl chain on the organic cation (for example, tetrafluoroborates, chlorides, nitrates, and trifluoroacetates exhibit complete miscibility with water) (Laus et al., 2005). The suitability of ionic liquids for the dissolution of cellulose has been the subject of various investigations by a growing number of working groups (Laus et al., 2005; Swatloski, Spear, Holbrey, & Rogers, 2002). Barthel investigated 1-*N*-butyl-3-methylimidazolium chloride, 1-*N*-ethyl-3-methylimidazolium chloride, 1-*N*-butyldimethylimidazolium chloride and 1-*N*-allyl-2,3-dimethylimidazolium bromide as solvents for cellulose (Barthel & Heinze, 2006). Another article describes studies on two chloride-based ILs: 1-butyl-3-methylimidazolium chloride and 1-allyl-3-methylimidazolium chloride. The first is a corrosive, toxic and extremely hygroscopic solid, and the second is viscous and has a reactive side-chain (Zhao et al., 2009). Kosan et al. studied the use of various ionic liquids (1-*N*-butyl-3-methylimidazolium chloride, 1-ethyl-3-methylimidazolium chloride, 1-*N*-butyl-3-methylimidazolium acetate, 1- ethyl-3-methylimidazolium acetate, and 1-*N*-butyl-2,3-dimethylimidazolium chloride) as solvents to dissolve cellulose (Kosan, Michels, & Meister, 2008).

According to studies of ionic liquids that were conducted for several years, one of the best liquids is 1-ethyl-3-methylimidazolium acetate (EMIMAc), which forms cellulose solutions with a concentration of 23 g/mol at 40 °C and solutions with a concentration of 16–25 % w/w at 90 °C (Isik, Sardon, & Mecerreyes, 2014). An important feature of EMIMAc is that it belongs to the group of room-temperature ionic liquids (RTILs) (Cao et al., 2009). Another advantage is its low toxicity of ED$_{50}$ = 2860 mg/dm^3 (Freire et al., 2011). Many publications describe conditions for the dissolution of cellulose in EMIMAc and the subsequent spinning of it. For example, Sundberg et al. worked with cellulose in very high concentrations. They prepared a 38.5 % solution of cellulose in EMIMAc, heated the mixture for 4 days at 70 °C, and precipitated the cellulose in ethanol (Sundberg et al., 2015).

Obtaining cellulose in the form of a solution enables the introduction of organic, inorganic or polymeric additives to obtain composite fibres. Rac-Rumijowska's team introduced silver nanoparticles during the formation of cellulose fibres via the NMMO method (Rac-Rumijowska, Fiedot, Karbownik, Suchorska-Woźniak, & Teterycz, 2017; Rac-Rumijowska, Maliszewska, Fiedot-Toboła, Karbownik, & Teterycz, 2019). Other studies describe the possibility of introducing iron oxide into cellulose composite fibres (Sun et al., 2008; Yadav, 2018). Andersson Trojer et al. obtained composite fibres from a cellulose solution in EMIMAc with the addition of silicon nanoparticles (Andersson Trojer, Olsson, Bengtsson, Hedlund, & Bordes, 2019). The additives are intended to change the properties of the CEL fibres, for example, to render them antibacterial, hydrophobic or conductive.

An interesting and modern material that is used to prepare polymer composites is graphene oxide (GO), which has many oxygen-containing functional groups (Ghosh et al., 2012; Guerrero-Contreras & Caballero-Briones, 2015). GO can be easily dispersed in water and organic solvents, e.g., DMF, tetrahydrofuran and ethylene glycol (Konkena & Vasudevan, 2012; Parades, Villar-Rodil, Martínez-Alonso, & Tascón, 2008; Texter, 2014; Yoon et al., 2013). The diversity of oxygen functional groups that are arranged on the GO surface facilitate its dispersion in polymers with functional groups to form durable bonds (Ghosh et al., 2012; Hwang et al., 2016). Teodoro et al. described the method for creating the GO/CEL mixture, which they applied on PA6 nanofibres, which were used ultimately as mercury detectors (Teodoro, Migliorini, Facure, & Correa, 2019). Another team obtained GO/CEL composite fibres from a solution of CEL in NaOH (Tian et al., 2014). Yang et al. coated functionalized cellulose yarn with graphene oxide (GO) for use in electronics (Yang, Jun, & Yun, 2019). The literature also discusses the possibility of coating cotton fibres with a GO dispersion and fixing them at elevated temperatures (Yaghoubidoust & Salimi, 2019). In contrast, Shao et al. described the possibility of bacterial cellulose synthesis in the presence of GO (Shao et al., 2016).

This paper presents a method for obtaining cellulose composite GO/CEL fibres that has not been described in the literature. Cellulose was dissolved in a low-temperature ionic liquid, namely, 1-ethyl-3-methylimidazolium acetate (EMIMAc) (Cao et al., 2009; Gupta, Hu, & Jiang, 2011), while GO was dispersed in DMF. Preparation of the spinning solution and wet fibre formation were conducted at room temperature, which has not been described in the literature so far. The fibre formation process involved extruding the spinning fluid into two baths: water and methanol. This study attempts to show that a small addition of graphene oxide into spinning liquids increases the strength parameters of GO/CEL fibres and increases the degree of crystallinity.

2. Experimental

2.1. Materials

Cellulose long fibres C 6663 (the average length of the single fibres was 120–140 μm, and the thickness of the fibres was 13–18 μm), 1-ethyl-3-methylimidazolium acetate (EMIMAc) with 97 % (w/w) purity, and graphite powder of <20 μm were purchased from Sigma-Aldrich.

Methanol (99.8 %), KMnO$_4$, H$_2$SO$_4$ with 98 % (w/w) purity, 30 % H$_2$O$_2$, and N,N-dimethylformamide (DMF) were purchased from Avantor Performance Materials Poland S.A. All the chemicals were used without further purification.

2.2. GO synthesis and preparation of the GO/DMF dispersion

Graphene oxide was obtained via a modified Hummers method (Hummers & Offeman, 1958). The GO synthesis and evaluation of its properties (XRD, DSC, FTIR) were highly similar to the processes in our earlier study (Fryczkowska, Sieradzka, Sarna, Fryczkowski, & Janicki, 2015). Wet graphene oxide was dried in a laboratory drier at 60 °C to obtain a brown precipitate, which was dispersed in DMF on an ultrasonic bath to obtain a 2.1 % GO/DMF dispersion.

2.3. Preparation and rheological studies of the spinning solutions

To prepare spinning solutions, suitable amounts of 2.1 % GO/DMF dispersion were introduced into the ionic liquid (EMIMAc), which was followed by intensive stirring for 10 min and sonication for 30 min in an Inter Sonic 1S-1 ultrasonicator at 35 kHz. Suitable amounts of cellulose were introduced into the dispersion thus obtained such that the CEL concentration in each spinning solution was 5 %. Then, each solution was mixed thoroughly using a rotary homogenizer and left to deaerate for 24 h. The deaeration process was based on the free removal of air bubbles that moved to the surface of the spinning solutions under atmospheric pressure. The amounts of the ingredients that were used in the preparation of the individual spinning solutions and their determinations are listed in Table 1.

The viscosity testing of the spinning liquids was conducted using a Myr V2-L rotational viscosity gauge that was equipped with an L3 spindle and a thermocouple (Especialidades Medicas Myr, SL, Tarragona, Spain). Rheological parameters, such as the viscosity activation energy (E) and constant A, were determined based on the Arrhenius-Guzman equation (formula 1):

$$\eta = A \cdot exp \left(E/RT \right) \tag{1}$$

where:

η - absolute viscosity [Pa × s], A - characteristic constant for a given liquid [-], E - activation energy of viscous flow [kJ/mol], R - gas constant [8.314 J/mol K], and T - temperature [K].

The results are summarized in Table 2.

2.4. Fibre formation

GO/CEL fibres were produced via the wet spinning solution method. For this purpose, a KDS-100 single syringe infusion pump (KD Scientific) that was equipped with a 10 cm^3 syringe and a needle with an internal diameter of 0.7 mm was used. The fibre extrusion rate was 0.18 cm^3/min. The stretch ratio was S = 1. The monofilament take-up velocity was 23 cm/min. The fibres were extruded at room temperature directly into a bath that contained distilled water (1) or methanol (2) (Table 3). The coagulation process lasted 30 min, and subsequently, the fibres were taken up onto a spool and dried with air at 60 °C. The fibre production scheme is illustrated in Fig. 1a.

Table 1
Compositions of the solutions for the fibre spinning.

Determination of the spinning solution	0	A	B	C	D
Amount of 2.1 % GO/DMF [g]	0	0.25	0.60	1.18	2.40
Amount of GO [g]	0	0.0052	0.0125	0.0249	0.0503
Amount of CEL [g]	2.5	2.5	2.5	2.5	2.5
Amount of EMIMAc [g]	47.50	47.25	46.89	46.29	45.05
W/w conc. of GO in fibre [%]	0	0.21	0.50	0.98	1.97
W/w conc. of CEL in fibre [%]	100	99.79	99.50	99.02	98.03

Table 2
Values of the rheological parameters of the spinning solutions.

Spinning solutions	η [mPa × s]	E [kJ/mol]	A [-]
0	14,610	25.16	1.99
A	14,010	44.45	2.72
B	11,525	42.58	2.67
C	9625	40.88	2.63
D	8425	38.83	2.59

where η - viscosity; E - energy of viscous flow activation; and A - characteristic constant for the liquid.

2.5. Structure and morphology analysis

The surfaces of the fibres and their cross-sections were observed using an OPTA-TECH optical microscope at 10x magnification. Images of the sample were captured using transmission mode.

Fibre tests were also conducted using a high-resolution Phenom ProX scanning electron microscope (SEM) from Thermo Fisher Scientific (Pik Instruments, Poland, Piaseczno) that was operated at 10 kV. Liquid nitrogen was used to prepare the cross-sections of the fibres, in which the samples were frozen and broken.

All measurements were conducted using a Nicolet 6700 FT-IR spectrometer (Thermo Electron Corp., Madison, WI, USA) that was equipped with a photoacoustic MTEC model 300 accessory. The following measurement parameters were used: resolution, 4 cm^{-1}; spectral range, $500-4000$ cm^{-1}; and number of scans, 64. Data collection and postprocessing were conducted using the OMNIC software (v. 8.0, Thermo Electron Corp.).

X-ray diffraction (XRD) investigations were conducted with a URD 63 Seifert diffractometer. Cu K⟨ radiation was used at 40 kV and 30 mA. A scintillation counter was used as a detector. Diffractograms were recorded from 3° to 60° with a step size of 0.1° and an acquisition time of 20 s per step. Each diffraction curve was corrected for polarization, the

Table 3
Physicochemical and mechanical properties of cellulose and GO/CEL composite fibres.

Fibre	Type of coagulant	U [%]	α [°]	F [cN]	E [%]	m$_l$ [tex]	W [cN/tex]	M [GPa]
0−1	water	80.0 ± 2.1	41.0 ± 2.1	244.60±56.36	10.01±2.37	28.20 ± 0.52	8.67±0.55	35.67±3.06
A-1	water	77.0 ± 1.7	39.0 ± 2.8	271.61±6.67	12.79±0.53	28.80 ± 1.22	9.43±0.60	59.00±3.88
B-1	water	82.0 ± 1.8	37.0 ± 2.1	265.22±16.95	7.44±1.01	25.40 ± 0.82	10.44±0.66	62.69±3.55
C-1	water	90.0 ± 1.9	32.0 ± 2.0	236.07±6.06	14.32±1.10	39.00 ± 0.95	6.05±0.38	48.92±6.57
D-1	water	94.0 ± 1.9	30.0 ± 1.2	195.32±7.98	5.12±0.49	27.80 ± 1.31	7.03±0.44	70.30±4.55
0−2	methanol	71.0 ± 1.7	32.0 ± 1.7	151.34±40.24	10.87±2.21	27.20 ± 1.09	5.56±0.35	35.99±4.02
A-2	methanol	73.0 ± 1.6	30.0 ± 2.0	331.49±34.81	20.06±4.51	26.00 ± 0.68	12.75±0.80	53.70±4.09
B-2	methanol	74.0 ± 1.8	29.0 ± 0.9	294.95±14.77	19.54±3.93	20.80 ± 0.45	14.18±0.90	83.34±3.89
C-2	methanol	79.0 ± 1.8	28.0 ± 2.1	318.12±6.40	19.93±1.41	32.60 ± 1.56	9.76±0.62	92.51±6.30
D-2	methanol	83.0 ± 1.8	27.0 ± 2.9	281.85±10.65	10.27±1.61	30.60 ± 0.69	9.21±0.58	81.91±3.49

U – water uptake; α – contact angle; F - breaking force; E – elongation at break; m$_l$ - linear density; W - tenacity; and M - elastic modulus.
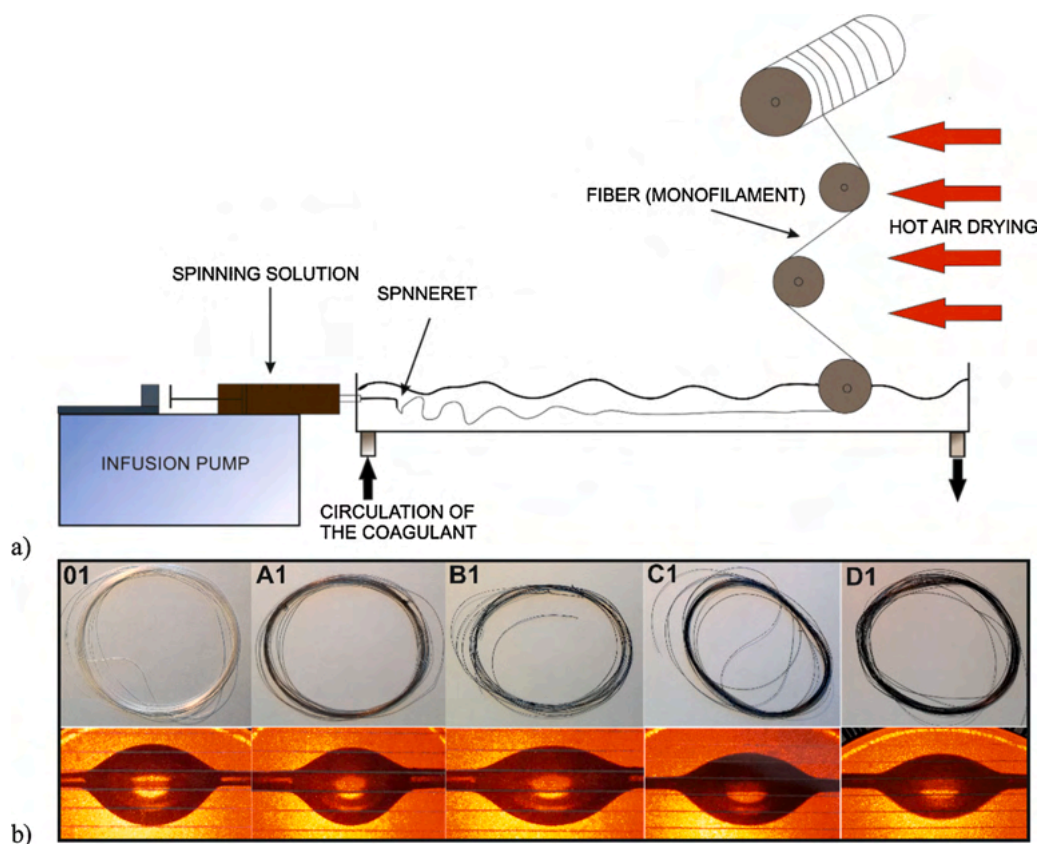

Fig. 1. a) The wet-spinning setup, which includes all stages for CEL and GO/CEL fibre spinning. b) Pure CEL and GO/CEL fibres that were obtained in water (at the top) with contact angle measurements (bottom).

Lorentz factor and incoherent scattering. The degree of crystallinity of the obtained fibres was determined on the basis of WAXS analysis. Each WAXS pattern was distributed into individual crystalline and amorphous components using the WaxsFit software (Rabiej, 2017). The shape of each peak was approximated using the Gaussian and Cauchy functions. The degree of crystallinity was calculated as the ratio of the sum of the surface areas under the crystalline peaks to the total area under the scattering curve.

Thermal studies (TGAs) of the fibres were conducted using a TA Instruments Q500 thermobalance. The obtained TG and DTG curves were analysed using the TA Instruments Universal v4.5 software package. Measurements were conducted under a nitrogen purge (flow 60 mL/min) with a heating rate of 20°/min from the ambient temperature to 650 °C.

2.6. Physicochemical and mechanical properties of fibres

To determine the water sorptions for pure cellulose (CEL) and composite (GO/CEL) fibres, the samples were weighed on an analytical balance, placed in beakers that contained distilled water and left for 60 min. Then, the fibres were removed and filtered off, the remaining water was removed with filter paper, and they were re-weighed. The water absorption (U) was calculated using the following formula (2), and the obtained results are summarized in Table 3.

$$U = \frac{W_w - W_d}{W_d} \times 100\% \tag{2}$$

where: W_w - wet fibre weight [g]; W_d - dry fibre weight [g]

Contact angle measurements were conducted using a PG-1 Pocket goniometer. A Hamilton syringe was used to form distilled water drops with a volume of 0.8 μl, which were placed on a single fibre (Fig. 1b).

The strength parameters were determined by considering the recommendations of ISO 5079 ("Textiles fibres - Determination of breaking force & elongation of individual fibres (ISO 5079 : 1995)," n. d.). The measurements were conducted using an Instron testing machine (Model 5544, Norwood, MA, USA) with a compression and stretching head with a measuring range of 0−10 N ("Technical-motion documentation of a resistance machine INSTRON, 2020). The tests were conducted at a strain rate of 10 mm/min for all samples. In our case, we studied GO/CEL fibres with different material composition, so as like research of He et al. we used only one strain rate for all fibres, which was 10 mm/min (He et al., 2012). This is directly due to the standard and the experience gained from working with cellulose fibres. To determine the strength parameters, 50 ruptures were conducted for each variant, and a random error that was equal to 2 % of the value of the average breaking force was assumed. The measuring distance between the jaws was 20 mm. The testing was conducted under normal climate conditions ("Textiles-Standard atmospheres for conditioning and testing (ISO 139:2005)," n.d.). The results are summarized in Table 3.

3. Results and discussion

3.1. Properties of the spinning liquids

The basic parameters that determine the quality and characteristics of spinning solutions are their rheological properties. These properties change with the solution composition and temperature, and if these are known, determination of the optimal processing conditions is possible. By conducting the tests, the results were obtained, and on their basis, the energy of viscous flow activation (E), the characteristic constant for the liquid (A) and the absolute viscosity (η) were determined. The values of the rheological parameters of the spinning solutions are summarized in Table 2.

The results demonstrate that the smallest addition of GO, which is 0.01 % in the case of solution A, results in a sharp decrease in viscosity (Table 2). The viscosity value for the pure cellulose solution (solution 0) is 14 610 mPa × s for a low concentration of 5 % w/w of CEL at room temperature, which is a satisfactory result compared to the viscosity values that were reported by Cao et al. (Cao et al., 2009). However, as the GO content in the CEL matrix increases, the viscosity values decrease in the following order: (solution A) 14 010 mPa × s; (solution B) 11 525 mPa × s; (solution C) 9 625 mPa × s; and (solution D) 8 425 mPa × s (Table 2). This effect is caused by the strong slip properties of GO in combination with the EMIMAc ionic liquid.

3.2. Structural and morphology studies

3.2.1. Fibre microstructure

The cellulose fibres (0) and composite cellulose fibres (A–D) that were obtained in the experiment differed in terms of colour with the amount of GO addition (Fig. 1b). Pure cellulose fibres 0 were colourless. However, the remaining fibres were characterized by shades of grey. The more GO that was added in the GO/CEL fibre, the darker its colour. In the wet formation process, differences in the coagulation rate of the fibres were observed among the coagulants that were used. The spinning solutions that were introduced into methanol were characterized by much shorter coagulation times than those that were coagulated in distilled water. This observed phenomenon significantly impacts the ordering of CEL and GO macromolecules in the entire volume of the fibre.

For pure cellulose fibres (0) and composite fibres (A–D), the samples were observed via transmission mode optical microscopy (Fig. 2).

The pure cellulose fibres (0−1; 0−2) are smooth and transparent, both in the longitudinal view and in the cross-section. It may indicate that they are largely amorphous, as reported by Sundberg et al. (Sundberg, Toriz, & Gatenholm, 2013).

Transmission mode optical microscopy enabled the observation of the presence of GO inclusions in GO/CEL composite fibres (Fig. 2). The more GO was added into the GO/CEL fibre, the darker the sample. The amount of GO was increased as follows: 0.21; 0.5; 0.98; and 1.97 % w/w. In the longitudinal and cross-sectional views of the A–D fibres, GO is well dispersed throughout the entire volume of the GO/CEL composite. Moreover, no phase separation is observed, even for the highest (1.97 %) GO concentration in the composite fibre.

Comparing images of the same composite fibres (Fig. 2) that were coagulated in water (1) with images of those that were coagulated in methanol (2), no significant differences were observed. Therefore, tests using scanning electron microscopy (SEM) were conducted.

In the SEM images (Fig. 3), it was observed that the method of coagulation of the fibres affects the morphology of their surfaces. According to surface microphotographs, small grooves were present along the fibres. Analysing the SEM images, the number of grooves on the fibres increases in the following order: 0, A, B, C, D. Moreover, the grooves in the fibres that were coagulated in methanol (0−2; A-2; B-2; C -2; D2) are shallower and the fibres are smoother than those that were coagulated in water (0−1; A-1; B-1; C-1; D-1). SEM microscopy also explained the differences in the contact angle values (Table 3), which were lower for smoother fibres (0−2; A-2; B-2; C-2; D2) than for fibres with more developed surfaces (0−1; A-1; B-1; C-1; D-1) and ranged from 27−32°. Studies have shown that the coagulation process of the GO/CEL composite in methanol is faster than in water, which results in differences in the surface structures of the obtained fibres, as observed in SEM images. The fibres are similar in appearance to the cellulose fibres that were described by Sundberg et al. (Sundberg et al., 2015).

3.2.2. FTIR analysis

The molecular structures of the cellulose and GO/CEL composite fibres that were obtained using the wet solution method and coagulated in distilled water (Fig. 4a) and in methanol (Fig. 4b) were examined via FTIR spectroscopy. The characteristic OH stretching bands that are responsible for the formation of hydrogen bonds are observed between
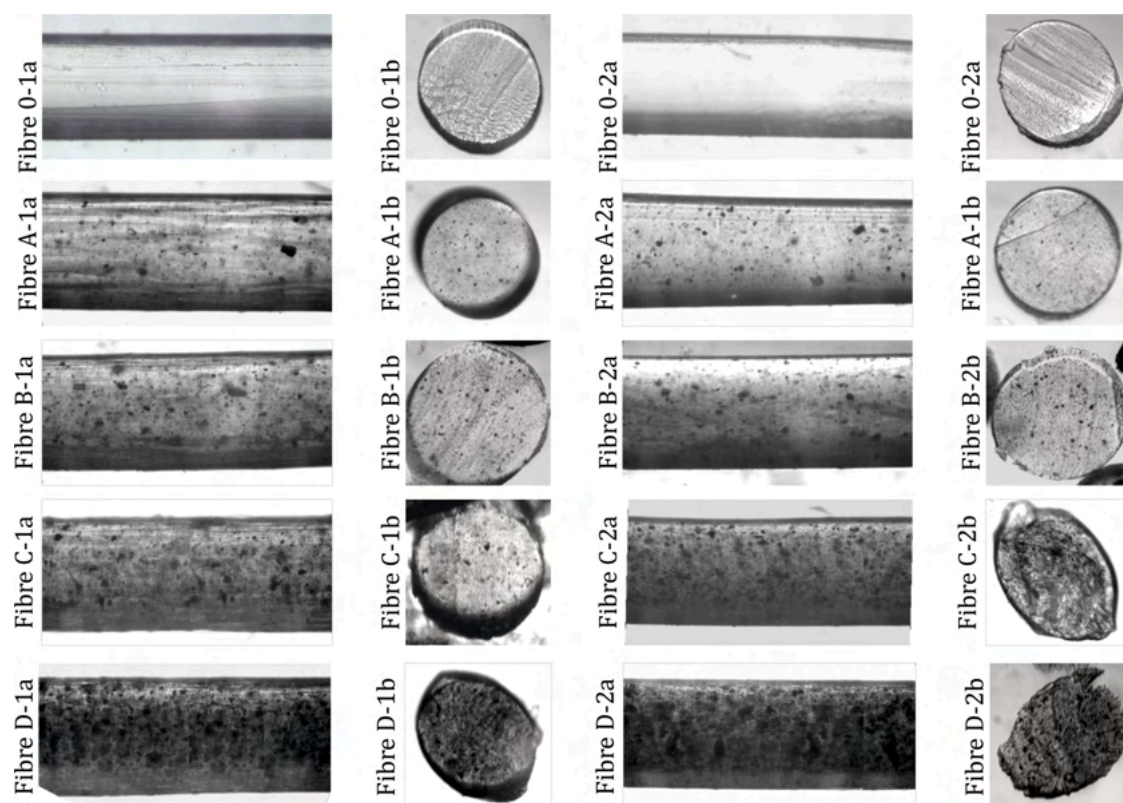
Fig. 2. Optical microscope images of the surfaces (a) and cross-sections (b) of fibres that were coagulated in water (1) and in methanol (2) (10x magnification).

$3700-2400$ cm^{-1} and at approximately 1640 cm^{-1}, similar to in (Tian et al., 2014). In addition, widening of this broad band is observed as the amount of GO that is introduced into the GO/CEL fibres is increased. The GO addition likely causes loosening of the structure between cellulose macromolecule chains and introduces additional hydroxyl groups. The band at a wavelength of approximately 2900 cm^{-1} corresponds to the effect of the stretching vibrations of the C–H oscillator. No significant differences are observed in this range of wave numbers; hence, the configuration of the groups that contain this oscillator is preserved. The band with a peak at approximately 1115 cm^{-1} is the effect of oscillation of etheric C—OC— groups between the rings and the band with a peak at approximately 1160 cm^{-1} is the result of asymmetric stretching vibrations of C—OC— (Fan, Dai, & Huang, 2012). For the GO/CEL composite fibres, band intensity increases are observed at wavelengths of approximately 1740 cm^{-1} and 1640 cm^{-1}, which correspond to the vibration of C=O groups in GO, as the amount of GO that is introduced to the cellulose fibres is increased (Teodoro et al., 2019).

EMIMAc can plasticize cellulose fibres. In the spectra of fibres that were coagulated in water (1) and in methanol (2), bands at wave numbers 1585 cm^{-1} and 1587 cm^{-1} are observed, which, according to Sundberg (1572 cm^{-1}), could be attributed to ionic liquid. However, the 1404 cm^{-1} band, which is characteristic for this ionic liquid, is not observed (Sundberg et al., 2013). The absence of these bands supports the removal of EMIMAc from the fibres in the process of spinning from a spinning solution that was composed of GO/CEL/DMF/EMIMAc.

3.2.3. XRD analysis

According to the literature, four crystal varieties of cellulose occur, which differ in terms of the shape of the unit cell and its parameters (Mahadeva & Kim, 2012). Native cellulose that has not been chemically treated is known as type I cellulose. Cellulose that has been regenerated after being dissolved in EMIMAc ionic liquid and precipitating in the form of fibre in water and in methanol has the characteristics of type II

cellulose. This phenomenon occurs when cellulose is dissolved in most known solvents to produce hydrated cellulose. The degree of crystallinity was investigated for GO/CEL fibres with various GO contents. The presence of type II crystal cellulose was detected in the supermolecular structures of all examined GO/CEL fibres. The type II crystal cellulose is significantly more abundant and better developed in fibres that were coagulated in water. The crystallite structure of the type II cellulose that was regenerated during methanol coagulation is only partially developed and is severely defective. This is manifested in extension and blurring of the peaks for the interference maxima that occur for the 2-theta results at $13°$, $20°$ and $21°$. Especially for the 2-theta angle of $13°$, the crystal peak is visible as an inflection that overlaps an amorphous halo. Hence, the coagulation of fibres in water promotes the process of recrystallization, which can also be associated with the rate of ionic liquid leaching from the fibres. The diffraction patterns for type I cellulose, type II cellulose that precipitated in water and in methanol and GO are compared in Fig. 5a.

The results demonstrate that the degree of crystallinity of fibres that were obtained in water ranged from 31 to 40.8 % and that of fibres that were obtained in methanol ranged from 21.6 to 26.2 % (Fig. 5b). According to an analysis of the results, the degree of crystallinity increases with the GO content in the cellulose matrix (Fig. 5b). The most dynamic increase in crystallinity occurs for fibres with GO contents of up to 0.5 %. For fibres with GO contents that exceed 0.5 %, the degree of crystallinity does not increase rapidly. This may indicate that there is no need to use higher concentrations of graphene oxide because GO in the GO/CEL fibre has occupied most of the available functional groups in the CEL polymer chain. The increase in the degree of crystallinity with the GO content in the fibres may be due to the presence of numerous hydrogen bonds, which enable the formation of clusters of ordered areas by connecting cellulose polymer chains via cellulose-graphene oxide combination.
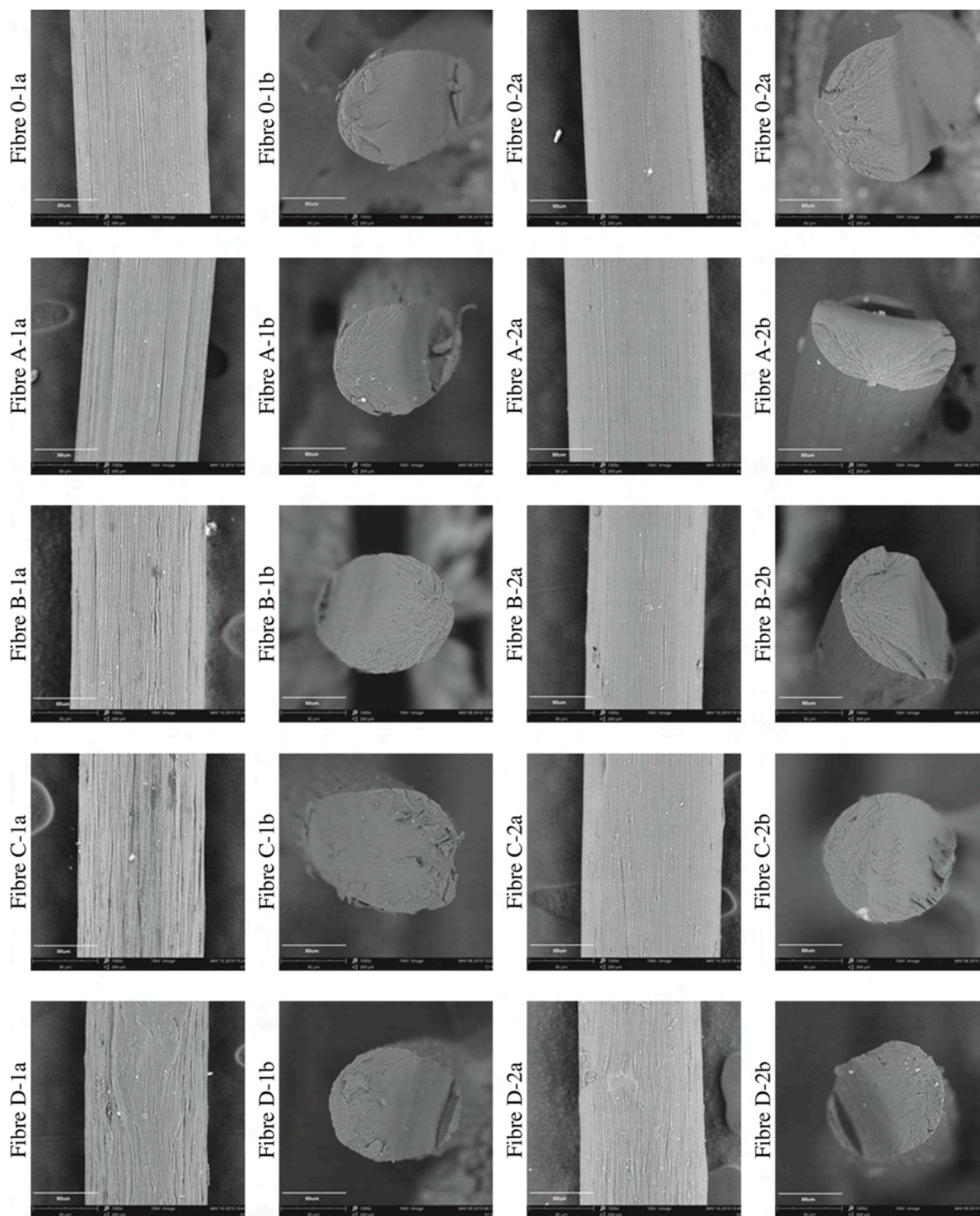
Fig. 3. SEM images for fibres: (a) surfaces and (b) cross-sections of fibres that were coagulated in water (1) and methanol (2) (1000x magnification).

3.2.4. TGA analysis

According to an analysis of the curves (TG) for samples of fibres that were coagulated in water (Fig. 6a), the water release process (from 6.7 % weight loss for fibres without GO (0−1) to 7.1 % for GO/CEL fibres (D-1)) occurs at up to approximately 200 °C and proceeds directly into a thermal decomposition process. The maximum for the DTG curves (which corresponds to the highest mass loss rate) for this effect is the lowest for fibres 0−1 (97.6 °C) and shifts towards higher temperatures by as much as 18.3 °C for fibres B-1. Moreover, the temperature at the beginning of thermal decomposition is the lowest for fibres without the addition of a modifier (199.7 °C), while the addition of GO causes a substantial increase in this temperature (the temperature of the extrapolated beginning of the transformation) for all modified fibres. The largest shift (by 16.8 °C) is observed for fibres A-1.
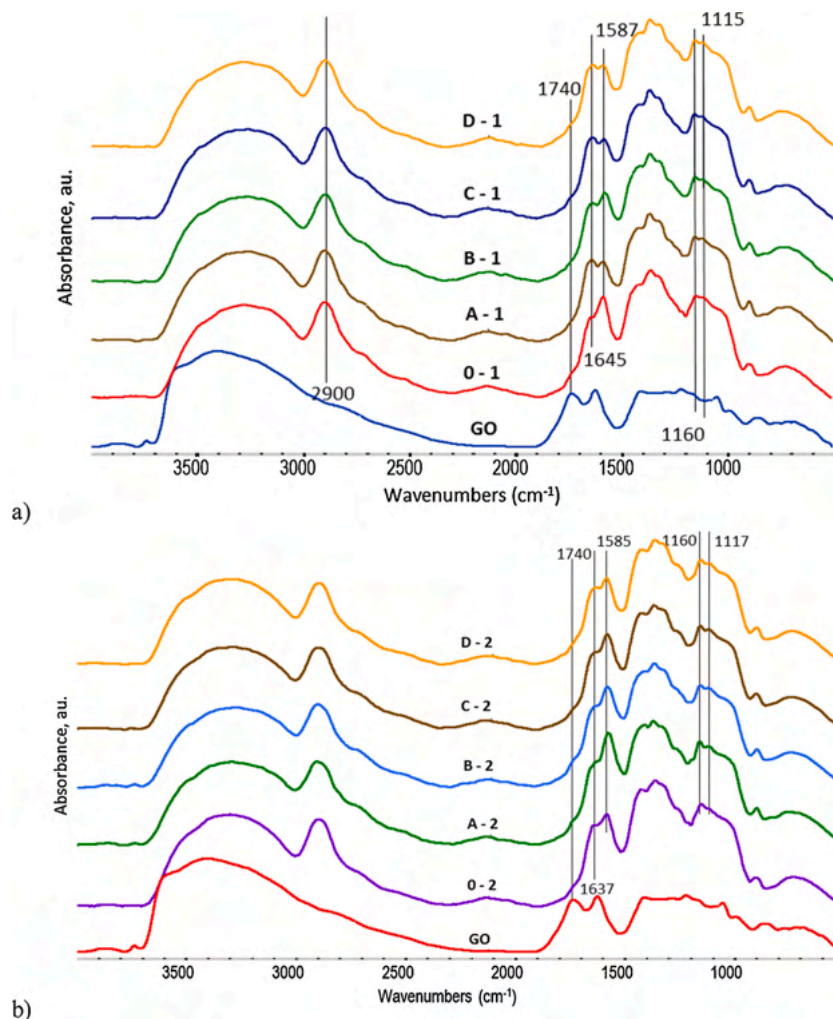
Fig. 4. FTIR spectra for pure cellulose (0), graphene oxide (GO) and GO/CEL (A-D) composite fibres that were coagulated in a) water (1) and b) methanol (2).

The trend is similar at the beginning of the thermal decomposition for fibres that were coagulated in methanol (Fig. 6b): The lowest decomposition onset temperature was recorded for the unmodified cellulose fibre (180.3 °C). The addition of GO to the fibre increases the decomposition temperature to 203.5 °C (for fibres D-2). The temperature of the onset of fibre degradation depends on the type of coagulant. Fibres that were coagulated in methanol degrade earlier than fibres that were coagulated in water.

The process of thermal decomposition of the tested fibres in all cases (regardless of the coagulant used) ends at a temperature that slightly exceeds 390 °C. The final decomposition stage for all samples occurs at almost the maximum rate at a temperature of approximately 436 °C (which corresponds to a weight loss of slightly over 6 %). The determination of the residue after heating the samples to 650 °C in a nitrogen atmosphere demonstrates an increased content of condensed carbon structures in the GO/CEL fibres. This content varies monotonically from 16.5 % to 19.1 % for the fibres that were coagulated in water and from 13.4 % to 16.6 % for the fibres that were solidified in methanol (Fig. 6b).

The presence of type II crystal cellulose (hydrated cellulose) was detected in the supermolecular structures of all cellulose fibres that were examined in this paper. The type II crystal cellulose was significantly more abundant and better developed in the fibres that were coagulated in water (Fig. 5b). The increase in the degree of structural ordering that was observed for fibres that were solidified in water exceeds 8 % for fibres without GO (Fig. 5b), thereby resulting in a significant shift in the thermal decomposition (by approximately 19 °C) towards higher temperatures (Fig. 6c).

3.3. Physicochemical and mechanical properties of the fibres

According to an analysis of the results that are summarized in Table 3, both the method of fibre coagulation and the amount of GO that is added into the cellulose matrix significantly affect the water absorption. Water sorption values that were determined for the fibres that were coagulated in water (1) exceed the values that were obtained for the fibres that were coagulated in methanol (2). For the fibres that were obtained from pure cellulose, the water sorption is 80 % (for fibres 0−1) and 71 % (for fibres 0−2). For all types of composite fibres (A–D), an increase in the water sorption is observed as the GO concentration is increased. It is concluded from this study that the addition of hydrophilic GO and the use of water as a coagulant increase the water absorption capacity of the GO/CEL fibres (from 77 % to 94 % for the A-1, B-1, C-1, and D-1 fibres). The obtained results are attributed to the fibre coagulation process, which is slower in water, thereby resulting in the formation of fibres with a higher degree of crystallinity (Fig. 5b) and accompanied by higher water sorption.

To evaluate the effect of the addition of GO into the CEL matrix and the effect of the coagulant on the properties of the obtained fibres, contact angle tests were conducted. Both synthetic and natural cellulose fibres are characterized by satisfactory hydrophilic properties. According to the results of the experiment, the selection of the coagulant decisively impacts the hydrophilicity of the obtained fibres (Table 3). Studies have shown that CEL and GO/CEL fibres that were coagulated in methanol (2) are characterized by lower contact angle values (32−27°) than fibres (1) that were coagulated in water (41−30°). Contact angle
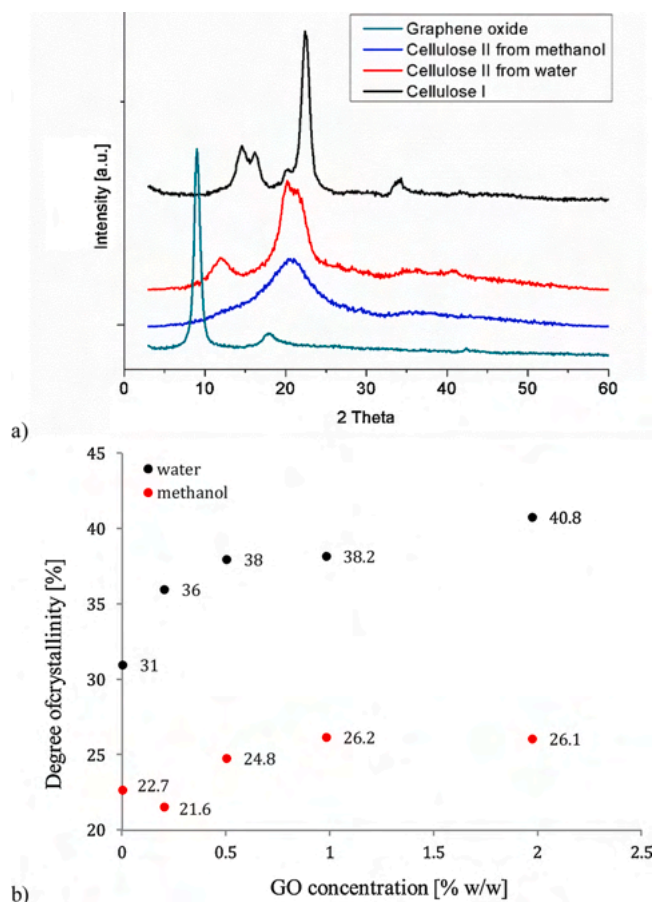
Fig. 5. a) A comparison of diffraction patterns for cellulose type I, cellulose type II that were coagulated in water and methanol, and pure GO. b) The dependence of the degree of crystallinity on the type of coagulant and the content of graphene oxide in GO/CEL fibres. The parameters were determined on the basis of WAXS analysis.

measurements that were obtained for fibres that were coagulated in methanol (2) may indicate that the surfaces of these fibres are more hydrophilic than those of fibres that were coagulated in water (1). Moreover, the contact angle values decrease as the proportion of hydrophilic GO addition in the composite fibres increases. Comparing the contact angle values for fibres that were obtained from the same spinning solutions but with different coagulants, it is concluded that coagulation in water causes the formation of micropores or microcracks on the surfaces of the fibres, which increases the contact angle values.

The linear density tests (Table 3) of the obtained fibres showed that the linear density was in the range of 20.8–39.0 tex. For fibres that were obtained from pure cellulose, the linear density was 28.2 tex (0−1) and 27.2 tex (0−2), similar to the values that were obtained by Shi et al. (Shi, Hou, Li, & Ge, 2017). In contrast, for composite fibres that contained up to 0.5 % w/w GO, decreases in the linear density to 25.4 tex (B-1) and 20.8 tex (B-2) are observed. The subsequent addition of portions of the nanoadditive into composite fibres results in increases in the linear density.

The cellulose and composite fibres are characterized by tenacity values of 5.56–14.18 cN/tex (Table 3), which are lower than those of typical cellulose fibres that are obtained using industrial technologies (Cai, Zhang, Guo, Shao, & Hu, 2010; Reddy & Yang, 2008, 2009). According to an analysis of the results, the cellulose fibres that were coagulated in methanol (0−2) are characterized by lower tenacity values (5.56 cN/tex) than the fibres that were coagulated in water (0−1), for which the strength is 8.67 cN/tex. According to the literature, the tenacity for commercial viscose fibres is 17.3 cN/tex (Michud et al.,

2016). An analysis of the results that were obtained for composite fibres A-1, B-1, A-2, and B-2 shows that there are observable increases in tenacity (9.4, 10.4, 12.8, and 14.2 cN/tex, respectively) relative to fibres without the addition. For composite fibres (C-1, ᴅ-1, C-2, and ᴅ-2) that contain more than 0.5 % GO, decreases in the strength are observed relative to the previously discussed fibres. This phenomenon may be associated with increases in the volume of the GO agglomerates inside the fibres, as shown in Fig. 2 (2C-1a, 2D1-a, 2C-2a, and 2D2-a). The large sizes of the agglomerates reduce the strength of the GO/CEL fibres. However, the obtained fibres have similar mechanical properties to the cellulose composite fibres that were obtained by other researchers. Shi et al. prepared luminescence cellulose fibre by using a NaOH/thiourea/aurea aqueous solvent system (Shi et al., 2017). They used highly similar equipment to obtain the fibres. The tenacity values are within the range of 0.97–1.78 cN/dtex.

From the results, it is concluded that during the formation of GO/CEL fibres, interactions occur between the oxygen groups on GO and the hydroxyl groups of the CEL chains. If the concentration of the nanoadditive in the fibres is low (up to 0.5 % GO), GO flakes are separated in the CEL matrix. During the recrystallization of cellulose (Fig. 5a), the process of regeneration of intra- and intermolecular hydrogen bonds occurs in the biopolymer and between GO and CEL molecules. However, when the amount of the additive in the composite fibres exceeds 0.5 %, intra- and intermolecular bonds are formed not only between cellulose chains but also between GO flakes. The result of these interactions is the formation of GO agglomerates in composite fibres. Therefore, it is concluded that the increase in the tenacity of the GO/CEL fibres is the result of intermolecular interactions that are caused by the formation of hydrogen bonds between oxygen functional groups on GO flakes and OH groups in CEL chains. In contrast, the decrease in the strength of the tested fibres is the result of an excess of GO, which causes the formation of agglomerates in the fibres, which reduce their strength.

The obtained results may also demonstrate that the rapid coagulation of CEL in methanol promotes the formation of fibres with a low degree of intramolecular structural ordering. This was supported by the results that were obtained via X-ray diffraction (WAXS), according to which the crystallinity of the fibres (2) was 21.6–26.1 % (Fig. 5b). In addition, it is concluded that the specific strength of the fibres that were coagulated in methanol (2) is statistically significantly higher than that of the fibres that were coagulated in water (1).

The results that are presented in Table 3 also demonstrate that the fibres that were coagulated in methanol (0−2; A-2, B-2, C-2, and ᴅ-2) are characterized by higher elongation at break values than those that were coagulated in water (0−1, A-1, B-1, C-1, and ᴅ-1). The values of elongation at break for fibres (2are 10.27–20.06 %, while those of fibres (1) are 5.12–14.32 %. The obtained results demonstrate that the fibres that were coagulated in methanol are more amorphous and, therefore, more plastic. Comparing with the results of other researchers (Shi et al., 2017), the test fibres have 3–4 times larger elongation at break values. It may seem that the high elongation at break values for fibres (2) may result from the presence of EMIMAc in the fibres due to their rapid coagulation. However, FTIR studies (Fig. 4) exclude the presence of this solvent. Thus, the elongation at break values of 10.87–20.06 are due to the high content of the amorphous phase in the fibres that were coagulated in methanol.

4. Conclusions

Studies have shown that it is possible to obtain composite fibres that are based on cellulose that is doped with graphene oxide. The proposed method consisted the use of a low-temperature ionic liquid (EMIMAc) into which GO dispersed in DMF was introduced, followed by cellulose. GO/CEL composite fibres were formed at room temperature via a wet spinning method and were coagulated in water or methanol. Optical microscopy and SEM images showed a homogeneous structure of the fibres and satisfactory dispersion of the nanoadditive. The structural
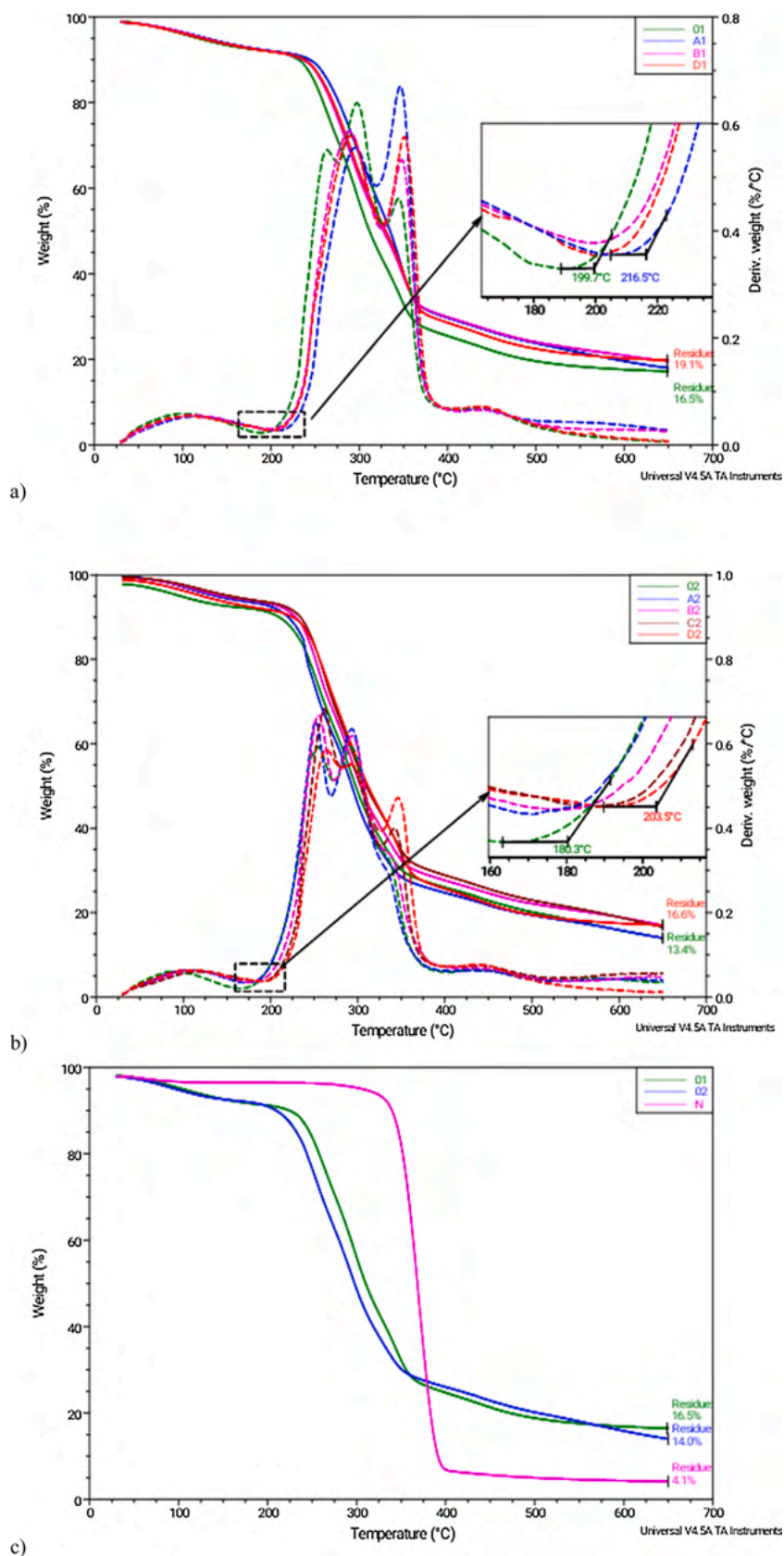
Fig. 6. TG and DTG curves for samples of cellulose fibres that were modified with graphene oxide (GO/CEL) with various modifier contents and coagulated in a) water and b) methanol. c) TG curves of cellulose fibres that were coagulated in water 0-1 (green) and methanol 0-2 (blue), and a curve for a sample of native cellulose -N- (pink).

tests (WAXS and TGA) showed that when water was used as a coagulant, GO/CEL fibres with a high degree of crystallinity of up to 40.8 % were obtained. Moreover, all obtained fibres retained their hydrophilic character (29–41 °) and high water sorption of up to ~ 94 %. The study of the strength properties showed that GO/CEL fibres are characterized by low tenacity values but high elongation at break (20.06 %). This study showed that the best parameters corresponded to fibres that contained no more than 0.5 % GO. The obtained fibres that contained GO, which exhibited biocidal properties, can be potentially used in disposable products for packaging (an additive to cellulose pulp), medical (protective clothing), and gardening (mulching nonwovens), among other applications.

Funding

CRediT authorship contribution statement

Tobiasz Gabryś: Conceptualization, Methodology, Validation, Formal analysis, Investigation, Writing - original draft, Visualization. **Beata Fryczkowska:** Conceptualization, Methodology, Writing - original draft, Writing - review & editing, Supervision. **Dorota Biniaś:** Investigation, Writing - original draft, Visualization. **Czesław Ślusarczyk:** Formal analysis, Investigation, Writing - original draft, Visualization. **Janusz Fabia:** Investigation, Writing - original draft, Visualization.

References

Andersson Trojer, M., Olsson, C., Bengtsson, J., Hedlund, A., & Bordes, R. (2019). Directed self-assembly of silica nanoparticles in ionic liquid-spun cellulose fibers. *Journal of Colloid and Interface Science, 553*, 167–176. https://doi.org/10.1016/j.jcis.2019.05.084

Barthel, S., & Heinze, T. (2006). Acylation and carbanilation of cellulose in ionic liquids. *Green Chemistry, 8*(3), 301–306. https://doi.org/10.1039/b513157j

Cai, T., Zhang, H., Guo, Q., Shao, H., & Hu, X. (2010). Structure and properties of cellulose fibers from ionic liquids. *Journal of Applied Polymer Science, 116*(5), 2658–2667. https://doi.org/10.1002/app

Cao, Y., Wu, J., Zhang, J., Li, H., Zhang, Y., & He, J. (2009). Room temperature ionic liquids (RTILs): A new and versatile platform for cellulose processing and derivatization. *Chemical Engineering Journal, 147*(1), 13–21. https://doi.org/10.1016/j.cej.2008.11.011

Fan, M., Dai, D., & Huang, B. (2012). Transform - Materials analysis. *Fourier transform infrared spectroscopy for natural fibres* (pp. 1–26). In Tech.. https://doi.org/10.5772/57353

Freire, M. G., Teles, A. R. R., Ferreira, R. A. S., Carlos, L. D., Lopes-Da-Silva, J. A., & Coutinho, J. A. P. (2011). Electrospun nanosized cellulose fibers using ionic liquids at room temperature. *Green Chemistry, 13*(11), 3173–3180. https://doi.org/10.1039/c1gc15930e

Fryczkowska, B., Sieradzka, M., Sarna, E., Fryczkowski, R., & Janicki, J. (2015). Influence of a graphene oxide additive and the conditions of membrane formation on the morphology and separative properties of poly(vinylidene fluoride) membranes. *Journal of Applied Polymer Science, 132*(46), 42789. https://doi.org/10.1002/app.42789

Ghosh, T., Biswas, C., Oh, J., Arabale, G., Hwang, T., Luong, N. D., … Nam, J. D. (2012). Solution-processed graphite membrane from reassembled graphene oxide. *Chemistry of Materials, 24*(3), 594–599. https://doi.org/10.1021/cm2033838

Guerrero-Contreras, J., & Caballero-Briones, F. (2015). Graphene oxide powders with different oxidation degree, prepared by synthesis variations of the Hummers method. *Materials Chemistry and Physics, 153*, 209–220. https://doi.org/10.1016/j.matchemphys.2015.01.005

Gupta, K. M., Hu, Z., & Jiang, J. (2011). Mechanistic understanding of interactions between cellulose and ionic liquids: A molecular simulation study. *Polymer, 52*(25), 5904–5911. https://doi.org/10.1016/j.polymer.2011.10.035

He, Y., Zhang, N., Gong, Q., Qiu, H., Wang, W., Liu, Y., … Gao, J. (2012). Alginate/graphene oxide fibers with enhanced mechanical strength prepared by wet spinning. *Carbohydrate Polymers, 88*(3), 1100–1108. https://doi.org/10.1016/j.carbpol.2012.01.071

Hummers, W. S., & Offeman, R. E. (1958). Preparation of graphitic oxide. *Journal of the American Chemical Society, 80*(6). https://doi.org/10.1021/ja01539a017, 1339–1339.

Hwang, T., Oh, J.-S., Yim, W., Nam, J.-D., Bae, C., Kim, H.-I., … Kim, K. J. (2016). Ultrafiltration using graphene oxide surface-embedded polysulfone membranes. *Separation and Purification Technology, 166*(2016), 41–47. https://doi.org/10.1016/j.seppur.2016.04.018

Isik, M., Sardon, H., & Mecerreyes, D. (2014). Ionic liquids and cellulose: Dissolution, chemical modification and preparation of new cellulosic materials. *International Journal of Molecular Sciences*. https://doi.org/10.3390/ijms150711922

Konkena, B., & Vasudevan, S. (2012). Understanding aqueous dispersibility of graphene oxide and reduced graphene oxide through p K a measurements. *The Journal of Physical Chemistry Letters, 3*(7), 867–872. https://doi.org/10.1021/jz300236w

Kosan, B., Michels, C., & Meister, F. (2008). Dissolution and forming of cellulose with ionic liquids. *Cellulose, 15*(1), 59–66. https://doi.org/10.1007/s10570-007-9160-x

Laus, G., Bentivoglio, G., Schottenberger, H., Kahlenberg, V., Kopacka, H., Roeder, T., … Sixta, H. (2005). Ionic liquids: Current dev elopments, potential and drawbacks for industr ial applications. *Lenzinger Berichte, 84*, 71–85. https://doi.org/10.2174/157017905774322640

Mahadeva, S. K., & Kim, J. (2012). Influence of residual ionic liquid on the thermal stability and electromechanical behavior of cellulose regenerated from 1-ethyl-3-methylimidazolium acetate. *Fibers and Polymers, 13*(3), 289–294. https://doi.org/10.1007/s12221-012-0289-3

Michud, A., Tanttu, M., Asaadi, S., Ma, Y., Netti, E., Kääriainen, P., & Sixta, H. (2016). Ioncell-F: Ionic liquid-based cellulosic textile fibers as an alternative to viscose and Lyocell. *Textile Research Journal, 86*(5), 543–552. https://doi.org/10.1177/0040517515591774

Parades, J. I., Villar-Rodil, S., Martínez-Alonso, A., & Tascón, J. M. D. (2008). Graphene oxide dispersions in organic solvents. *Langmuir, 24*(19), 10560–10564. https://doi.org/10.1021/la801744a

Pinkert, A., Marsh, K. N., Pang, S., & Staiger, M. P. (2009). Ionic liquids and their interaction with cellulose. *Chemical Reviews, 109*(12), 6712–6728. https://doi.org/10.1021/cr9001947

Rabiej, M. (2017). Application of the particle swarm optimization method for the analysis of wide-angle X-ray diffraction curves of semicrystalline polymers. *Journal of Applied Crystallography, 50*(5), 221–230. https://doi.org/10.1107/S1600576714014782

Rac-Rumijowska, O., Fiedot, M., Karbownik, I., Suchorska-Woźniak, P., & Teterycz, H. (2017). Synthesis of silver nanoparticles in NMMO and their in situ doping into cellulose fibers. *Cellulose, 24*(3), 1355–1370. https://doi.org/10.1007/s10570-016-1168-7

Rac-Rumijowska, O., Maliszewska, I., Fiedot-Toboła, M., Karbownik, I., & Teterycz, H. (2019). Multifunctional nanocomposite cellulose fibers doped in situ with silver nanoparticles. *Polymers, 11*(3), 562. https://doi.org/10.3390/polym11030562

Reddy, N., & Yang, Y. (2008). Characterizing natural cellulose fibers from velvet leaf (Abutilon theophrasti) stems. *Bioresource Technology, 99*(7), 2449–2454. https://doi.org/10.1016/j.biortech.2007.04.065

Reddy, N., & Yang, Y. (2009). Properties of natural cellulose fibers from hop stems. *Carbohydrate Polymers, 77*(4), 898–902. https://doi.org/10.1016/j.carbpol.2009.03.013

Shao, W., Wang, S., Liu, H., Wu, J., Zhang, R., Min, H., … Huang, M. (2016). Preparation of bacterial cellulose/graphene nanosheets composite films with enhanced mechanical performances. *Carbohydrate Polymers, 138*, 166–171. https://doi.org/10.1016/j.carbpol.2015.11.033

Shi, C., Hou, X., Li, X., & Ge, M. (2017). Preparation and characterization of persistent luminescence of regenerated cellulose fiber. *Journal of Materials Science Materials in Electronics, 28*(1), 1015–1021. https://doi.org/10.1007/s10854-016-5622-y

Sun, N., Swatloski, R. P., Maxim, M. L., Rahman, M., Harland, A. G., Haque, A., … Rogers, R. D. (2008). Magnetite-embedded cellulose fibers prepared from ionic liquid. *Journal of Materials Chemistry, 18*(3), 283–299. https://doi.org/10.1039/b713194a

Sundberg, J., Guccini, V., Håkansson, K. M. O., Salazar-Alvarez, G., Toriz, G., & Gatenholm, P. (2015). Controlled molecular reorientation enables strong cellulose fibers regenerated from ionic liquid solutions. *Polymer (United Kingdom), 75*, 119–124. https://doi.org/10.1016/j.polymer.2015.08.035

Sundberg, J., Toriz, G., & Gatenholm, P. (2013). Moisture induced plasticity of amorphous cellulose films from ionic liquid. *Polymer, 54*(24), 6555–6560. https://doi.org/10.1016/j.polymer.2013.10.012

Swatloski, R. P., Spear, S. K., Holbrey, J. D., & Rogers, R. D. (2002). Dissolution of cellulose with ionic liquids. *Journal of the American Chemical Society, 124*(18), 4974–4975. https://doi.org/10.1021/ja025790m [pii].

Technical-motion documentation of a resistance machine INSTRON (n.d.).

Teodoro, K. B. R., Migliorini, F. L., Facure, M. H. M., & Correa, D. S. (2019). Conductive electrospun nanofibers containing cellulose nanowhiskers and reduced graphene oxide for the electrochemical detection of mercury(II). *Carbohydrate Polymers, 207* (Ii), 747–754. https://doi.org/10.1016/j.carbpol.2018.12.022

Texter, J. (2014). Graphene dispersions. *Current Opinion in Colloid & Interface Science, 19* (2), 163–174. https://doi.org/10.1016/j.cocis.2014.04.004

Textiles fibres - Determination of breaking force and elongation of individual fibres (ISO 5079:1995). (n.d.).

Textiles-Standard atmospheres for conditioning and testing (ISO 139:2005). (n.d.).

Tian, M., Qu, L., Zhang, X., Zhang, K., Zhu, S., Guo, X., … Sun, Y. (2014). Enhanced mechanical and thermal properties of regenerated cellulose/graphene composite fibers. *Carbohydrate Polymers, 111*, 456–462. https://doi.org/10.1016/j.carbpol.2014.05.016

Wang, S., Lu, A., & Zhang, L. (2016). Recent advances in regenerated cellulose materials. *Progress in Polymer Science, 53*, 169–206. https://doi.org/10.1016/j.progpolymsci.2015.07.003

Yadav, M. (2018). Study on thermal and mechanical properties of cellulose/iron oxide bionanocomposites film. *Composites Communications, 10*(May), 1–5. https://doi.org/10.1016/j.coco.2018.04.010

Yaghoubidoust, F., & Salimi, E. (2019). A simple method for the preparation of antibacterial cotton fabrics by coating graphene oxide nanosheets. *Fibers and Polymers, 20*(6), 1155–1160. https://doi.org/10.1007/s12221-019-8540-1

Yang, H. Y., Jun, Y., & Yun, Y. J. (2019). Ultraviolet response of reduced graphene oxide/ natural cellulose yarns with high flexibility. *Composites Part B Engineering, 163* (November 2018), 710–715. https://doi.org/10.1016/j.compositesb.2019.01.051

Yoon, K. Y., An, S. J., Chen, Y., Lee, J. H., Bryant, S. L., Ruoff, R. S., … Johnston, K. P. (2013). Graphene oxide nanoplatelet dispersions in concentrated NaCl and

stabilization of oil/water emulsions. *Journal of Colloid and Interface Science, 403*, 1–6. https://doi.org/10.1016/j.jcis.2013.03.012

Zhao, H., Jones, C. L., Baker, G. A., Xia, S., Olubajo, O., & Person, V. N. (2009). Regenerating cellulose from ionic liquids for an accelerated enzymatic hydrolysis. *Journal of Biotechnology, 139*(1), 47–54. https://doi.org/10.1016/j. jbiotec.2008.08.009

Nanocomposite Cellulose Fibres Doped with Graphene Oxide and Their Biocidal Properties

Tobiasz Maksymilian Gabryś [1,*] , Beata Fryczkowska [2] , Alicja Machnicka [2] and Tadeusz Graczyk [1]

1 Department of Material Science, Faculty of Materials, Civil and Environmental Engineering, University of Bielsko-Biala, Willowa 2, 43-309 Bielsko-Biala, Poland; tgraczyk@ath.bielsko.pl

2 Department of Environmental Protection and Engineering, Faculty of Materials, Civil and Environmental Engineering, University of Bielsko-Biala, Willowa 2, 43-309 Bielsko-Biala, Poland; bfryczkowska@ath.bielsko.pl (B.F.); amachnicka@ath.bielsko.pl (A.M.)

* Correspondence: tgabrys@ath.bielsko.pl

Abstract: The paper presents a method of obtaining composite cellulose fibres (CEL) doped with graphene oxide (GO) and the influence of GO nanoparticles on the structure and properties of the obtained fibres. Composite fibres (GO/CEL) were prepared using wet method from 5% CEL solutions in 1-ethyl-3-methylimidazolium acetate (EMIMAc) containing GO (0; 0.21; 0.50; 0.98; 1.97% *w/w*) dispersion in N,N-dimethylformamide (DMF). The fibres were coagulated in distilled water and methanol. Optical microscopy allowed us to demonstrate a good degree of GO additive dispersion in the CEL matrix. Surface morphology was examined by scanning electron microscopy (SEM) and infrared spectroscopy (FTIR), which indicated interactions between the matrix and the additive. Strength tests have shown that GO/CEL fibres are characterised by high values of elongation at break (7.7–19.5%) and tenacity (~133–287 [MPa]). The obtained composite fibres are characterized by good biocidal properties against Gram-negative bacteria (*Escherichia coli*), Gram-positive bacteria (*Staphilococcus aureus*), and fungi *Candida albicans*, and the resistance to microorganisms depends on the surface zeta potential value and the isoelectric point (IEP) of GO/CEL fibres.

Keywords: graphene oxide; cellulose; composite fibres; biocidal properties; zeta potential; isoelectric point

1. Introduction

Natural cellulose fibres are produced by the world of plants (e.g., cotton, sisal, jute, hemp). As a result of chemical treatment of wood cellulose, fibres from regenerated cellulose are obtained. There are many cellulose dissolution systems that can dissolve this biopolymer. Some of them include: N-methylmorpholine-N-oxide (NMMO), ionic liquids (ILs), LiCl/N,N-dimethylacetamide (LiCl/DMAc), NaOH aqua solution, alkali/urea and NaOH/thiourea aqueous solution, tetrabutyl ammonium fluoride/dimethyl sulfoxide, metal complex solutions, and molten inorganic salt hydrates [1]. Woven, knitted and non-woven fabrics are made of cellulose fibres and are used for everyday textile products. The hydrophilic and porous structure of cellulose stimulates the attachment and growth of pathogenic bacteria. Therefore, extensive research is being carried out to impart antibacterial properties to cellulose. The simplest method is surface modification of the fibres. Another method is incorporation of biocidal additives into the spinning liquids (in situ) and then forming composite fibres. Ibrahim et al. applied nanoparticles of metal oxides-ZrO, ZnO, and TiO_2 onto the surface of cotton fibres [2], while another team introduced CuO into bacterial cellulose [3]. Other researchers introduced silver nanoparticles in the process of cotton mercerization [4]. Lakshmanan et al. obtained jute fibres coated with silver ions [5]. Rac-Rumijowska described the possibility of introducing silver nanoparticles into the NMMO cellulose spinning solution [6]. The literature also describes more complicated systems in which cotton fabric was modified by the mixture of tetraethoxysilane (TEOS)

and triclosan (TC)-(2,4,4′-trichloro-2′-hydroxydiphenyl ether) or TEOS and quaternary ammonium salt [7].

An interesting and modern material used to prepare polymer composites is graphene oxide (GO), which has many different oxygen-containing functional groups [8]. GO can be easily dispersed in water and organic solvents, e.g., DMF, tetrahydrofuran, and ethylene glycol [9,10]. The diversity of oxygen functional groups arranged on the GO surface makes it easy to be dispersed in polymer with functional groups to form durable bonds [11]. Thanks to its specific structure, graphene oxide has a number of interesting properties. The most important of them are bactericidal and fungicidal properties, used in many composite materials, such as fibres or membranes [12–14]. In general, the development of antimicrobial activity for GO proceeds in three steps: (1) Deposition of nanosheets on the bacterial surface, (2) membrane disruption by sharp nanosheets, and (3) the ensuing superoxide anion-independent oxidation [15,16]. The discussed bactericidal properties result from the interactions between GO and bacterial cells. These involve mechanical damage of cell walls and destruction of lipid layers, resulting in oxidative stress and, consequently, death of a cell [17,18]. The mechanism of the destruction of bacterial and fungal cells by GO is closely determined by such GO properties as: Concentration, particle size, oxygen group content, agglomerate size, chemical purity, and pathogen incubation time [19–21]. The results of the studies by other researchers also indicate a connection between biocidal properties and the surface charge determined on the basis of the surface zeta potential [22]. Thus, the biocidal properties of GO/CEL materials may depend on the surface charge and the isoelectric point value [23].

The literature widely describes various methods of obtaining cellulose composites with the addition of GO. Most reports in the literature concern composites in the form of cellulose membranes [24–26], granules [27,28], hydrogels [29], and aerogels [30] with the addition of GO. Unfortunately, there are few reports describing the use of GO for the production of fibres with biocidal properties. One of the simpler methods is coating cotton fabric with the GO dispersion [31]. Yang et al. coated amine-functionalized cellulose yarn with the GO dispersion [32]. Tian's team produced cellulose composite fibres using the NaOH aqua solution method [33]. Teodoro et al. described the method of creating the GO/CEL nanofibers, which were used as mercury detectors [34]. Other researchers obtained bacterial cellulose in the presence of GO, producing a composite material [35–37].

This paper presents the results of research on cellulose composite GO/CEL fibres, obtained according to the procedure described in our earlier publication [38]. The fibres were formed by wet spinning method using 5% CEL solutions in ionic liquid: 1-ethyl-3-methylimidazolium acetate (EMIMAc) with GO/DMF addition. The process of fibre formation, consisting of extrusion spinning liquid into different baths: Water and methanol. The paper demonstrates the influence of GO additive on the structural and mechanical properties of the obtained composite fibres. It proves the relationship between the surface zeta potential and the isoelectric point, and the biocidal properties of GO/CEL fibres against Gram-negative bacteria (*Escherichia coli*), Gram-positive bacteria (*Staphilococus aureus*), and *Candida albicans* fungi. The obtained composite fibres based on CEL doped with GO may find potential applications in the widely understood medical industry.

2. Materials and Methods

2.1. Materials

Cellulose long fibres C 6663, 1-ethyl-3-methylimidazolium acetate (EMIMAc) 97% (*w/w*) purity, graphite powder <20 μm, and Triton X-100 were purchased from Sigma-Aldrich. Methanol (99.8%), $KMnO_4$, H_2SO_4, with 98% (*w/w*) purity, 30% H_2O_2, *N,N*-dimethyloformamide (DMF) purchased from Avantor Performance Materials Poland S.A. (Gliwice, Poland). All the chemicals were used without further purification.

Graphene oxide was obtained according to modified Hummers method [39]. In brief, 1 g of $NaNO_3$, 46 mL of H_2SO_4, and 2 g of graphite powder were placed in a flask in an ice bath. After stirring for 30 min, 6 g of $KMnO_4$ was added in small portions so that the

temperature of the mixture did not exceed 20 °C. After adding all KMnO$_4$ and waiting for 5 min, the mixture was heated to 35 °C and stirred at this temperature for 4 h. Then, 92 mL of distilled water was carefully added in portions. Finally, the unreacted KMnO$_4$ was removed. For this purpose, 80 mL of distilled water at 60 °C and 50 mL of 30% H$_2$O$_2$ were added. The obtained GO was centrifuged and washed several times with distilled water until the wash water reached pH 7. Wet GO was dried in an oven at 60 °C, turning into a brown solid. The resulting GO powder was dispersed in DMF using an ultrasonic bath to prepare the 2.1% *w/w* GO/DMF dispersion.

2.2. Preparation of Fibres

To prepare spinning solutions, suitable amounts of 2.1% GO/DMF dispersion were introduced into the ionic liquid (EMIMAc), which was followed by intensive stirring for 10 min and sonication for 30 min in an Inter Sonic 1S-1 ultrasonicator at 35 kHz. Suitable amounts of cellulose were introduced into the dispersion thus obtained such that the CEL concentration in each spinning solution was 5%. Then, each solution was mixed thoroughly using a rotary homogenizer and left to deaerate for 24 h. The deaeration process was based on the free removal of air bubbles that moved to the surface of the spinning solutions under atmospheric pressure. The amounts of the ingredients that were used in the preparation of the individual spinning solutions are the same and described in detail in our previous publication [38]. The percentage concentrations of CEL and GO content in individual fibres are shown in Table 1.

Table 1. Percentage concentrations of cellulose fibres (CEL) and graphene oxide (GO) in individual fibres.

Determination of the Obtained Fibres	0	A	B	C	D
W/w conc. of GO in fibre [%]	0	0.21	0.50	0.98	1.97
W/w conc. of CEL in fibre [%]	100	99.79	99.50	99.02	98.03

CEL and GO/CEL fibres were produced via the wet spinning solution method (Figure 1). For this purpose, a KDS-100 single syringe infusion pump (KD Scientific) that was equipped with a 10 mL syringe and a needle with an internal diameter of 0.7 mm was used. The fibre extrusion rate was 0.18 mL/min. The stretch ratio was S = 1. The monofilament take-up velocity was 23 cm/min. The fibres were extruded at room temperature directly into a bath that contained distilled water (1) or methanol (2). The coagulation process lasted 30 min, and subsequently, the fibres were taken up onto a spool and dried with air at 60 °C.
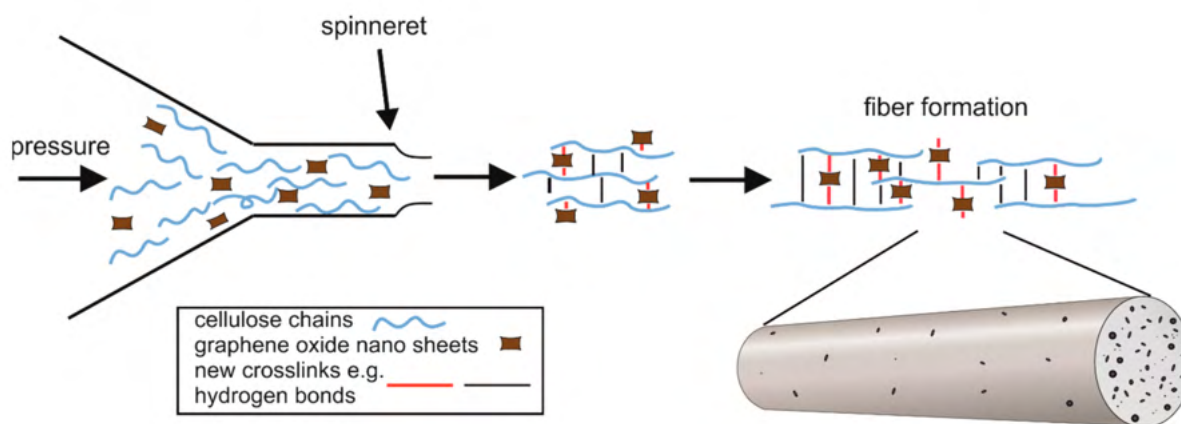

Figure 1. Diagram of the GO/CEL fibre forming process showing the distribution of GO particles in the cellulose matrix.

We know from our own experience in working with GO/CEL membranes that cellulose composites may contain residual ionic liquid inside the material [25]. Therefore, the fibres obtained in the experiment were subjected to the washing process. The washing process of cellulose and nanocomposite fibres was carried out by using the home laundry washing method. The washing solution was prepared by dissolving 1 g of non-ionic surfactants Triton X-100 (Sigma-Aldrich, Poznan, Poland) in 400 mL of distilled water, and the fibres to solution weight ratio was 1:50. The fibres were immersed in a washing solution at 50 °C and mixed for 60 min. After washing, the fibres were rinsed two times in clean water and air dried (Figure 2).

Figure 2. The photo shows pure cellulose fibres (**0**) and GO/CEL composite fibres (**A–D**). The obtained fibres look identical, regardless of the coagulation method (water-1; methanol-2).

2.3. Research Methods Used

The surfaces and cross-sections of the fibres were observed using an optical microscope (OPTA-TECH, Warsaw, Poland) at $10\times$ magnification. Images of the sample were captured using transmission light mode.

Fibre tests were also conducted using a high-resolution Phenom ProX scanning electron microscope (SEM) from Thermo Fisher Scientific (Pik Instruments, Piaseczno, Poland) that was operated at 10 kV. Liquid nitrogen was used to prepare the cross-sections of the fibres, in which the samples were frozen and broken. The fibres' thicknesses were measured from the surface images using FibreMetric software developed by PhenomWorld.

Nicolet 6700 FT-IR spectrometer (Thermo Electron Corp., Madison, WI, USA) equipped with a photoacoustic MTEC model 300 accessory was used in the FTIR (infrared spectroscopy) spectroscopic analysis. The following measurement parameters were used: Resolution, 4 cm^{-1}; spectral range, 500–4000 cm^{-1}; and number of scans, 64. Data collection and post-processing were conducted using the OMNIC software (v. 8.0, Thermo Electron Corp., Madison, WI, USA.).

Raman spectroscopy was performed with a Witec Raman Alpha M300+ spectrometer (WITec Corp., Ulm, Germany), with laser Nd-YAG at 532 nm, a laser power of approximately 1 mW, a spectral resolution of 2 cm^{-1}, and a long working distance objective Olympus LMPLFLN 20X (Olympus Corp., Warsaw, Poland).

The zeta potential was measured using the streaming potential method applied to electrokinetic analyser SurPASS 3 (Anton Paar GmBH, Graz, Austria) according to Helmholtz-Smoluchowski equation Equation (1).

$$\zeta = \frac{dU}{d\Delta p} \times \frac{\eta}{\varepsilon \, x \, \varepsilon_0} \times k \tag{1}$$

where: ζ is calculated zeta potential; U is measured streaming potential; Δp is pressure difference across the sample; η is viscosity of electrolyte solution; ε_0 is vacuum permittivity; ε is dielectric constant of the electrolyte; and k is electrolyte conductivity.

The zeta potential measurements were carried out in a cylindrical cell, into which fibre samples were introduced, then the cell was placed in the testing device and rinsed with electrolyte: 0.001 M KCl. Measurements of the zeta potential were carried out for the pH range of 3 to 10. Appropriate amounts of 0.1 M HCl and then 0.1 M KOH were dosed into the tested solution. Three washing cycles and four zeta potential measurements were performed for each pH value. During the tests, the isoelectric point (IEP) was also determined for each of the tested samples.

The strength parameters were determined by considering the recommendations of ISO 5079 ("Textiles fibres-Determination of breaking force and elongation of individual fibres (ISO 5079: 1995)," n.d.). The measurements were conducted using an Instron testing machine (Model 5544, Norwood, MA, USA) with a compression and stretching head with a measuring range of 0–10 N ("Technical-motion documentation of a resistance machine INSTRON," n.d.). The tests were conducted at a strain rate of 10 mm/min for all samples. To determine the strength parameters, 50 ruptures were conducted for each variant, and a random error that was equal to 2% of the value of the average breaking force was assumed. The measuring distance between the jaws was 20 mm. The testing was conducted under normal climate conditions ("Textiles-Standard atmospheres for conditioning and testing (ISO 139:2005)," n.d.).

The microbiological studies were performed as follows. The specimens were exposed to bacteria and fungi capable of causing human infections, i.e., gram-positive Staphylococcus aureus, gram-negative Escherichia coli, and Candida albicans fungi. Microorganisms (reference strains) were purchased from the American Type Culture Collection (ATCC, Kielpin, Poland). The bacteria were grown on blood agar at $36 \pm 2\,^\circ$C for 24 h. Blood agar is an enriched culture medium. The medium is non-selective, used to grow anaerobic, aerobic, gram-negative, and gram-positive bacteria as well as fungi. The ingredient is agar and most frequently sheep's blood. Candida albicans was grown on Sabouraud agar. Sabouraud medium is used in microbiology to grow fungi. Its basic ingredients include agar, distilled water, growth sources (glucose, peptone), and antibiotics. The latter most often include penicillin, streptomycin, or chloramphenicol, used to inhibit the growth of bacteria, as is the acidic pH. The grown cultures were rinsed with 1 mL of physiological NaCl saline solution. Using a sterile pipette, 0.1 mL of the microorganism suspension was drawn and transferred to selective agars by inoculating "spread plates". In this case, the following media were used to cultivate the microorganisms: Chapman agar-*S. aureus*, MacConkey agar-*E. coli*, and Candida-*C. albicans*.

Chapman agar is a selective-multiplication medium used for the cultivation of staphylococci. It takes advantage of the fact that these bacteria are able to grow in high concentrations of sodium chloride. Chapman agar contains 7.5% NaCl solution (to inhibit the growth of bacteria other than staphylococci), growth sources (broth, peptone), mannitol, and phenol red. MacConkey Agar is a selective medium used in microbiology for the cultivation of gram-negative bacteria. The components that differentiate bacteria are: Lactose and pigments. The crystal violet contents inhibits the growth of gram-positive bacteria, while neutral red colours the lactose-fermenting microorganisms. MacConkey Agar differentiates gram-negative bacteria into lactose-fermenting (Lac+) and non-fermenting (Lac-). Those microorganisms that can ferment lactose contained in agar (e.g., *Escherichia coli*, *Klebsiella* sp.) acidify the medium to a pH value of <6.8. This leads to the formation of red-pink colonies. Lactose-negative bacteria such as Salmonella or Shigella consume peptones; they grow in the form of white/transparent colonies, because neutral red is colourless in neutral pH.

Candida agar, on the other hand, is used for the multiplication and quick identification of Candida yeasts. The cells of individual species, thanks to characteristic enzymes, break down the colour compounds present in the chromogenic mixture and by absorbing

the dyes acquire different colours, which facilitates their identification. The selective factor of the medium, limiting the growth of bacteria, is chloramphenicol and lowered pH.

In the next stage of microbiological studies, samples of whole (1.5 cm long) and comminuted (0.5 mm long) GO/CEL fibres were placed on the central part of Petri dishes (with appropriate agars) (these fibres were test samples). The tests prepared in this way were placed in a laboratory incubator and incubated at the temperature of $36 \pm 2\,°C$ for 24 h. The experiment was performed three times for each type of composite fibre. A control sample (cellulose fibre 01 and 02) was also made. After the incubation process, the zones of inhibition of microorganism growth around the fibres were measured. The growth inhibition zones were analysed using optical microscope equipped with a camera (Opta-Tech, Warsaw, Poland).

3. Results and Discussion

3.1. General Characteristics of Fibres

The paper describes a method of obtaining fibres from pure cellulose and cellulose-based composite fibres with the addition of GO. Fibres were obtained using wet method from cellulose solution in EMIMAc, by coagulation in water (1) or methanol (2).

The molecular structure of the fibres surface was investigated using the FTIR spectroscopy. FTIR studies performed for the fibre samples after the washing process allowed for the evaluation of the ionic liquid removal. The spectra of pure cellulose and composite fibres did not differ from the spectra obtained for the CEL and GO/CEL membranes described in our earlier publication [40]. The results of the study are summarized in Table 2.

Table 2. Summary of the most important bonds appearing in the infrared spectroscopy (FTIR) spectra of CEL and GO/CEL fibres.

Samples	The FTIR Peaks (cm^{-1}) *	Bond Type
All fibres	3400–2400	Wide band of the elastic O–H vibrations in the hydrogen bonds
All fibres	2900	Stretching vibrations of the C–H oscillator
Composite fibres	1645 (1); 1637 (2)	Vibration of C=O groups in GO
All fibres	1160	Asymmetric stretching vibrations of C–O–C in the pyranose ring
All fibres	1115 (1); 1117 (2)	Oscillation of etheric C–O–C groups between the pyranose rings

Where *: (1)—fibres coagulated in water; (2)—fibres coagulated in methanol.

FTIR spectroscopy (Table 2) indicated that the fibres obtained by coagulation in water (1) and in methanol (2) did not differ in their chemical structure and contained the same bands. The characteristic wide band ($3700 \div 2400$ cm^{-1}) of the elastic O–H indicating the formation of hydrogen bonds between GO and CEL. The GO addition probably causes loosening of the structure between cellulose macromolecule chains and introduces additional hydroxyl groups. For GO/CEL composite fibres, band intensities are observed at a wavelength of approximately 1640 cm^{-1} corresponding to the vibration of C=O groups in GO along with the amount of GO introduced to the cellulose fibres [41]. However, the 1404 cm^{-1} band, which is characteristic for this ionic liquid, was not observed [42]. The absence of this band was confirmed through the removal of EMIMAc from the fibres in the washing process. Our studies showed no significant shifts or changes in the peaks, indicating the incorporation of GO probably did not result in any change in the chemical structures of cellulose [43]. To investigate the interaction between cellulose and GO, Raman spectra of the GO and GO/CEL were performed. The GO displayed two characteristic peaks at ~1315 cm^{-1} (D peak) and ~1590 cm^{-1} (G peak), respectively. No shift was observed in the GO/CEL composite like in other publications [44].

The method of GO dispersion in the CEL matrix influences physicochemical, structural, and functional properties of composite fibres. Optical microscopy allows a quick analysis of the structure of the examined fibres (Figure 3). The pure cellulose fibres (01; 02) are smooth and transparent in the longitudinal view. Transmission mode optical microscopy enabled the observation of the presence of GO inclusions in GO/CEL composite fibres (Figure 3). The more GO (0.21; 0.5; 0.98; and 1.97 % *w/w*) was added into the GO/CEL fibre, the darker the sample. GO is well dispersed throughout the entire volume of the GO/CEL composite.
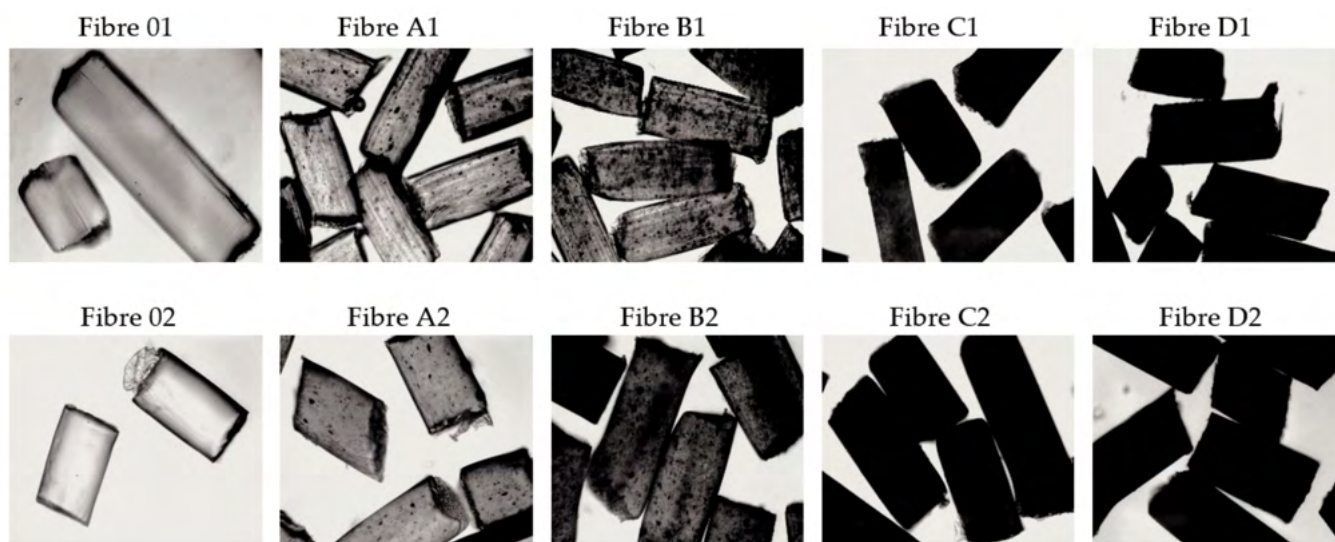
Figure 3. Optical microscope images of the surfaces of fibres that were coagulated in water (1) and in methanol (2) (10× magnification).

SEM microscopy (Figure 4) allowed us to analyse the surface of pure cellulose fibres (0–1; 0–2) and GO/CEL fibres coagulated in water (1) and in methanol (2). The pictures show that all the fibres coagulated in methanol (2) in general have a smooth surface and fine efflorescence. The more GO in composite fibres (2), the less surface efflorescence and more shallow cracks along the fibre. On the other hand, the fibres coagulated in water (1) show numerous grooves extending along the fibre. The more GO in the fibres (1), the deeper and more numerous the cracks on the surface. The surface morphology of the examined fibres is the result of the fibre coagulation method. The use of methanol results in almost immediate precipitation of the fibres in the coagulation bath. The coagulation of the fibres in water, in turn, is a slower process, and the slow penetration of the fibre can lead to the formation of a porous structure. We described similar observations for GO/CEL composite membranes, examining the effect of the coagulant and the amount of GO additive on their porosity [40].

The diameter of all obtained fibres before (nw) and after the washing process was measured using the FibreMetric software. An example of tests on a selected sample is shown in Figure 5, and the obtained results of thickness measurements are summarized in Table 3.
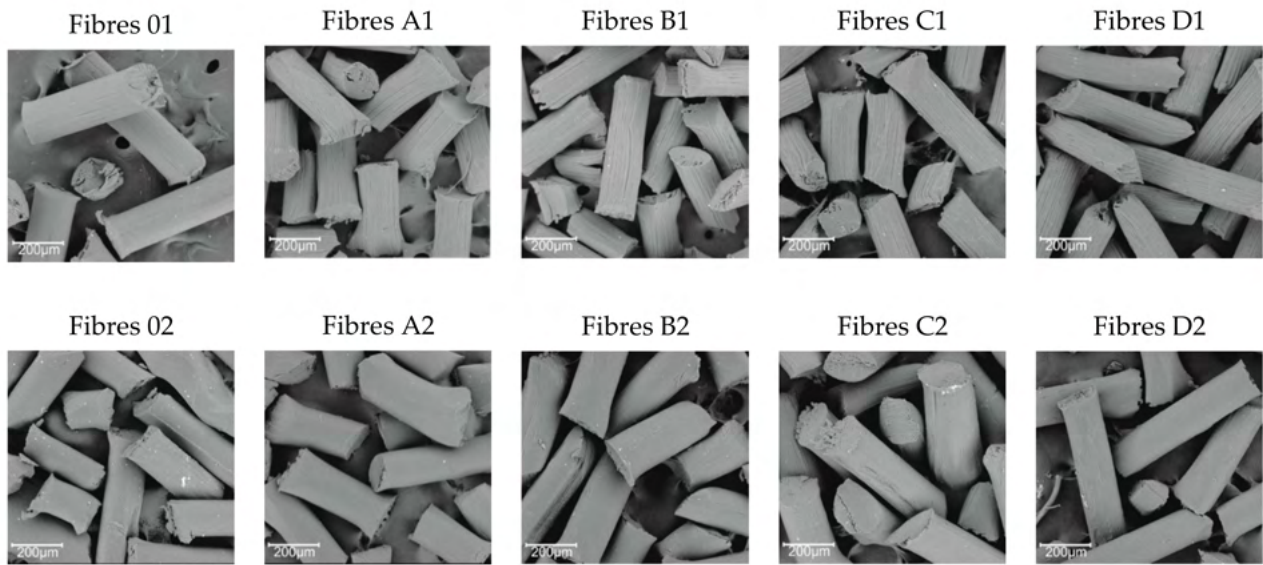
Figure 4. SEM (scanning electron microscopy) images for surfaces fibres that were coagulated in water (1) and methanol (2) (300× magnification).
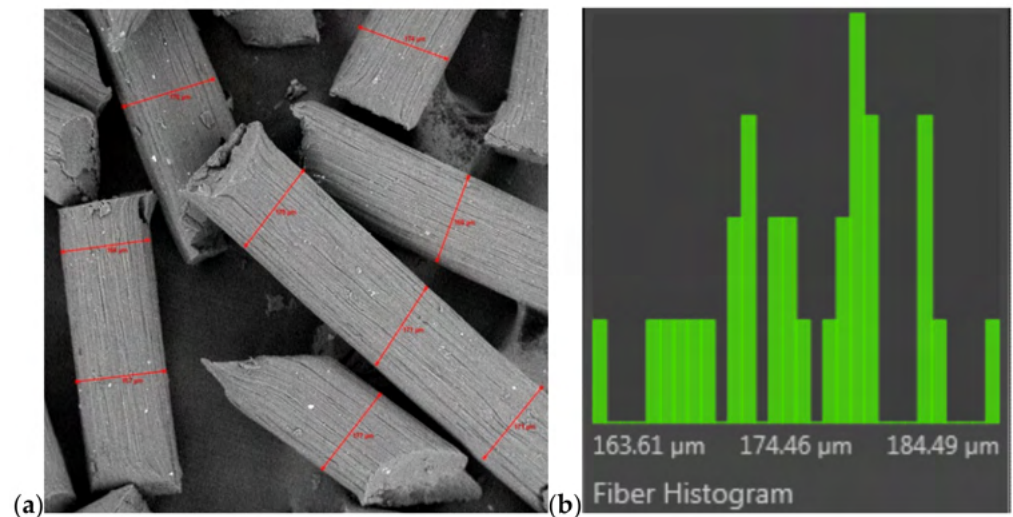

Figure 5. A measurement of thickness fibres by using the FibreMetric software; (**a**) surface of fibres (300× magnification) and (**b**) histogram (an example for fibres C1).

Table 3. Summary of the median values of results of the fibre thickness measurements.

Fibre Thickness (before Washing) (μm)									
01nw	A1nw	B1nw	C1nw	D1nw	02nw	A2nw	B2nw	C2nw	D2nw
183 ± 6	175 ± 6	174 ± 8	174 ± 5	165 ± 5	156 ± 14	182 ± 7	187 ± 8	186 ± 8	180 ± 7
Fibre Thickness (after Washing) (μm)									
01	A1	B1	C1	D1	02	A2	B2	C2	D2
169 ± 6	151 ± 5	156 ± 7	148 ± 5	147 ± 7	141 ± 7	163 ± 12	165 ± 4	165 ± 8	150 ± 9

nw—sample not washed.

The process of coagulation of fibres in methanol (Table 3—not washed fibres "nw") is relatively fast. The polarity of this solvent is 1.7 [D], which accelerates the coagulation process of 02 fibres. On the other hand, the coagulation of 01 fibres in water is closely related to the polarity of the water molecule, which is 1.85 [D], slowing down the process of washing away the ionic liquid. The effect of these interactions is the thickness of CEL fibres, which is: 156 μm and 183 μm (for 02nw fibres and 01nw fibres), respectively. The thicknesses of GO/CEL fibres (Table 3—not washed fibres "nw"), on the other hand, have slightly different values, which may be related to interactions at the molecular level. Thus, a general conclusion can be drawn that the more GO additive, the more interactions between CEL and GO and between GO nanoparticles themselves. The discussed interactions were observed as a broad band of 3400–2400 cm^{-1} (Table 2). While interactions between GO nanoparticles, which resulted in the formation of agglomerates, were observed in Figure 3.

When analysing the results of the fibres' thickness measurements after the washing process (Table 3—fibres after washing), it can be observed, as a general tendency, that this process reduces the thickness of all the tested fibres. During washing, individual fibres lose 7–15% of their thickness. The observed phenomenon is probably the result of the removal of the ionic liquid (EMIMAc) from the inside of the fibres, which was confirmed by FTIR studies (Table 2).

Some regularities can be observed when comparing the thicknesses of all the composite fibres listed in Table 3. For samples A1, B1, A2, and B2, a slight increase in thickness is observed as the amount of GO addition increases. On the other hand, the thickness of the 1.97% GO fibres is lower than in the C1 and C2 samples. This phenomenon is probably the result of an excess of GO addition, which causes the formation of large amounts of agglomerates in samples D1 and D2.

The obtained results prompted us to analyse the influence of the fibre formation process, the composition of the spinning solution, and the washing process on the mechanical properties of the produced CEL and GO/CEL fibres.

First, elongation at break was analysed for all fibres tested before the washing process (Table 4—fibres before washing). The studies have shown that for the fibres coagulated in water (1), the elongation at break values are low. Apart from this, there are no significant dependencies between elongation at break for individual fibre samples. Elongation at break for pure cellulose (01nw) was ~10%, for composite fibres (A1nw-C1nw) it was ~7–~14%, while for sample D1nw it had the lowest value of ~5%. For composite fibres obtained by the second method (2), there is a clear increase in elongation at break to the value of ~20% for A2nw-C2nw fibres, i.e., fibres containing 0.21–0.98% *w/w* of GO. On the other hand, for the D2nw fibres and for the 02nw fibres, the elongation at break values are similar, i.e., ~10%. Therefore, it can be concluded that the addition of 1.97% *w/w* of GO to the cellulose matrix is too much.

The same studies were carried out for the samples of washed fibres (Table 4—fibres after washing). It turned out that the washing process increases elongation at break by about 80% for the fibres coagulated in methanol (02). For fibres 01, the increase was also present, but at ~30%. The obtained results are higher than those described in the work by Cao et al. [45]. However, for all composite fibres, a decrease in elongation at break as a function of increasing amount of GO was noted. All values of elongation at break for CEL and GO/CEL fibres fall within the range characteristic for commercial cellulose fibres, i.e., 6–10% [46].

Table 4. Mechanical test results.

	Fibres before Washing [38]				Fibres after Washing		
	E (%) *	W (MPa) *	M (GPa) *		E (%)	W (MPa)	M (GPa)
01nw *	10.01 ± 2.37	137.22 ± 34.36	35.67 ± 3.06	**01**	13.05 ± 0.92	223.61 ± 13.28	7.91 ± 0.07
A1nw *	12.79 ± 0.53	149.35 ± 6.66	59.00 ± 3.88	**A1**	11.9 ± 1.37	188.92 ± 25.87	7.41 ± 0.45
B1nw *	7.44 ± 1.01	165.86 ± 13.91	62.69 ± 3.55	**B1**	9.5 ± 1.45	219.70 ± 20.06	8.52 ± 0.59
C1nw *	14.32 ± 1.10	95.80 ± 4.38	48.92 ± 6.57	**C1**	8.75 ± 0.51	132.75 ± 11.11	5.30 ± 0.51
D1nw *	5.12 ± 0.49	111.38 ± 6.78	70.30 ± 4.55	**D1**	7.45 ± 0.77	167.26 ± 9.23	6.97 ± 0.70
02nw *	10.87 ± 2.21	88.06 ± 25.18	35.99 ± 4.02	**02**	10.25 ± 1.90	228.67 ± 28.05	8.81 ± 0.91
A2nw *	20.06 ± 4.51	202.11 ± 25.27	53.70 ± 4.09	**A2**	8.55 ± 1.34	287.32 ± 20.01	10.71 ± 0.82
B2nw *	19.54 ± 3.93	224.33 ± 15.72	83.34 ± 3.89	**B2**	7.7 ± 1.41	172.16 ± 13.75	6.56 ± 0.55
C2nw *	19.93 ± 1.41	154.54 ± 6.20	92.51 ± 6.30	**C2**	7.65 ± 1.01	189.65 ± 15.21	7.41 ± 0.69
D2nw *	10.27 ± 1.61	146.31 ± 8.46	81.91 ± 3.49	**D2**	19.55 ± 1.25	193.41 ± 21.09	6.25 ± 0.69

where: *—is nw-not washed sample, E—elongation at break; W—tenacity; M—elastic modulus.

Analysing the tenacity results for GO/CEL fibres (Table 4), it is evident that the fibre samples coagulated in methanol (2)—both not washed and washed—generally have higher tenacity values as compared to the corresponding samples of fibres coagulated in water (1). Moreover, for all series of composite fibres, the tenacity increase is observed as the GO content rises to 0.5% *w/w*, then it decreases with its lowest values for samples containing 1.97% of GO. The observed tenacity changes are similar to the changes in the thickness of the examined fibres (Table 3). These studies show that during the process, a reconstruction of the internal structure takes place, accompanied by an increase in fibres tenacity and elongation at break. Comparing the obtained results with the literature data [46], it can be concluded that the obtained fibres have good tenacity, higher than that of regenerated cellulose, which is 69–170 [MPa].

The next area of study was determining the elastic modulus (Table 4). This parameter has higher values for all samples of unwashed fibres (nw), and after the washing process, all values of the elastic modulus drop sharply, e.g., by 83% for fibres 02 and 93% for fibres C2. Therefore, it can be assumed that during washing, the components responsible for fibre stiffness are washed out of all the tested fibres. The elastic modulus values for GO/CEL fibres do not depend on the coagulant (water or methanol) used in the fibre formation process. However, they are slightly dependent on the amount of GO addition in the cellulose matrix. As the content of GO in unwashed fibres (nw) increases, so do the values of the elastic modulus. On the other hand, the opposite is true for unwashed fibres. The most interesting case are fibres containing 0.5% of GO additive in the cellulose matrix. In all tests of their mechanical properties, the results of B1 and B2 differ from the others, which may indicate that these composite fibres are characterized by the best quantitative composition.

3.2. Biocidal Properties of GO/CEL Fibres

Microbiological studies were carried out for both GO/CEL fibres and for the corresponding pure cellulose fibres. The following human pathogens were selected for the study: Gram-negative bacteria (*E. coli*), gram-positive bacteria (*S. aureus*), and fungi (*C. albicans*), and the sample photos taken with an optical microscope are presented in Figure 6.
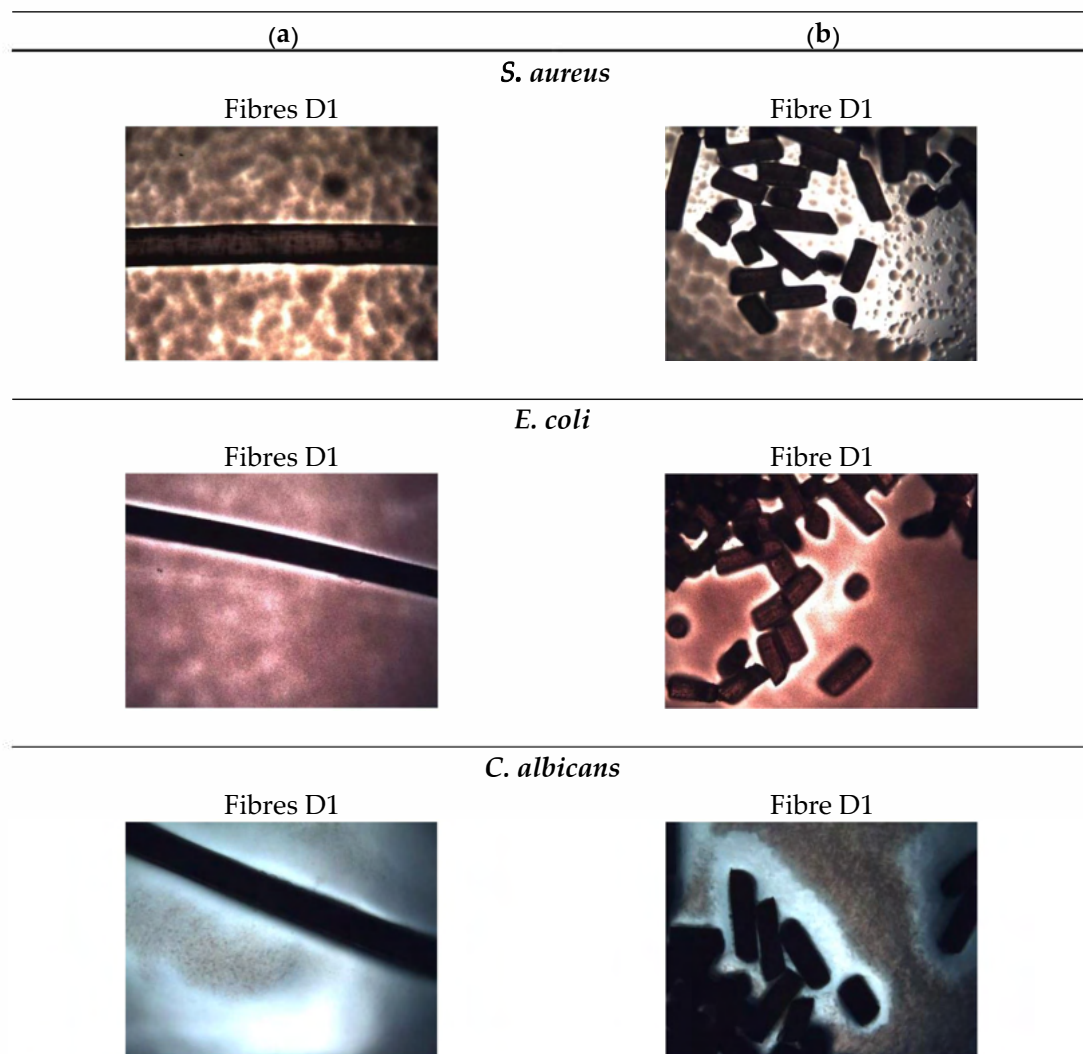
Figure 6. Photographs of microbiological tests of fibres with the highest amount of GO (D1). The photos show the tests for samples of: (**a**) Whole fibres; (**b**) fibre sections. The photos were taken after 24 h of *S. aureus*, *E. coli*, and *C. albicans* incubation.

At the beginning, the impact of composite fibres on the multiplication or stopping the growth of Gram-negative *E. coli bacteria* was analysed. For GO/CEL fibres, the size of the *E. coli* inhibition zones depends on the form of the test sample. In general, samples coagulated in water A1–D1 and tested in the form of whole fibres (Figure 7a) have inhibition zones ranging from ~39.9 μm to ~64.4 μm, which increase as the concentration of GO in the fibres increase. The same fibres, but prepared in the form of small sections (Figure 7b), are characterized by slightly larger inhibition zones, which range from ~59.2 μm to ~72.8 μm. The test results obtained for GO/CEL fibres coagulated in methanol (2) A2–D2 were similar. The fibres tested as a whole (Figure 7c) were characterized by inhibition zones in the range of ~50.7–~67.6 μm. Whereas the same fibres, but cut into small lengths (Figure 7d), demonstrated the inhibition zones from ~47.9 μm to ~93.9 μm. It could, therefore, be concluded that the inhibition of *E. coli* multiplication is more intense if the GO/CEL fibre samples are cut into pieces.
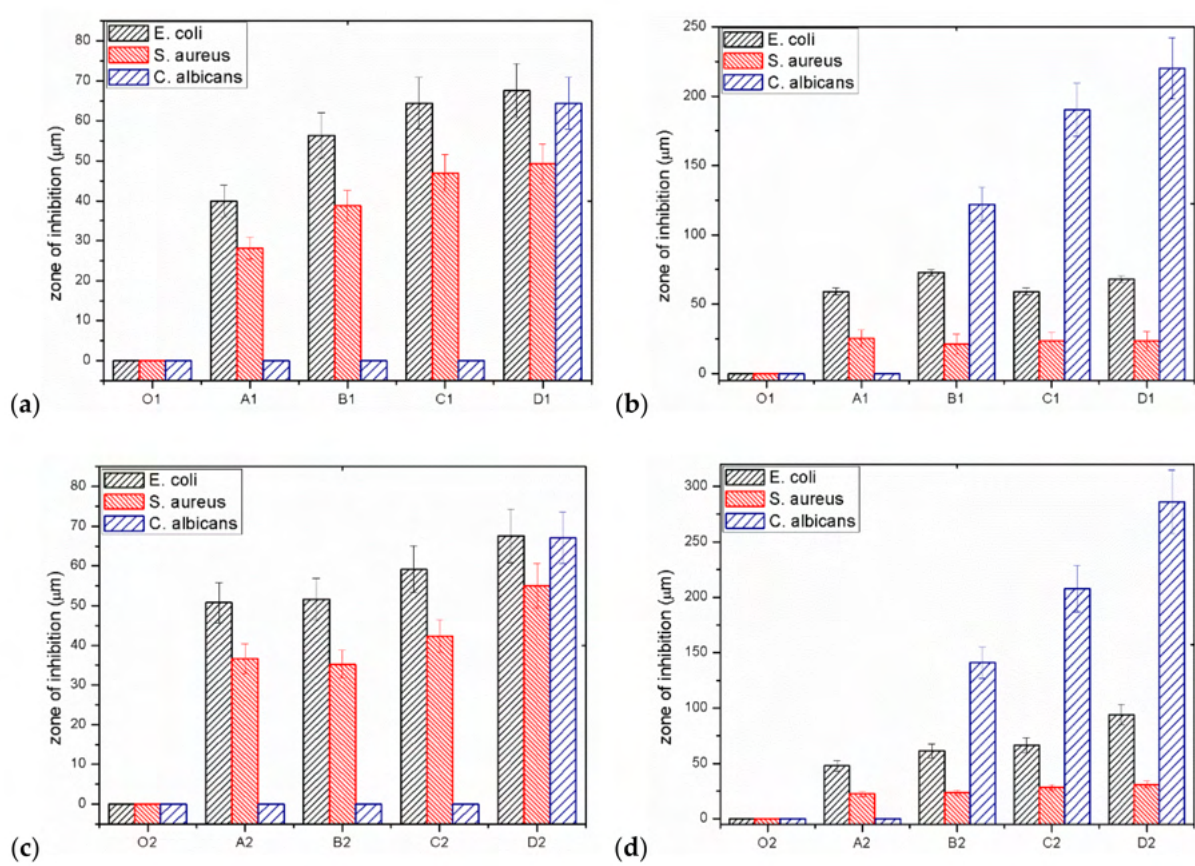
Figure 7. Results of the inhibition zone measurements for individual micro-organisms: (**a**) Whole fibres; (**b**) short sections of water coagulated fibres (1); (**c**) whole fibres; (**d**) short sections of fibres coagulated in methanol (2).

Another tested microorganism was the gram-positive bacteria, *S. aureus*. Additionally, in this case, the size of the inhibition zones of *S. aureus* depends on the form of the test sample. Samples coagulated in water A1–D1, tested in the form of whole fibres (Figure 7a), are characterized by inhibition zones from ~28.2 μm to ~49.3 μm. The same samples, but in the form of staple fibres (Figure 7b), have smaller inhibition zones ranging from ~21.1 μm to ~25.4 μm. On the other hand, the test results obtained for the GO/CEL fibres coagulated in methanol (2) A2–D2 showed that the fibres tested as a whole (Figure 7c) were characterized by inhibition zones range of ~35.2–~47.0 μm. Whereas the same fibres, but cut into small lengths (Figure 7d), demonstrated slightly smaller inhibition zones ranging from ~23.5 μm to ~31.0 μm. The conclusion of the studies would be that the inhibition of *S. aureus* multiplication is more intense on the surface of GO/CEL fibres.

The last microorganisms used were fungi, *C. albicans*. The results of the tests presented in Figure 7a,c show that the fungus multiplication stops when the composite fibre samples (D1, D2) contain the highest amount of GO addition (1.97% *w/w*). For samples of fibres cut into sections (Figure 7b,d), on the other hand, the degree of stopping the pathogen multiplication increases with the increase in the content of the GO additive. In the studies of fibres coagulated in water (Figure 7b), the inhibition zone of *C. albicans* is high, ranging from ~122.1 μm to ~220 μm, and includes samples containing 0.5–1.97% *w/w* of GO. While for fibres coagulated in methanol (Figure 7d), the degree of inhibition is in the range of ~140.9 μm to ~286.4 μm for fibre samples: B2; C2; D2. It should therefore be concluded that the inhibition of *C. albicans* multiplication is more intense if GO/CEL fibre samples are cut into pieces and contain at least 0.5% of GO in the cellulose matrix.

Measurements of the microorganism inhibition zones (Figure 7) showed that even a small addition of GO results in a biocidal effect. The greater the effect is, the higher the concentration of GO in the tested fibres. In contrast, for the reference fibre samples (01 and

02), as expected, no inhibition zones were found. An interesting phenomenon is also the divergence in the width of the inhibition zones between the fibre samples with the same compositions, but a different coagulant. These differences may result from the structure of the fibre surface as observed using SEM in Figure 4. All fibres coagulated in methanol have a smooth surface, and those coagulated in water have fine grooves, which may hinder the access of bacteria to their surface.

The general conclusion of the microbiological studies is that for all GO/CEL fibres, the size of the inhibition zones depends on the method of sample preparation and takes the highest values for fibres cut into sections (Figure 7b,d). The explanation for this phenomenon can be found in the anatomical structure and properties of individual microorganisms.

E. coli have a rod shape of 2×0.8 μm and are composed of a thin cell membrane. The shape of the bacterial allows it to adhere to the surface and to the cross-section of the GO/CEL fibre (Figure 8). The microscopic studies (Figure 3) show that GO particles are present on the surface of composite fibres in a small amount only. However, smaller and larger clusters of these nanoparticles occur inside of the fibres. The knowledge of the structure of GO/CEL fibres and the structure of *E. coli* cells allows us to understand the phenomenon of stopping the growth of this pathogen. The smaller inhibition zone observed in Figure 7a,c results from the presence of GO that is lower on the surface than inside the fibre (Figure 7b,c).
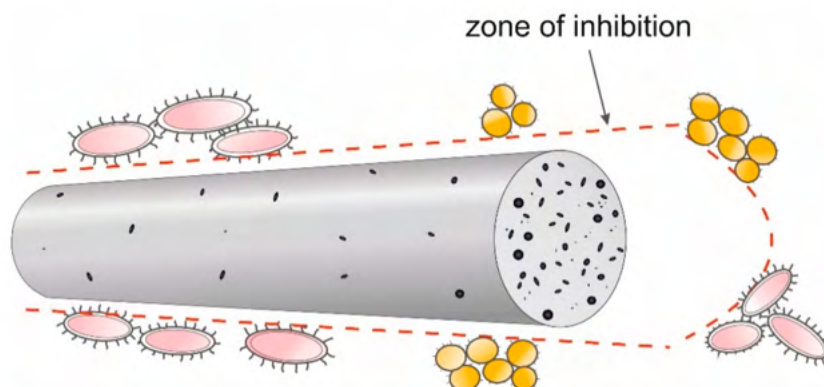
Figure 8. Model of pathogen cell destruction on the surface and at the cross-section of the fibre.

S. aureus bacteria, on the other hand, are spherical in shape, with dimensions of 1×0.8 μm and a thick cell wall. All these factors make the pathogen difficult to be destroyed by GO nanoparticles, both on the surface and in the cross-sections of GO/CEL fibres (Figure 8). This results in smaller inhibition zones that are observed in Figure 7.

C. albicans is a fungus which in the presence of sugars—in our case cellulose—forms a biofilm that sticks tightly to the surface of the fibre. Only a large amount of GO in the cellulose matrix inhibits its development. Therefore, the surfaces of composite fibres containing 1.97% of GO (Figure 7a,c), and the cross-sections of fibres containing 0.5% to 1.97% of GO, are resistant to *C. albicans* (Figure 7b,d).

The conducted microbiological tests clearly indicate the bactericidal effect of GO. Its mechanism can be explained in two ways. The first one concerns the mechanical damage to the bacterial cell walls, which in turn leads to metabolic disorders, oxidative stress, and cell death. This process is widely described by many researchers, among others in [47,48]. The second mechanism of GO influence on microorganisms is relatively little known. It consists in introducing surface functional groups that change the surface charge properties of materials. The functional groups in GO are hydroxyl and carboxyl groups, which determine its negative charge (zeta potential ~39 mV). This affects the surface charge parameter and, consequently, the isoelectric point (IEP) [22]. The experimental works

described in the literature indicate the link of IEP with antimicrobial activity [23], therefore we analysed the zeta potential of the GO/CEL fibre surface.

The dependence of the degree of bactericidal properties on the zeta potential was determined based on the isoelectric point (IEP) of the CEL and GO/CEL fibres. For this purpose, measurements of the zeta potential of all obtained fibres were performed in the pH range of 3 to 10, and the results are summarized in Figure 9. Pure CEL fibres, as compared to composite fibres, show a more negative zeta potential value, which results from the large number of hydroxyl groups present in cellulose. The addition of GO (which also has numerous oxygen groups) to the cellulose matrix causes the formation of hydrogen bonds between cellulose and graphene oxide. As a result, as the concentration of GO in the fibres increases, the acidic nature of the GO/CEL fibres decreases, which is expressed by a change in the shape of the $\zeta = f$ (pH) curve into a more inert one. It is related to the shift of the IEP towards higher pH values and the "flattening" of the curve [49].
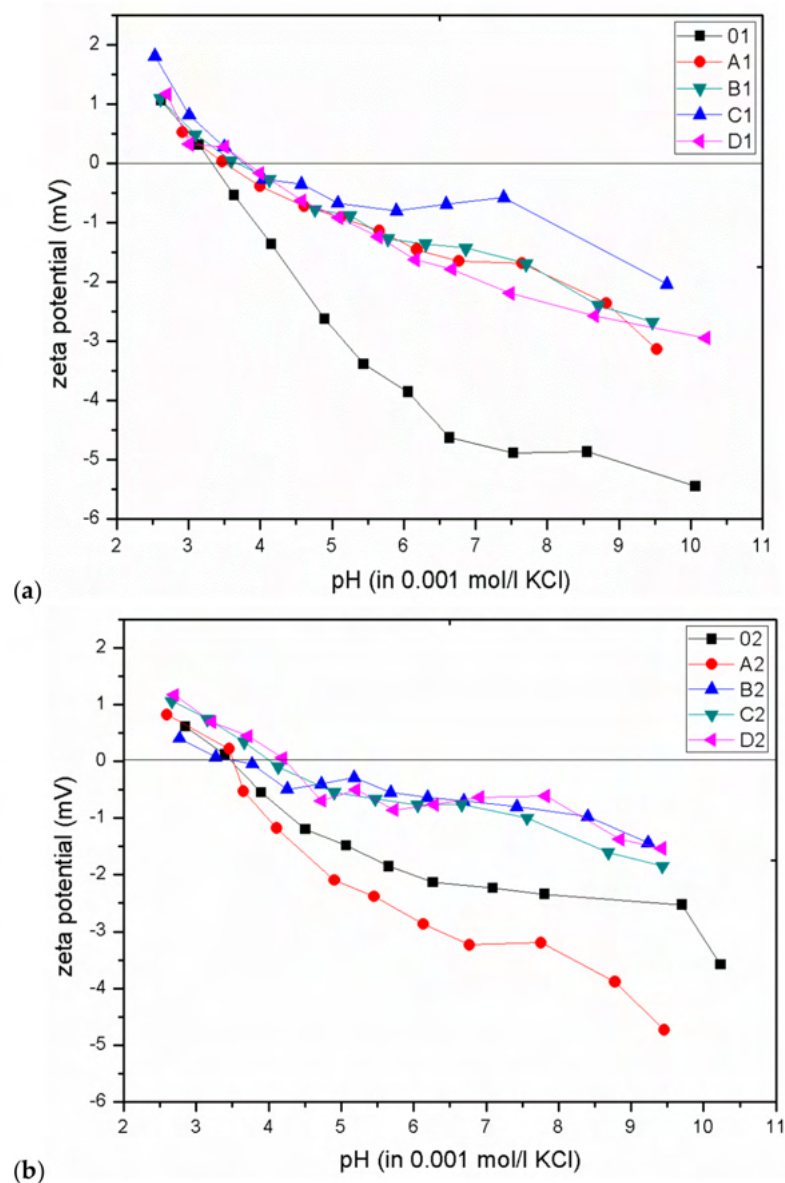
Figure 9. The dependence of the zeta potential on the pH value for CEL and GO/CEL fibres coagulated in water (**a**) and methanol (**b**). Straight line designates the isoelectric point (IEP) (where $\zeta = 0$ mV).

The bactericidal properties of GO/CEL fibres mainly result from the increase in the IEP value, which is confirmed by the work of other researchers [22,23]. Analysis of the our research shows that for fibres coagulated in water (01; A1; B1; C1; D1), the IEP values are within in the range of 3.3–3.8. On the other hand, for fibres coagulated in methanol (02; A2; B2; C2; D2), the IEP values range from 3.5 to 4.2. In both cases, the IEP values increase with the increase of GO concentration in composite fibres. The relationship between the IEP value and the size of the pathogen inhibition zones for all obtained fibres is shown in Figure 10.
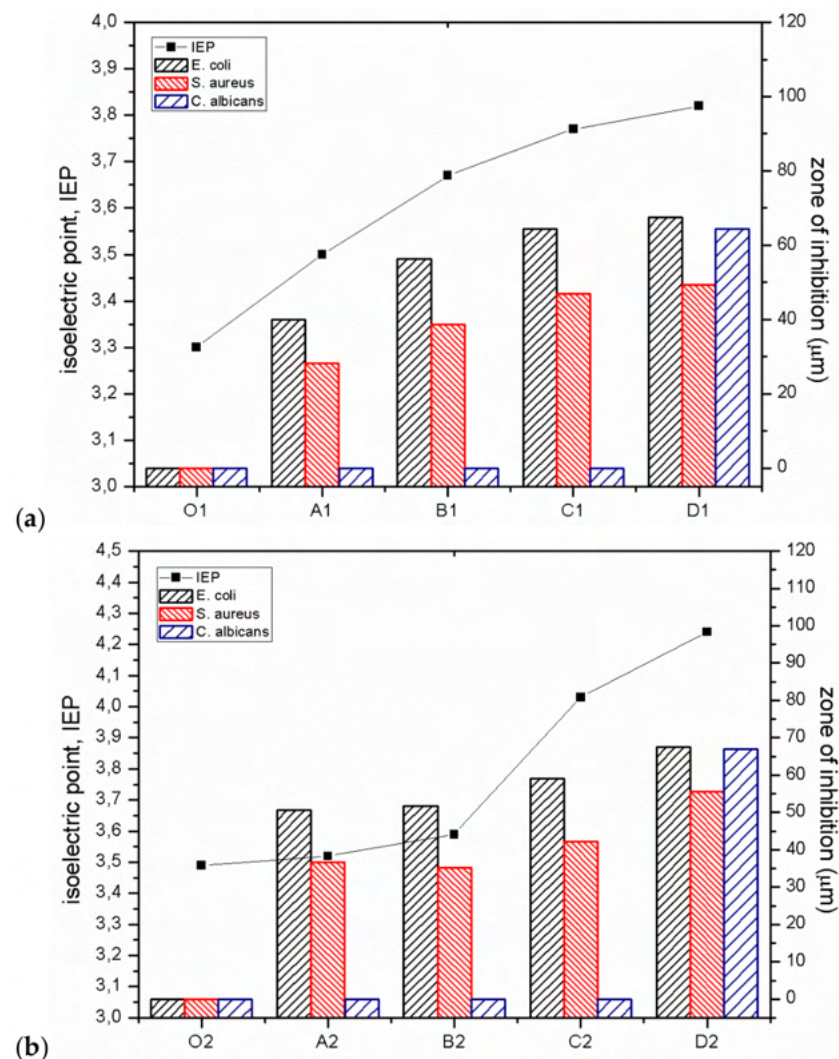
Figure 10. Antimicrobial activity (shown as the zone of inhibition) and IEP of CEL and GO/CEL fibres coagulated in water (**a**) and coagulated in methanol (**b**) on bacteria *E. coli*, *S. aureus*, and fungi *C. albicans*.

The results of the research indicate a close correlation between the IEP value and bactericidal properties (Figure 10), both in the case of gram-negative (*E. coli*) and gram-positive (*S. aureus*) bacteria. It was observed that an increase in IEP results in increased bactericidal activity. This relationship is very well visible for fibres coagulated in water (Figure 10a), but also in the case of fibres coagulated in methanol (Figure 10b). The reduction of the negative surface charge of composite fibres (Figure 9) and the higher value of the zeta potential are accompanied by the bactericidal effect. This effect is caused by the formation of hydrogen bonds and electrostatic interactions between the surface of GO/CEL fibres and the bacterial cell wall, which prevents the absorption of nutrients and causes cell

death [15,50]. Therefore, electrostatic interactions between GO/CEL fibres and the negative surface charge of bacteria are possible, which inhibits the growth of bacteria [51].

4. Conclusions

A simple method of obtaining composite fibres containing a wide range of concentrations of GO (from 0.21% to 1.97%) in the CEL matrix was developed. The method enables good dispersion of the nano-additive in the polymer matrix, which was confirmed by optical microscopy. The addition of nanoparticles also influenced the mechanical properties of the formed GO/CEL fibres. Composite fibres were characterized by high elongation at break and tenacity. FTIR studies enabled us to observe the formation of GO-CEL intermolecular hydrogen bonds. An additional feature of GO/CEL fibres are biostatic properties, confirmed by the study, preventing the development of bacteria (*E. coli* and *S. aureus*) and fungi (*C. albicans*) on their surface and cross-section. The size of the inhibition zones is proportional to the concentration of GO in the fibres. The zeta potential study allowed us to determine the surface charge and IEP values, the increase of which is responsible for the increased biocidal effect of GO/CEL fibres. The obtained composite fibres based on CEL doped with GO may find potential applications in the widely understood medical industry.

Author Contributions: Conceptualization. T.M.G. and B.F.; methodology. T.M.G. and B.F.; validation. T.M.G., A.M., T.G.; formal analysis. T.M.G. and B.F.; investigation. T.M.G., A.M., T.G.; writing—original draft preparation. T.M.G. and B.F.; writing—review and editing. T.M.G. and B.F.; visualization. T.M.G. and B.F.; supervision. B.F.; project administration. B.F. All authors have read and agreed to the published version of the manuscript.

Institutional Review Board Statement: Not applicable.

Informed Consent Statement: Not applicable.

Conflicts of Interest: The authors declare no conflict of interest.

References

1. Wang, S.; Lu, A.; Zhang, L. Recent advances in regenerated cellulose materials. *Prog. Polym. Sci.* **2016**, *53*, 169–206. [CrossRef]
2. Ibrahim, N.A.; Eid, B.M.; El-Aziz, E.A.; Abou Elmaaty, T.M.; Ramadan, S.M. Multifunctional cellulose-containing fabrics using modified finishing formulations. *RSC Adv.* **2017**, *7*, 33219–33230. [CrossRef]
3. Almasi, H.; Jafarzadeh, P.; Mehryar, L. Fabrication of novel nanohybrids by impregnation of CuO nanoparticles into bacterial cellulose and chitosan nanofibers: Characterization, antimicrobial and release properties. *Carbohydr. Polym.* **2018**, *186*, 273–281. [CrossRef] [PubMed]
4. Tang, B.; Kaur, J.; Sun, L.; Wang, X. Multifunctionalization of cotton through in situ green synthesis of silver nanoparticles. *Cellulose* **2013**, *20*, 3053–3065. [CrossRef]
5. Lakshmanan, A.; Chakraborty, S. Coating of silver nanoparticles on jute fibre by in situ synthesis. *Cellulose* **2017**, *24*, 1563–1577. [CrossRef]
6. Rac-Rumijowska, O.; Fiedot, M.; Karbownik, I.; Suchorska-Woźniak, P.; Teterycz, H. Synthesis of silver nanoparticles in NMMO and their in situ doping into cellulose fibers. *Cellulose* **2017**, *24*, 1355–1370. [CrossRef]
7. Foksowicz-Flaczyk, J.; Walentowska, J.; Przybylak, M.; Maciejewski, H. Multifunctional durable properties of textile materials modified by biocidal agents in the sol-gel process. *Surf. Coat. Technol.* **2016**, *304*, 160–166. [CrossRef]
8. Guerrero-Contreras, J.; Caballero-Briones, F. Graphene oxide powders with different oxidation degree, prepared by synthesis variations of the Hummers method. *Mater. Chem. Phys.* **2015**, *153*, 209–220. [CrossRef]
9. Konkena, B.; Vasudevan, S. Understanding aqueous dispersibility of graphene oxide and reduced graphene oxide through p K a measurements. *J. Phys. Chem. Lett.* **2012**, *3*, 867–872. [CrossRef]
10. Texter, J. Graphene dispersions. *Curr. Opin. Colloid Interface Sci.* **2014**, *19*, 163–174. [CrossRef]
11. Ghosh, T.; Biswas, C.; Oh, J.; Arabale, G.; Hwang, T.; Luong, N.D.; Jin, M.; Lee, Y.H.; Nam, J. Do Solution-processed graphite membrane from reassembled graphene oxide. *Chem. Mater.* **2012**, *24*, 594–599. [CrossRef]
12. Liu, S.; Zeng, T.H.; Hofmann, M.; Burcombe, E.; Wei, J.; Jiang, R.; Kong, J.; Chen, Y. Antibacterial activity of graphite, graphite oxide, graphene oxide, and reduced graphene oxide: Membrane and oxidative stress. *ACS Nano* **2011**, *5*, 6971–6980. [CrossRef] [PubMed]
13. Machnicka, A.; Fryczkowska, B. Bioactive membranes from cellulose with a graphene oxide admixture. *J. Ecol. Eng.* **2018**, *19*, 231–240. [CrossRef]

14. Fryczkowska, B.; Machnicka, A.; Biniaś, D.; Ślusarczyk, C.; Fabia, J. The influence of graphene addition on the properties of composite rGO/PAN membranes and their potential application for water disinfection. *Membranes* **2020**, *10*, 58. [CrossRef] [PubMed]

15. Tang, J.; Chen, Q.; Xu, L.; Zhang, S.; Feng, L.; Cheng, L.; Xu, H.; Liu, Z.; Peng, R. Graphene Oxide–Silver Nanocomposite As a Highly Effective Antibacterial Agent with Species-Specific Mechanisms. *ACS Appl. Mater. Interfaces* **2013**, *5*, 3867–3874. [CrossRef]

16. Anand, A.; Unnikrishnan, B.; Wei, S.C.; Chou, C.P.; Zhang, L.Z.; Huang, C.C. Graphene oxide and carbon dots as broad-spectrum antimicrobial agents-a minireview. *Nanoscale Horiz.* **2019**, *4*, 117–137. [CrossRef]

17. Tu, Y.; Lv, M.; Xiu, P.; Huynh, T.; Zhang, M.; Castelli, M.; Liu, Z.; Huang, Q.; Fan, C.; Fang, H.; et al. Destructive extraction of phospholipids from Escherichia coli membranes by graphene nanosheets. *Nat. Nanotechnol.* **2013**, *8*, 594–601. [CrossRef]

18. Song, B.; Zhang, C.; Zeng, G.; Gong, J.; Chang, Y.; Jiang, Y. Antibacterial properties and mechanism of graphene oxide-silver nanocomposites as bactericidal agents for water disinfection. *Arch. Biochem. Biophys.* **2016**, *604*, 167–176. [CrossRef]

19. Wu, X.; Tan, S.; Xing, Y.; Pu, Q.; Wu, M.; Zhao, J.X. Graphene oxide as an efficient antimicrobial nanomaterial for eradicating multi-drug resistant bacteria in vitro and in vivo. *Colloids Surf. B Biointerfaces* **2017**, *157*, 1–9. [CrossRef]

20. Zhang, X.F.; Gurunathan, S. Biofabrication of a novel biomolecule-assisted reduced graphene oxide: An excellent biocompatible nanomaterial. *Int. J. Nanomed.* **2016**, *11*, 6635–6649. [CrossRef]

21. He, J.; Zhu, X.; Qi, Z.; Wang, C.; Mao, X.; Zhu, C.; He, Z.; Li, M.; Tang, Z. Killing dental pathogens using antibacterial graphene oxide. *ACS Appl. Mater. Interfaces* **2015**, *7*, 5605–5611. [CrossRef]

22. Kelly, A.M.; Kaltenhauser, V.; Mühlbacher, I.; Rametsteiner, K.; Kren, H.; Slugovc, C.; Stelzer, F.; Wiesbrock, F. Poly(2-oxazoline)-derived contact biocides: Contributions to the understanding of antimicrobial activity. *Macromol. Biosci.* **2013**, *13*, 116–125. [CrossRef]

23. Mühlbacher, I.; Wiesbrock, F. *Self—Disinfectant Surfaces—Correlation Between Antimicrobial Activity and Zeta Potential*; Institute for Chemistry and Technology of Materials: Graz, Austria, 2015.

24. Kim, C.J.; Khan, W.; Kim, D.H.; Cho, K.S.; Park, S.Y. Graphene oxide/cellulose composite using NMMO monohydrate. *Carbohydr. Polym.* **2011**, *86*, 903–909. [CrossRef]

25. Ślusarczyk, C.; Fryczkowska, B. Structure-property relationships of pure cellulose and GO/CEL membranes regenerated from ionic liquid solutions. *Polymers* **2019**, *11*, 1178. [CrossRef]

26. Huang, H.D.; Liu, C.Y.; Li, D.; Chen, Y.H.; Zhong, G.J.; Li, Z.M. Ultra-low gas permeability and efficient reinforcement of cellulose nanocomposite films by well-aligned graphene oxide nanosheets. *J. Mater. Chem. A* **2014**, *2*, 15853–15863. [CrossRef]

27. Mahmoudian, S.; Wahit, M.U.; Imran, M.; Ismail, A.F.; Balakrishnan, H. A facile approach to prepare regenerated cellulose/graphene nanoplatelets nanocomposite using room-temperature ionic liquid. *J. Nanosci. Nanotechnol.* **2012**, *12*, 5233–5239. [CrossRef]

28. Gabrys, T.; Fryczkowska, B. Preparing and using cellulose granules as biodegradable and long-lasting carriers for artificial fertilizers. *J. Ecol. Eng.* **2018**, *19*, 111–122.

29. Si, H.; Luo, H.; Xiong, G.; Yang, Z.; Raman, S.R.; Guo, R.; Wan, Y. One-step in situ biosynthesis of graphene oxide-bacterial cellulose nanocomposite hydrogels. *Macromol. Rapid Commun.* **2014**, *35*, 1706–1711. [CrossRef]

30. Zhang, J.; Cao, Y.; Feng, J.; Wu, P. Graphene-oxide-sheet-induced gelation of cellulose and promoted mechanical properties of composite aerogels. *J. Phys. Chem. C* **2012**, *116*, 8063–8068. [CrossRef]

31. Yaghoubidoust, F.; Salimi, E. A simple method for the preparation of antibacterial cotton fabrics by coating graphene oxide nanosheets. *Fibers Polym.* **2019**, *20*, 1155–1160. [CrossRef]

32. Yang, H.Y.; Jun, Y.; Yun, Y.J. Ultraviolet response of reduced graphene oxide/natural cellulose yarns with high flexibility. *Compos. Part. B Eng.* **2019**, *163*, 710–715. [CrossRef]

33. Tian, M.; Qu, L.; Zhang, X.; Zhang, K.; Zhu, S.; Guo, X.; Han, G.; Tang, X.; Sun, Y. Enhanced mechanical and thermal properties of regenerated cellulose/graphene composite fibers. *Carbohydr. Polym.* **2014**, *111*, 456–462. [CrossRef]

34. Teodoro, K.B.R.; Migliorini, F.L.; Facure, M.H.M.; Correa, D.S. Conductive electrospun nanofibers containing cellulose nanowhiskers and reduced graphene oxide for the electrochemical detection of mercury (II). *Carbohydr. Polym.* **2019**, *207*, 747–754. [CrossRef]

35. Luo, H.; Ao, H.; Li, G.; Li, W.; Xiong, G.; Zhu, Y.; Wan, Y. Bacterial cellulose/graphene oxide nanocomposite as a novel drug delivery system. *Curr. Appl. Phys.* **2017**, *17*, 249–254. [CrossRef]

36. Nandgaonkar, A.G.; Wang, Q.; Fu, K.; Krause, W.E.; Wei, Q.; Gorga, R.; ALucia, L. A one-pot biosynthesis of reduced graphene oxide (RGO)/bacterial cellulose (BC) nanocomposites. *Green Chem.* **2014**, *16*, 3195–3201. [CrossRef]

37. Shao, W.; Wang, S.; Liu, H.; Wu, J.; Zhang, R.; Min, H.; Huang, M. Preparation of bacterial cellulose/graphene nanosheets composite films with enhanced mechanical performances. *Carbohydr. Polym.* **2016**, *138*, 166–171. [CrossRef]

38. Gabryś, T.; Fryczkowska, B.; Biniaś, D.; Ślusarczyk, C.; Fabia, J. Preparation and properties of composite cellulose fibres with the addition of graphene oxide. *Carbohydr. Polym.* **2020**, *254*, 117436. [CrossRef]

39. Hummers, W.S.; Offeman, R.E. Preparation of graphitic oxide. *J. Am. Chem. Soc.* **1958**, *80*, 1339. [CrossRef]

40. Fryczkowska, B.; Biniaś, D.; Ślusarczyk, C.; Fabia, J.; Janicki, J. Properties and application of cellulose membranes with graphene oxide addition for removal of heavy metals from aqueous solutions. *Desalin. Water Treat.* **2018**, *117*, 66–77. [CrossRef]

41. Wan, C.; Li, J. Graphene oxide/cellulose aerogels nanocomposite: Preparation, pyrolysis, and application for electromagnetic interference shielding. *Carbohydr. Polym.* **2016**, *150*, 172–179.

42. Sundberg, J.; Toriz, G.; Gatenholm, P. Moisture induced plasticity of amorphous cellulose films from ionic liquid. *Polymer* **2013**, *54*, 6555–6560. [CrossRef]

43. Rouf, T.B.; Kokini, J.L. Biodegradable biopolymer—Graphene nanocomposites. *J. Mater. Sci.* **2016**, *51*, 9915–9945. [CrossRef]

44. Clarification of GO Acted as a Barrier Against the Crack Propagation of the Cellulose Composite Films. Elsevier Enhanced Reader. Available online: https://reader.elsevier.com/reader/sd/pii/S0266353814003273?token=0A4E982BFAC5CC81EDFA46E82B8 D36B0AA4944F8A2DFC75B5FD2BAF80AC6F5CC067FDD906AB666461F7663AB175FFE21 (accessed on 21 December 2020).

45. Cao, Y.; Wu, J.; Zhang, J.; Li, H.; Zhang, Y.; He, J. Room temperature ionic liquids (RTILs): A new and versatile platform for cellulose processing and derivatization. *Chem. Eng. J.* **2009**, *147*, 13–21. [CrossRef]

46. Wypych, G. Cellulose. In *Handbook of Polymers*; ChemTecPublishing: Toronto, ON, Canada, 2012; pp. 25–29, ISBN 9781895198478.

47. Chen, H.; Gao, D.; Wang, B.; Palmieri, V.; Lauriola, M.C.; Ciasca, G. The graphene oxide contradictory effects against human pathogens. *Nanotechnology* **2017**, *28*, 1–18.

48. Xiao, S.; Lu, X.; Gou, L.; Li, J.; Ma, Y.; Liu, J.; Yang, K.; Yuan, B. Graphene oxide as antibacterial sensitizer: Mechanically disturbed cell membrane for enhanced poration efficiency of melittin. *Carbon NY* **2019**, *149*, 248–256. [CrossRef]

49. Luxbacher, T. *The Zeta Potential for Solid Surface Analysis*, 1st ed.; Anton Paar GmbH: Graz, Austria, 2014.

50. Luo, X.; Zhong, J.; Zhou, Q.; Du, S.; Yuan, S.; Liu, Y. Cationic reduced graphene oxide as self-aligned nanofiller in the epoxy nanocomposite coating with excellent anticorrosive performance and its high antibacterial activity. *ACS Appl. Mater. Interfaces* **2018**, *10*, 18400–18415. [CrossRef]

51. Kumar, R.; Oves, M.; Ameelbi, T.; Al-Makishah, N.H.; Barakat, M.A. Hybrid chitosan/polyaniline-polypyrrole biomaterial for enhanced adsorption and antimicrobial activity. *J. Colloid Interface Sci.* **2017**, *490*, 488–496. [CrossRef]

MDPI

Article

Preparation of an Active Dressing by In Situ Biosynthesis of a Bacterial Cellulose–Graphene Oxide Composite

Tobiasz Gabryś [1,]* , Beata Fryczkowska [2] , Janusz Fabia [1] and Dorota Biniaś [2]

1   Department of Material Science, Faculty of Materials, Civil and Environmental Engineering,
     University of Bielsko-Biala, Willowa 2, 43-309 Bielsko-Biala, Poland; jfabia@ath.bielsko.pl
2   Department of Environmental Protection and Engineering, Faculty of Materials,
     Civil and Environmental Engineering, University of Bielsko-Biala, Willowa 2, 43-309 Bielsko-Biala, Poland;
     bfryczkowska@ath.bielsko.pl (B.F.); dbinias@ath.bielsko.pl (D.B.)
*   Correspondence: tgabrys@ath.bielsko.pl

Abstract: This paper presents a simple method of obtaining a bacterial cellulose (BC) composite with the addition of graphene oxide (GO) using an in situ method and studies the influence of GO nanoparticles on the structure and properties of the obtained membranes. Microorganisms obtained from Golden Delicious apple vinegar were used to obtain the BC. During the biosynthesis, GO was introduced in the amounts of 3.7, 5.4 and 7.1% *w/w*. The resulting BC/GO composite was characterized by high water content (~400%), a thickness of about 1.1 mm (in wet form) and a cellulose nanofiber diameter of ~100 nm. The possibility of using the resulting composite membranes as potential active dressings with the sustained-release analgesic medicine—paracetamol—was investigated. The BC/GO composite membranes were characterized by a medicine sorption of 60 mg/g of BC, a slow desorption time, a constant medicine concentration over time and an 80% paracetamol release rate after 24 h. The morphology of membrane surfaces and cross-sections were examined by means of scanning electron microscopy (SEM). Infrared spectroscopy (FTIR), X-ray structure studies (WAXS) as well as thermal analysis (TGA) demonstrated the presence of GO in the BC matrix and interactions between the matrix and the additive.

Keywords: bacterial cellulose; graphene oxide; biosynthesis; composite membranes; nanofibers

1. Introduction

Cellulose is an inexpensive and readily available biopolymer synthesized by plants. It is obtained by the processing of coniferous and deciduous trees, as well as by recycling used paper. Plant-based cellulose occurs together with supporting substances such as lignin, pectin and hemicellulose. Such a chemical composition does not affect the wide possibilities of application of this biopolymer. However, when used as a biomaterial, 100% cellulose content products are expected. For this purpose, BC can be employed.

BC can be synthesized by different bacteria, including Gram-negative bacteria, such as *Gluconacetobacter xylinus* [1,2], *Agrobacterium* [3] and *Rhizobium* [4], and Gram-positive bacteria, such as *Sarcina* [5]. As many as 59 strains of bacteria from ripe fruit and vegetables that can synthesize BC have already been isolated and tested [5].

Cellulose can also be produced in vitro, i.e., using the cell-free enzyme system. This method employs enzymes derived from bacteria or fungi [6–9]. The cell-free system method has many advantages over bacteria-based methods. It uses less glucose, and the efficiency of the process is higher than that obtained with bacteria. The resulting fibers are characterized by larger diameters than in the method based on the use of microorganisms [9]. Cellulose produced by means of cell-free enzyme systems is characterized by better physicochemical and structural properties [10]. BC is synthesized in the bacterial cell membrane from nucleotide-activated glucose [11]. Bacteria synthesize BC through the pores of the cell membrane in the form of fibrils composed of D-glucose units, which are connected by

β-1,4-glycosidic bonds. Bacteria synthesize cellulose nanofibers through 50 to 80 channels located on the surface of the bacterial cell membrane [10]. In the first stage of synthesis, glucan chains form protofibrils, which combine into nanofibrils to form a compact, ultrathin three-dimensional network [11]. The resulting BC fibers have a diameter of up to 100 nm and a length of 10 μm [12]. The production rate of BC is approximately 200,000 glucose units per second [13]. Single BC fibers are 100 times thinner than those of plant origin, and the nano-nonwoven fabric produced during synthesis is characterized by a high water retention index [10]. The BC synthesis mechanism influences some specific properties of the material, such as: specific surface area (high aspect ratio of fibers with diameter 20–100 nm), porosity, mechanical strength (Young's modulus 15–18 GPa), degree of crystallinity (up to 80%) and polymerization, high water-holding capacity (over 100 times of its own weight) or biodegradability [5,12]. As a hydrogel, BC has the ability to absorb, store and desorb large amounts of water, which is possibly due to its nanofiber structure [14]. This makes BC an excellent biomedical material, along with biopolymers such as chitosan, alginates, or hyaluronic acid and collagen [15]. BC, combined with those biopolymers, forms composite materials. The literature describes the possibility of synthesizing BC/chitosan composite as a dressing material for the treatment of various types of wounds, burns and ulcers [16] or as a tissue culture material (scaffold) [17]. BC/alginate composites are used in tissue engineering [18]. Additionally, the combination of three biopolymers, BC/alginate/chitosan, makes it possible to obtain an antibacterial dressing [19]. BC can also be combined with hyaluronic acid [20] and collagen [21,22], and the resulting composites can be used in bone regeneration.

BC is also potentially useful in 3D printing [23,24]. The literature provides a method of printing with an ink containing acetic bacteria, which produces BC directly in the resulting printout, creating a tissue scaffold [25]. To print BC, composites with alginates are formed and scaffolds for cartilage culture are obtained by means of an electromagnetic jet printer [26]. This polymer can be chemically modified to obtain a three-dimensional material that has potential for application in soft tissue engineering [27].

There are several methods of modifying BC in order to give it new, previously undescribed properties. Two known methods of BC modification are in situ and ex situ [4]. The ex situ modification is relatively simple and consists of introducing additives or nano-additives to the finished BC product. Barud et al. obtained a non-genotoxic and non-cytotoxic BC/silk fibroin composite [28]. Other researchers have modified BC by introducing polyethylene glycol, silver nanoparticles or zinc oxide [4]. The literature also mentions the possibility of chemical modification of BC by reaction of hydroxyl groups of cellulose with gelatin [29], hydroxyapatite [4], graphene oxide [30] and proteins [12].

The second method of BC modification is the in situ method, which consists of introducing additives or nanoparticles that are soluble in water to form dispersion with it, directly into the culture medium. There are many scientific reports of BC modified with the use of electrically conductive polymers [31], carbon nanoadditives, including graphene [32] or graphene oxide [33,34]. The use of carbon nanoadditives increases the specific surface area of the composite, increasing its porosity, improving its strength properties and giving it electrically conductive properties [32].

The third method of BC modification is solvent dissolution–regeneration. This method consists of dissolving BC, then introducing the modifier, followed by BC regeneration. Jayani et al. obtained probiotic carriers by dissolving BC in trifluoroacetic acid, mixing with polyvinyl alcohol (PVA) solution, and then producing nanofibers via electrospinning [35].

Graphene oxide (GO) is a particularly interesting carbon nanomaterial that can be used to produce a BC composite. Known as a two-dimensional nanomaterial with many oxygen functional groups on its surface, graphene oxide links strongly to BC, forming hydrogen bonds [36]. The literature reports on many types of BC/GO nanocomposites with different conformations, developed for absorbents for the elimination of pollutants. Luo et al. reported a method of preparing ultra-strong BC/GO nanocomposites by multiple in situ layer-by-layer assembly steps which consisted of spraying GO dispersed medium

onto a growing static BC membrane [36]. In addition, graphene nanosheets have been incorporated into BC growing membranes by spraying to obtain flexible and highly conductive nanopapers for applications in energy storage devices [32,37]. In the area of biomedicine, these carbon-based materials have been used for the development of biosensors, in tissue engineering and as delivery carriers for genes or medicines [38]. To date, none of the GO applications have been approved for clinical trials due to issues related to potential toxicity in model animals, and there are several recent studies in which the in vitro biocompatibility and antimicrobial activity of nanocomposites containing GO have been assessed [39,40]. BC/GO hydrogels have been developed in static and dynamic cultivation to develop systems for the release of medicines such as doxorubicin hydrochloride or ibuprofen, although low release profiles have been obtained [30,36,41].

The experiment describes a simple method of obtaining a composite of BC with the addition of graphene oxide (in the amounts of 3.7, 5.4 and 7.1% w/w) using the in situ method. In this study, microorganisms obtained from Golden Delicious apple vinegar, rather than selected bacterial strains, were used. No additional nutrients for bacterial growth were added. Additions such as peptone, yeast extract, citric acid and Na_2HPO_4 were not used in the BC for synthesis [14]. Instead, a simple method is proposed for synthesizing the BC/GO composite with the following properties: (~400%) and wet thickness (~1100 μm), as well as cellulose nanofiber diameter of ~100 nm. The physicochemical properties of BC/GO could be used as a potential active dressing with prolonged analgesic effect. BC/GO composite membranes are characterized by paracetamol sorption at the level of 60 mg/g of BC and a slow desorption time, releasing approximately 80% of the medicine after 24 h. Structural tests (WAXS, FTIR, TGA) confirm the presence of GO in membranes and its influence on physicochemical properties.

2. Materials and Methods

2.1. Chemicals

The reagents for the preparation of liquid medium and purification of obtained BC included saccharose (≥99%) and potassium hydroxide (≥97%) purchased from Sigma-Aldrich.

The reagents for the production of graphene oxide included: graphite powder < 20 μm purchased from Sigma-Aldrich and potassium permanganate (≥99%), sulfuric acid (98%) and hydrogen peroxide (30%) purchased from Avantor Performance Materials Poland S.A (Gliwice, Poland). Graphene oxide (GO) was obtained using the modified Hummers method [42]. GO synthesis description and testing of its properties (XRD, DSC, FTIR) were very similar to those of our earlier work [43]. After the synthesis was completed, the concentration of GO in wet graphene oxide was checked by drying it in a drying apparatus at 60 °C until constant weight. The wet graphene oxide was then dispersed in water to obtain 50 ppm dispersion. Graphite with a particle size < 20 μm was used following previous research on the biocidal properties of GO flakes of various particle sizes [44].

The reagents used to prepare phosphate-buffered saline (PBS) included: sodium chloride, potassium chloride and disodium hydrogen phosphate purchased from Sigma-Aldrich (Poznan, Poland). PBS solution with the following composition was prepared: NaCl 8 g/L, KCl 0.2 g/L and Na_2HPO_4 1.44 g/L. A pH of 7.4 was obtained by adding the appropriate amount of 0.1 M NaOH.

Paracetamol Kabi (10 mg/mL) was purchased from Fresenius Kabi Polska sp. z o.o.

2.2. Culture Medium

Acetate fermentation of Golden Delicious apples from organic cultivation located in the Silesian Voivodship was carried out. First, a sterilized 1000 mL jar was filled to one-third with apples cut into pieces. The fruit was covered with a solution of water with sucrose (80 g of sucrose dissolved in 1 L of water), which was initially sterilized in an autoclave at 121 °C for 15 min. Finally, the jar was covered with sterile gauze. The contents of the jar were thoroughly mixed 2 times a day. After 2–3 days, it was possible to observe the formation of gas bubbles in the jar, which indicated the alcoholic fermentation reaction

in progress, ending when the fruit fell to the bottom of the jar. The solution was then separated from the fruit, poured back into the jar and covered with sterile gauze. From this point on, the process of acetic acid fermentation began and the "mother of vinegar", which includes BC, live bacteria and yeast, was formed. The fermentation process was completed after 3 weeks. The BC formed in the reaction was gently removed from the surface of the solution, transferred to a sterilized jar and then covered with a small amount of apple cider vinegar. The "mother of vinegar" and apple cider vinegar were stored in the refrigerator.

2.3. Production and Purification of BC

For the production of BC, a liquid sucrose medium with a concentration of 110 g/L was prepared and then sterilized in an autoclave at 121 °C for 15 min. A total of 800 mL of liquid sucrose medium, 200 mL of apple cider vinegar obtained earlier and a 1×1 cm fragment of "mother of vinegar" were placed in a sterilized 2000 mL laboratory beaker, and then mixed thoroughly. The pH of the medium was also measured and found to be pH = 3.5. Then, the mixture prepared in this way was divided into 4 parts and placed in sterilized 300 mL beakers (Table 1).

Table 1. Designation of samples and their composition.

Sample Designation	BC/0	BC/GO/I	BC/GO/II	BC/GO/III
Incubation time [h]/[days]	Amount of GO added [mL] (GO dispersion with a concentration of 50 ppm)			
96/4	-	10	10	10
144/6	-	10	10	10
192/8	-	-	10	10
240/10	-	-	-	10
BC content [% *w/w*]	100	96.3	94.6	92.9
GO content [% *w/w*]	0	3.7	5.4	7.1

Each vessel was covered with a watch glass and then transferred to an incubator preheated to 25 °C. The synthesis of BC was carried out for 12 days by adding appropriate amounts of GO dispersion to the consecutive samples (Table 1). As a result of our previous research on the optimization of GO concentration, a solution with a concentration of 50 ppm was selected. Solutions with lower concentrations of GO at 10 and 25 ppm did not affect the BC synthesis. A 100 ppm solution of GO, on the other hand, stopped the synthesis of BC.

The stages of this part of the experiment as well as the process of introducing the GO dispersion onto the surface of BC are presented in Figure 1.

After completion of the reaction, membranes from pure BC (BC/0) and from modified BC (BC/GO/I; BC/GO/II; BC/GO/III) were removed from the beakers and rinsed with distilled water to remove residual medium.

Then, the process of purifying the membranes of organic residues (bacterial cells) was carried out (Figure 2). For this purpose, each membrane was placed in a separate 300 mL beaker containing 100 mL of 2% *w/w* aqueous solution of KOH [30]. The purification process was carried out at 80 °C for 1 h under static conditions. Then, the membranes were washed several times with distilled water until the reaction was neutral.
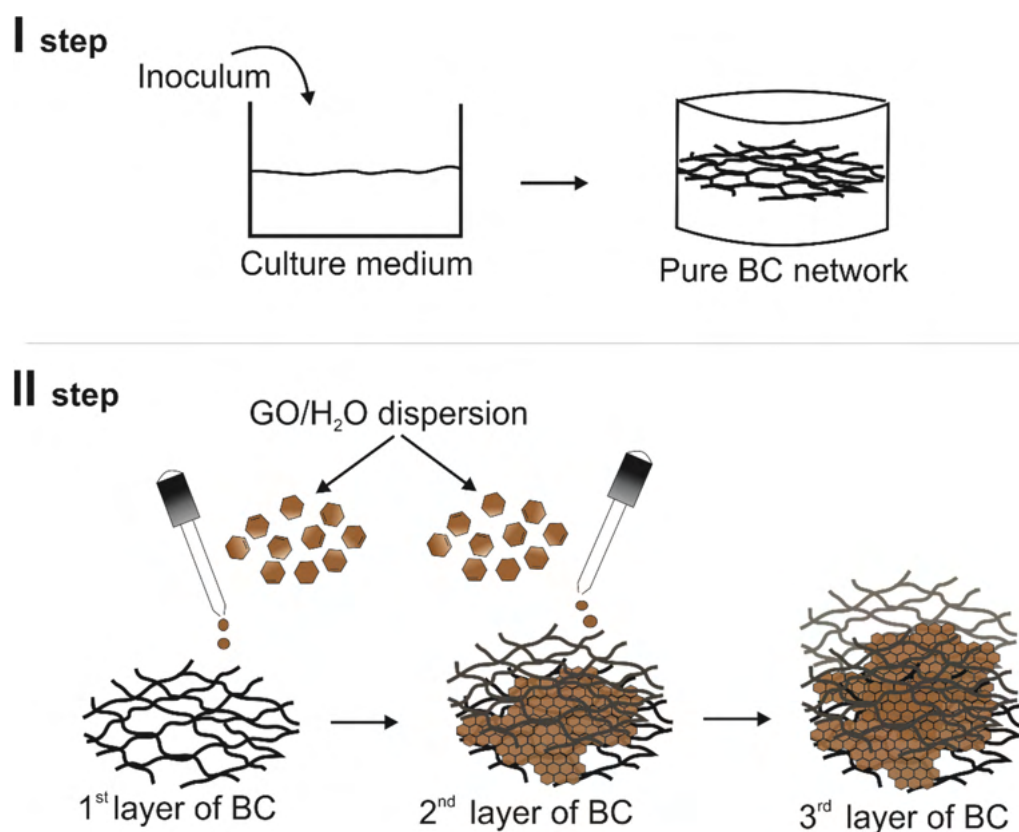
Figure 1. The process of obtaining modified BC.

2.4. Thickness Measurement

After completion of the reaction, membranes from pure BC (BC/0) and from modified BC (BC/GO/I, BC/GO/II, BC/GO/III) were removed from the beakers and rinsed with distilled water to remove residual medium. Then, discs with a diameter of 2 cm were cut from the wet membranes. The membrane was placed on a glass plate and the thickness measurements were made (Figure 2). For this purpose, a YATO YT-7201 electronic thickness gauge was used. For all obtained membranes, 20 measurements were made (Figure 2), and the obtained results are reported in Table 2.

In addition to measuring the thickness when wet, the thickness of the dry membranes was also measured. Initially, the membranes were air-dried until a constant weight was obtained. Thickness measurements were made using an electronic thickness gauge (El-metron MG-411, Zabrze, Poland). In order to avoid spot-crushing of the membrane, a cover glass was used and placed on the membrane at the point where its thickness was measured. Twenty measurements were made for each membrane, and the obtained results are summarized in Table 2.

Table 2. Summary of the results of thickness and water absorption measurements for wet and dry membranes.

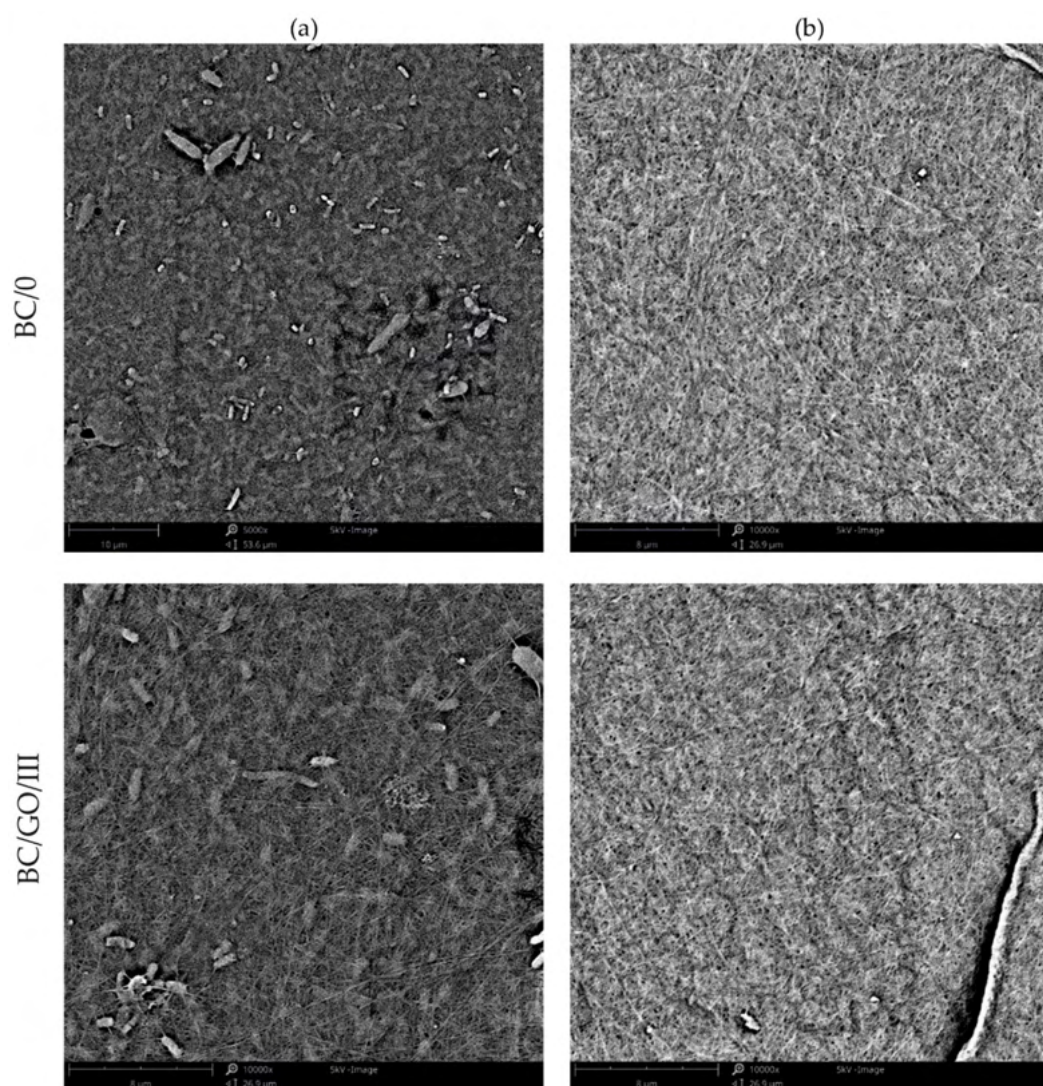| Sample Designation	BC/0	BC/GO/I	BC/GO/II	BC/GO/III
Thickness of wet membranes [μm]	470.0 ± 8.1	1070.0 ± 74.8	1110.1 ± 37.4	1180.0 ± 24.5
Thickness of dry membranes [μm]	30.4 ± 7.1	46.6 ± 7.9	44.8 ± 12.7	36.0 ± 12.8
Water content in wet membranes [%]	358.7 ± 45.0	361.9 ± 43.2	408.0 ± 48.4	306.3 ± 37.9
Water absorption of dry membranes [%]	97.4 ± 5.1	96.8 ± 4.5	96.3 ± 3.9	96.6 ± 4.0

Figure 2. SEM photo of the membrane made from pure BC/0 and sample BC/GO/III: (**a**) after the synthesis process—with visible bacterial cells; (**b**) after KOH purification process.

2.5. Measurement of Water Content in Wet Samples and Water Absorption in Dry Samples

The water content was measured for wet and dry membranes. Initially, samples of wet membranes with a diameter of 6 cm were transferred to aluminum dishes with a diameter of 9 cm, and then weighed on a laboratory electronic moisture balance (Radwag MA 110.R, Radom, Poland) with an accuracy of 0.0001 g. The membrane drying process was carried out at 80 °C until a constant mass was obtained.

The discs of membranes dried during the test described above were used to measure the water absorption. The membranes placed on aluminum dishes were soaked in distilled water added in such an amount as to cover their surface and left for 1 h. After this time, the water was removed from the dishes. The excess water was then collected from the membrane using filter paper and the weighing was repeated.

Twenty measurements were made for each wet and dry membrane, and the obtained results are summarized in Table 2.

2.4. Thickness Measurement

After the purification and neutralization process of the obtained membranes, their thickness was measured. For this purpose, discs with a diameter of 2 cm were cut from the wet membranes. The membranes were then placed on a glass plate and the thicknesses were read using an electronic micrometer screw (YATO YT-7201). For all obtained membranes, 20 measurements were made (Figure 3), and the obtained results are summarized in Table 2.

(**a**)

(**b**)

Figure 3. Samples of wet membranes placed on glass, prepared for thickness measurement; (**a**) top view; (**b**) side view.

2.6. In Vitro Study of Bioactive Substance Release

The kinetics of the active substance release from the membranes was studied in phosphate-buffered saline (PBS), which mimics the ion concentration, osmolarity and pH of human body fluids. Paracetamol, which is commonly used as a strong analgesic and antipyretic medicine, was selected for the sorption studies of biologically active substances. At the beginning, a standard curve was prepared. For this purpose, 4 solutions containing PBS (as a solvent) and paracetamol at a concentration of 5.0, 10.0, and 20.0 ppm were prepared. The solutions were tested using a UV-Vis spectrophotometer (Thermo Scientific, Evolution 220, Waltham, MA, USA), at a wavelength of λ = 243 nm, using PBS as the reference solution.

Then, the sorption and desorption of paracetamol from the membranes obtained in the test, wet BC/0 and BC/GO/I, BC/GO/II, BC/GO/III membranes were placed in 100 ppm, dissolved in PBS. The beakers with the membrane samples were left at room temperature for 24 h. After this time, samples of the solution were taken from the beakers and the absorbance was measured using the UV-Vis spectrophotometer at the wavelength of λ = 243 nm, determining the amount of medicine adsorbed by each tested membrane.

2.5. Measurement of Water Content in Wet Samples and Water Absorption in Dry Samples

The water content was measured for wet and dry membranes. Initially, samples wet membranes with a diameter of 6 cm were transferred to aluminum dishes with a ameter of 9 cm, and then weighed on a laboratory electronic moisture balance (Radw MA 110 R, Radom, Poland) with an accuracy of 0.0001 g. The membrane drying pro

Table 2. Summary of the results of thickness and water absorption measurements for wet and membranes.

Sample Designation	BC/0	BC/GO/I	BC/GO/II	BC/GO/III
Thickness of wet membranes [μm]	470.0 ± 8.1	1070.0 ± 74.8	1110.1 ± 37.4	1180.0 ± 24.
Thickness of dry membranes [μm]	30.4 ± 7.1	46.6 ± 7.9	44.8 ± 5.7	36.0 ± 12.8
Water content in wet membranes [%]	358.7 ± 45.0	361.9 ± 43.2	408.0 ± 48.4	506.3 ± 37.9
Water absorption of dry membranes [%]	97.4 ± 5.1	96.8 ± 4.5	96.3 ± 3.9	96.6 ± 4.0

In addition to measuring the thickness when wet, the thickness of the dry membra was also measured. Initially, the membranes were air-dried until a constant weight v obtained. Thickness measurements were made using an electronic thickness gau (Elmetron MG-411, Zabrze, Poland). In order to avoid spot-crushing of the membran cover glass was used and placed on the membrane at the point where its thickness v measured. Twenty measurements were made for each membrane, and the obtained sults are summarized in Table 2.

Studies on medicine desorption from membranes followed thereafter. Membranes soaked in paracetamol were transferred to separate beakers, each containing 100 mL of PBS solution, and stirred using a magnetic stirrer at 37 °C. Samples of the solution from these membranes were taken every 10 min and the absorbance values were read. After the measurement, the test solutions were returned to the beakers. The cumulative release factor (C_r) was determined using the following formula, similar to that calculated in the publication [30]:

$$C_r = \left(\frac{C_t}{C_0} \right) * 100\% \tag{1}$$

where C_t is concentration released at time t and C_0 is the concentration of paracetamol in membranes.

2.7. Characterization of BC

Membrane surface and cross-section tests were carried out using a high-resolution Phenom ProX scanning electron microscope (SEM) from Thermo Fisher Scientific (Pik Instruments, Poland, Piaseczno), operating at 10 kV. The fiber thicknesses were measured based on the surface images using FiberMetric software developed by PhenomWorld (v. 2.9.0, Eindhoven, The Netherlands). A total of 1000 fiber thickness measurements were taken for each type of membrane. To prepare the cross-sections of the membranes, liquid nitrogen was used, in which the samples were frozen and then broken. The samples were previously coated with a 10 nm gold layer using a Leica EM ACE 200 low-vacuum coater (Vienna, Austria).

The surfaces of the membranes were observed using an OPTA-TECH optical microscope at $10\times$ magnification. The images were taken using the transmission method, in the light passing through the sample.

Wide-angle X-ray scattering (WAXS) studies were performed using URD-65 Seifert diffractometer (Freiberg, Germany) employing the Bragg–Brentano reflection geometry method. CuKα radiation (λ = 1.54 Å) was emitted at an accelerating voltage of 40 kV and an anode current of 30 mA. The monochromatization of the radiation beam was achieved by a graphite monochromatizer placed across the monochromatized beam. A scintillation counter was used as a detector. The tests were carried out in the range of 2θ from 5 to 60° in steps of 0.1°.

Fourier Transform Infrared Spectroscopy (FTIR) measurements were taken using a Nicolet 6700 FT-IR spectrometer (Thermo Electron Corp., Madison, WI, USA) equipped with a photoacoustic MTEC model 300 accessory. The following measurement parameters were used: resolution, 4 cm^{-1}; photoacoustic detector; number of scans, 256. For each sample, the spectra were collected over the range of 4000 to 500 cm^{-1}. Data collection and post-processing were performed using OMNIC software (v. 9.0, Thermo Electron Corp., Madison, WI, USA).

Thermogravimetric analysis were performed using TA Instruments Q500 Thermogravimetric Analyzer. The measurements were conducted in a nitrogen atmosphere (flow 60 mL/min), in the temperature range of 30 to 500 °C and at a heating rate of 20°/min. TG and DTG curves were analyzed using Universal V2.6D TA Instruments software.

3. Results and Discussion

This study describes the possibility of obtaining BC and composites of BC with graphene oxide in situ. The study used microorganisms obtained from Golden Delicious apple vinegar as the literature provides many examples of isolating bacterial strains from fruits and vegetables [5].

The membranes obtained in the experiment, made of pure BC (BC/0) and composite membranes (BC/GO/I, BC/GO/II, BC/GO/III), were treated with KOH. This treatment process is designed to remove organic matter such as bacterial cells. Figure 2a clearly shows the bacterial rods entangled between the BC filaments. On the other hand, in the SEM

ple vinegar as the literature provides many examples of isolating bacterial strains from fruits and vegetables [5].

The membranes obtained in the experiment, made of pure BC (BC/0) and composite membranes (BC/GO/I, BC/GO/II, BC/GO/III), were treated with KOH. This treatment process is designed to remove organic matter such as bacterial cells. Figure 2a clearly shows the bacterial rods entangled between the BC filaments. On the other hand, in the SEM photo, after the alkali washing process (Figure 2b), the bacterial cells are gone, and only the BC filaments are visible.

At the beginning of the research, the physicochemical properties of the membranes, such as the thickness and water absorption, were determined for both pure cellulose (BC/0) and composite (BC/GO/I, BC/GO/II, BC/GO/III) membranes. The obtained results are summarized in Figure 4.

(a)

(b)
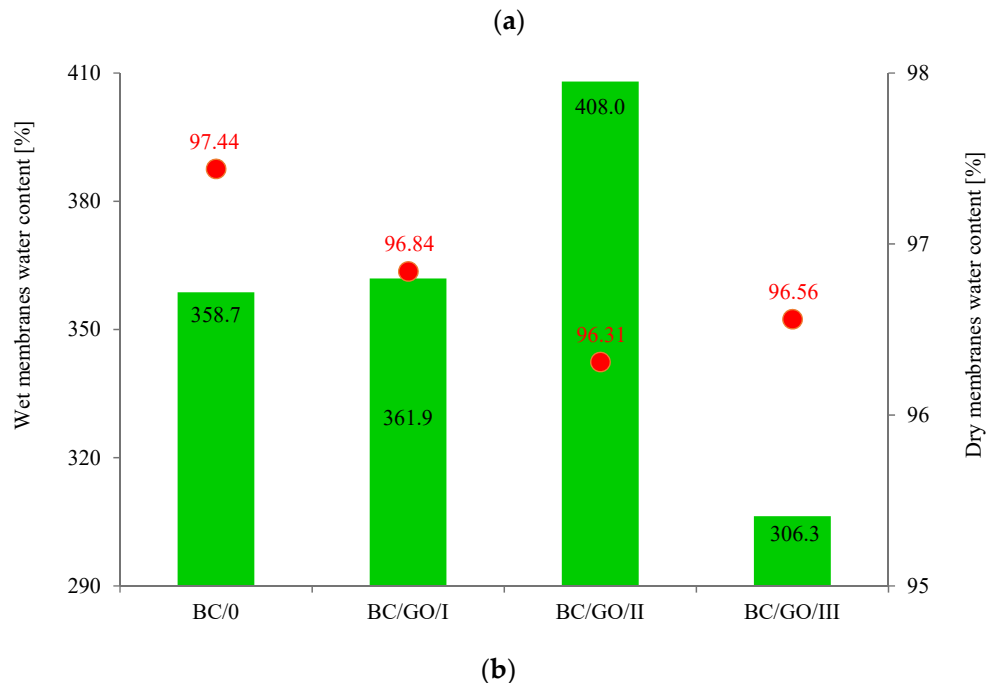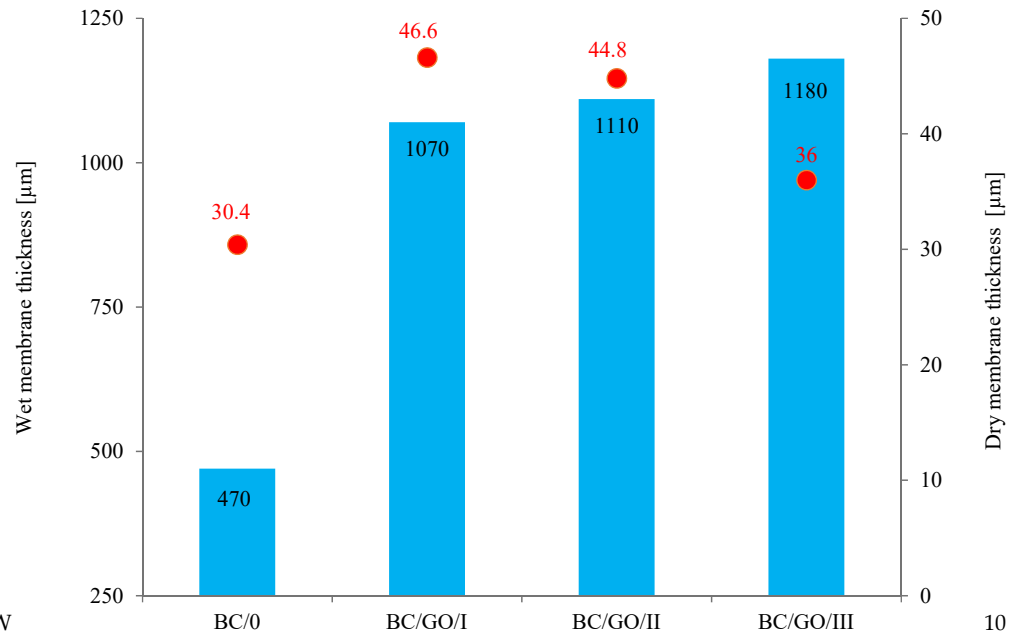
Figure 4. (a) Dependence of the thickness of wet and dry membranes on the content of GO in the sample; (b) water content of wet membranes and water absorption of dry membranes.

As Figure 4a demonstrates, the addition of GO to the growing inoculum significantly increases the thickness of the cellulose composite membranes. For wet membranes, the membrane thickness values increase from 470 μm (BC/0) to 1070, 1110 and 1180 μm for BC/GO/I, BC/GO/II and BC/GO/III membranes, respectively, which is an increase of over 130%. Thus, the addition of GO promotes an increase in the amount of BC produced or the thickness of the nanofibers formed. In addition, it is observed that an increase in the GO contents in the sample (3.7; 5.4; 7.1% of GO) results in a slight increase in the thickness of the composite membrane samples. However, after drying of all tested membranes, their

over 130%. Thus, the addition of GO promotes an increase in the amount of BC produced or the thickness of the nanofibers formed. In addition, it is observed that an increase in the GO contents in the sample (3.7; 5.4; 7.1% of GO) results in a slight increase in the thickness of the composite membrane samples. However, after drying of all tested membranes, their thickness drops drastically to 30.4 μm for BC/0. It is closely related to the formation of inter- and intramolecular hydrogen bonds during drying of cellulose [45,46]. Moreover, an increase in the amount of GO added to the BC/GO/III sample in the amount of up to 7.1% *w/w* probably causes the formation of additional hydrogen bonds, which have a direct impact on the formation of a more compact structure, resulting in a decrease in the thickness of this membrane.

Studies have also shown that the water content of wet membranes ranges from 306.3 to 408.0% (Figure 4b). For pure BC membranes, the water content is ~359%. The addition of GO in the amount of 5.4% *w/w* causes an approx. 14% increase in the water content in the BC/GO/II membrane. The result obtained for the BC/GO/III wet membrane may suggest that the presence of GO caused the formation of additional hydrogen bonds.

The water absorption tests carried out for dry membranes (Figure 4b) demonstrated that this property is practically independent of the type of membrane; it ranges from approx. 96% to approx. 97% for the BC/0 membrane. Lower water absorption values for dry membranes BC/GO/I, BC/GO/II and BC/GO/III may also prove the formation of additional hydrogen bonds between BC and GO [36].

Analyzing the sorption properties (Figure 5a) of the obtained membranes against paracetamol, it can be concluded that the medicine is well-sorbed on the membranes obtained in the experiment. The amount of adsorbed medicine is 63.3 mg/g BC (for the BC/0 membrane), and this slightly decreases with the increase in GO content in composite membranes to the value of 62.4 mg/g BC (for the BC/GO/III membrane). The desorption tests, on the other hand, showed that the composite membranes desorbed more paracetamol than the BC/0 sample (34.9 mg/g BC), in the following order: BC/GO/III (42.0 mg/g BC), BC/GO/II (41.7 mg/g BC) and BC/GO/I (35.3 mg/g BC).

Interesting results were obtained during the study of the kinetics of the medicine release from the tested membranes (Figure 5b). They show that the BC/0 sample desorbs paracetamol slowly but steadily; however, the release rate is less than 55%. On the other hand, the membrane with the lowest GO content (3.7% *w/w*) is characterized by a more intense medicine desorption in the initial phase of the release, which slows down after 40 min and remains at the level of ~55%. The medicine substance release curves for the BC/GO/III and BC/GO/II composite membranes have similar characteristics, and their release rates after 24 h are high, amounting to ~67%. The results obtained in the study of the release of paracetamol from BC-based composite membranes with the addition of GO reach values that are much higher than those described by the team of Urbin et al. [30].
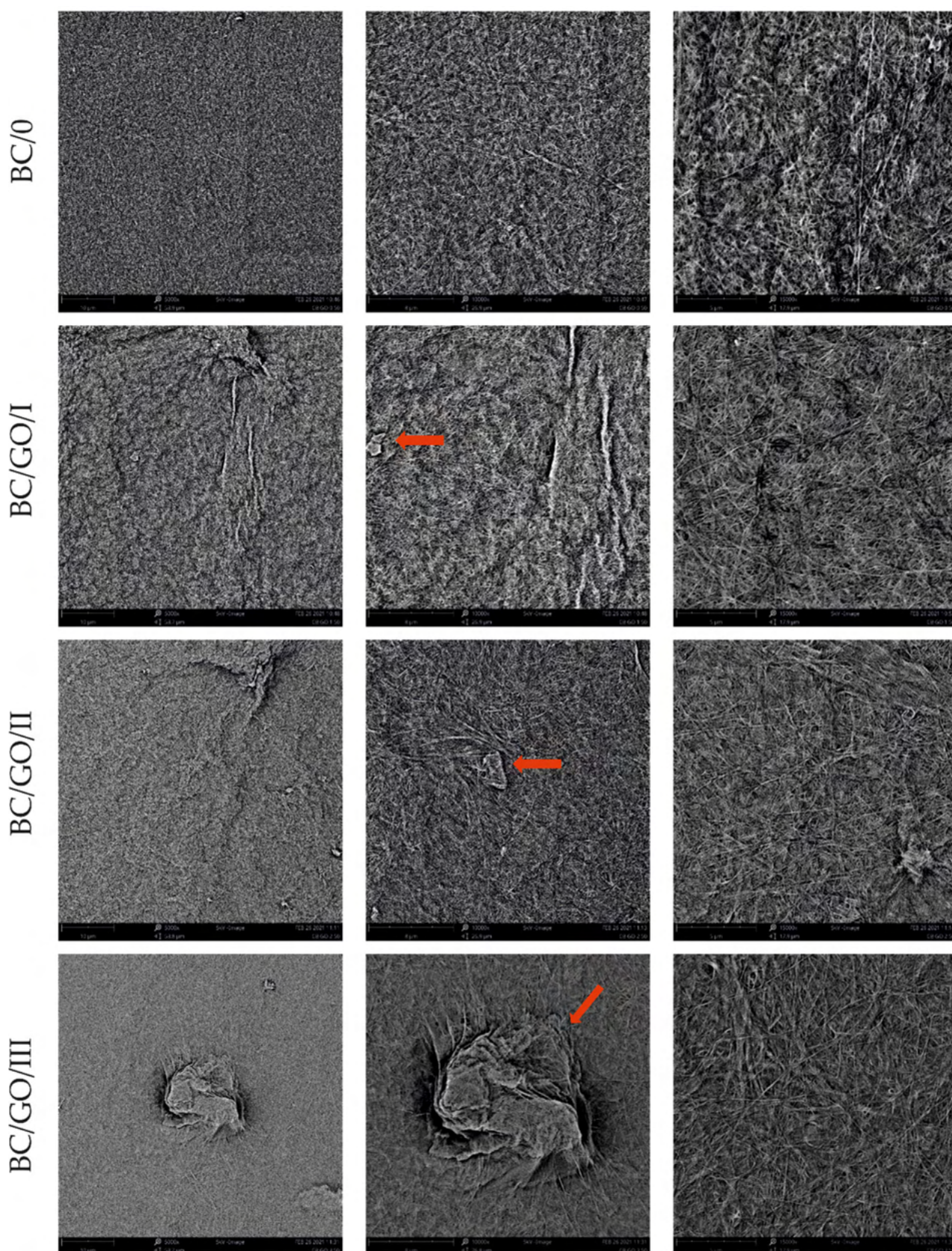
The examination of the physicochemical properties of the membranes was supplemented with microscopic examinations. The use of scanning electron microscopy allowed for the analysis of the surface of the obtained membranes, their cross-sections and the thickness of cellulose nanofibers that make up the membrane structure.

The SEM photos (Figure 6) clearly show that the membranes are made of BC nanofibers, the arrangement of which on the surface is completely random, as in the classic nonwoven fabric. Additionally, for the membranes BC/GO/I, BC/GO/II and BC/GO/III, the presence of inclusions (red arrow), which come from the GO addition, can be observed. SEM studies have shown that the graphene oxide flakes do not appear directly on the surface of composite membranes but are covered with the web of BC nanofibers.

Scanning electron microscopy also allowed observing fractures of the obtained membranes. The sample photos show a pure BC membrane (Figure 7). In Figure 7 of the BC/0 membrane, we can see that the membrane is made of nanofibers that are arranged in layers, parallel to each other.
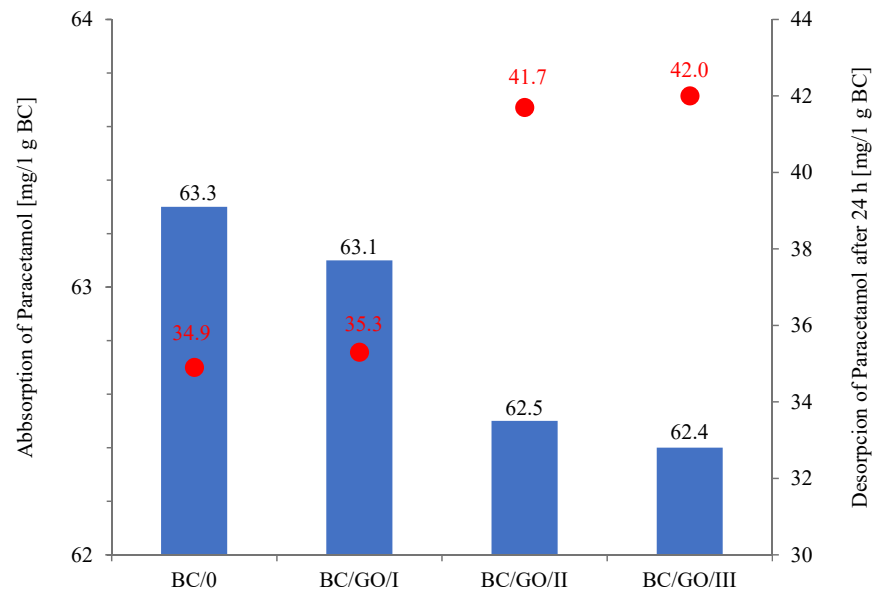
(**a**)
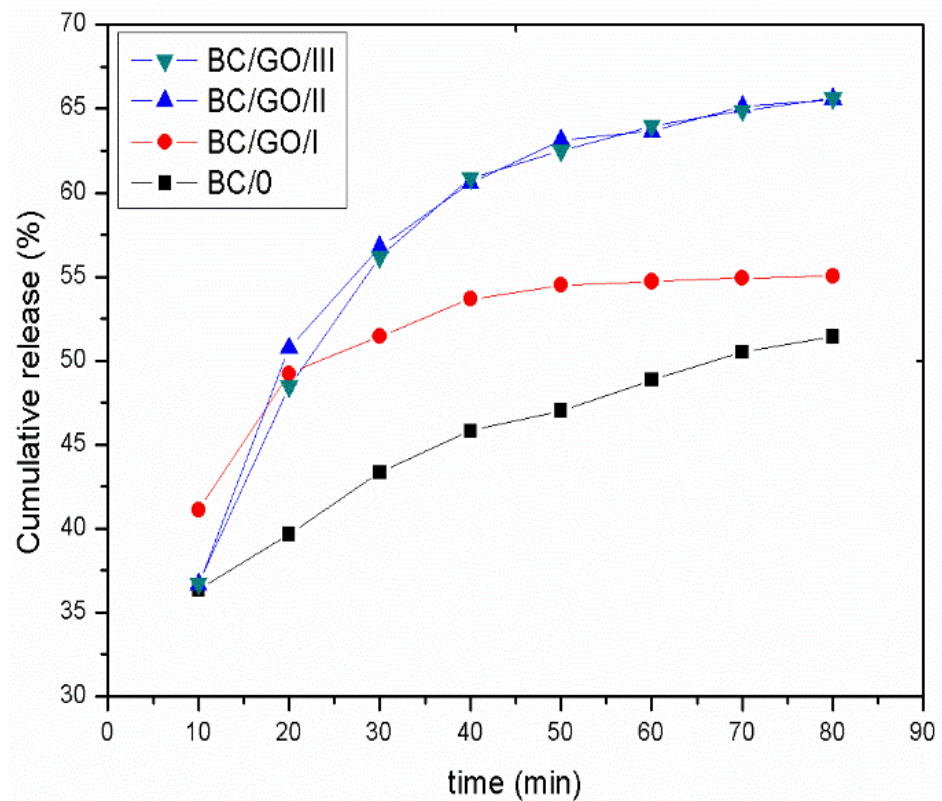
(**b**)

Figure 5. (**a**) Graph of active substance absorption on membranes and active substance desorption from membranes after 24 h; (**b**) Paracetamol release from pure cellulose (BC/0) and composite (BC/GO/I, BC/GO/II, BC/GO/III) membranes to PBS solution.

Interesting results were obtained during the study of the kinetics of the medicine release from the BC membranes (Figure 5b). They show that the BC/0 sample desorbs paracetamol slowly but steadily; however, the release rate is less than 55%. On the other hand, the membrane with the lowest GO content (3.7% *w/w*) is characterized by a more

Figure 6. SEM pictures of the surface of BC (BC/0) samples and BC/GO/I, BC/GO/II, BC/GO/III composites at a magnification of 5000×, 10,000×, 15,000×.

Figure 6. SEM pictures of the surface of BC (BC/0) samples and BC/GO/I, BC/GO/II, BC/GO/III composites at a magnification of 5000×, 10,000×, 15,000×.

Scanning electron microscopy also allowed observing fractures of the obtained membranes. The sample photos show a pure BC membrane (Figure 7). In Figure 7 of the BC/0 membrane, we can see that the membrane is made of nanofibers that are arranged in lay-

Table 3. Thickness dispersion of BC fibers in the following membranes: BC/0, BC/GO/I, BC/GO/II and BC/GO/III, compared using FiberMetric software: (a) photo of the sample with measurements (at 10,000× magnification); (b) a histogram of BC fibers diameter distribution; (c) mean fiber diameter (nm) measured in the test range from 0 to 100 nm.

	(a)	(b)	(c)
BC/0		67.39 nm 85.79 nm 97.34 nm	÷ 91 nm 89 ÷ 91 nm
BC/GO/I		53.74 nm 85.70 nm 100.77 nm	÷ 100 nm 98 ÷ 100 nm
BC/GO/II		44.91 nm 85.95 nm 100.98 nm	÷ 98 nm 96 ÷ 98 nm
BC/GO/III		37.46 nm 85.41 nm 100.98 nm	÷ 100 nm 97 ÷ 100 nm

(a) **(b)**
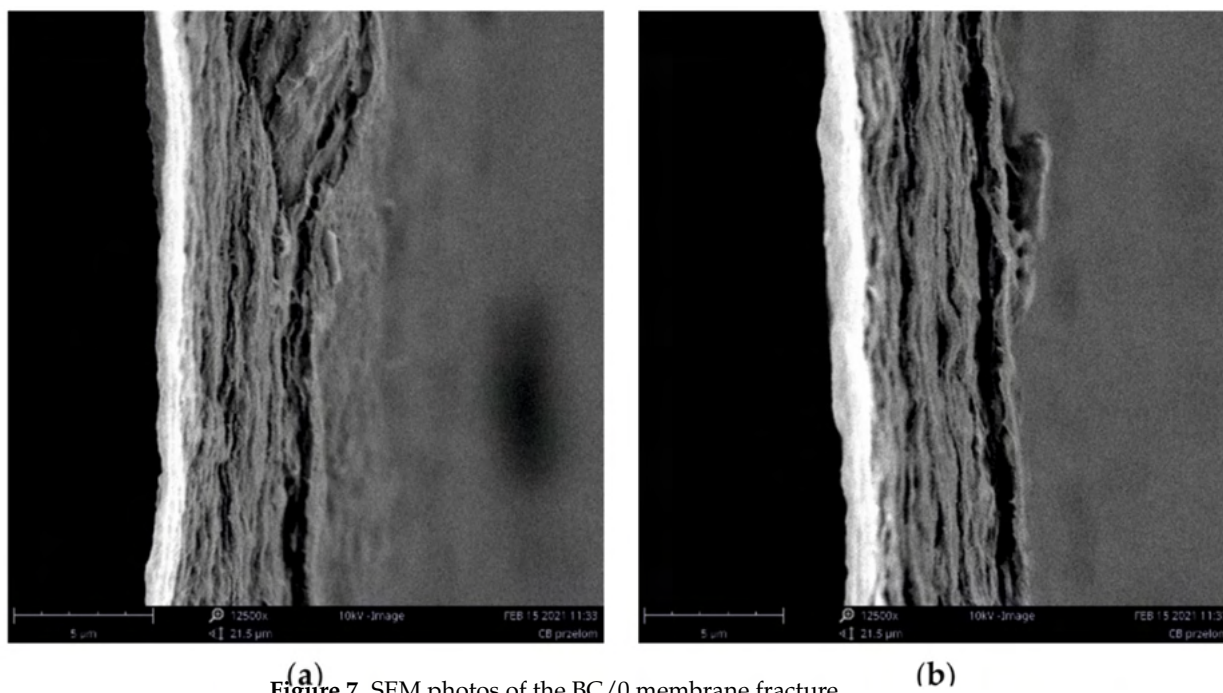
Figure 7. SEM photos of the BC/0 membrane fracture.

Measurements of the thickness of the BC fibers forming the membranes (Table 3) demonstrated that the thinnest fibers with a diameter of 85 ± 91 nm were characteristic of the BC/0 membrane, which is consistent with the literature reports [47]. The thickness of the composite fibers, on the other hand, was slightly larger and ranged from 96 to 100 nm for subsequent membranes. Therefore, it can be concluded that the addition of GO strongly influences the process of the membrane and allows perturbing the process of their formation, which confirms the results described in the literature [32]. Moreover, in the histograms (Table 3), pure BC fibers can be observed to have a low thickness spread, unlike the composite membranes.

The presence of GO in the inoculum results in a slight increase in the thickness of the BC fibers that form composite membranes. The thickness of the fibers seems to be related to the thickness of the membranes themselves (Table 2) for both wet and dry membranes. Thicker cellulose fibers form thicker composite membranes (BC/GO/I, BC/GO/II, BC/GO/III). In the case of wet membranes, the thicker BC fibers form a loose structure that contains a lot of water in the inter-fiber spaces. However, after drying the composite, membrane thickness is still 20 to 56% greater than that of the BC/0 membranes. However, a decrease in the thickness of dry membranes is observed as the GO content of the composite increases. This may be related to the amount of hydrogen bonding between cellulose particles and graphene oxide, which results in a very dense membrane.

Optical microscopy allows observing the structure of BC membranes and the degree of dispersion of the GO additive in the BC/GO/I, BC/GO/II and BC/GO/III membranes (Figure 8).
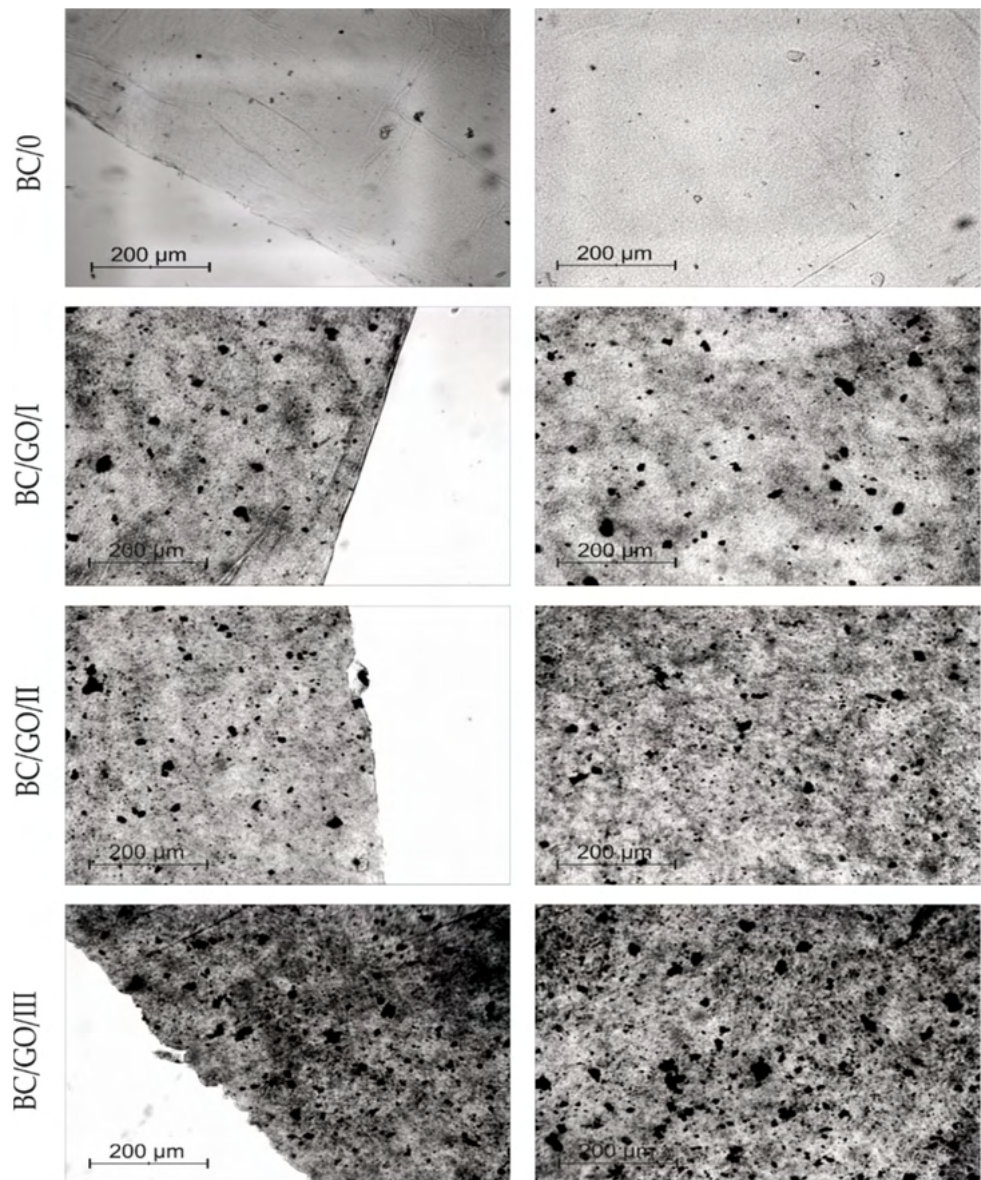
Figure 8 clearly shows the effect of the amount of GO on the internal structure of the obtained membranes. Membrane BC/0 is practically transparent, with the exception of small, foreign impurities on its surface. On the other hand, the photographs of the BC/GO/I, BC/GO/II and BC/GO/III membranes show clear GO inclusions present in the transparent structure of the dry BC. The GO additive is not uniformly dispersed. This may indicate that GO introduced into the reaction was woven into the network of BC nanofibers randomly. Moreover, it should be noted that in the photographs of the composite membranes (Figure 8), no agglomeration of the GO additive is observed. They only show an increase in the number of GO flakes in the direction from the BC/GO/I membrane, through BC/GO/II membrane to BC/GO/III membrane, in line with the amount of GO addition. We know from our own experience that the aqueous dispersion of GO in solutions with an acidic pH, which in our case is 3.5, does not tend to form agglomerates.

a decrease in the thickness of dry membranes is observed as the GO content of ~~posite~~ increases. This may be related to the amount of hydrogen bonding betwe~~...~~ ~~lose~~ particles and graphene oxide, which results in a very dense membrane.

Optical microscopy allows observing the structure of BC membranes and th~~...~~ of dispersion of the GO additive in the BC/GO/I, BC/GO/II and BC/GO/III me~~...~~ (Figure 8).

Figure 8. Optical microscope photos of BC (BC-0) samples and BC/GO/I, BC/GO/II, BC/GO/III composites.

The research on the structure of the obtained membranes was extended by the WAXS study. The structural parameters of the obtained cellulose membranes were determined on the basis of WAXS diffraction curves. The crystallinity index (CI) of obtained materials was determined on the basis of WAXS analysis by the peak deconvolution method [48]. For this purpose, each WAXS pattern was distributed into individual crystalline and amorphous components using the WaxsFit software [49]. This software was also used to calculate the crystallinity index. In the software, deconvolution is performed by means of an approximation method. It consists of the construction of a theoretical curve, which is composed of functions related to individual crystalline peaks and amorphous maxima. The shape of each peak was approximated using a linear combination of the Gaussian and Cauchy's functions. The parameters of these functions are found through best fitting of the theoretical curve to the experimental one using a suitable optimization procedure. The theoretical curve was fitted to the experimental data using Rosenbrock's double-criteria optimization method, which is described by Rabiej et al. [50]. The crystallinity index was determined as the ratio of the sum of the surface areas under the crystalline peaks to the total area under the scattering curve. An example of the distribution of BC XRD diffraction

The shape of each peak was approximated using a linear combination of the Gauss Cauchy's functions. The parameters of these functions are found through best fit the theoretical curve to the experimental one using a suitable optimization procedu theoretical curve was fitted to the experimental data using Rosenbrock's double-optimization method, which is described by Rabiej et al. [50]. The crystallinity ind determined as the ratio of the sum of the surface areas under the crystalline peaks total area under the scattering curve. An example of the distribution of BC XRD diff pattern into crystalline and amorphous components with the use of this software is

pattern into crystalline and amorphous components with the use of this software is shown in Figure 9a.

(**b**)

Figure 9. (**a**) Distribution of XRD diffraction patterns into crystalline and amorphous compo nents; (**b**) Summary of diffractograms of pure BC (BC/0) and composites (BC/GO/I, BC/GO/II, BC/G BC/GO/III) as well as pure GO membranes.

Figure 9b shows the WAXS diffraction patterns of pure cellulose (BC/0) membr composite membranes (BC/GO/I, BC/GO/II, BC/GO/III) and GO. The curves show the acteristic peaks for type I cellulose, whose angular positions fall at 2 Theta of 14.5°, and 22.7° and correspond to the planes (100), (010) and (110), respectively [51,52]. means that the addition of GO did not change the structure of the BC, as no signif shifts were observed. The WAXS curve for the GO, in turn, shows one characteristic intensity peak at 2 Theta of 11°. The intensity of the 14.5° peak is much higher than t

characteristic peaks for type I cellulose, whose angular positions fall at 2 Theta of 14.5°, 16.7° and 22.7° and correspond to the planes (100), (010) and (110), respectively [51,52]. This means that the addition of GO did not change the structure of the BC, as no significant shifts were observed. The WAXS curve for the GO, in turn, shows one characteristic high intensity peak at 2 Theta of 11°. The intensity of the 14.5° peak is much higher than that at 16.7°, which results from the typical features of BC [53]. Analyzing the shape of the curves for composite membranes (BC/GO/I, BC/GO/II, BC/GO/III), one can see slight fluctuations within the 2 Theta scattering angle of 11°, which are not present in the case of pure cellulose (BC/0). This is undoubtedly the effect of the presence of GO in the cellulose matrix of these membranes.

The conducted research shows that the degree of crystallinity of pure BC (BC/0) is high and amounts to 66%. This is a typical value for BC, a polymer of high chemical purity [41]. Analysis of the results also indicates a decrease in the degree of crystallinity with an increase in the GO content in the cellulose matrix. GO addition in the amount of 3.7, 5.4 and 7.1% w/w reduces the degree of crystallinity to 51, 47 and 40% for BC/GO/I, BC/GO/II and BC/GO/III samples, respectively. Dhar et al. in their work described a similar correlation but with reduced graphene oxide, whereby a higher concentration of GO decreased the crystallinity index up to 5% [41]. This phenomenon is explained by the fact that additives, and especially nanoadditives, disturb the formation process of BC nanofibrils, so that there is a minority of highly ordered crystalline areas in the overall structure of the material [54]. Troncoso et al. in their work described in detail how graphene nanoadditives can interfere with the formation of BC nanofibrils, thus reducing the degree of crystallinity [32].

In order to investigate the interactions between BC and the GO additive, FTIR spectroscopy studies were performed. Figure 10 summarizes the FTIR curves for the tested membranes.
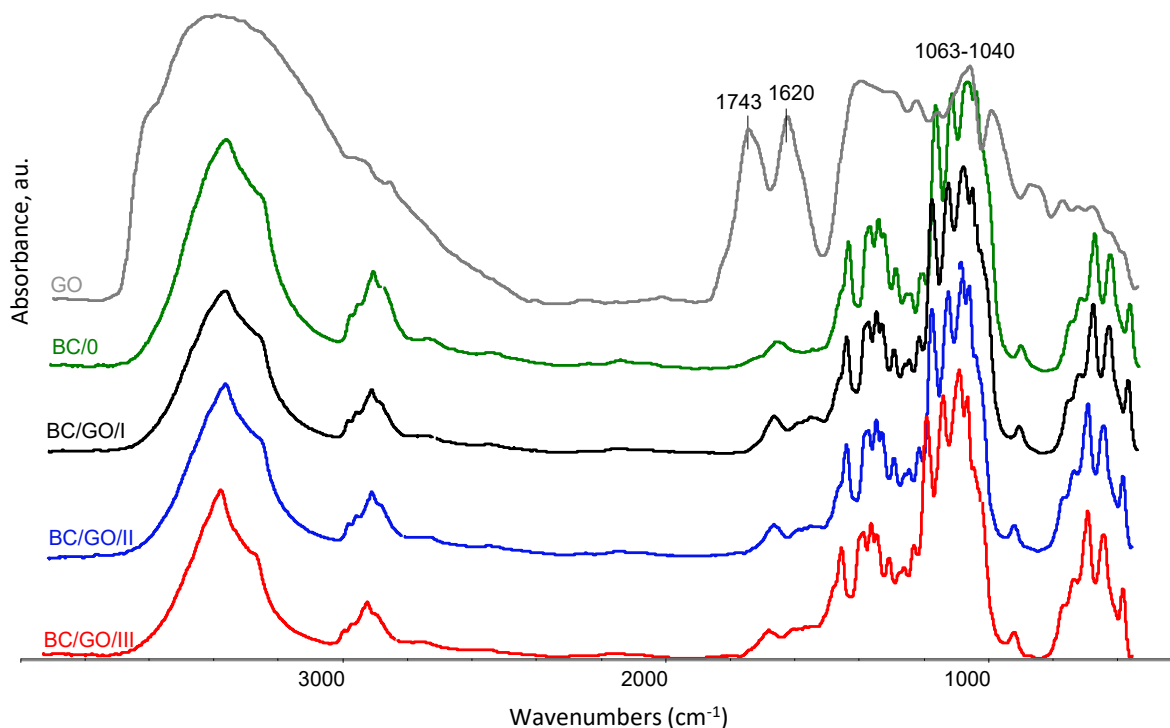

Figure 10. Summary of FTIR spectra for the following samples: BC (BC/0), BC/GO/I, BC/GO/II and BC/GO/III membranes and GO. The spectra were recorded in the range of 4000 ÷ 400 cm⁻¹.

The comparison of FTIR spectra (Figure 10) shows that the samples of BC with the GO addition (BC/GO/I, BC/GO/II, BC/GO/III) retained all the characteristic features of the pure BC bands, which confirms the behavior of this chemical structure. In all the obtained spectra, a characteristic broad absorption band of the O-H group stretching vibrations appears at wave numbers in the range of approximately 3600 ÷ 3240 cm⁻¹. There is also a slight decrease in intensity and bandwidth at a maximum of 3350 cm⁻¹ for the stretching

pure BC bands, which confirms the behavior of this chemical structure. In all the obtained spectra, a characteristic broad absorption band of the O-H group stretching vibrations appears at wave numbers in the range of approximately $3600 \div 3240$ cm^{-1}. There is also a slight decrease in intensity and bandwidth at a maximum of 3350 cm^{-1} for the stretching vibrations of the O-H oscillators along with the amount of GO added to BC. This may indicate the formation of alkali cellulose as a result of its treatment with potassium hydroxide. The spectra show characteristic vibration bands of the C-H group in cellulose I and cellulose II, at 2895 cm^{-1} and 1334 cm^{-1} [54]. The presence of these bands proves that the introduction of subsequent portions of GO during the synthesis has no effect on this group. There are no significant changes in the wavenumber range: 1162 cm^{-1}, 1113 cm^{-1}, 1063 cm^{-1} or 1040 cm^{-1} of the C–O–C group, occurring in the glucopyranose ring and ether bridges [55]. Additionally, the effects of GO on skeletal oscillators, resulting in bands at the wavenumbers around 896 cm^{-1}, are not observed. In Figure 10, a slight increase in the intensity of the bands can also be observed at 1652 cm^{-1} and 1576 cm^{-1} for the samples of composite membranes BC/GO/I, BC/GO/II and BC/GO/III. These peaks correspond to the C=C double bond vibrations in ring structures, which are one of the main bands characteristic of GO [56,57].

Based on the analysis of the thermogravimetric study results (Figure 11), it can be concluded that the process of thermal dissociation of the BC matrix of the tested membranes takes place in a single stage and in a fairly wide temperature range: from approx. 250 to 400 °C. The temperature of the extrapolated beginning of the matrix degradation process, determined on the basis of DTG curves, is the lowest for the BC/0 membrane (298.6 °C) and the highest for the BC/GO/III membrane (317.4 °C). The temperature of the maximum thermal decomposition rate of membranes in nitrogen atmosphere, expressed as the location of the respective maxima on the DTG curves is also the lowest for the sample without the GO addition (366.7 °C) and increases monotonically as the modifier content increases up to 376.6 °C for BC/GO/III membrane. It should be noted, however, that the characteristic thermal decomposition temperatures for the membranes modified with GO, vary only slightly as a function of GO content.
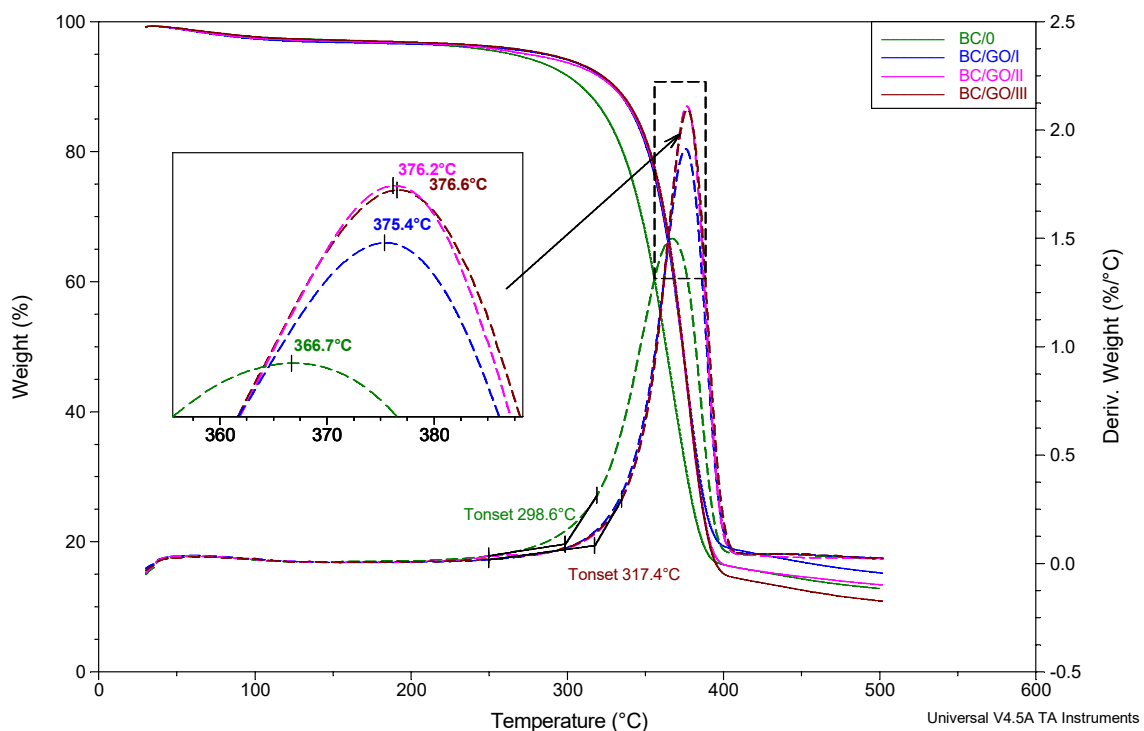
Figure 11. Summary of TG and dTG curves for membrane BC/0, BC/GO/I, BC/GO/II, BC/GO/III samples. Heating rate 20°/min, N$_2$ atmosphere flow 60 mL/min.

4. Conclusions

A simple method of obtaining composite membranes from BC, containing the addition of GO (from 3.7 to 5.1% *w/w*), was developed. The in situ bioreaction method ensured the optimal pH of the solution (pH = 3.5), preventing GO agglomeration, and optical mi-

4. Conclusions

A simple method of obtaining composite membranes from BC, containing the addition of GO (from 3.7 to 5.1% *w/w*), was developed. The in situ bioreaction method ensured the optimal pH of the solution (pH = 3.5), preventing GO agglomeration, and optical microscopy confirmed the good dispersibility of the nanoadditive in the BC matrix. The possibility of using the obtained composite membranes as a potential active dressing with sustained-release analgesic medicine—paracetamol—was also investigated. The BC/GO wet composite membranes selected for these tests (~400% water content in the membrane, thickness of ~1100 μm, BC nanofiber diameter of ~100 nm) were characterized by a slow desorption time, constant drug concentration over time and a high drug release rate after 24 h (~80%). The morphology of the surface and cross-sections of the obtained membranes, examined using SEM, did not show any significant differences in their structure, but revealed the presence of GO flakes woven into the structure of BC nanofibers. The SEM analysis and the study of the degree of crystallinity (WAXS) confirmed the effect of the GO addition on the large dispersion of the BC nanofiber diameter and the related decrease in crystallinity from 66% (for the BC/0 sample) to 40% (for the BC/GO/III sample). Infrared spectroscopy (FTIR), X-ray structure studies (WAXS) as well as thermal analysis (TGA) demonstrated the presence of GO in the BC matrix and interactions between the matrix and the additive. The shift of the characteristic temperatures of the BC thermal degradation process, with the temperature of the highest process rate —in the extreme case (BC/0 membrane) by less than 10 °C and the temperature of the extrapolated onset of transformation—being up to nearly 19 °C, clearly demonstrates the increase in thermal stability of the tested membranes influenced by GO.

Institutional Review Board Statement: Not applicable.

Informed Consent Statement: Not applicable.

Data Availability Statement: Not applicable.

Conflicts of Interest: The authors declare no conflict of interest.

References

1. Torres, F.G.; Troncoso, O.P.; Lopez, D.; Grande, C.; Gomez, C.M. Reversible stress softening and stress recovery of cellulose networks. *Soft Matter* **2009**, *5*, 4185–4190. [CrossRef]
2. Iguchi, M.; Yamanaka, S.; Budhiono, J.A. Review Bacterial cellulose—A masterpiece of nature's arts. *J. Mater. Sci.* **2000**, *35*, 261–270. [CrossRef]
3. Thompson, M.A.; Onyeziri, M.C.; Fuqua, C. Function and Regulation of Agrobacterium Tumefaciens Cell Surface Structures That Promote Attachment. In *Agrobacterium Biology. Current Topics in Microbiology and Immunology*; Gelvin, S., Ed.; Springer: Cham, Switzerland, 2018; Volume 418, pp. 143–184, ISBN 9783030032562.
4. Stumpf, T.R.; Yang, X.; Zhang, J.; Cao, X. In situ and ex situ modifications of bacterial cellulose for applications in tissue engineering. *Mater. Sci. Eng. C* **2018**, *82*, 372–383. [CrossRef]
5. Tanskul, S.; Amornthatree, K.; Jaturonlak, N. A new cellulose-producing bacterium, Rhodococcus sp. MI 2: Screening and optimization of culture conditions. *Carbohydr. Polym.* **2013**, *92*, 421–428. [CrossRef] [PubMed]
6. Omadjela, O.; Narahari, A.; Strumillo, J.; Mélida, H.; Mazur, O.; Bulone, V.; Zimmer, J. BcsA and BcsB form the catalytically active core of bacterial cellulose synthase sufficient for in vitro cellulose synthesis. *Proc. Natl. Acad. Sci. USA* **2013**, *110*, 17856–17861. [CrossRef]
7. Kim, Y.; Ullah, M.W.; Ul-Islam, M.; Khan, S.; Jang, J.H.; Park, J.K. Self-assembly of bio-cellulose nanofibrils through intermediate phase in a cell-free enzyme system. *Biochem. Eng. J.* **2019**, *142*, 135–144. [CrossRef]

8. Purushotham, P.; Cho, S.H.; Díaz-Moreno, S.M.; Kumar, M.; Nixon, B.T.; Bulone, V.; Zimmer, J. A single heterologously expressed plant cellulose synthase isoform is sufficient for cellulose microfibril formation in vitro. *Proc. Natl. Acad. Sci. USA* **2016**, *113*, 11360–11365. [CrossRef]

9. Ullah, M.W.; Ul-Islam, M.; Khan, S.; Kim, Y.; Park, J.K. Innovative production of bio-cellulose using a cell-free system derived from a single cell line. *Carbohydr. Polym.* **2015**, *132*, 286–294. [CrossRef]

10. Manan, S.; Wajid Ullah, M.; Ul-Islam, M.; Shi, Z.; Gauthier, M.; Yang, G. Bacterial cellulose: Molecular regulation of biosynthesis, supramolecular assembly, and tailored structural and functional properties. *Prog. Mater. Sci.* **2022**, *129*, 100972. [CrossRef]

11. Wenhua, Z.X.; Liheng, G.; Wu, C.; Runge, L.J.Y.Z.T. A comparison of cellulose nanofibrils produced from Cladophora glomerata algae and bleached eucalyptus pulp. *Cellulose* **2016**, *23*, 493–503. [CrossRef]

12. Gorgieva, S.; Trček, J. Bacterial cellulose: Production, modification and perspectives in biomedical applications. *Nanomaterials* **2019**, *9*, 1352. [CrossRef] [PubMed]

13. Rajwade, J.M.; Paknikar, K.M.; Kumbhar, J.V. Applications of bacterial cellulose and its composites in biomedicine. *Appl. Microbiol. Biotechnol.* **2015**, *99*, 2491–2511. [CrossRef] [PubMed]

14. Rambo, C.R.; Recouvreux, D.O.S.; Carminatti, C.A.; Pitlovanciv, A.K.; Antônio, R.V.; Porto, L.M. Template assisted synthesis of porous nanofibrous cellulose membranes for tissue engineering. *Mater. Sci. Eng. C* **2008**, *28*, 549–554. [CrossRef]

15. Ozdil, D.; Aydin, H.M. Polymers for medical and tissue engineering applications. *J. Chem. Technol. Biotechnol.* **2014**, *89*, 1793–1810. [CrossRef]

16. Ciechańska, D. Multifunctional bacterial cellulose/chitosan composite materials for medical applications. *Fibres Text East Eur.* **2004**, *12*, 69–72.

17. Kim, J.; Cai, Z.; Lee, H.S.; Choi, G.S.; Lee, D.H.; Jo, C. Preparation and characterization of a Bacterial cellulose/Chitosan composite for potential biomedical application. *J. Polym. Res.* **2011**, *18*, 739–744. [CrossRef]

18. Kirdponpattara, S.; Khamkeaw, A.; Sanchavanakit, N.; Pavasant, P.; Phisalaphong, M. Structural modification and characterization of bacterial cellulose-alginate composite scaffolds for tissue engineering. *Carbohydr. Polym.* **2015**, *132*, 146–155. [CrossRef]

19. Wichai, S.; Chuysinuan, P.; Chaiarwut, S.; Ekabutr, P.; Supaphol, P. Development of bacterial cellulose/alginate/chitosan composites incorporating copper (II) sulfate as an antibacterial wound dressing. *J. Drug Deliv. Sci. Technol.* **2019**, *51*, 662–671. [CrossRef]

20. Jia, Y.; Huo, M.; Huang, H.; Fu, W.; Wang, Y.; Zhang, J.; Jia, S. Preparation and characterization of bacterial cellulose/hyaluronic acid composites. *Proc. Inst. Mech. Eng. Part N J. Nanoeng. Nanosyst.* **2015**, *229*, 41–48. [CrossRef]

21. Noh, Y.K.; Dos Santos Da Costa, A.; Park, Y.S.; Du, P.; Kim, I.H.; Park, K. Fabrication of bacterial cellulose-collagen composite scaffolds and their osteogenic effect on human mesenchymal stem cells. *Carbohydr. Polym.* **2019**, *219*, 210–218. [CrossRef]

22. Saska, S.; Teixeira, L.N.; Tambasco De Oliveira, P.; Minarelli Gaspar, A.M.; Lima Ribeiro, S.J.; Messaddeq, Y.; Marchetto, R. Bacterial cellulose-collagen nanocomposite for bone tissue engineering. *J. Mater. Chem.* **2012**, *22*, 22102–22112. [CrossRef]

23. Wang, Q.; Sun, J.; Yao, Q.; Ji, C.; Liu, J.; Zhu, Q. 3D printing with cellulose materials. *Cellulose* **2018**, *25*, 4275–4301. [CrossRef]

24. Khan, S.; Ul-Islam, M.; Ullah, M.W.; Zhu, Y.; Narayanan, K.B.; Han, S.S.; Park, J.K. Fabrication strategies and biomedical applications of three-dimensional bacterial cellulose-based scaffolds: A review. *Int. J. Biol. Macromol.* **2022**, *209*, 9–30. [CrossRef] [PubMed]

25. Schaffner, M.; Rühs, P.A.; Coulter, F.; Kilcher, S.; Studart, A.R. 3D printing of bacteria into functional complex materials. *Sci. Adv.* **2017**, *3*, eaao6804. [CrossRef] [PubMed]

26. Markstedt, K.; Mantas, A.; Tournier, I.; Martínez Ávila, H.; Hägg, D.; Gatenholm, P. 3D bioprinting human chondrocytes with nanocellulose-alginate bioink for cartilage tissue engineering applications. *Biomacromolecules* **2015**, *16*, 1489–1496. [CrossRef]

27. Hospodiuk-Karwowski, M.; Bokhari, S.M.Q.; Chi, K.; Moncal, K.K.; Ozbolat, V.; Ozbolat, I.T.; Catchmark, J.M. Dual-charge bacterial cellulose as a potential 3D printable material for soft tissue engineering. *Compos. Part B Eng.* **2022**, *231*, 109598. [CrossRef]

28. Marins, J.A.; Soares, B.G.; Dahmouche, K.; Ribeiro, S.J.L.; Barud, H.; Bonemer, D. Structure and properties of conducting bacterial cellulose-polyaniline nanocomposites. *Cellulose* **2011**, *18*, 1285–1294. [CrossRef]

29. Khan, S.; Ul-Islam, M.; Ikram, M.; Islam, S.U.; Ullah, M.W.; Israr, M.; Jang, J.H.; Yoon, S.; Park, J.K. Preparation and structural characterization of surface modified microporous bacterial cellulose scaffolds: A potential material for skin regeneration applications in vitro and in vivo. *Int. J. Biol. Macromol.* **2018**, *117*, 1200–1210. [CrossRef]

30. Urbina, L.; Eceiza, A.; Gabilondo, N.; Corcuera, M.Á.; Retegi, A. Tailoring the in situ conformation of bacterial cellulose-graphene oxide spherical nanocarriers. *Int. J. Biol. Macromol.* **2020**, *163*, 1249–1260. [CrossRef]

31. Peng, S.; Fan, L.; Wei, C.; Liu, X.; Zhang, H.; Xu, W.; Xu, J. Flexible polypyrrole/copper sulfide/bacterial cellulose nanofibrous composite membranes as supercapacitor electrodes. *Carbohydr. Polym.* **2017**, *157*, 344–352. [CrossRef]

32. Troncoso, O.P.; Torres, F.G. Bacterial cellulose—Graphene based nanocomposites. *Int. J. Mol. Sci.* **2020**, *21*, 6532. [CrossRef] [PubMed]

33. Luo, H.; Ao, H.; Li, G.; Li, W.; Xiong, G.; Zhu, Y.; Wan, Y. Bacterial cellulose/graphene oxide nanocomposite as a novel drug delivery system. *Curr. Appl. Phys.* **2017**, *17*, 249–254. [CrossRef]

34. Song, S.; Liu, Z.; Zhang, J.; Jiao, C.; Ding, L.; Yang, S. Synthesis and Adsorption Properties of Novel Bacterial Cellulose/Graphene Oxide/Attapulgite Materials for Cu and Pb Ions in Aqueous Solutions. *Materials* **2020**, *13*, 3703. [CrossRef] [PubMed]

35. Jayani, T.; Sanjeev, B.; Marimuthu, S.; Uthandi, S. Bacterial Cellulose Nano Fiber (BCNF) as carrier support for the immobilization of probiotic, Lactobacillus acidophilus 016. *Carbohydr. Polym.* **2020**, *250*, 116965. [CrossRef] [PubMed]

36. Luo, H.; Dong, J.; Yao, F.; Yang, Z.; Li, W.; Wang, J.; Xu, X. Layer-by-Layer Assembled Bacterial Cellulose / Graphene Oxide Hydrogels with Extremely Enhanced Mechanical Properties. *Nano-Micro Lett.* **2018**, *10*, 42. [CrossRef]
37. Eng, A.Y.S.; Chua, C.K.; Pumera, M. Facile labelling of graphene oxide for superior capacitive energy storage and fluorescence applications. *Phys. Chem. Chem. Phys.* **2016**, *18*, 9673–9681. [CrossRef]
38. Oliveira Barud, H.G.; Barud, H.D.S.; Cavicchioli, M.; Do Amaral, T.S.; De Oliveira Junior, O.B.; Santos, D.M.; De Oliveira Almeida Petersen, A.L.; Celes, F.; Borges, V.M.; De Oliveira, C.I.; et al. Preparation and characterization of a bacterial cellulose/silk fibroin sponge scaffold for tissue regeneration. *Carbohydr. Polym.* **2015**, *128*, 41–51. [CrossRef]
39. Gabryś, T.M.; Fryczkowska, B.; Machnicka, A.; Graczyk, T. Nanocomposite cellulose fibres doped with graphene oxide and their biocidal properties. *Polymers* **2021**, *13*, 204. [CrossRef]
40. Song, B.; Zhang, C.; Zeng, G.; Gong, J.; Chang, Y.; Jiang, Y. Antibacterial properties and mechanism of graphene oxide-silver nanocomposites as bactericidal agents for water disinfection. *Arch. Biochem. Biophys.* **2016**, *604*, 167–176. [CrossRef]
41. Dhar, P.; Etula, J.; Bankar, S.B. In Situ Bioprocessing of Bacterial Cellulose with Graphene: Percolation Network Formation, Kinetic Analysis with Physicochemical and Structural Properties Assessment. *ACS Appl. Bio Mater.* **2019**, *2*, 4052–4066. [CrossRef]
42. Hummers, W.S.; Offeman, R.E. Preparation of Graphitic Oxide. *J. Am. Chem. Soc.* **1958**, *80*, 1339. [CrossRef]
43. Sieradzka, M.; Fryczkowski, R.; Fryczkowska, B.; Biniaś, D. Influence of solvents on low-temperature reduction- -exfoliation of graphene oxide. *Polimery* **2017**, *62*, 841–847. [CrossRef]
44. Machnicka, A.; Fryczkowska, B. Bioactive membranes from cellulose with a graphene oxide admixture. *J. Ecol. Eng.* **2018**, *19*, 231–240. [CrossRef]
45. Wei, X.; Wang, Y.; Li, J.; Wang, F.; Chang, G.; Fu, T.; Zhou, W. Effects of temperature on cellulose hydrogen bonds during dissolution in ionic liquid. *Carbohydr. Polym.* **2018**, *201*, 387–391. [CrossRef] [PubMed]
46. Kannam, S.K.; Oehme, D.P.; Doblin, M.S.; Gidley, M.J.; Bacic, A.; Downton, M.T. Hydrogen bonds and twist in cellulose microfibrils. *Carbohydr. Polym.* **2017**, *175*, 433–439. [CrossRef]
47. Guhados, G.; Wan, W.; Hutter, J.L. Measurement of the elastic modulus of single bacterial cellulose fibers using atomic force microscopy. *Langmuir* **2005**, *21*, 6642–6646. [CrossRef]
48. Park, S.; Baker, J.O.; Himmel, M.E.; Parilla, P.A.; Johnson, D.K. Cellulose crystallinity index: Measurement techniques and their impact on interpreting cellulase performance. *Biotechnol. Biofuels* **2010**, *3*, 10. [CrossRef]
49. Rabiej, M. Application of the particle swarm optimization method for the analysis of wide-angle X-ray diffraction curves of semicrystalline polymers. *J. Appl. Crystallogr.* **2017**, *50*, 221–230. [CrossRef]
50. Rabiej, M.; Rabiej, S. *Analiza Rentgenowskich Krzywych Dyfrakcyjnych Polimerów za Pomocą Programu Komputerowego Waxsfit*, 1st ed.; Garbarczyk, J., Broda, J., Eds.; Wydawnictwo Akademii Techniczno-Humanistycznej w Bielsku-Białaj: Bielsko Biała, Poland, 2006; ISBN 83-89086-39-5.
51. Yao, Q.; Fan, B.; Xiong, Y.; Jin, C.; Sun, Q.; Sheng, C. 3D assembly based on 2D structure of Cellulose Nanofibril/Graphene Oxide Hybrid Aerogel for Adsorptive Removal of Antibiotics in Water. *Sci. Rep.* **2017**, *7*, 45914. [CrossRef]
52. Singhsa, P.; Narain, R.; Manuspiya, H. Physical structure variations of bacterial cellulose produced by different Komagataeibacter xylinus strains and carbon sources in static and agitated conditions. *Cellulose* **2018**, *25*, 1571–1581. [CrossRef]
53. Tokoh, C.; Takabe, K.; Sugiyama, J.; Fujita, M. Cellulose synthesized by Acetobacter xylinum in the presence of plant cell wall polysaccharides. *Cellulose* **2002**, *9*, 65–74. [CrossRef]
54. Paquin, F.; Rivnay, J.; Salleo, A.; Stingelin, N.; Silva, C. Multi-phase semicrystalline microstructures drive exciton dissociation in neat plastic semiconductors. *J. Mater. Chem. C* **2015**, *3*, 10715–10722. [CrossRef]
55. Pinto, S.C.; Gonçalves, G.; Sandoval, S.; López-Periago, A.M.; Borras, A.; Domingo, C.; Tobias, G.; Duarte, I.; Vicente, R.; Marques, P.A.A.P. Bacterial cellulose/graphene oxide aerogels with enhanced dimensional and thermal stability. *Carbohydr. Polym.* **2020**, *230*, 115598. [CrossRef] [PubMed]
56. Luo, H.; Ao, H.; Peng, M.; Yao, F.; Yang, Z.; Wan, Y. Effect of highly dispersed graphene and graphene oxide in 3D nanofibrous bacterial cellulose scaffold on cell responses: A comparative study. *Mater. Chem. Phys.* **2019**, *235*, 121774. [CrossRef]
57. Luo, H.; Dong, J.; Xu, X.; Wang, J.; Yang, Z.; Wan, Y. Exploring excellent dispersion of graphene nanosheets in three-dimensional bacterial cellulose for ultra-strong nanocomposite hydrogels. *Compos. Part A Appl. Sci. Manuf.* **2018**, *109*, 290–297. [CrossRef]

103

GO-Enabled Bacterial Cellulose Membranes by Multistep, In Situ Loading: Effect of Bacterial Strain and Loading Pattern on Nanocomposite Properties
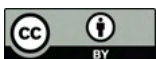
Tobiasz Gabryś [1],* , Beata Fryczkowska [2] , Urška Jančič [3] , Janja Trček [4] and Selestina Gorgieva [3]

1   Department of Material Engineering, Faculty of Materials, Civil and Environmental Engineering, University of Bielsko-Biala, ul. Willowa 2, 43-309 Bielsko-Biala, Poland
2   Department of Environmental Protection and Engineering, Faculty of Materials, Civil and Environmental Engineering, University of Bielsko-Biala, ul. Willowa 2, 43-309 Bielsko-Biala, Poland
3   Institute of Engineering Materials and Design, Faculty of Mechanical Engineering, University of Maribor, Smetanova ul. 17, 2000 Maribor, Slovenia
4   Department of Biology, Faculty of Natural Sciences and Mathematics, University of Maribor, Koroška Cesta 160, 2000 Maribor, Slovenia
*   Correspondence: tgabrys@ath.bielsko.pl

Abstract: This paper presents the results of research on the preparation and properties of GO/BC nanocomposite from bacterial cellulose (BC) modified with graphene oxide (GO) using the in situ method. Two bacterial strains were used for the biosynthesis of the BC: *Komagataeibacter intermedius* LMG 18909 and *Komagataeibacter sucrofermentans* LMG 18788. A simple biosynthesis method was developed, where GO water dispersion was added to reinforced acetic acid-ethanol (RAE) medium at concentrations of 10 ppm, 25 ppm, and 50 ppm at 24 h and 48 h intervals. As a result, a GO/BC nanocomposite membrane was obtained, characterized by tensile strength greater by 150% as compared with the pure BC (~50 MPa) and lower volume resistivity of ~$4 \cdot 10^9$ $\Omega \times$ cm. Moreover, GO addition increases membrane thickness up to ~10% and affects higher mass production, especially with low GO concentration. All of this may indicate the possibility of using GO/BC membranes in fuel cell applications.

Keywords: bacterial cellulose; graphene oxide; nanocomposite; structural analysis

1. Introduction

Cellulose is a widely available biopolymer synthesized mainly by plants, as well as fungi, protozoa, and prokaryotes [1]. Chemically, it is a linear homopolysaccharide composed of 3000–14,000 D-glucopyranose molecules linked with β-1,4-glycosidic bonds [2]. Plant-derived cellulose also contains other biopolymers, such as hemicelluloses and lignins. These compounds can be removed using chemical treatment and purification methods before further processing [3,4].

A fascinating pure form of cellulose is bacterial cellulose (BC). It is composed of linear β-1,4-glucan chains forming protofibrils, which combine into nanofibrils to form a compact, three-dimensional network [5]. The diameter of a single BC fibril does not exceed 100 nm and the product obtained in this bioreaction is in the form of a flat membrane [6,7]. One of the ways to synthesize BC is acetic fermentation, carried out in the presence of microorganisms, including gram-positive and gram-negative bacteria [8–12].

BC possess a relatively large specific surface area, high porosity, high flexibility, and mechanical strength (GPa-scale), as well as a high degree of crystallinity, reaching as far as 80% [13–15]. An exceptional feature of the BC is its ability to absorb, store, and desorb large amounts of water (more than 200 times its dry weight). This property is closely related to the structure of BC. Another very important feature of BC is biodegradability by many

microorganisms, although not by the human body [16]. Moreover, it is a durable and environmentally friendly product. BC is applied in pharmacology and biomedicine [2,17–20] and can also be used in textiles, cosmetics, and food products [21,22]. In addition, the potential applications of BC include air purification, water treatment, food storage or energy conversion, electronic paper, audio membrane, and so on [22–24].

In order to give the BC membrane new, unique properties, it can be modified using methods such as ex situ, in situ, or solvent dissolution-regeneration [11]. The most important criterion differentiating these methods is that the ex situ method introduces additives onto the finished BC product. The literature describes many examples of the preparation of BC composites; e.g., with silk fibroin, proteins, gelatin, silver nanoparticles, zinc oxide, hydroxyapatite, or graphene oxide (GO) [11,14,25–27]. The in situ modification method introduces additives or nanoparticles that are soluble in water or form dispersion with it, directly into the BC culture medium used at the beginning of biosynthesis. In this one-step process, nanoadditives intertwine with the emerging network of BC nanofibers [11,14,28,29]. The literature describes the possibility of obtaining composites based on BC membranes with the addition of electrically conductive polymers as well as graphene and GO [13,29–31]. The third method of BC modification is solvent dissolution-regeneration. It involves dissolving BC; adding additives or nanoadditives, e.g., polypyrrole/carbon nanotubes or polyvinyl alcohol; and then precipitating the obtained composite [32,33].

An interesting and intensively researched nanoadditive is GO, a two-dimensional nanomaterial with different types of oxygen functional groups on its surface [34]. GO easily forms stable dispersions with water and other organic solvents, e.g., DMF and ethylene glycol [35,36]. The presence of many oxygen functional groups on the GO surface promotes the formation of dispersions with solutions of other polymers, which also have functional groups [37].

BC is undoubtedly such a polymer, featuring hydroxyl groups in its structure, thanks to which it can form hydrogen bonds with GO [38]. The methods of obtaining BC nanocomposites with GO are particularly well known. The literature describes a GO-modified BC nanocomposite, which can potentially be applied to remove impurities [29,31]. Other researchers have described a method of obtaining a multi-layer and durable BC/GO composite material, where GO was applied on the surface of the forming BC film [38]. In turn, Urbina et al. reported the in situ method to obtain bacterial cellulose-graphene oxide spherical nanocarriers where the GO was directly added to the medium [14]. Moreover, GO has been introduced into the BC network to prepare conductive nano papers as an innovative energy storage device [13,39]. The use of carbon nano additives can improve the properties of the nanocomposites such as porosity and strength and provide it with electro-conductive properties. Therefore, improving these parameters, which in the case of biomaterials are particularly important, increases the application capabilities. All of this allows for the potential use of such a nanocomposite as an adsorbent, scaffold, or dressing material [40–43]. Carbon-related nanomaterials can be used as biomaterials in tissue engineering and drugs carriers [14,44].

This paper presents research results about BC membranes modified with GO using a multistep, in situ loading method. This method was chosen to solve a critical challenge—GO agglomeration in the BC production medium. Two acetic acid bacterial strains were used to produce BC and GO/BC nanocomposites—*Komagataeibacter intermedius* and *Komagataeibacter sucrofermentans*. Their effect and loading pattern on GO/BC nanocomposite properties were studied to obtain homogeneous novel membranes that take advantage of the outstanding properties of BC and GO, including improved resistivity—an important property in fuel cell membrane application. The work is a continuation of our previous article, differing in that specific strains of bacteria were used and research was carried out confirming the possibilities of practical application, including mechanical and physico-chemical tests [45].

2. Materials and Methods

2.1. Chemicals

The reagents used for the preparation of RAE medium and purification of obtained BC were as follows: D-glucose (≥99%), peptone from meat enzymatic digest, and sodium hydroxide (≥97%, pellets) purchased from Sigma Aldrich (Darmstadt, Germany); yeast extract and micro agar purchased from Duchefa Biochemie (Haarlem, The Netherlands); disodium hydrogen phosphate dihydrate purchased from Merck (Darmstadt, Germany); citric acid purchased from Caleo (Graz, Austria); and acetic acid (99.8%) and ethanol (96%) purchased from Honeywell (Charlotte, NC, USA). The reagents for the production GO included the following: graphite powder < 20 μm purchased from Sigma-Aldrich, potassium permanganate (≥99%), and sulfuric acid (98%) and hydrogen peroxide (30%) purchased from Avantor Performance Materials Poland S.A. (Gliwice, Poland). GO synthesis description and testing of its properties (XRD, DSC, FTIR) were described in our earlier work [46].

2.2. Microorganisms

Komagataeibacter intermedius LMG 18909 and *Komagataeibacter sucrofermentans* LMG 18788 were maintained and precultured in the Laboratory of Microbiology, Department of Biology, Faculty of Natural Sciences and Mathematics, University of Maribor.

2.3. Medium

The RAE medium for bacterial cellulose production was selected on the basis of our experience and literature data [47]. RAE media were used for both types of bacteria (*K. intermedius* and *K. sucrofermentans*). Liquid RAE media consisted of glucose (40 g/L), peptone from meat (10 g/L), yeast extract (10 g/L), $Na_2HPO_4 \times 2H_2O$ (3.38 g/L), citric acid (1.37 g/L), acetic acid (10 mL/L), and ethanol (10 mL/L). Solid RAE media for the bacteria revitalization and inoculation process consisted of the same ingredients as well as agar (10 g/L). Before use, all of the media were autoclaved at 121 °C for 20 min with the glucose solution autoclaved separately. Moreover, acetic acid and ethanol were added to the medium after the autoclaving process. The pH of the media was 4.1.

2.4. Growth Conditions

The bioprocesses were performed in 250 mL Erlenmeyer flasks equipped with a membrane screw cup. The flask containing 50 mL RAE media was inoculated with a single bacterial colony and incubated in a water bath for 7 days at 30 °C. For the first 24 h, the flasks were agitated by linear shaking at 120 rpm; after this, the shaking was discontinued and the bioprocess continued under static conditions. In this way, samples of reference bacterial cellulose were obtained, referred to as iBC (in the case of *K. intermedius*) and sBC (in the case of *K. sucrofermentans*).

In order to synthesize the GO/BC nanocomposite, GO water dispersion with a concentration of 10 ppm, 25 ppm, and 50 ppm was added to the RAE liquid medium. Owing to the chemical structure of GO and its possible reduction above 80 °C, the dispersion was not autoclaved. Unfortunately, already at the first dose (3.33 mL and 5 mL) in contact with the RAE medium, the GO nanoparticles aggregated and sedimented (Figure 1).

Therefore, it was decided to introduce the GO nanoadditive into the BC culture in small portions. In the GO/BC nanocomposite, GO water dispersion with a concentration of 10 ppm, 25 ppm, and 50 ppm was applied to the surface of the generated BC network in two ways. The first consisted of applying 5 mL of GO dispersion with a given concentration after 48 h and 96 h, while the second consisted of applying 3.33 mL of GO dispersion at the given concentration after 48 h, 72 h, and 96 h. In both cases, in the end, the amount of dispersion applied was the same, with only the volume of doses and time intervals being variable. Thus, a layer-by-layer nanocomposite material with GO and BC was obtained with two replications for each treatment. Figure 2 shows the process of applying GO dispersion on the BC surface, similar to our previous publication [45].

Figure 1. Visible aggregates of GO in RAE liquid medium (at pH = 4.1).

Therefore, it was decided to introduce the GO nanoadditive into the BC culture in small portions. In the GO/BC nanocomposite, GO water dispersion with a concentration of 10 ppm, 25 ppm, and 50 ppm was applied to the surface of the generated BC network in two ways. The first consisted of applying 5 mL of GO dispersion with a given concentration after 48 h and 96 h, while the second consisted of applying 3.33 mL of GO dispersion at the given concentration after 48 h, 72 h, and 96 h. In both cases, in the end, the amount of dispersion applied was the same, with only the volume of doses and time intervals being variable. Thus, a layer-by-layer nanocomposite material with GO and BC was obtained with two replications for each treatment. Figure 2 shows the process of applying GO dispersion to the BC surface, similar to our previous publication [45].
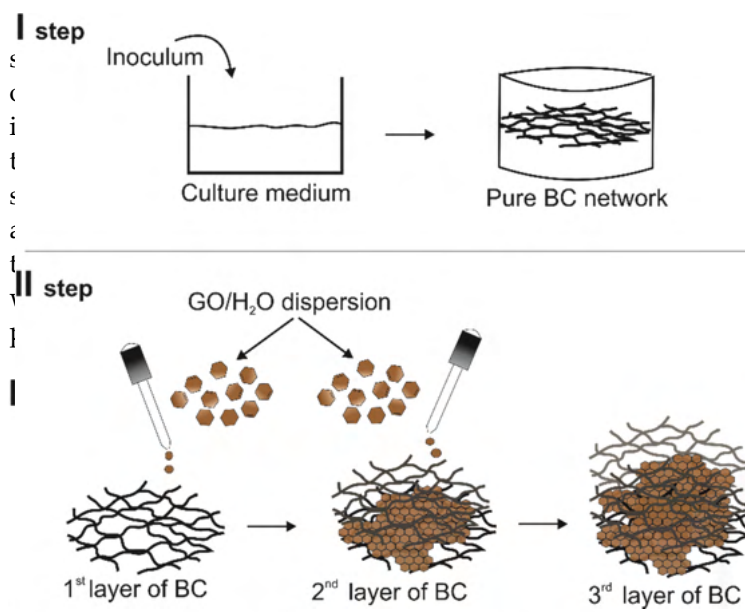

Figure 2. The loading process of GO/H₂O application onto the BC network surface [45].

The designations of pure BC samples and GO/BC nanocomposite are summarized in Table 1.

Table 1. Designation of the obtained BC and GO/BC nanocomposites.

K. intermedia	*K. sucrofermentans*	GO Dispersion Concentration [ppm]	GO Loading Dose	Intervals of Loadings [hour]
iBC	sBC	-	-	-
iBC_10/2	sBC_10/2	10		
iBC_25/2	sBC_25/2	25	2 × 5.0 mL	48/48
iBC_50/2	sBC_50/2	50		
iBC_10/3	sBC_10/3	10		
iBC_25/3	sBC_25/3	25	3 × 3.33 mL	48/24/24
iBC_50/3	sBC_50/3	50		

2.5. Purification Process

After incubation, the BC and GO/BC nanocomposites were taken from the bioprocess and rinsed with MiliQ water to remove any residual media. Then, each GO/BC nanocomposite was placed in a beaker with 100 mL of 0.5 M NaOH. The purification process was carried out in a water bath at 80 °C for 1 h with a linear shaking speed of 70 rpm. Then, bioreaction products were washed several times with MiliQ water until a neutral pH

2.5. Purification Process

After incubation, the BC and GO/BC nanocomposites were taken from the bioprocess and rinsed with MiliQ water to remove any residual media. Then, each GO/BC nanocomposite was placed in a beaker with 100 mL of 0.5 M NaOH. The purification process was carried out in a water bath at 80 °C for 1 h with a linear shaking speed of 70 rpm. Then, bioreaction products were washed several times with MiliQ water until a neutral pH was obtained. Figure 3 presents sample photos of GO/BC nanocomposites (from the left: sBC_10/3, sBC_25/3, sBC_50/3) before and after the neutralization process.
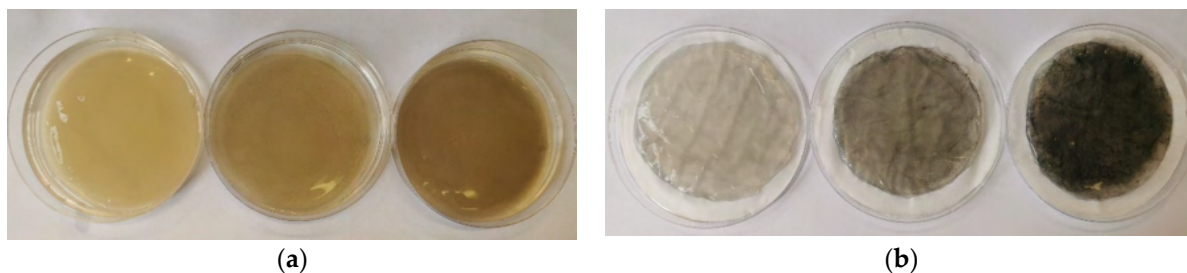

(**a**)   (**b**)

Figure 3. Examples of GO/BC nanocomposite samples with 10 ppm, 25 ppm, and 50 ppm (from left to right) GO concentration, before (**a**) and after (**b**) the neutralization process in 0.5 M NaOH.

2.6. ζ Potential Analysis of GO Dispersions

The ζ potential measurements were performed to determine the stability of the GO dispersion in the liquid culture medium. For this purpose, Litesizer 500 (Anton Paar, Graz, Austria) with a unique Omega measuring cuvette was used. The measurement was taken in a thermostated cell at a temperature of 25 °C using Milli-Q water. The ζ potential was measured in a pH range from 2 to 12, being adjusted by NaOH (0.01 M) and HCl (0.01 M).

2.7. Physicochemical Properties

Initially, the GO/BC membranes obtained in the experiment were dried and then weighed on a Sartorius analytical balance with an accuracy of 0.0001 g to determine the weight of individual samples.

The thickness of the dry GO/BC nanocomposites was measured using a digital micrometer (Inside, 3109 Series, Zamudio, Spain). Before measurements, the GO/BC nanocomposites were conditioned for 24 h at room temperature. Each value is the average of four measurements made randomly along each of the GO/BC nanocomposites.

The water contact angle (CA) measurements were carried out using an OCA 35 optical device (DataPhysic Instruments GmbH, Filderstadt, Germany) equipped with a video measuring system with an optical camera and a high-performance table adapter. The volume of the Milli-Q water droplet was 3 μL. All measurements were performed at room temperature, in triplicates, with average and standard deviation reported.

The tensile modulus (MPa), tensile strength (MPa), and elasticity (%) of the GO/BC nanocomposite were determined using Shimadzu, AG-X plus 10 kN electromechanical universal testing machine. Dry GO/BC nanocomposite samples with specimen dimensions of 10 mm × 20 mm were mounted vertically. The effective clamping distance was 25 mm. The application of tensile force (10 kN load cell) proceeded at 1 mm min⁻¹. Three or five specimens were tested per sample and average values and standard deviations were calculated.

The measurements of the volume resistivity of the obtained GO/BC nanocomposite were carried out in accordance with ASTM D275 standard using the Keithley meter model 6517A (Cleveland, OH, USA) and the Keithley test chamber, model 8009 (Cleveland, OH, USA). Samples of the test material were placed in a measuring cell between the electrode system. The measurement was carried out at a voltage of 50 V DC during an electrification time of 10 s. For each sample, five measurements were taken, from which an average value was determined. A measurement was also carried out for a reference sample without the addition of GO to demonstrate the effect of this additive on the electrical properties of the test material. A diagram showing the volume resistivity measurement method is shown in Figure 4.
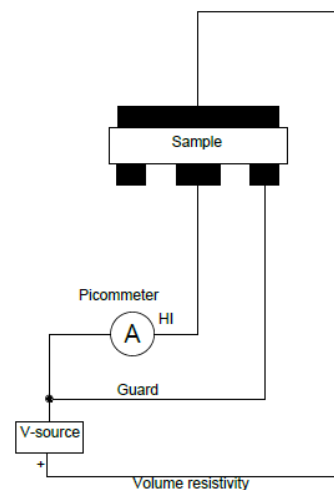
time of 10 s. For each sample, five measurements were taken, from which an average value was determined. A measurement was also carried out for a reference sample without the addition of GO to demonstrate the effect of this additive on the electrical properties of the test material. A diagram showing the volume resistivity measurement method is shown in Figure 4.

Figure 4. Diagram of the volume resistivity measurement technique.

The volume resistivity was measured by applying a voltage potential to opposite sides of the sample, measuring the resulting current flowing through the sample and then converting according to the following formula:

$$\rho = \frac{V \times 22.9}{I \times t} \ [\Omega \times cm]\tag{1}$$

Where ρ is the volume resistivity of the sample; V is the voltage applied; I is the measured current; t is the mean thickness of the sample expressed in centimeters; and 22.9 is the constant characteristic of the electrode geometry.

2.8. Structural Analysis

GO/BC nanocomposite surface observation was carried out using a high-resolution Phenom ProX scanning electron microscope (SEM) from Thermo Fisher Scientific (Pik Instrument, Piaseczno, Poland), operating at 10 kV. The samples were previously coated with a 20 nm gold layer using a Leica EM ACE200 low-vacuum coater (Wetzlar, Germany). The chemical structure of GO/BC nanocomposite materials with different GO concentrations was analyzed using a Spectrum GX FTIR spectrometer (PerkinElmer, Waltham, Massachusetts, USA) with a Golden Gate ATR attachment and a diamond crystal. The transmission spectra were obtained within the range of 4000–650 cm^{-1}, with 16 scans and a resolution of 4 cm^{-1}. Reference samples (iBC and sBC) were scanned in parallel. All scans were performed at room temperature.

Wide-angle X-ray scattering (WAXS) studies were performed using a D2 Phaser diffractometer (Bruker AXS GmbH, Karlsruhe, Germany) using the Bragg–Brentano reflection geometry method. CuKα radiation (λ = 1.54 Å) was emitted at an accelerating voltage of 30 kV and an anode current of 10 mA. A scintillation counter was used as a detector. The tests were carried out in the range of 2θ from 5° to 60° in steps of 0.03° and acquisition time of 0.25 s per one step. Before the measurements, a small piece of material was cut, placed on a quartz crystal holder, and measured at room temperature.

Thermogravimetric investigations were performed using a TA Instruments Q500 Thermogravimetric Analyzer (New Castle, DE, USA). The measurements were conducted in a nitrogen atmosphere (flow 60 mL/min), in the temperature range from 30 to 500 °C, at a heating rate of 20°/min. TG and DTG curves were analyzed using Universal V2.6D TA Instruments software (New Castle, DE, USA).

2.9. Statistical Methods

The results of the study were subjected to statistical analysis consisting of the application of Student's t-test for independent paired samples at a 5% level of significance.

3. Results and Discussion

3.1. ζ Potential of GO Dispersion and Stability of GO in RAE Medium

Because of the fact that GO is in the form of nanosheets, its stability in liquid dispersions is an essential parameter as it affects its distribution pattern within the final GO/BC nanocomposites to which it has been added. Therefore, before starting the experiment, it was necessary to explore how GO would behave within the culture medium upon its application to BC. The liquid RAE medium used has a pH of about 4.1. Therefore, $\zeta = f$ (pH) was measured in a wide range of pH from 2 to 12 (Figure 5), which covers the pH of interest.
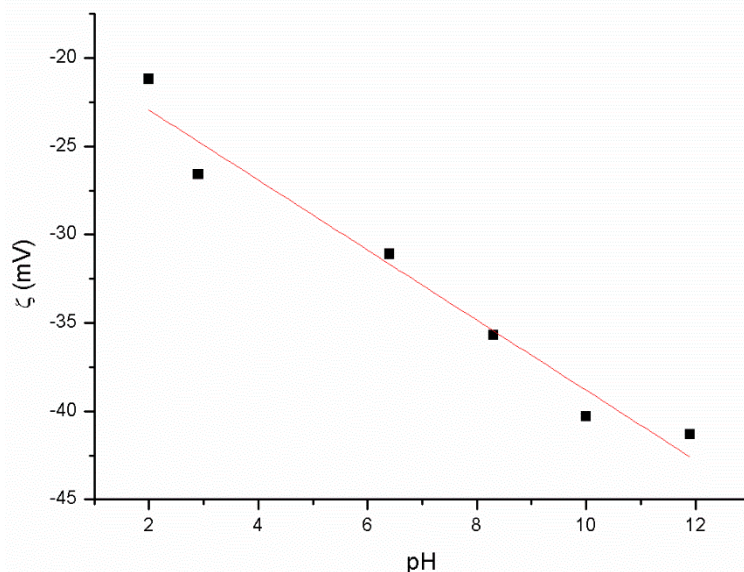

Figure 5. Zeta potential (ζ) of GO/H$_2$O dispersion in pH dependency.

The analysis showed (Figure 5) that the ζ potential of the GO water dispersion is about −27 mV at pH 4.1, which indicates its stability under these conditions [48]. A team of other researchers obtained almost identical results. Kártić et al. confirmed in his work that the zeta potential for GO at the same pH value ranges from −50 mV to −20 mV, and at pH of 4, the zeta potential was −30 mV [49]. However, research on the water dispersion of GO and its dispersion in a complex environment such as the RAE medium differs significantly. Therefore, despite the stability of GO at pH 4.1 in the water environment, in the initial effect of contact with the RAE, the GO medium underwent aggregation and sedimentation (Figure 4). The results obtained by us differ from those described in the literature, which reports that the addition of GO dispersion to the liquid medium did not cause its aggregation [30]. This may result from using a different medium, e.g., Hestrin–Scharmann (HS) [14,28]. The reason behind aggregation is a high presence of ions in the RAE medium, causing extensive charge screening. Because of this, the diffuse electric double layer around the particle surfaces is thinner, causing van der Waals force to dominate the interparticle interaction [50]. This is according to the classical theory of dispersion stability developed by Derjaguin, Landau, Verwey, and Overbeek (DLVO) [51].

As the aggregation state strongly depends on the time window investigated [50], we assume that spreading GO dispersion on already formed BC in a few intervals will hinder the aggregation owing to the limited time for contact among the particles.

3.2. General Characteristics of the Obtained Material

As a result of the experiment, pure BC and a library of GO/BC nanocomposite were obtained, photos of which are presented in Figure 6. The photographs show a change in color along with the amount of nanoadditive introduced. The reference samples (iBC

As the aggregation state strongly depends on the time window investigated [50], we assume that spreading GO dispersion on already formed BC in a few intervals will hinder the aggregation owing to the limited time for contact among the particles.

3.2. General Characteristics of the Obtained Material

As a result of the experiment, pure BC and a library of GO/BC nanocomposite were obtained, photos of which are presented in Figure 6. The photographs show a change in color along with the amount of nanoadditive introduced. The reference samples (iBC and sBC) are colourless and almost identical to the naked eye. As the concentration of GO used increases (10, 25, and 50 ppm respectively), the colour of the samples becomes darker. For samples iBC_50/2 and sBC_50/3, individual GO aggregation sites are visible as darker points.
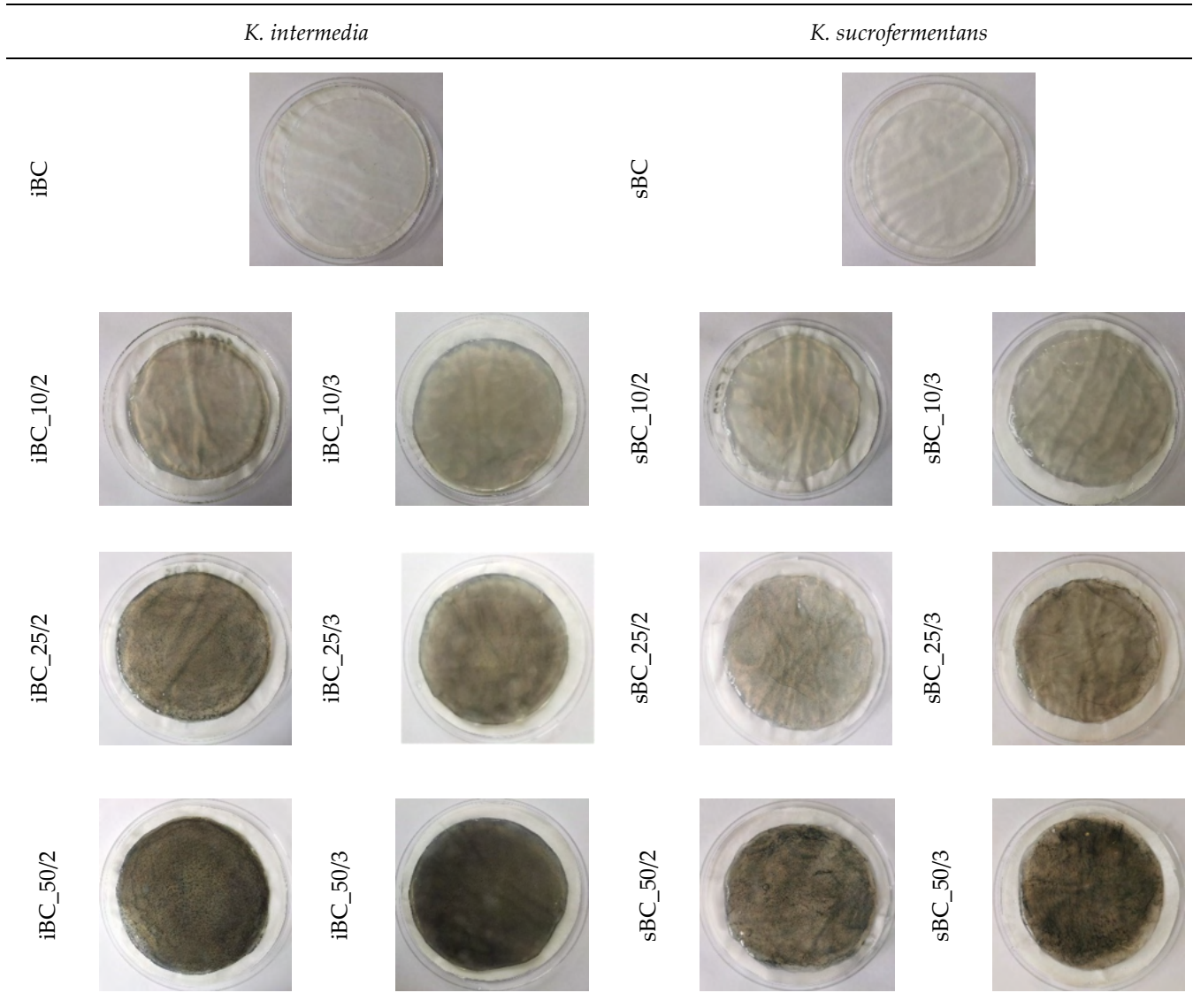

Figure 6. Photos of obtained pure BC and GO/BC nanocomposites.

In order to characterize the obtained pure BC and GO/BC nanocomposites, the following measurements were carried out: production yield; thickness; FTIR; XRD; contact angle; SEM; and mechanical, thermal (TG, dTG), and electrical properties.

Production yield measured from obtained dry material (Figure 7) indicates that *K. sucrofermentans* is a better producer of BC than *K. intermedius* in the absence of additives. Under the same conditions, it produced 12% more BC dry matter. An interesting fact is that, in the case of *K. intermedius*, regardless of the GO loading time intervals, a trend of increasing the mass of the GO/BC nanocomposites with an increase in the concentration of GO dispersion is observed. It ranges from 24% (iBC_25/3) to 39% (iBC_10/3) as compared with the iBC control sample without the addition of GO. In the case of *K. sucrofermentans*, this relationship looks different and is more closely related to the GO loading methodology, i.e., frequency and single dose. Applying GO at intervals of 48/24/24 h, as described in Table 1, results in a light decrease trend in the mass of the obtained nanocomposite, with

increasing the mass of the GO/BC nanocomposites with an increase in the concentration of GO dispersion is observed. It ranges from 24% (iBC_25/3) to 39% (iBC_10/3) as compared with the iBC control sample without the addition of GO. In the case of *K. sucrofermentans*, this relationship looks different and is more closely related to the GO loading methodology, i.e., frequency and single dose. Applying GO at intervals of 48/24/24 h, as described in Table 1, results in a light decrease trend in the mass of the obtained nanocomposite, with an increase in the concentration of GO. A similar effect occurs with samples sBC_10/2, sBC_25/2, and sBC_50/2.
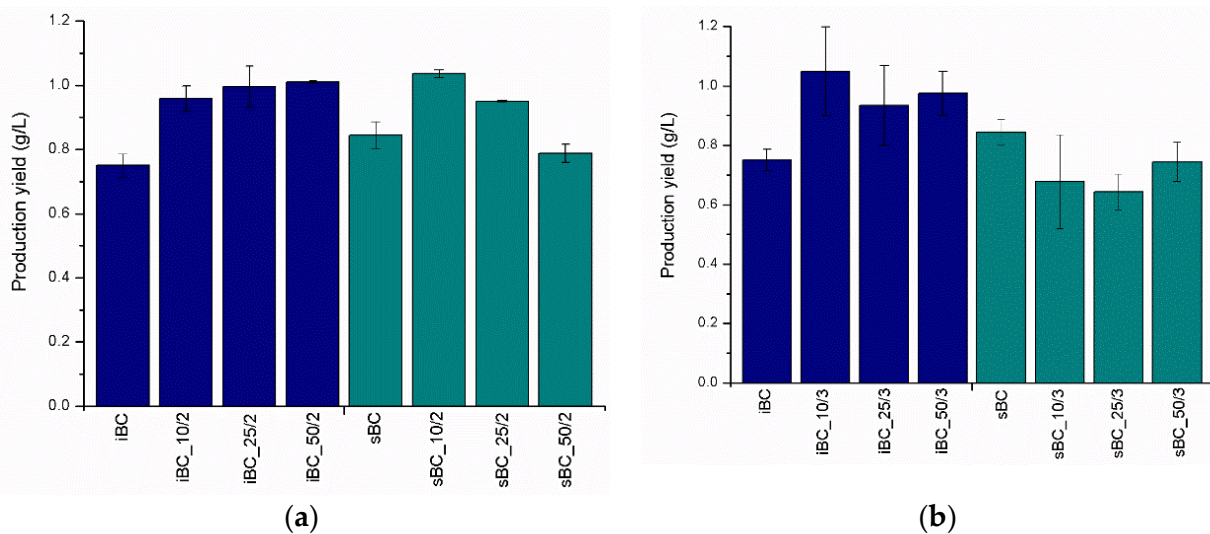

(**a**)   (**b**)

Figure 7. Production yield (g/L) of dry BC and GO/BC nanocomposites with (**a**) two and (**b**) three GO loading steps.

The analysis of the thickness of dry GO/BC nanocomposites (Table 2) shows mainly the differences in the thickness of the obtained nanocomposite depending on the strain used. The use of *K. intermedius* results in an initial BC production of about a 20% thicker membrane than in the case of the *K. sucrofermentans* strain. Thus, the difference between the average thickness values of the iBC and sBC samples is statistically significant. This phenomenon is observed for both pure BC (iBC and sBC) and the ones doped two and three times with GO. The addition of GO during BC synthesis was shown an impact on the thickness of all GO/BC nanocomposite membranes. The highest increases in BC mass are observed in the sBC_10/2 sample and amount to as much as 38%. Thus, the results we obtained confirm that the created reaction conditions favor the biosynthesis of BC.

Table 2. Thickness of dry material BC and GO/BC nanocomposites.

Thickness of Material after Drying [µm]			
iBC	23.3 ± 1.2	sBC	18.0 ± 0.9
iBC_10/2	26.6 ± 7.4	sBC_10/2	24.8 ± 7.7
iBC_25/2	23.6 ± 6.7	sBC_25/2	23.4 ± 7.1
iBC_50/2	26.1 ± 6.4	sBC_50/2	17.9 ± 3.3
iBC_10/3	25.0 ± 4.2	sBC_10/3	18.7 ± 3.3
iBC_25/3	23.1 ± 5.1	sBC_25/3	19.7 ± 5.7
iBC_50/3	23.5 ± 4.2	sBC_50/3	20.5 ± 3.4

3.3. Structural Analysis

The SEM images (Figure 8) show that GO/BC nanocomposites are made of nanofibers to form a compact 3D tight network, where individual fibrils are randomly distributed. The SEM analysis does not show GO nanosheets on the surface of GO/BC nanocomposites. This may indicate that GO is entangled between nanofibers in deeper layers. This may result from the method of applying GO to the surface of the forming nanofiber network, with individual layers being arranged alternately, and the first and last layer formed by BC. In addition, the microphotographs show no residues of bacterial cells, which proves their thorough removal during the neutralization process in NaOH. In addition, the analysis of the microphotographs indicates the existence of characteristic differences between pure bacterial cellulose synthesized by individual strains. The sBC sample, unlike iBC, shows a

sites. This may indicate that GO is entangled between nanofibers in deeper layers. This may result from the method of applying GO to the surface of the forming nanofiber network, with individual layers being arranged alternately, and the first and last layer formed by BC. In addition, the microphotographs show no residues of bacterial cells, which proves their thorough removal during the neutralization process in NaOH. In addition, the analysis of the microphotographs indicates the existence of characteristic differences between pure bacterial cellulose synthesized by individual strains. The sBC sample, unlike iBC, shows a more compact, less porous structure, where the nanofibers adhere closely to each other. In iBC, on the other hand, it is possible to easily distinguish individual nanofibers from the rest of the cellulose matrix.
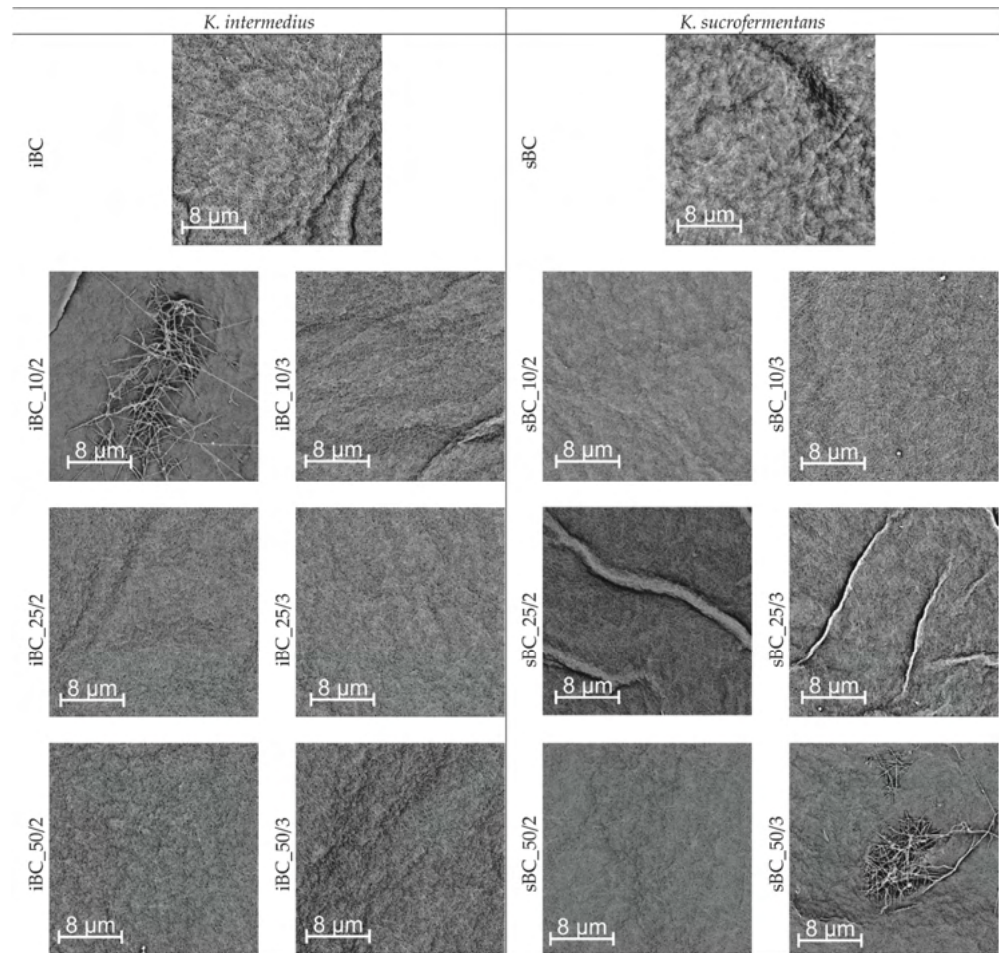

Figure 8. SEM microphotographs of all nanofiber membranes obtained using both bacterial strains. Magnification: 100,000×.

The FTIR spectrographs of GO (Figure 9) show the presence of peaks at 3000–3600, 1730, 1621, and 1030 cm^{-1}, which correspond to a very broad adsorption of -OH groups, two most characteristic peaks corresponding to the stretching vibrations of carboxyl C=O, -C=C- (stretching mode of sp^2 network), and C-O-C groups, respectively [52]. BC shows characteristic FTIR peaks for cellulose type I at 3348, 2892, 1636, 1429, and 1061 cm^{-1}, corresponding to the hydroxyl (-OH) stretching vibrations, -CH asymmetric stretching, hydroxyl (-OH) bending vibrations, CH$_2$ symmetric bending, and bond of glycosidic bridges (C-O-C and C-O skeletal stretching) [14,28].

In the case of GO/BC nanocomposite membranes (Figure 10), the characteristic BC peaks appear in the same location without big differences (Figure 9). In these samples, no peaks characteristic of GO can be seen, which may be caused by a too low concentration and strong dispersion of GO nanoparticles in the cellulose matrix with no new peaks found. The peak in some samples, the maximum of which is 2350 cm^{-1}, is derived from CO$_2$ in the atmospheric air.
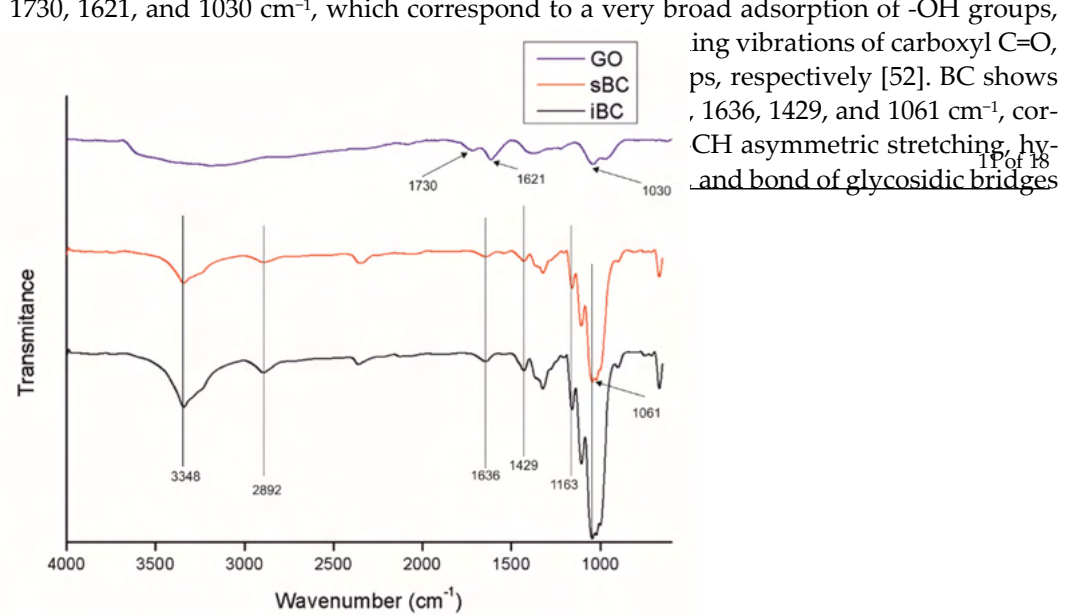
1730, 1621, and 1030 cm⁻¹, which correspond to a very broad adsorption of -OH groups, ...ing vibrations of carboxyl C=O, ...ps, respectively [52]. BC shows ..., 1636, 1429, and 1061 cm⁻¹, cor-...CH asymmetric stretching, hy-...and bond of glycosidic bridges

Figure 9. FTIR spectra of GO and neat BC produced by *K.intermedius* and *K.sucrofermentans*. The spectra range from 4000 cm⁻¹ to 650 cm⁻¹.

In the case of GO/BC nanocomposite membranes (Figure 10), the characteristic BC peaks appear in the same location without big differences (Figure 9). In these samples, no peaks characteristic of GO can be seen, which may be caused by a too low concentration and strong dispersion of GO nanoparticles in the cellulose matrix with no new peaks derived from
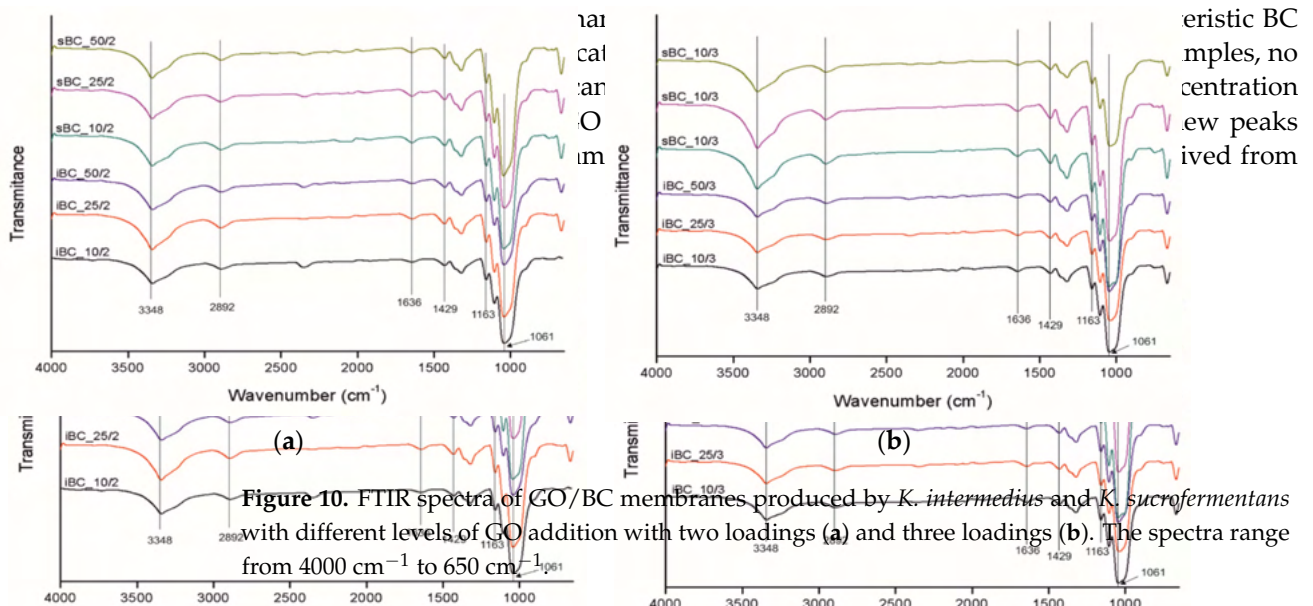

(a)

(b)

Figure 10. FTIR spectra of GO/BC membranes produced by *K. intermedius* and *K. sucrofermentans* with different levels of GO addition with two loadings (**a**) and three loadings (**b**). The spectra range from 4000 cm⁻¹ to 650 cm⁻¹.

The crystallinity index (CI) of obtained materials was determined based on WAXS analysis by the peak deconvolution method [53]. For this purpose, each WAXS pattern was distributed into individual crystalline and amorphous components using the WaxsFit software [54]. In this software, deconvolution is performed by means of an approximation method. It consists of the construction of a theoretical curve, which is composed of functions related to individual crystalline peaks and amorphous maxima. The shape of each peak was approximated using a linear combination of the Gaussian and Cauchy's functions. The parameters of these functions are found through the best fitting of the theoretical curve to the experimental one using a suitable optimization procedure. The theoretical curve was fitted to the experimental data using the Rosenbrock's double-criteria optimization method described by Rabiej et al. [55]. The crystallinity index was determined as the ratio of the sum of the surface areas under the crystalline peaks to the total area under the scattering curve. An example of the distribution of bacterial cellulose XRD diffraction pattern into crystalline and amorphous components using this software is shown in Figure 11A.

curve was fitted to the experimental data using the Rosenbrock's double-criteria optimization method described by Rabiej et al. [55]. The crystallinity index was determined as the ratio of the sum of the surface areas under the crystalline peaks to the total area under the scattering curve. An example of the distribution of bacterial cellulose XRD diffraction pattern into crystalline and amorphous components using this software is shown in Figure 11a.
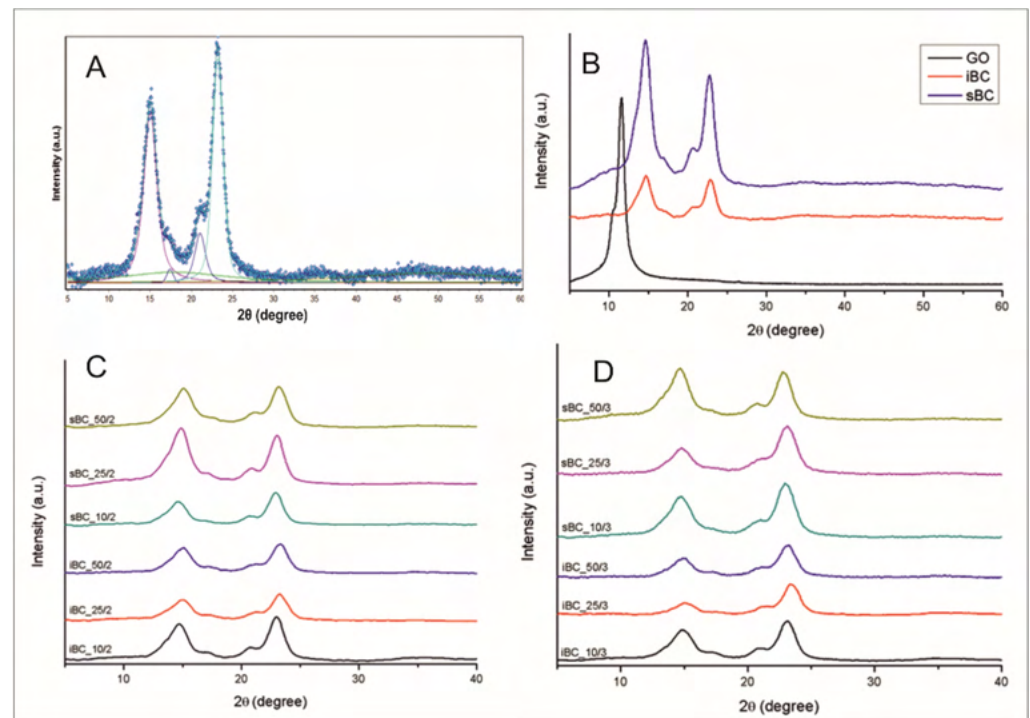

Figure 11. Distribution of XRD pattern for sBC sample into crystalline and amorphous components (**A**), XRD patterns of GO and neat BC produced by *K. intermedius* and *K. sucrofermentans* (**B**), and XRD patterns of GO/BC nanocomposites with different levels of GO addition with two loadings (**C**) and three loadings (**D**).

Analysis of X-ray curves of GO/BC nanocomposites (Figure 11C,D) as well as reference samples (Figure 11B) clearly indicates the presence of characteristic peaks that are easy to identify. In the case of BC membranes (Figure 10b), there are four characteristic crystalline peaks for cellulose I, where 2θ equals 14.6°, 16.8°, 20.6°, and 22.8°, corresponding to crystal planes (1 −1 0), (110), and (200), respectively [38,53]. The peak for 2θ at 20.6° is the result of the overlapping scattering coming from two planes (012) and (102). It occurs when crystallites are not oriented in the sample relative to the crystallographic axis c. Scattering from these planes is weak and often not registered, and even poor orientation eliminates it [56].

XRD results for GO/BC nanocomposites also indicate the presence of these peaks without significant shifts compared with reference samples made of pure BC. This indicates that the crystalline structure of BC has not changed after the introduction of GO into the cellulose matrix. In addition, it was found that, in the GO/BC nanocomposite XRD curves, regardless of the GO concentration, there is no GO-specific peak for 2θ at 11°. This may indicate the good distribution of GO nanoparticles throughout the volume of the cellulose matrix [14,38,57]. The analysis of the degree of crystallinity indicates that the addition of GO does decrease the cryatallinity index (Table 3). Dhar et al. in their work described a similar correlation but with rGO, whereby a higher concentration of rGO decreased the crystallinity index by up to 5% [28]. Rashidian et al. came to similar conclusions, which in turn showed that the GO addition reduced CI by 10 percentage points compared with neat BC [58]. This is because of all kind of additives, especially nanoadditives, impede the formation process of BC nanofibrils, which form highly ordered crystalline areas [59].

scribed a similar correlation but with rGO, whereby a higher concentration of rGO decreased the crystallinity index by up to 5% [28]. Rashidian et al. came to similar conclusions, which in turn showed that the GO addition reduced CI by 10 percentage points compared with neat BC [58]. This is because of all kind of additives, especially nanoadditives, impede the formation process of BC nanofibrils, which form highly ordered crystalline areas [59].

Table 3. Crystallinity index (%) of obtained BC and GO/BC nanocomposites.

	Crystallinity Index (CI) [%]		
iBC	70.9	sBC	64.8
iBC_10/2	70.1	sBC_10/2	65.7
iBC_25/2	69.6	sBC_25/2	65.3
iBC_50/2	69.5	sBC_50/2	63.0
iBC_10/3	68.4	sBC_10/3	67.3
iBC_25/3	66.9	sBC_25/3	66.0
iBC_50/3	65.1	sBC_50/3	65.9

The surface hydrophilicity of obtained BC and GO/BC nanocomposites was determined by measuring the contact angle (Figure 12). The water contact angle values show an increasing trend linked with GO concentration in all GO/BC nanocomposites (Figure 13). This means that GO addition decreases the hydrophilicity of GO/BC nanocomposites. A similar dependence was demonstrated by research studies of Urbina et al., where the swelling ratio of water was lower along with the increase in GO content. Further, this is known to be strictly related to the hydrophilicity of the material surface [14]. The explanation of this fact by Huang et al. may be that GO might not have been homogeneously dispersed in the cellulose matrix and that GO tended to aggregate [60]. It is worth noting that all nanocomposites obtained using *K. sucrofermentans* are characterized by significantly higher contact angle values as compared with those obtained with *K. intermedius*. In the case of the iBC sample, it was impossible to measure CA because, when the drop was applied to the surface of the membrane, the drop was immediately absorbed by the material. However, all obtained BC and GO/BC nanocomposites demonstrate hydrophilicity, with their contact angle being lower than 90°. Exemplary microphotographs taken during the contact angle measurement are shown in Figure 12.
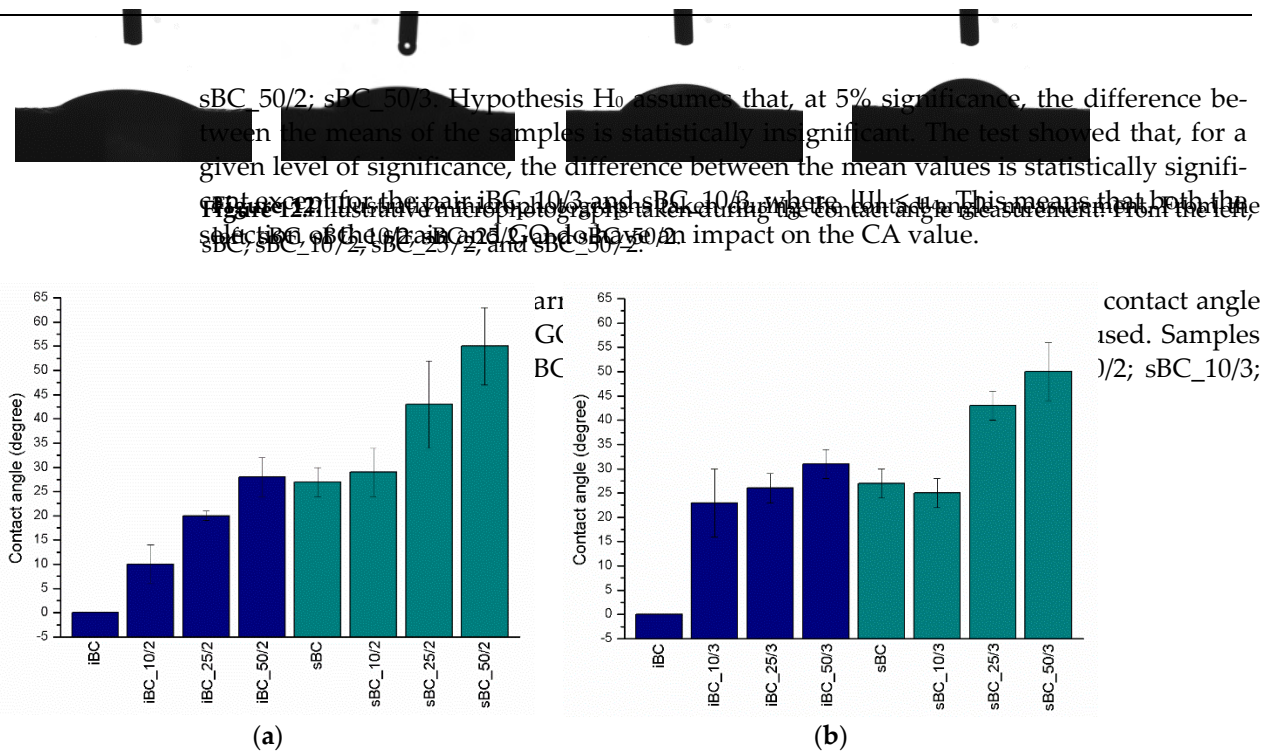
sBC_50/2; sBC_50/3. Hypothesis H$_0$ assumes that, at 5% significance, the difference between the means of the samples is statistically insignificant. The test showed that, for a given level of significance, the difference between the mean values is statistically significant except for the pair iBC_10/3 and sBC_10/3, where |U| < u$_\alpha$. This means that both the selection of the strain and GO loading have an impact on the CA value.

Figure 13. Contact angle of BC and GO/BC nanocomposite with two GO loadings (**a**) and three GO loadings (**b**).

The mechanical properties of the obtained nanofiber membranes are presented in Table 4. Significant differences between the reference samples and those containing GO are noticeable. The tensile strength values for the iBC and sBC samples were 19.41 ± 1.2 and 17.34 ± 4.2 MPa, respectively. The results of the statistical analysis comparing iBC and sBC samples in terms of mechanical parameters (tensile strength, tensile modulus, and elongation) at the significance level of 5% showed that, in terms of the first criterion, the

A statistical test was carried out comparing the average values of the contact angle in terms of the number of GO doses and in terms of the bacterial strain used. Samples were tested sequentially: iBC_10/2; iBC_10/3; iBC_50/2; iBC_50/3; sBC_10/2; sBC_10/3; sBC_50/2; sBC_50/3. Hypothesis H_0 assumes that, at 5% significance, the difference between the means of the samples is statistically insignificant. The test showed that, for a given level of significance, the difference between the mean values is statistically significant except for the pair iBC_10/3 and sBC_10/3, where $|U| < u_\alpha$. This means that both the selection of the strain and GO do have an impact on the CA value.

The mechanical properties of the obtained nanofiber membranes are presented in Table 4. Significant differences between the reference samples and those containing GO are noticeable. The tensile strength values for the iBC and sBC samples were 19.41 ± 1.2 and 17.34 ± 4.2 MPa, respectively. The results of the statistical analysis comparing iBC and sBC samples in terms of mechanical parameters (tensile strength, tensile modulus, and elongation) at the significance level of 5% showed that, in terms of the first criterion, the difference between the means of the samples is not significant, i.e., $|U| <$ in α, while in terms of the other two parameters, these samples differ significantly, where $|U| > u_\alpha$, which means that the type of bacterial strain under specific conditions affects these parameters. Interesting conclusions can be drawn based on the results for the samples containing the smallest addition of GO (iBC_10/3 and sBC_10/2), for which the tensile strength values increased more than threefold and were 60.9 MPa and 51.51 MPa, respectively, which proves that the effect of GO on material strength is positive. This phenomenon is linked to the interaction between GO and the cellulose matrix like hydrogen bond formation [38,58]. Moreover, the 3D structure of the GO network can improve this parameter. The addition of GO at higher concentrations, during both two- and three-fold loading, resulted in a gradual decrease in breaking strength, which, however, was still 1.5 times higher as compared with the samples without the addition of GO. Considering the fact that GO, like all nanoadditives, shows the ability to agglomerate, in the cellulose matrix as well, it can be assumed that this was the cause of material weakening at higher concentrations (25 ppm and 50 ppm) and a decrease in strength.

Table 4. Mechanical properties of BC and GO/BC nanocomposites.

Sample	Tensile Strength (MPa)	Tensile Modulus (MPa)	Elongation (%)
iBC	19.41 ± 1.2	1614 ± 29	1.46 ± 0.17
iBC_10/2	39.22 ± 0.87	1115 ± 127	1.65 ± 0.17
iBC_25/2	55.84 ± 1.47	2231 ± 175	2.56 ± 0.63
iBC_50/2	30.01 ± 2.69	2301 ± 171	1.86 ± 0.26
iBC_10/3	60.93 ± 10.51	2508 ± 271	2.59 ± 0.40
iBC_25/3	45.38 ± 11.17	1252 ± 247	3.17 ± 0.69
iBC_50/3	43.02 ± 13.31	3401 ± 490	1.69 ± 0.35
sBC	17.34 ± 4.2	1426 ± 24	0.69 ± 0.29
sBC_10/2	51.51 ± 7.01	2586 ± 72	1.49 ± 0.29
sBC_25/2	48.16 ± 3.51	1529 ± 172	2.33 ± 0.82
sBC_50/2	22.21 ± 1.52	2344 ± 324	0.95 ± 0.16
sBC_10/3	42.20 ± 11.49	1405 ± 287	1.15 ± 0.54
sBC_25/3	38.78 ± 2.38	2714 ± 546	2.05 ± 0.36
sBC_50/3	38.44 ± 4.06	1917 ± 396	2.59 ± 0.31

Thermogravimetric analysis (Figure 14) shows that the thermal degradation process of the obtained material is a single step and occurs from approximately 250 to 400 °C. The temperature at the beginning of the degradation process (based on DTG curves) is the lowest for the iBC membrane (298.6 °C) and the highest for the iBC_50 membrane (317.4 °C). The temperature of the maximum thermal decomposition is also the lowest for the reference sample iBC (366.7 °C) and increases monotonically together with the content of the GO nanoadditive up to 376.6 °C for the iBC_50 membrane. For sBC membranes,

of the obtained material is a single step and occurs from approximately 250 to 400 °C. The temperature at the beginning of the degradation process (based on DTG curves) is the lowest for the iBC membrane (298.6 °C) and the highest for the iBC_50 membrane (317.4 °C). The temperature of the maximum thermal decomposition is also the lowest for the reference sample iBC (366.7 °C) and increases monotonically together with the content of the GO nanoadditive up to 376.6 °C for the iBC_50 membrane. For sBC membranes, the temperature of the initial thermal degradation point is the lowest for the sBC sample (298.2 °C) and the highest for the sample with the maximum GO content: sBC_50 (315.2 °C). Moreover, in this case, the monotonicity of the decomposition process is preserved, which is manifested by an increase in the degradation temperature of more than 7 °C (sample sBC_50) in relation to the reference sample without the addition of GO (370.2 °C). It follows that GO causes a significant shift at the extrapolated temperature of the beginning of the decomposition and the actual temperature of thermal degradation. A similar relationship has been observed by us in the case of GO/CEL fibers and described in another paper [60,61].
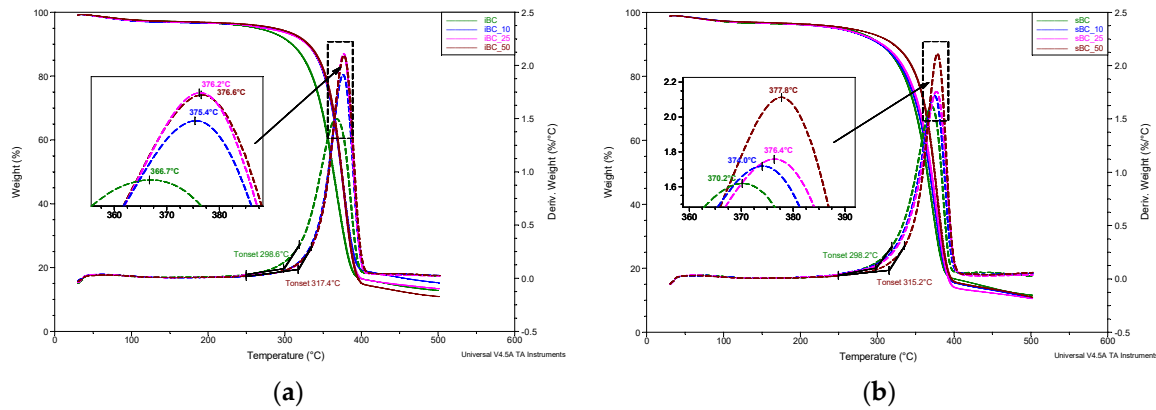

Figure 14. TG and DTG curves of the studied *K. intermedius* (**a**) and *K. sucrofermentans* (**b**) bacterial cellulose samples with different levels of GO addition.

The analysis of the volume resistivity results obtained for BC and GO/BC nanocomposites (Table 5) shows the differences in resistivity depending on the amount of the nanoadditive introduced and the method of its incorporation. The values range from 10^{11} $\Omega \times$ cm for pure cellulose reference samples to 10^{9} $\Omega \times$ cm (iBC_50/2 and sBC_50/2). The results show a trend of decreasing resistivity with an increase in GO content in the material. Despite the fact that GO is a carbon nanoadditive, it conducts electricity poorly. This is because of the presence of a large number of carbon groups with sp^3 hybridization. Nevertheless, its presence in the cellulose matrix of the obtained GO/BC membranes reduces the volume resistivity by two orders of magnitude. The greatest influence of GO on the change in resistivity of the obtained material was observed for the series of samples subjected to double BC loading in GO dispersion, for both *K. intermedius* and *K. sucrofermentans strains.* This may result from the fact that the single dose of loading, which in this case was 5 mL (Table 1), aggregated on the neat BC surface and was not evenly absorbed into the formed network of cellulose nanofibers. As a result, local areas containing more GO reduce the volume resistivity.

Table 5. Volume resistivity of the obtained BC and GO/BC nanocomposites.

Volume Resistivity ($\Omega \times$ cm)			
K. intermedius		*K. sucrofermentans*	
iBC	3.5×10^{11}	sBC	5.5×10^{11}
iBC_10/2	8.7×10^{10}	sBC_10/2	3.9×10^{11}
iBC_25/2	1.4×10^{10}	sBC_25/2	9.7×10^{10}
iBC_50/2	4.4×10^{9}	sBC_50/2	7.5×10^{9}
iBC_10/3	7.7×10^{10}	sBC_10/3	2.5×10^{11}
iBC_25/3	6.5×10^{10}	sBC_25/3	2.0×10^{11}
iBC_50/3	6.1×10^{10}	sBC_50/3	8.8×10^{10}

4. Conclusions

This paper presents research results on BC membranes modified with GO using a multistep, in situ loading method. This method was chosen with the aim of solving a critical

challenge—agglomeration of GO in the medium used for BC production. Two acetic acid bacterial strains were used to produce BC and BC-GO nanocomposites—*Komagataeibacter intermedius* and *Komagataeibacter sucrofermentans*. The obtained GO/BC nanocomposite material was characterized in terms of structural and physicochemical aspects. The results of the study indicate a significant influence of GO on the properties of GO/BC nanocomposites, including a decrease in volume resistivity by two orders of magnitude (iBC_50/2 ~4.4 × 10^9). WAXS analysis as well as thermal analysis (TG, DTG) demonstrated interactions between BC and GO, which are visible in a decrease in the degree of crystallinity. In addition, as a result of the addition of GO to the cellulose matrix, a monotonic increase in the thermostability of the material was noted, significantly increasing the temperature of thermal decomposition from 366.7 °C (iBC) to 376.2 °C (iBC_50).

References

1. Wertz, J.L.; Bédué, O.; Bédué, O.; Mercier, J.P. Biosynthesis of cellulose. In *Cellulose Science and Technology*; Hubert, G., Ed.; EPFL Press: Lausanne, Switzerland, 2010; pp. 46–80.
2. Saraiva, N.; Cavaco, G.; Portela, R.P.; Leal, C.R.; Almeida, A.P.C.; Sobral, R.G.; Almeida, P.L. Crosslinked bacterial cellulose hydrogels for biomedical applications. *Eur. Polym. J.* **2022**, *177*, 111438.
3. Martínez-Sanz, M.; Mikkelsen, D.; Flanagan, B.; Gidley, M.J.; Gilbert, E.P. Multi-scale model for the hierarchical architecture of native cellulose hydrogels. *Carbohydr. Polym.* **2016**, *147*, 542–555. [PubMed]
4. Wertz, J.L.; Bédué, O.; Mercier, J.P. Structure and Properties od Cellulose. In *Cellulose Science and Technology*; Hubert, G., Ed.; EPFL Press: Lausanne, Switzerland, 2010; pp. 87–140.
5. Xiang, Z.; Gao, W.; Chen, L.; Lan, W.; Zhu, J.Y.; Runge, T. A comparison of cellulose nanofibrils produced from *Cladophora glomerata* algae and bleached eucalyptus pulp. *Cellulose* **2016**, *23*, 493–503.
6. Cannon, R.E.; Anderson, S.M. Biogenesis of Bacterial Cellulose. *Crit. Rev. Microbiol.* **2008**, *17*, 435–447.
7. Dumitriu, S. *Polysaccharides: Structural Diversity and Functional Versatility*; Dekker, M., Ed.; CRC Press: Boca Raton, FL, USA, 2005.
8. Torres, F.G.; Troncoso, O.P.; Lopez, D.; Grande, C.; Gomez, C.M. Reversible stress softening and stress recovery of cellulose networks. *Soft Matter* **2009**, *5*, 4185–4190. [CrossRef]
9. Iguchi, M.; YAMANAKA Ajinomoto Central Research, S.; Budhiono, J.A. Review Bacterial cellulose—A masterpiece of nature's arts. *J. Mater. Sci.* **2000**, *35*, 261–270.
10. Thompson, M.A.; Onyeziri, M.C.; Fuqua, C. Function and Regulation of Agrobacterium Tumefaciens Cell Surface Structures That Promote Attachment. In Agrobacterium Biology. In *Current Topics in Microbiology and Immunology*; Gelvin, S., Ed.; Springer: Cham, Switzerland, 2018; Volume 418, pp. 143–184. ISBN 9783030032562.
11. Stumpf, T.R.; Yang, X.; Zhang, J.; Cao, X. In situ and ex situ modifications of bacterial cellulose for applications in tissue engineering. *Mater. Sci. Eng. C* **2018**, *82*, 372–383. [CrossRef]
12. Tanskul, S.; Amornthatree, K.; Jaturonlak, N. A new cellulose-producing bacterium, *Rhodococcus* sp. MI 2: Screening and optimization of culture conditions. *Carbohydr. Polym.* **2013**, *92*, 421–428.
13. Troncoso, O.P.; Torres, F.G. Bacterial cellulose—Graphene based nanocomposites. *Int. J. Mol. Sci.* **2020**, *21*, 6532.
14. Urbina, L.; Eceiza, A.; Gabilondo, N.; Corcuera, M.Á.; Retegi, A. Tailoring the in situ conformation of bacterial cellulose-graphene oxide spherical nanocarriers. *Int. J. Biol. Macromol.* **2020**, *163*, 1249–1260. [CrossRef]
15. Czaja, W.; Krystynowicz, A.; Bielecki, S.; Brown, R.M. Microbial cellulose—The natural power to heal wounds. *Biomaterials* **2006**, *27*, 145–151. [PubMed]
16. Portela, R.; Leal, C.R.; Almeida, P.L.; Sobral, R.G. Bacterial cellulose: A versatile biopolymer for wound dressing applications. *Microb. Biotechnol.* **2019**, *12*, 586–610. [CrossRef] [PubMed]

17. Pértile, R.A.N.; Moreira, S.; Gil Da Costa, R.M.; Correia, A.; Guardão, L.; Gartner, F.; Vilanova, M.; Gama, M. Bacterial cellulose: Long-term biocompatibility studies. *J. Biomater. Sci. Polym. Ed.* **2012**, *23*, 1339–1354. [CrossRef]

18. Saska, S.; Scarel-Caminaga, R.M.; Teixeira, L.N.; Franchi, L.P.; Dos Santos, R.A.; Gaspar, A.M.M.; De Oliveira, P.T.; Rosa, A.L.; Takahashi, C.S.; Messaddeq, Y.; et al. Characterization and in vitro evaluation of bacterial cellulose membranes functionalized with osteogenic growth peptide for bone tissue engineering. *J. Mater. Sci. Mater. Med.* **2012**, *23*, 2253–2266.

19. Torres, F.G.; Commeaux, S.; Troncoso, O.P. Biocompatibility of Bacterial Cellulose Based Biomaterials. *J. Funct. Biomater.* **2012**, *3*, 864–878. [PubMed]

20. Żywicka, A.; Ciecholewska-Juśko, D.; Charęza, M.; Drozd, R.; Sobolewski, P.; Junka, A.; Gorgieva, S.; El Fray, M.; Fijałkowski, K. Argon plasma-modified bacterial cellulose filters for protection against respiratory pathogens. *Carbohydr. Polym.* **2022**, *302*, 120322. [CrossRef]

21. Almeida, T.; Silvestre, A.J.D.; Vilela, C.; Freire, C.S.R. Bacterial nanocellulose toward green cosmetics: Recent progresses and challenges. *Int. J. Mol. Sci.* **2021**, *22*, 2836. [CrossRef] [PubMed]

22. Moradi, M.; Jacek, P.; Farhangfar, A.; Guimarães, J.T.; Forough, M. The role of genetic manipulation and in situ modifications on production of bacterial nanocellulose: A review. *Int. J. Biol. Macromol.* **2021**, *183*, 635–650. [CrossRef]

23. Liu, X.; Souzandeh, H.; Zheng, Y.; Xie, Y.; Zhong, W.H.; Wang, C. Soy protein isolate/bacterial cellulose composite membranes for high efficiency particulate air filtration. *Compos. Sci. Technol.* **2017**, *138*, 124–133.

24. Razavi, R.; Molaei, R.; Moradi, M.; Tajik, H.; Ezati, P.; Shafipour Yordshahi, A. Biosynthesis of metallic nanoparticles using mulberry fruit (*Morus alba* L.) extract for the preparation of antimicrobial nanocellulose film. *Appl. Nanosci.* **2020**, *10*, 465–476.

25. Marins, J.A.; Soares, B.G.; Dahmouche, K.; Ribeiro, S.J.L.; Barud, H.; Bonemer, D. Structure and properties of conducting bacterial cellulose-polyaniline nanocomposites. *Cellulose* **2011**, *18*, 1285–1294.

26. Gorgieva, S.; Trček, J. Bacterial cellulose: Production, modification and perspectives in biomedical applications. *Nanomaterials* **2019**, *9*, 1352. [CrossRef] [PubMed]

27. Khan, S.; Ul-Islam, M.; Ikram, M.; Islam, S.U.; Ullah, M.W.; Israr, M.; Jang, J.H.; Yoon, S.; Park, J.K. Preparation and structural characterization of surface modified microporous bacterial cellulose scaffolds: A potential material for skin regeneration applications in vitro and in vivo. *Int. J. Biol. Macromol.* **2018**, *117*, 1200–1210. [CrossRef]

28. Dhar, P.; Etula, J.; Bankar, S.B. In Situ Bioprocessing of Bacterial Cellulose with Graphene: Percolation Network Formation, Kinetic Analysis with Physicochemical and Structural Properties Assessment. *ACS Appl. Bio Mater.* **2019**, *2*, 4052–4066.

29. Luo, H.; Ao, H.; Li, G.; Li, W.; Xiong, G.; Zhu, Y.; Wan, Y. Bacterial cellulose/graphene oxide nanocomposite as a novel drug delivery system. *Curr. Appl. Phys.* **2017**, *17*, 249–254.

30. Peng, S.; Fan, L.; Wei, C.; Liu, X.; Zhang, H.; Xu, W.; Xu, J. Flexible polypyrrole/copper sulfide/bacterial cellulose nanofibrous composite membranes as supercapacitor electrodes. *Carbohydr. Polym.* **2017**, *157*, 344–352.

31. Song, S.; Liu, Z.; Zhang, J.; Jiao, C.; Ding, L.; Yang, S. Synthesis and Adsorption Properties of Novel Bacterial Cellulose/Graphene Oxide/Attapulgite Materials for Cu and Pb Ions in Aqueous Solutions. *Materials* **2020**, *13*, 3703.

32. Wang, L.; Hu, S.; Ullah, M.W.; Li, X.; Shi, Z.; Yang, G. Enhanced cell proliferation by electrical stimulation based on electroactive regenerated bacterial cellulose hydrogels. *Carbohydr. Polym.* **2020**, *249*, 116829. [CrossRef] [PubMed]

33. Jayani, T.; Sanjeev, B.; Marimuthu, S.; Uthandi, S. Bacterial Cellulose Nano Fiber (BCNF) as carrier support for the immobilization of probiotic, Lactobacillus acidophilus 016. *Carbohydr. Polym.* **2020**, *250*, 116965. [CrossRef]

34. Guerrero-Contreras, J.; Caballero-Briones, F. Graphene oxide powders with different oxidation degree, prepared by synthesis variations of the Hummers method. *Mater. Chem. Phys.* **2015**, *153*, 209–220. [CrossRef]

35. Konkena, B.; Vasudevan, S. Understanding aqueous dispersibility of graphene oxide and reduced graphene oxide through p K a measurements. *J. Phys. Chem. Lett.* **2012**, *3*, 867–872. [CrossRef] [PubMed]

36. Texter, J. Graphene dispersions. *Curr. Opin. Colloid Interface Sci.* **2014**, *19*, 163–174. [CrossRef]

37. Ghosh, T.; Biswas, C.; Oh, J.; Arabale, G.; Hwang, T.; Luong, N.D.; Jin, M.; Lee, Y.H.; Nam, J. Do Solution-processed graphite membrane from reassembled graphene oxide. *Chem. Mater.* **2012**, *24*, 594–599. [CrossRef]

38. Luo, H.; Dong, J.; Yao, F.; Yang, Z.; Li, W.; Wang, J.; Xu, X. Layer-by-Layer Assembled Bacterial Cellulose/Graphene Oxide Hydrogels with Extremely Enhanced Mechanical Properties. *Nano-Micro Lett.* **2018**, *10*, 42. [CrossRef]

39. Eng, A.Y.S.; Chua, C.K.; Pumera, M. Facile labelling of graphene oxide for superior capacitive energy storage and fluorescence applications. *Phys. Chem. Chem. Phys.* **2016**, *18*, 9673–9681.

40. Torres, F.G.; Arroyo, J.J.; Troncoso, O.P. Bacterial cellulose nanocomposites: An all-nano type of material. *Mater. Sci. Eng. C* **2019**, *98*, 1277–1293. [CrossRef]

41. Torgbo, S.; Sukyai, P. Bacterial cellulose-based scaffold materials for bone tissue engineering. *Appl. Mater. Today* **2018**, *11*, 34–49. [CrossRef]

42. Pourali, P.; Razavianzadeh, N.; Khojasteh, L.; Yahyaei, B. Assessment of the cutaneous wound healing efficiency of acidic, neutral and alkaline bacterial cellulose membrane in rat. *J. Mater. Sci. Mater. Med.* **2018**, *29*, 90. [CrossRef]

43. Abeer, M.M.; Cairul, M.; Amin, I.M.; Martin, C.; Kebangsaan Malaysia, U.; Raja, J.; Aziz, M.A.; Lumpur, K. A review of bacterial cellulose-based drug delivery systems: Their biochemistry, current approaches and future prospects. *J. Pharm. Pharmacol.* **2014**, *66*, 1047–1061.

44. Oliveira Barud, H.G.; Barud, H.D.S.; Cavicchioli, M.; Do Amaral, T.S.; De Oliveira Junior, O.B.; Santos, D.M.; De Oliveira Almeida Petersen, A.L.; Celes, F.; Borges, V.M.; De Oliveira, C.I.; et al. Preparation and characterization of a bacterial cellulose/silk fibroin sponge scaffold for tissue regeneration. *Carbohydr. Polym.* **2015**, *128*, 41–51.

45. Gabryś, T.; Fryczkowska, B.; Fabia, J.; Biniaś, D. Preparation of an Active Dressing by In Situ Biosynthesis of a Bacterial Cellulose–Graphene Oxide Composite. *Polymers.* **2022**, *14*, 2864. [CrossRef] [PubMed]

46. Sieradzka, M.; Fryczkowski, R.; Fryczkowska, B.; Biniaś, D. Influence of solvents on low-temperature reduction—Exfoliation of graphene oxide. *Polimery* **2017**, *62*, 841–847.

47. Sokollek, S.J.; Hammes, W.P. Description of a starter culture preparation for vinegar fermentation. *Syst. Appl. Microbiol.* **1997**, *20*, 481–491.

48. Mianehrow, H.; Moghadam, M.H.M.; Sharif, F.; Mazinani, S. Graphene-oxide stabilization in electrolyte solutions using hydroxyethyl cellulose for drug delivery application. *Int. J. Pharm.* **2015**, *484*, 276–282. [PubMed]

49. Kartick, B.; Srivastava, S.K.; Srivastava, I. Green synthesis of graphene. *J. Nanosci. Nanotechnol.* **2013**, *13*, 4320–4324. [CrossRef] [PubMed]

50. Szabo, T.; Maroni, P.; Szilagyi, I. Size-dependent aggregation of graphene oxide. *Carbon.* **2020**, *160*, 145–155.

51. Derjaguin, B.V. On the repulsive forces between charged colloid particles and on the theory of slow coagulation and stability of lyophobe sols. *Trans. Faraday Soc.* **1939**, 203–215. [CrossRef]

52. Dimiev, A.M.; Polson, T.A. Contesting the two-component structural model of graphene oxide and reexamining the chemistry of graphene oxide in basic media. *Carbon* **2015**, *93*, 544–554.

53. Park, S.; Baker, J.O.; Himmel, M.E.; Parilla, P.A.; Johnson, D.K. Cellulose crystallinity index: Measurement techniques and their impact on interpreting cellulase performance. *Biotechnol. Biofuels* **2010**, *3*, 10.

54. Rabiej, M. Application of the particle swarm optimization method for the analysis of wide-angle X-ray diffraction curves of semicrystalline polymers. *J. Appl. Crystallogr.* **2017**, *50*, 221–230.

55. Rabiej, M.; Rabiej, S. *Analiza Rentgenowskich Krzywych Dyfrakcyjnych Polimerów za Pomocą Programu Komputerowego WAXSFIT*, 1st ed.; Garbarczyk, J., Broda, J., Eds.; Wydawnictwo Akademii Techniczno-Humanistycznej w Bielsku-Białaj: Bielsko Biała, Poland, 2006; ISBN 83-89086-39-5.

56. French, A.D. Idealized powder diffraction patterns for cellulose polymorphs. *Cellulose* **2014**, *21*, 885–896.

57. Yao, Q.; Fan, B.; Xiong, Y.; Jin, C.; Sun, Q.; Sheng, C. 3D assembly based on 2D structure of Cellulose Nanofibril/Graphene Oxide Hybrid Aerogel for Adsorptive Removal of Antibiotics in Water. *Sci. Rep.* **2017**, *7*, 45914. [PubMed]

58. Rashidian, E.; Babaeipour, V.; Khodamoradi, N.; Omidi, M. Synthesis and characterization of bacterial cellulose/graphene oxide nano-biocomposites. *Polym. Compos.* **2021**, *42*, 1–9. [CrossRef]

59. Feng, Y.; Zhang, X.; Shen, Y.; Yoshino, K.; Feng, W. A mechanically strong, flexible and conductive film based on bacterial cellulose/graphene nanocomposite. *Carbohydr. Polym.* **2012**, *87*, 644–649. [CrossRef] [PubMed]

60. Huang, Y.; Zeng, M.; Ren, J.; Wang, J.; Fan, L.; Xu, Q. Preparation and swelling properties of graphene oxide/poly(acrylic acid-co-acrylamide) super-absorbent hydrogel nanocomposites. *Colloids Surfaces A Physicochem. Eng. Asp.* **2012**, *401*, 97–106. [CrossRef]

61. Gabryś, T.; Fryczkowska, B.; Biniaś, D.; Ślusarczyk, C.; Fabia, J. Preparation and properties of composite cellulose fibres with the addition of graphene oxide. *Carbohydr. Polym.* **2020**, *254*, 117436. [PubMed]

9. Wykaz pozostałego dorobku naukowego autora rozprawy

Oprócz wymienionych w punkcie 5 artykułów będących trzonem niniejszej rozprawy, mgr inż. Tobiasz Gabryś jest również autorem lub współautorem następujących publikacji:

- T. Gabryś, B. Fryczkowska „Preparing and using cellulose granules as biodegradable and long-lasting carriers for artificial fertilizers" *Journal of Ecological Engineering*, vol. 19, iss. 4, s. 111-122 (2018)
  punktacja MEiN: 70
- T. Gabryś „Modyfikowana włóknina wiskozowa jako nowoczesny i biodegradowalny materiał ściółkujący stosowany w rolnictwie" *Środowisko przyrodnicze jako obszar badań : praca zbiorowa pod red. Adama Młynarczyka*, Poznań : Bogucki Wydawnictwo Naukowe, (2020)
  punktacja MEiN: 20
- T. Gabryś, B. Fryczkowska, J. Grzybowska-Pietras, D. Biniaś „Modification and properties of cellulose nonwoven fabric – multifunctional mulching material for agricultural applications" *Materials*, vol. 14, iss. 15, s. 1-16 (2021)
  IF = 3,748; punktacja MEiN: 140
- T. Gabryś, B. Fryczkowska „Using sheeps wool as an additive to the growing medium and its impact on plant development on the example of Chlorophytum comosum" *Journal of Ecological Engineering,* vol. 23, iss. 6, s. 205-212 (2022)
  punktacja MEiN: 70

Ponadto autor rozprawy jest współautorem trzech patentów:

- T. Gabryś, B. Fryczkowska, J. Janicki, „Modyfikowane granule celulozowe oraz sposób wytwarzania modyfikowanych granuli celulozowych", Patent RP nr 240317. Punktacja MEiN: 75
- T. Gabryś, B. Fryczkowska, J. Janicki, „Sposób modyfikacji agrowłókniny z włóknin celulozowych oraz modyfikowana agrowłóknina z włókien celulozowych", Patent RP nr 240812. Punktacja MEiN: 75
- T. Gabryś, B. Fryczkowska, J. Janicki, „Sposób otrzymywania fungicydów/bakteriocydów na bazie tlenku grafenu oraz fungicydy/bakteriocydy na bazie tlenku grafenu", Patent RP nr 242394. Punktacja MEiN: 75

Doktorant odbył cztery staże naukowe w następujących podmiotach:

- Przedsiębiorstwo Górnicze SILESIA, Laboratorium Analiz Powietrza i Urobku (2018r.).
- Zakład Przetwórstwa Materiałów Polimerowych „Polowat", Laboratorium Jakości Regranulatu PET (2019r.).
- Staż w projekcie realizowanym przez University of Applied Sciences and Art z firmą EuroChem pt. „Optimization of a method to construct ternary phase diaGrams, KCl-CaCl$_2$-water at 35°C". Antwerpia, Belgia (od 1.07.2018 r. do 1.09.2018 r.).
- Staż doktorski realizowany w Institute of Engineering Materials and Desing dotyczący badań nad otrzymywaniem i właściwościami celulozy bakteryjnej modyfikowanej *in situ* tlenkiem grafenu. University of Maribor, Słowenia (od 1.09.2021 r. do 1.11.2021 r.).

Lista projektów, w których autor brał udział obejmuje:

- Grant NCBiR *„Koncentraty grafenu do zastosowań w technologii druku 3D*", POIR.04.01.04-00-0018/19-00. Wykonawca.
- Grant NCBiR „*Materiały termoizolacyjne o zwiększonej izolacyjności zawierające grafen*" , POIR.04.01.02-00-0062/16. Wykonawca.
- ProGram Erasmus +, „*Otrzymywanie i właściwości celulozy bakteryjnej modyfikowanej in situ tlenkiem grafenu*". Projekt realizowany z funduszy Interdyscyplinarnej Szkoły Doktorskiej ATH oraz Uniwersytetu w Mariborze, w Słowenii.

Otrzymane nagrody i wyróżnienia:

- Finalista konkursu „EKOinnowatorzy" realizowanego przez Instytut Zrównoważonej Energetyki za prezentację dorobku badań pro-ekologicznych (08.12.2022 r.).
- Wyróżnienie w konkursie „StRuNa", w kategorii „Projekt roku 2020 Science" za projekt pt. „*Graphite meets graphene: towards a cleaner environment*" (15.11.2020 r.).
- Pierwsze miejsce na Międzynarodowej konferencji „Innowacyjne pomysły młodych naukowców: Nauka-Start'up-Przemysł" za referat

pt. *„Zastosowanie tlenku grafenu jako bezpiecznego dla środowiska fungicydu i bakteriocydu stosowanego w uprawie roślin*” (12.05.2020 r.).

- Pierwsze miejsce na „V Ogólnopolskiej Sesji Studenckich Kół Naukowych” (Zachodniopomorski Uniwersytet Technologiczny w Szczecinie) za referat pt. *„Zastosowanie tlenku grafenu w rolnictwie na przykładzie oprysków oraz mat podsiąkowych*” (22-23.11.2019 r.).

- Drugie miejsce na „V Ogólnopolskiej Sesji Studenckich Kół Naukowych” (Zachodniopomorski Uniwersytet Technologiczny w Szczecinie) za referat pt. „*Otrzymywanie i właściwości włókien celulozowych modyfikowanych tlenkiem grafenu*” (22-23.11.2019 r.).

- Stypendium Ministra Nauki i Szkolnictwa Wyższego za wybitne osiągnięcia (01.2018 r.).

- Pierwsze miejsce na „III Ogólnopolskiej Sesji Studenckich Kół Naukowych” (Zachodniopomorski Uniwersytet Technologiczny w Szczecinie) za referat pt. *„Zastosowanie granulek celulozowych jako długodziałających nośników nawozów mineralnych*” (24-25.11.2017 r.).

Ponadto autor rozprawy brał czynny udział w następujących konferencjach:

- Międzynarodowa konferencja „EPNOE International Polysaccharide Conference”, Aveiro, Portugalia. Prezentacja posteru pt. ”Preparation and properties of cellulose fibers with Graphene oxide addition” (21-25.10.2019 r.).

- Międzynarodowa konferencja „X-ray Investigations of polymer structure”, Ustroń, Polska. Prezentacja posteru pt.”Structure of cellulose fibers with graphene oxide addition” (3-6.12.2019 r.).

- Międzynarodowa konferencja „Innowacyjne pomysły młodych naukowców: Nauka-Start’up-Przemysł”, online. Wygłoszenie referatu pt. „Zastosowanie tlenku grafenu jako bezpiecznego dla środowiska fungicydu i bakteriocydu stosowanego w uprawie roślin” (12.05.2020 r.).

- Ogólnopolska konferencja pt. „Środowisko przyrodnicze jako obszar badań”, online. Wygłoszenie referatu pt. „Modyfikowana włóknina wiskozowa jako nowoczesny i biodegradowalny materiał ściółkujący stosowany w rolnictwie” (28.05.2020 r.).

- Międzynarodowa konferencja „EuroScience Open Forum", Triest, Włochy. Wygłoszenie referatu pt. „Graphite meets graphene: towards a cleaner environment" (2-6.09.2020 r.).

- XIII Interdyscyplinarna Konferencja Naukowa Tygiel 2021. Wygłoszenie referatu pt. "Celuloza bakteryjna modyfikowana tlenkiem grafenu jako nowoczesny bośnik leków" (25-28.03.2021 r.).

- Ogólnokrajowa konferencja pt. "Koncentraty grafenowe w przetwórstwie tworzyw sztucznych". Współorganizator (18.11.2021 r.).

- Ogólnokrajowa konferencja/konkurs pt. „EKOinnowatorzy 2022". Wygłoszenie referatu na temat prowadzonych badań proekologicznych (8.12.2022 r.).